DETERMINATION OF THE ENERGY MAGNITUDE M_E: APPLICATION TO RAPID RESPONSE PURPOSES AND INSIGHTS TO REGIONAL/LOCAL VARIABILITIES

Domenico Di Giacomo

Thesis submitted for the degree in Doctor rerum naturalium

Institut für Erd- und Umweltwissenschaften, Universität Potsdam,
Karl-Liebknecht-Strasse 24, Haus 27, 14476 Potsdam, Germany
June, 2010

Published online at the
Institutional Repository of the University of Potsdam:
URL http://opus.kobv.de/ubp/volltexte/2011/5076/
URN urn:nbn:de:kobv:517-opus-50768
http://nbn-resolving.org/urn:nbn:de:kobv:517-opus-50768

I herewith declare that I have produced this paper without the prohibited assistance of third parties and without making use of aids other than those specified; notions taken over directly or indirectly from other sources have been identified as such. This paper has not previously been presented in identical or similar form to any other German or foreign examination board.

Potsdam, 05.07.2010

Domenico Di Giacomo

“The only man who makes no mistakes is the man who never does anything.”

- Theodore Roosevelt.

Acknowledgements

During the years of my PhD I had the luck and opportunity to interact with many members of the Section 2.1 of the GeoForschungsZentrum Potsdam. I first would like to thank my advisor Jochen Zschau for his help and support and for the suggestions to improve this manuscript. I am deeply indebted to Stefano Parolai not only for his constant guidance and patience that helped me to face and understand various aspects of seismology, but also for his support that has gone well beyond the research aspects of my PhD. I owe a special thank to Peter Bormann. It has been an honor and a pleasure to work with him and I will remember the many useful discussions but also his extraordinary enthusiasm and passion that I will always consider as a model for the future. Helmut Grosser deserves a special thank for his guidance since the beginning of my PhD, for the bright explanations about the earthquake source which at the beginning appeared dark to me, and for being always kindhearted towards me. My sincere gratitude to Rongjiang Wang for his simulation codes, essentials for my work. Many thanks are due to Joachim Saul of the GEOFON group for providing the data and for sharing his results.

I have benefited from Dino Bindi for his wonderful way of explaining difficult arguments, and Kevin Fleming for his company and invaluable English proof-reading. I am grateful to Adrien Oth and the ECGS Luxembourg for the support during last year of the PhD. Thanks to Susanne Köster for her kindness and precious help. I have enjoyed the company of other members of the section Heiko Woith, Claus Milkereit, Birger Lühr, Frank Roth, Sebastian Hainzl, Ralph Bauz, Regina Milkereit, Erwin Günther, Dorina Kroll, Ute Borchert, Manoochehr Shirazaei, Nicolas Le Corvec, Stefanie Donner, Silke Eggert, Ade Anggraini, Lifeng Wang, Katja Müller,

Ingo Veit, Sergio Rosa Cintas, Sebastian Rudolph, Marc Wieland and Max Pittore.

I would like to say a thank *gigante* to Matteo, Angelo, Marco, Andrea, Joel, and Geraldine Giselle for sharing the difficult moments but especially for making the cold Berlin-Potsdam so hot and warm.

Thanks to the "*Milanese*" Marco, Ezio, Gabriele and Simone for their friendship during these years.

Finally, I am thankful to my family for the constant support and in particular to my sister Maria for being always there for me.

Abstract

Recent large earthquakes put in evidence the need of improving and developing robust and rapid procedures to properly calculate the magnitude of an earthquake in a short time after its occurrence. The most famous example is the 26 December 2004 Sumatra earthquake, when the limitations of the standard procedures adopted at that time by many agencies failed to provide accurate magnitude estimates of this exceptional event in time to launch early enough warnings and appropriate response.

Being related to the radiated seismic energy E_S, the energy magnitude M_E is a good estimator of the high frequency content radiated by the source which goes into the seismic waves. However, a procedure to rapidly determine M_E (that is to say, within 15 minutes after the earthquake occurrence) was required. Here it is presented a procedure able to provide in a rapid way the energy magnitude M_E for shallow earthquakes by analyzing teleseismic *P*-waves in the distance range 20°-98°. To account for the energy loss experienced by the seismic waves from the source to the receivers, spectral amplitude decay functions obtained from numerical simulations of Greens functions based on the average global model AK135Q are used.

The proposed method has been tested using a large global dataset (~1000 earthquakes) and the obtained rapid M_E estimations have been compared to other magnitude scales from different agencies. Special emphasis is given to the comparison with the moment magnitude M_W, since the latter is very popular and extensively used in common seismological practice. However, it is shown that M_W alone provide only limited information about the seismic source properties, and that disaster management organizations would

benefit from a combined use of M_W and M_E in the prompt evaluation of an earthquake's tsunami and shaking potential. In addition, since the proposed approach for M_E is intended to work without knowledge of the fault plane geometry (often available only hours after an earthquake occurrence), the suitability of this method is discussed by grouping the analyzed earthquakes according to their type of mechanism (strike-slip, normal faulting, thrust faulting, etc.). No clear trend is found from the rapid M_E estimates with the different fault plane solution groups. This is not the case for the M_E routinely determined by the U.S. Geological Survey, which uses specific radiation pattern corrections. Further studies are needed to verify the effect of such corrections on M_E estimates.

Finally, exploiting the redundancy of the information provided by the analyzed dataset, the components of variance on the single station M_E estimates are investigated. The largest component of variance is due to the intra-station (record-to-record) error, although the inter-station (station-to-station) error is not negligible and is of several magnitude units for some stations. Moreover, it is shown that the intra-station component of error is not random but depends on the travel path from a source area to a given station. Consequently, empirical corrections may be used to account for the heterogeneities of the real Earth not considered in the theoretical calculations of the spectral amplitude decay functions used to correct the recorded data for the propagation effects.

Zusammenfassung

Starke Erdbeben in letzter Zeit zeigten deutlich den steigenden Bedarf nach einer Verbesserung und Entwicklung von stabilen und schnellen Methoden, um die Magnitude eines Erdbebens korrekt innerhalb kürzester Zeit nach dessen Auftreten zu ermitteln. Das bisher bekannteste Fallbeispiel in diesem Zusammenhang stellt das Sumatra-Erdbeben vom 26 Dezember 2004 dar. Dieses außergewöhnliche Ereignis zeigte deutlich die Grenzen der bisher gängigen und von den meisten Behörden zu dieser Zeit verwendeten Methoden zur Ermittlung der Erdbebenmagnitude. So konnte für dieses Beben mit den gängigen Ansätzen zeitnah die Magnitude nicht korrekt bestimmt werden , um eine angemessene Frühwarnung und entsprechende Gegenmaßnahmen einzuleiten.

Die Energiemagnitude M_E steht in direkter Verbindung mit der abgestrahlten seismischen Energie E_S und stellt somit eine guten Abschätzung für den Hochfrequenzanteil dar, der von der Quelle ausgestrahlt wird und in die seismischen Wellen einfließt. Eine Methode, welche eine schnelle Ermittlung von M_E ermöglicht (d.h. innerhalb von maximal 15 Minuten nach dem Erdbeben) wäre in diesem Falle benötigt worden. Im Rahmen dieser Arbeit wird eine Methode vorgestellt, die eine solche schnelle Ermittlung der Energiemagnitude M_E für oberflächennahe Erdbeben ermöglicht, indem teleseismische *P*-Wellen im Bereich von 20°-98° analysiert werden. Um den Energieverlust der seismischen Wellen von deren Quelle bis zu den Empfängern angemessen zu berücksichtigen, werden spektrale Amplituden-Abnahmefunktionen verwendet, welche aus numerischen Simulationen von Greenschen Funktionen basierend auf dem durchschnittlichen globalen Modell AK135Q abgeleitet werden.

Die vorgestellte Methode wurde mit einem umfangreichen globalen Datensatz (ca. 1000 Erdbeben) getestet, und die zeitnah ermittelten M_E-Abschätzungen wurden mit anderen Magnitudenskalen verschiedener Behörden verglichen. Ein Vergleich mit der Momentenmagnitude M_W war hierbei von besonderem Interesse, da diese

Skala heutzutage weitverbreitet ist und häufig zum Einsatz kommt. Es zeigt sich jedoch, dass M_W alleine nur begrenzte Informationen über die seismischen Herdeigenschaften liefern kann, und dass Organisationen des Katastrophenmagements von einer kombinierten Nutzung von M_W und M_E gerade hinsichtlich der unmittelbaren Evaluierung des tsunamigenen Potentials und der Erschütterungswirkung eines Erdbebens profitieren könnten. Die verwendete Methode zur Ermittlung von M_E kommt ohne Wissen über die geometrischen Eigenschaften der Verwerfungszone aus (diese sind meist erst Stunden nach einem Erbeben verfügbar). Entsprechend wird die Eignung dieser Methode durch Eingruppierungen der analysierten Erdbeben nach ihrem Wirkungsmechanismus (Scherbruch, Abschiebung, Aufschiebung, etc.) diskutiert. Für die schnelle Abschätzung von M_E ist kein klarer Trend unter Verwendung der verschiedenen Herdflächenlösungen erkennbar. Für M_E-Werte, welche standardmäßig vom U.S. Geological Survey mit speziellen Korrekturwerten für die Abstrahlungscharakteristika ermittelt werden, trifft dies jedoch nicht zu. Weitere Untersuchungen sind nötig, um die Auswirkungen solcher Korrekturen auf die M_E-Abschätzungen zu verifizieren.

Indem die Redundanz der Informationen des analysierten Datensatzes ausgenutzt wurde, konnte die Varianz bei den Einzelstations-M_E-Abschätzungen untersucht werden. Die größte Abweichung zeigt sich aufgrund von Intra-Stations-Fehlern (record-to-record), wenngleich auch der Inter-Stations-Fehler (station-to-station) nicht vernachlässigbar ist; so nimmt er für einige Stationen mehrere Magnitudeneinheiten an. Des Weiteren konnte gezeigt werden, dass der Intra-Stations-Anteil des Gesamtfehlers nicht zufällig ist, sondern abhängig vom Wellenweg von einem Quellgebiet zu einer bestimmten Station. Folglich können empirische Korrekturen dazu benutzt werden, den Heterogenitäten der realen Erde gerecht zu werden, welche heutzutage nicht in den theoretischen Kalkulationen der spektralen Amplituden-Abnahmefunktionen zur Korrektur der aufgezeichneten Daten verwendet werden.

Table of Contents

List of Tables and Figures

CHAPTER 1

1.1 Introduction

The magnitude of an earthquake is one of the most used parameters to quantify the earthquake "*strength*" and, therefore, to evaluate an earthquake's damage potential. In addition, its determination in a short time after the earthquake occurrence is of primary importance for disaster management organizations, especially in case of very large earthquakes. In fact, a prompt and reasonably accurate initial estimate of an earthquake's damage potential is of great importance for improved guidance of the rapid response activities. This is particularly the case when earthquakes occur in areas that are not well monitored by near- or real-time local networks. Then estimates of the fundamental parameters hypocenter location and earthquake magnitude may have to be based on teleseismic data only. A well-known example is the recent great 26 December, 2004, Sumatra earthquake, for which the standard procedure for magnitude determinations adopted at many agencies failed to correctly and promptly evaluate the actual magnitude of this exceptional earthquake, with the result of launching no warning before the devastating tsunami that stroke a wide area of the Indian Ocean.

However, over the past decades, many magnitude scales have been developed, and each of them has a different meaning and provides information about a particular aspect of the earthquake source.

The first magnitude scale was introduced by Richter (1935) after analyzing local seismogram recordings in California (Richter or local magnitude M_L). This was the first attempt to create a magnitude scale linked to the physical characteristics of the seismic source, independently of the

earthquake effects. In particular, the intention of Richter (1935) was to relate the earthquake magnitude with the amount of energy released by the seismic source. Since then, the magnitude concept evolved and after Gutenberg (1945a, b, c) and Gutenberg and Richter (1956a, b) other magnitude scales have been developed by considering teleseismic recordings. In this way the magnitude determination for all the earthquakes recorded on a global scale became routine practice. Still, the basic idea was to provide magnitude estimations related to the energy released by the source, as testified by the so-called classical Gutenberg-Richter relationships:

$$\log E_S = 2.4 m_B - 1.2, \qquad (1)$$

and

$$\log E_S = 1.5 M_S + 4.8. \qquad (2)$$

where E_S is the seismic energy (Haskell, 1964) measured in Joule, m_B is the body-wave magnitude (measured between about 2 and 20 s, Abe 1981) and M_S is the surface wave magnitude (measured at periods around 20 s). (Note: in this thesis log always means $\log_{10}$).

Therefore, E_S was recognized as a fundamental parameter to characterize the earthquake source, although its direct calculation from the recorded seismograms was not possible at that time. Especially Eq. (2) has been used for decades to have a rough estimation of the energy released by the earthquakes, but only in recent years, thanks to the deployment of high quality digital broadband seismometers worldwide, direct measurements of E_S became achievable on a routine basis. After the pioneer work of Wyss (1968), who first integrated squared digital seismograms to calculate the radiated energy, Boatwright and Choy (1986) proposed a method to directly estimate E_S from velocity broadband recordings and, later, the energy magnitude M_E has been

introduced (Choy and Boatwright, 1995; Bormann et al., 2002; Choy et al., 2006):

$$M_E = 2/3(\log E_S - 4.4) \qquad (3).$$

However, after the introduction of the seismic moment M_0 (Aki, 1966), it became popular to evaluate the "*size*" of an earthquake via the moment magnitude M_W proposed by Kanamori (1977) and Hanks and Kanamori (1979). M_W is a modern magnitude scale related to the well-defined physical parameter of the source as the seismic moment $M_0 = \mu\ A\ D$ (where μ = rigidity, A = rupture area, D = average displacement over the fault) via:

$$M_W = 2/3(\log M_0 - 9.1) \qquad (4)$$

with M_0 given in Nm. As such, M_W is used in many seismological applications (ShakeMap, seismic hazard studies, etc.) as it is assumed to be the best magnitude parameter to evaluate an earthquake's damage potential.

Nevertheless, despite its popularity, M_W provides only limited information about the earthquake source, especially regarding its high frequency content (e.g., Beresnev, 2009), which is the most relevant for the evaluation of an earthquake's shaking potential. To this regard M_E is more appropriate than M_W (Boatwright and Choy, 1986; Bormann et al., 2002; Choy and Kirby, 2004; Di Giacomo et al., 2010a).

In sum, the different magnitude scales mentioned so far have been developed following one of two possible approaches:

1. measuring amplitudes of different wave types (*P*- and *S*-waves, surface waves) and related periods;
2. assessing distinct and well-defined physical parameters of the seismic source (like M_0 and E_S).

To the latter belong the two modern magnitude scales M_W and M_E, which do not suffer of saturation as the classical ones (Kanamori, 1983;

Bormann et al., 2002; Bormann and Saul, 2009a). This is a feature of primary importance and attractive for disaster management organizations, especially in case for very large earthquakes. In recent years procedures to calculate in a rapid way the earthquake magnitude focused especially on M_W (e.g., Okal and Talandier, 1989; Sipkin, 1994; Tsuboi et al., 1995), and, after the occurrence of the 26 December, 2004, Sumatra earthquake, further improvements have been proposed (Kanamori and Rivera, 2008) and also considering proxies for estimating it (Lomax et al., 2007; Bormann and Saul, 2008, 2009b; Lomax and Michelini, 2009a).

With regard to M_E, the National Earthquake Information Center (NEIC) of the U.S. Geological Survey (USGS) delivers M_E determinations generally only hours after the earthquake occurrence. The USGS uses the method of Boatwright and Choy (1986), which requires knowledge of the fault plane solution and depth in order to apply the corrections for specific radiation pattern. Such corrections cannot be implemented in real-time observational conditions until a suitable source mechanism solution is available. The latter information, however, is normally not available 15-30 minutes (or hours in many cases) after the earthquake origin time (OT). Yet, the method of Boatwright and Choy (1986) normally adopts revised and accurate depth and focal mechanisms solutions (either from broadband waveform modelling or moment tensor solutions), and this requires more time to release the $M_{E(USGS)}$ solution.

In this context, a procedure to rapidly calculate M_E was required and one of the main goals of this work is to develop it. The scopes and the structure of the thesis are described in more detail in the next section.

1.2 Objective and structure of the thesis

The primary aim of the thesis is to develop a procedure suitable for implementation in rapid response systems to determine the energy magnitude M_E within 10-15 min after an earthquake occurrence, even for very large ones occurring in remote areas. Here are considered only shallow earthquakes (source depth $h < 70$ km) since they represent the events with higher damage potential and, therefore, of greater importance for rapid response purposes. After having described the developed procedure, it will be shown that the information provided by M_E is of essential not only for scientific studies of the seismic source but also for the purpose of better evaluating the earthquake's effects. Indeed, the use of a unique magnitude parameter like M_W is not able to provide a complete picture of the source properties, whereas already by complementing M_W with M_E would be of great help for the evaluation of the impact of an earthquake in terms of shaking and tsunami generation.

In **Chapter 2** the origins of the M_E relationship (outlining the differences with the derivation of the M_W formula) and, shortly, the basic concepts of the definition, meaning and calculation of the radiated seismic energy E_S are recalled. Then, the procedure to rapidly determine E_S and, therefore, M_E, is illustrated starting by the core of the proposed approach, which consists of the use of theoretical pre-calculated spectral amplitude decay functions for different frequencies. The latter have been computed from numerical simulations of Green's functions given the reference Earth model AK135Q.

In **Chapter 3** the suitability of the method is discussed considering a large global dataset of ~1000 earthquakes ($5.5 \leq M_W \leq 9.0$) and comparing the rapid M_E determinations with M_E and M_W from other agencies and also with

the classical magnitude estimates M_S, m_B and m_b. The importance of complementing M_W and M_E will be emphasized by discussing some representative earthquakes. In addition, the magnitude characteristics of tsunami and tsunamigenic earthquakes occurred in the last ~20 years will be also discussed.

In **Chapter 4** the redundancy of the information provided by the large dataset analyzed (a total of ~48,000 single stations M_E determinations from recordings of 476 seismic stations deployed worldwide) is exploited to asses the origins of the variance of the rapid M_E estimates due to:

1. the station characteristics (inter-station variability), related to shallower Earth structure below a given seismic station;
2. the propagation paths (intra-station variability), related to specific source-station paths.

Finally, in **Chapter 5** the conclusions of the thesis are summarized along with the outlook.

Most of the results shown in **Chapter 2 and 3** have been published in two papers, the first one in *Geophysical Research Letters* (*GRL*) in 2008 and the second in *Geophysical Journal International* (*GJI*) in 2010. The former introduces the spectral amplitude decay functions and the basic idea of the procedure for implementation in rapid response systems, and the latter reports the improvements applied to the procedure and shows the suitability of the approach by considering a large global dataset (comparisons of M_W and M_E, with examples of representative earthquakes). The results related to the magnitude characteristics of tsunami and tsunamigenic earthquakes discussed at the end of **Chapter 3** are included in a paper submitted to *Natural Hazards* (*Nat. Haz.*).

Moreover, the origins and differences of the M_E and M_W formulas outlined in **Chapter 2** are part of a paper submitted to *Journal of Seismology* (*JOSE*).

Finally, the results shown in **Chapter 4** have been submitted to *Physics of the Earth and Planetary Interiors* (*PEPI*).

The papers are not single-author manuscripts, but I am the first author and primary investigator of the two published papers (in *GRL* and *GJI*) and of the submitted to *Nat. Haz.* and *PEPI*. The paper submitted to *JOSE* I co-authored with P. Bormann.

CHAPTER 2

2.1 The derivation of the M_E relationship and how it relates to M_W

Choy and Boatwright (1995) scaled the energy magnitude M_E in a similar way as Kanamori (1977) scaled M_W with the Gutenberg-Richter relationship (2). Starting from their direct measurements of E_S, they plotted $\log E_S$ over M_S and determined from a standard least-square regression the best fitting straight line with the prescribed slope of 1.5 as in Eq. (2), and inserting M_E in place of M_S. However, doing so, they derived the constant 4.4 instead of the constant 4.8 in relation (2), as the former constant yielded a better average fit through the data cloud. Nevertheless, Choy and Boatwright decided in their 1995 paper: "For consistency with historical computations as well as with other types of magnitude that have been derived from the Gutenberg-Richter formula, we retain the original constants". Thus they arrived at

$$M_E = (2/3)\log E_S - 3.2 = (\log E_S - 4.8)/1.5 \qquad (5)$$

with E_S given in Joule. However, in subsequent papers they reverted to the better fitting constant of 4.4 and changed Eq. (5) to (Choy et al., 2006)

$$M_E = (2/3)\log E_S - 2.9. \qquad (6).$$

However, as recommended by Bormann et al. (2002), to avoid occasional rounding errors of 0.1 magnitude units (m.u.) (the constant in Eq. (6) should be 2.9333… instead of 2.9), today the Eq. (3) is accepted as standard also at NEIC/USGS.

Before outlining the link between Eq. (2) and Eq. (3), the derivation of M_W is here recalled. Kanamori (1977) used the following relationship between

the strain energy drop W and M_0 for the case of *complete stress drop* $\Delta\sigma$ in the source and with μ = rigidity of the medium in the source area:

$$W = W_0\ (=E_S) = (\Delta\sigma/2\mu)\ M_0. \qquad (7).$$

[The condition of *complete stress drop* is met when the final average stress (σ_1) and the frictional stress (σ_f) are identical (Orowan, 1960). However, the rupture process may deviate from this condition. The final stress σ_1 may be larger than σ_f in the case of *partial stress drop* (Brune, 1970) or smaller than σ_f in the case of *frictional overshoot* (Savage and Wood, 1971)]. Further, Kanamori assumed μ = 3-6 × 10^{11} dyn/cm^2 = 3-6 × 10^4 MPa in the source area under average crust-upper mantle conditions, and, on the basis of elastostatic considerations (as earlier Knopoff, 1958), that also the *stress drop is nearly constant* with values between some 20 and 60 bars = 2-6 ×10^7 dyn/cm^2 = 2-6 MPa *for very large earthquakes*. With the assumptions made on μ and $\Delta\sigma$ Eq. (7) can be written as

$$E_S = W_0 \approx M_0/(2 \times 10^4) \qquad (8)$$

or

$$E_S/M_0 = 5 \times 10^{-5} = \text{constant} \qquad (9a),$$

$$\log(E_S/M_0) = -4.3 = \text{constant} \qquad (9b),$$

which are also known as Kanamori's conditions.

Kanamori (1977) used Eq. (9) to introduce the non-saturating moment-magnitude scale M_W by substituting it for M_S in Eq. (2):

$$\log E_S = \log M_0 - 4.3 = 1.5M_W + 4.8 \qquad (10),$$

and when resolving it for M_W:

$$M_W = (\log M_0 - 4.3 - 4.8)/1.5 = (\log M_0 - 9.1)/1.5 \qquad (11).$$

Thus, if all these conditions were correct, one could easily calculate E_S from known M_0 via Eq. (9). However, the ratio $E_S/M_0 = \Theta$ is not constant (see,

e.g., Choy and Boatwright, 1995; Newmann and Okal, 1998; Weinstein and Okal, 2005) and varies over about three orders of magnitude. By using Θ, the relationships for M_W and M_E, according to Bormann and Di Giacomo (2010), can be rewritten as:

$$M_W = (\log M_0 + \Theta_K - 4.8)/1.5 \qquad (12),$$

(Θ_K = -4.3, identifying Θ under the Kanamori's condition),

and

$$M_E = (\log M_0 + \Theta - 4.4)/1.5 \qquad (13),$$

which yield, after few more steps, to the following relationship:

$$M_E = M_W + (\Theta + 4.7)/1.5 = M_W + [\log(E_S/M_0) + 4.7]/1.5 \qquad (14).$$

As a result of the last three equations, the link between M_W and M_E becomes evident but also why they may differ of several m.u. Therefore, it is of primary importance to complement these two modern magnitude scales in the characterization of the earthquake source. In contrast to M_W, M_E is sensitive to the variability of the stress conditions governing the earthquake rupture process, which, in turn, determine the amount of energy going into the seismic waves. This amount can be determined via M_W only if Kanamori's conditions are satisfied. To further explain this point, in Fig. 2.1 an average theoretical source spectrum (ω^{-2} model, Aki, 1967; Brune, 1970; Houston and Kanamori, 1986) is shown**.**

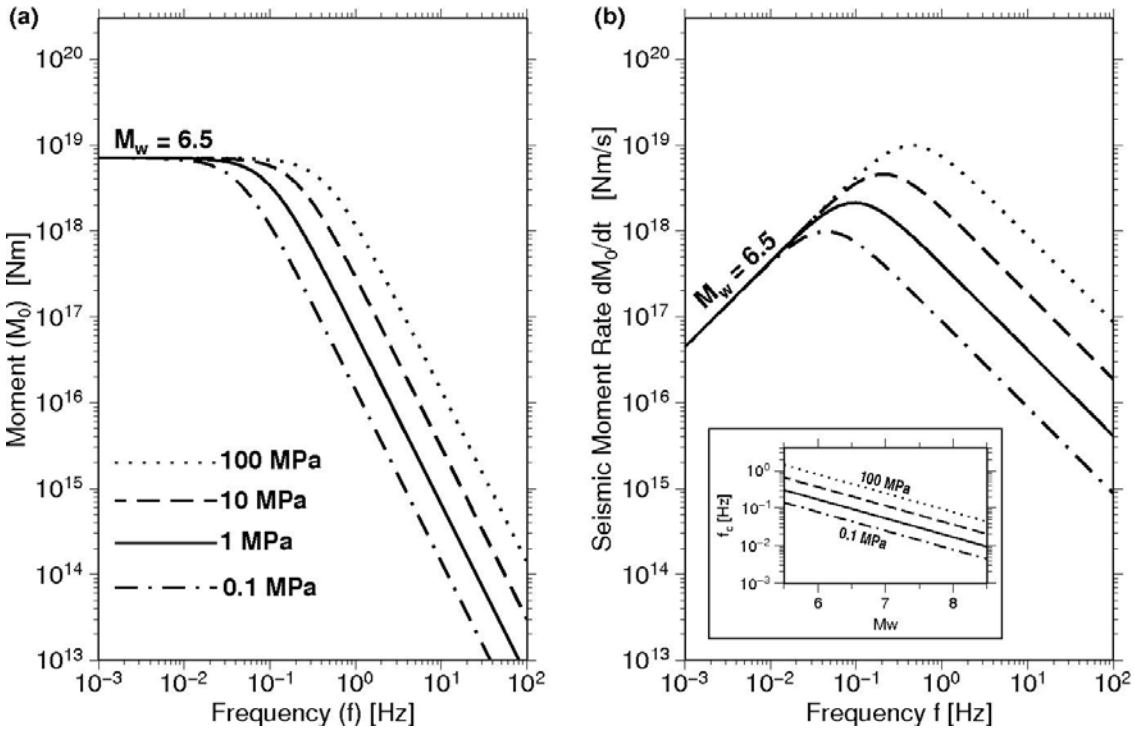

Fig. 2.1: a) Far-field "source spectra" of ground displacement amplitudes for a ω^{-2} model as a function of frequency f, scaled to seismic moment M_0 and the equivalent moment magnitude $M_W = 6.5$ for different stress-drop $\Delta\sigma$ in units of MPa. b) The same for ground motion velocity amplitudes, scaled to seismic moment rate and M_W. The maximum of E_S is concentred around the corner frequency $f_c = c\beta(\Delta\sigma/M_0)^{1/3}$, with β assumed to be 3.75 km/s, c = 0.49 and the stress drop $\Delta\sigma = 3$ MPa. The inset in Fig. 2.1b shows the variation of f_c in a wider range of M_w for $\Delta\sigma$ varying in increments of one order between 0.1 and 100 MPa.

Variations in stress drop for the theoretical curves do not play a role in their low-frequency amplitudes, where the determination of M_0 and M_W must be performed. On the contrary, variations in stress drop are very important for the final amount of E_S and, therefore, of M_E, since by definition of E_S (see following section), frequencies not only below but especially above the corner frequency, where the source spectra are peaked, must be considered.

2.2 Definition and calculation of E_S

This section recalls some of the theoretical basics and assumptions underlying the calculation of the radiated seismic energy E_S in the teleseismic

range (for more details, the reader is referred to, for example, Haskell, 1964; Rudnicki and Freund, 1981; Vassiliou and Kanamori, 1982; Boatwright and Fletcher, 1984; Boatwright and Choy, 1986; Venkataraman and Kanamori, 2004a).

The radiated seismic energy E_S is an important physical parameter of the seismic source. It describes the fraction of the overall energy budget involved in the earthquake source process that goes into elastic seismic waves energy. The latter is determined by the dynamics of the source process. According to Rudnicki and Freund (1981), E_S depends on the change of stress conditions during the fault rupture:

$$E_S = \int_{-\infty}^{\infty} \int_S \left[-\sigma_{ij} \gamma_j \dot{u}_i \right] dS dt \qquad (15)$$

where $\dot{u}_i$ = particle velocity, σ_{ij} = stress change associated with the fault displacement u_i, γ_j = unit vector normal to the surface S and pointing outward from the source, and t = time. This definition holds in the far-field, i.e., the radius of the surface S is much larger than the dimension of the earthquake source. Rudnicki and Freund (1981) have shown that Eq. (15) is equivalent to another one often used in seismology and proposed by Haskell (1964):

$$E_S = \int_{-\infty}^{\infty} \int_S \rho \left[\alpha \dot{u}_\alpha^{\,2} + \beta \dot{u}_\beta^{\,2} \right] dS dt \qquad (16)$$

where ρ = density, α and β = P- and S-wave velocities in the medium, $\dot{u}_\alpha$ and $\dot{u}_\beta$ = far-field velocity records of P- and S-waves, respectively. These records must be corrected for the energy loss due to the geometrical spreading and anelastic attenuation of P- and S-waves during their travel from the seismic source to the receivers. This is equivalent to saying that E_S in the far-field is proportional to the time derivative of the moment rate function $\ddot{M}(t)$. Recalling

that the ground motion $u_{\alpha,\beta}(t)$ at distance r from the source depends on the moment rate $\dot{M}(t)$ (e.g., Aki and Richards, 1980)

$$u_\alpha(t) = \frac{R_\alpha(\theta,\phi)}{4\pi r\alpha^3}\dot{M}(t) \qquad (17a)$$

$$u_\beta(t) = \frac{R_\beta(\theta,\phi)}{4\pi r\beta^3}\dot{M}(t) \qquad (17b)$$

where $R_\alpha(\theta,\phi)$ and $R_\beta(\theta,\phi)$ are the radiation patterns for *P*- and *S*-waves, respectively, and that it is easier to perform the correction for propagation effects in the frequency domain, by using Parseval's identity the equation for E_S can be finally written as:

$$\begin{aligned} E_S &= \left(\frac{1}{15\pi\rho\alpha^5}+\frac{1}{10\pi\rho\beta^5}\right)\int_{-\infty}^{\infty}\left|\dot{\hat{M}}(f)\right|^2 df \\ &= \left(\frac{2}{15\pi\rho\alpha^5}+\frac{1}{5\pi\rho\beta^5}\right)\int_{0}^{\infty}\left|\dot{\hat{M}}(f)\right|^2 df \qquad (18) \\ &\approx \left(\frac{2}{15\pi\rho\alpha^5}+\frac{1}{5\pi\rho\beta^5}\right)\int_{f_1}^{f_2}\left|\dot{\hat{M}}(f)\right|^2 df \end{aligned}$$

where f is the frequency and f_1 and f_2 are the lower and upper bounds of the integration, respectively. [In theory E_S would require the integration from 0 to ∞ frequency, but this is not achievable in practice. In the next section the effect of the bandwidth limitation of the integration on M_E will be discussed].

Eq. (18) holds for point sources, i.e., sources smaller than the analyzed wavelengths and neglecting directivity effects (see, e.g., Venkataraman and Kanamori, 2004a). Under these conditions, it is normal practice to analyze only the *P*-waves of seismograms recorded in the teleseismic range, since they present some advantage with respect to *S*-waves: (1) they are the faster waves and therefore arrive first at the seismic stations. This is essential for rapid earthquake magnitude determinations and (2) they are less affected than *S*-waves by energy loss during wave propagation.

2.2.1 Estimating the effect of the limited bandwidth of analysis on M_E estimations

The limits of the integration f_1 and f_2 in Eq. (18) may affect the estimation of E_S and, therefore, of M_E. Different authors (e.g., Di Bona and Rovelli, 1988; Singh and Ordaz, 1994; Ide and Beroza, 2001) already investigated the effect of the bandwidth limitations on energy estimations. In particular, Ide and Beroza (2001) pointed out that for an ω^{-2} model over the 80% of E_S is carried by waves of higher frequencies than the corner frequency.

In order to get a measure of the magnitude-dependent underestimation of M_E, ΔM_E, the source models of Fig. 2.1 are considered for different values of moment magnitude ($5.5 \leq M_W \leq 8.5$) assuming that they are roughly representative for most shallow earthquakes. Moreover, in order to assess the possible influence of variations in stress drop on such estimates, the same model was applied for $\Delta\sigma$ varying in increments of one order between 0.1 and 100 MPa. The chosen range of variations in $\Delta\sigma$ encompasses most of the published data (e.g., Abercrombie, 1995; Grosser et al., 1998; Kanamori and Brodsky, 2004; Parolai et al., 2007; Venkataraman and Kanamori, 2004b). The estimation of ΔM_E is simply performed from the difference between the M_E obtained from E_S considering frequencies between 0.001 Hz and 16 Hz (limits representing a bandwidth able to reasonably approach the whole energy radiated by the theoretical ω^{-2} curves in the considered range of magnitudes, although they are not realistic in routine seismological practice of teleseismic M_E estimations) and the one from frequencies between 12.4 mHz and 1 Hz (limits adopted in the calculation of M_E of the procedure proposed in this thesis and described in the following sections). The ω^{-2} curves are shown in

Fig. 2.2 for earthquakes with M_W = 5.5 and 8.5 along with the relative frequency limits of integration to estimate ΔM_E.

Table 1 (Bormann and Di Giacomo, 2010) summarises the magnitude-dependent underestimation of M_E. An E_S procedure operating in the bandwidth range from 12.4 mHz to 1 Hz may underestimate M_E of ~0.7 m.u. for moderate earthquakes (e.g., M_W = 5.5) with very high stress drop and thus $f_c > f_2$. Taking out this extreme case, the bias in M_E due to bandwidth limitations is negligible (that is to say < 0.1 m.u.) for strong to great earthquakes with M_W between about 6.5 and 8.5 for typical intermediate $\Delta\sigma$ between about 1 to 10 MPa (Kanamori and Brodsky, 2004). However, the underestimation of M_E may reach 0.2-0.3 m.u for moderate to strong earthquakes (M_W between about 5.5 and 6.5) with $\Delta\sigma \geq 10$ MPa (possibly $f_c > f_2$), or for great earthquakes ($M_W > 8$) with $\Delta\sigma < 1$ MPa (possibly $f_c < f_1$).

However, these values must be used with caution and can only be a rough guideline of the possible range of M_E underestimations, because the values were obtained from a common yet simple source model, which can not account for source spectra complexities under real conditions.

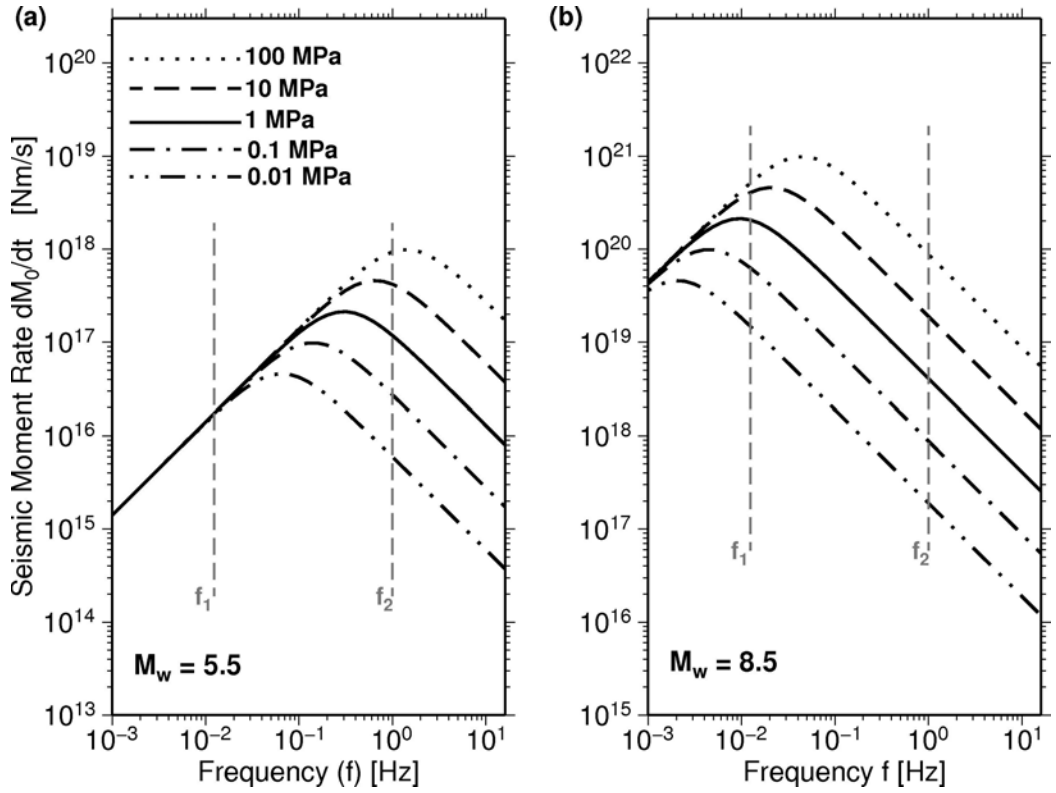

Fig. 2.2: a) Far-field "source spectra" of ground motion velocity amplitudes for a ω^{-2} model as a function of frequency f, scaled to seismic moment rate for a $M_W = 5.5$ for different stress-drop $\Delta\sigma$ in units of MPa, with the gray dashed lines representing the frequency limits f_1 and f_2 used in the procedure to obtain E_S described later. b) The same for $M_W = 8.5$. The frequency limits of this picture, 0.001 Hz and 16 Hz, are the one used in the estimation of ΔM_E reported in Table 1.

Table 1. Estimations of ΔM_E on the basis of the ω^{-2} model. For explanation see text.

$\Delta\sigma$ (MPa)	ΔM_E for $M_W = 5.5$	ΔM_E for $M_W = 6.5$	ΔM_E for $M_W = 7.5$	ΔM_E for $M_W = 8.5$
0.1	0.05	0.02	0.05	0.25
1	0.13	0.03	0.02	0.10
10	0.30	0.08	0.02	0.03
100	0.66	0.19	0.05	0.02

2.3 Correction for the wave propagation effects

A previously mentioned, the calculation of E_S requires the correction of the observed spectra over a broad frequency range for the geometrical spreading and the frequency-dependent attenuation experienced by the seismic

waves during propagation from the source to the receivers. These wave propagation phenomena determine energy losses which must be recovered. Correction for the propagation effects is one of the most challenging tasks in seismological practice, since — in contrast to seismic moment determination — also the high frequency part of the source spectrum must be considered (Fig. 2.1 and 2.2). In addition, correcting frequencies > 1 Hz requires detailed knowledge of the Earth fine structure and attenuation properties, also below the seismic station, which is often not available. As a consequence, E_S is usually calculated only for earthquakes with magnitudes above ~5 by using teleseismic recordings at epicentral distance $\Delta \geq 20°$. This allows modelling the Earth filter effects reasonably accurate by assuming an average 1-D layered structure.

In order to perform the correction for the wave propagation effects in a rapid way, spectral amplitude decay functions for different frequencies must be computed. This is due to the frequency-dependent energy loss of the recorded seismic waves, as already pointed out by Duda and Yanovskaya (1993). Moreover, such functions must be applicable to the whole Earth, since the procedure proposed here is intended to serve global seismic network centers, and must be available in a tabulated form in order to perform the correction for the various propagation effects in one simple step. In order to satisfy these requirements, the calculation of these functions has been performed by using the reference Earth model AK135Q (Kennett et al., 1995; Montagner and Kennett, 1996, plotted in solid lines in Fig. 2.3, along with the PREM model by Dziewonski and Anderson, 1981, which is used for the computation of M_W by many agencies and authors) and the simulation code QSSP, which calculates the Green's functions for the spherical Earth (Wang, 2009, pers. comm.). This simulation code is based on the propagator algorithm

proposed by Gilbert and Backus (1968) but extended with the orthonormalization technique (Wang, 1999) to ensure the numerical stability.

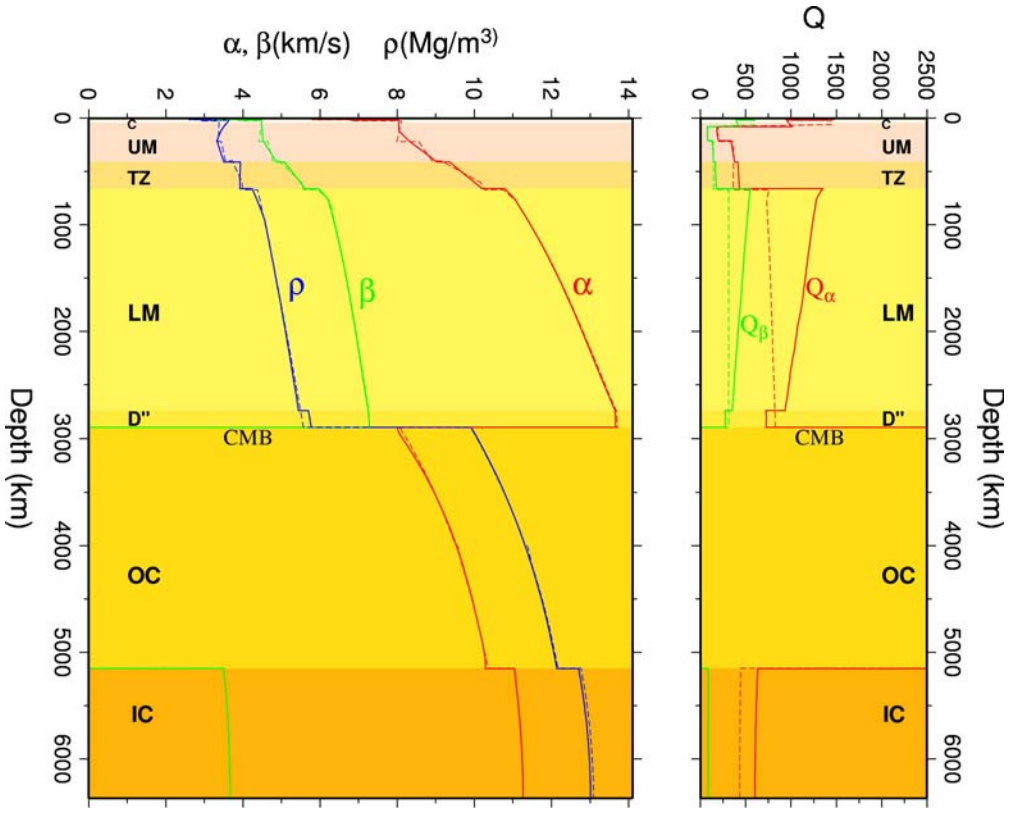

Fig. 2.3: Comparison between the reference Earth models AK135Q (Kennett et al., 1995; Montagner and Kennett, 1996) and PREM (Dziewonski and Anderson, 1981). The solid lines refer to AK135Q, the dashed line to PREM. C = crust, UM = upper mantel, TZ = transition zone, LM = lower mantle, D″ = transition layer between mantle and core, CMB= core-mantle boundary, OC = outer core, IC = inner core. The *P*- (α, red) and *S*-waves (β, green) velocities differ more in the UM and TZ than in the LM; the difference in the *Q* factor (right side) is more significant.

The advantage of using numerical simulations with respect to empirical approaches consists in that, starting from a known point source function, all propagation effects at different frequencies can be accounted for. *P*-wave teleseismic seismograms (source depth at 33 km) have been computed (see Fig. 2.4) in increments of 1° in the distance range 20°-35°, and steps of 2.5° from 35° onwards. For the distance range 20°-35° a denser spatial sampling has been used because *P*-waves observed in this range are more affected by

the larger variations in velocity and attenuation in the upper mantle and transition zone (see Fig. 2.3). [In **Chapter 4** it will be also shown that the use of stations between 20°-30° is empirically justified since no bias is introduced in the final M_E determination including stations in this distance range, but at the same time the procedure for rapid response purposes can be launched earlier].

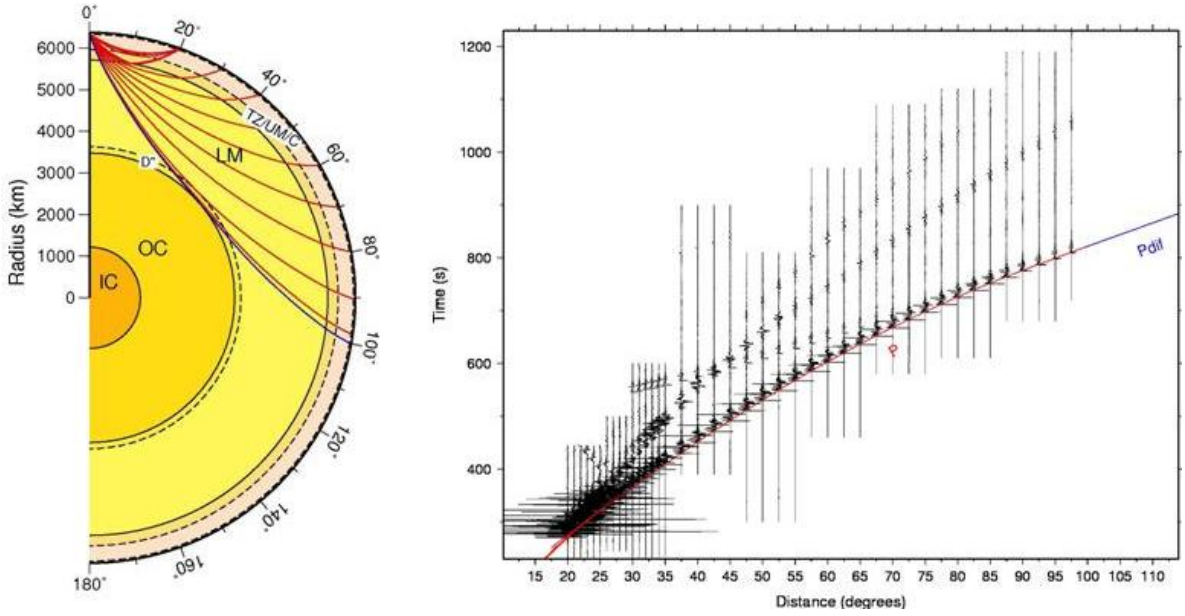

Fig. 2.4: Left: Representative *P*-wave ray paths for the model AK135Q. The ray for the 100° distance is marked in blue to highlight the beginning of the *P*-waves interactions with the OC beyond 98° distance; Right: example of numerical simulations of *P*-waves. The theoretical arrivals of the *P* (red) and *Pdif* (blue) phases are also marked. See text for details.

Furthermore, since the method is designed to work without prior knowledge of the fault plane and slip geometry, for each distance a set of time series resulting from different combinations of the focal parameters strike, dip and rake have been computed. The values of the strike, dip and rake have been allowed to vary in steps of 15° over the focal sphere. From the simulated time series the amplitude decay functions have been derived as follows: for each simulated distance, the Fourier spectra of the *P*-wave trains have been

computed and, then, the spectral amplitude decay at each distance at a given frequency has been extracted. Then the median, the 25th and the 75th percentile of the amplitude decay functions at each distance have been computed. The frequency dependence of the amplitude decay functions in Fig. 2.5 (modified after Di Giacomo et al., 2008) is highlighted by plotting them for periods between 1 s and 16 s in increments of one octave. As expected, Fig. 2.5 clearly shows that the amplitude decay is higher for shorter periods (higher frequencies), and that the difference between the functions for longer periods gets progressively smaller, with the percentile ranges for 8 s and 16 s already nearly overlapping.

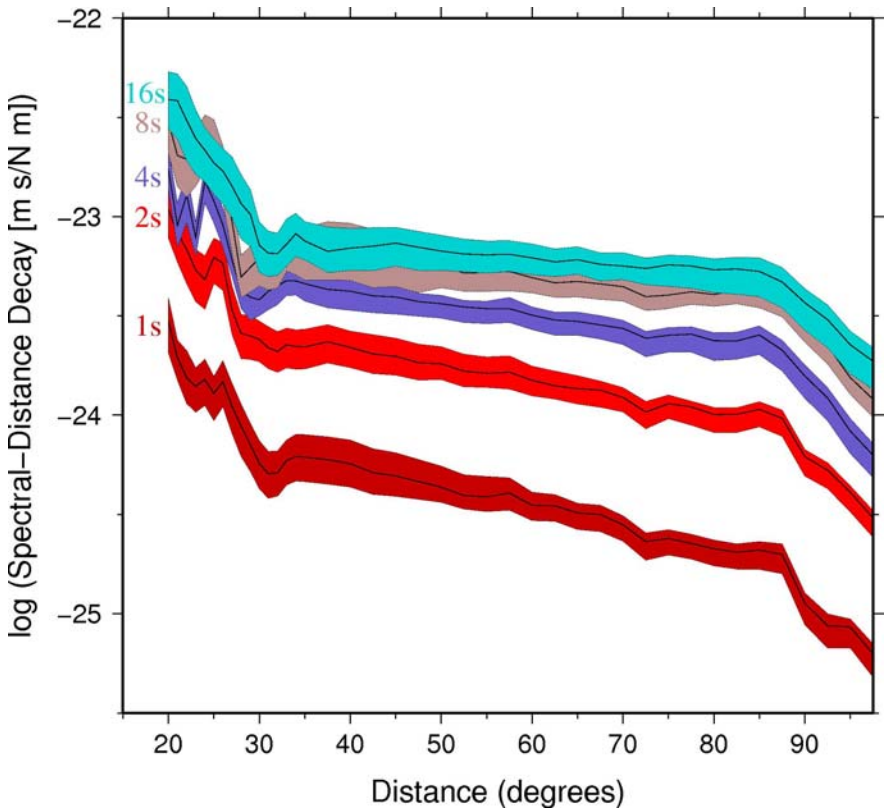

Fig. 2.5: Spectral amplitude decay functions for periods between 1 s and 16 s in steps of one octave. The solid lines represent the median spectral amplitude decay function for a given period, the shaded area represent the 25th and 75th percentile.

Even the influence on the amplitude decay functions of different phases (like *PP*) arriving between the first *P* and *S*-wave arrivals has also been investigated, but no significant changes in the theoretical functions have been observed.

The functions are available in a tabulated form for each frequency as function of distance. This allows the proposed approach to account for the various propagation effects in a simple and robust way. In practice, to correct the velocity spectra recorded at the seismic stations, the median amplitude decay functions for frequencies (periods) between f_2 = 1 Hz (1 s) and f_1 = 12.4 mHz (~80 s) in steps of 1/3 of one octave are used, so that an adequate number of frequencies is available when the integration of the corrected power velocity spectra is executed. The simulation code QSSP for the spherical Earth provided more reliable Green's functions in the low frequency range than the reflectivity code (Wang 1999) with the flat Earth approximation. Therefore, the lower bound f_1 of the frequency band considered in the calculation of E_S in the proposed procedure has been extended from 16.6 mHz (Di Giacomo et al., 2008) to 12.4 mHz (Di Giacomo et al., 2010a). The upper bound of the integration, instead, is fixed at 1 Hz (1 s) since the *Q* model was obtained from data in the significant period between 1 - 3000 s only (Montagner and Kennett, 1996). For shorter periods the decay functions are not reliable, as their spectral decay is too large when compared with that of the real data. This effect is even larger for the short-periods spectral amplitude decay functions from the PREM model, which are compared in Fig. 2.6 with the ones from the AK135Q model. For longer periods the difference (not shown here) of the spectral amplitude decay functions based on the AK135Q and PREM models is negligible.

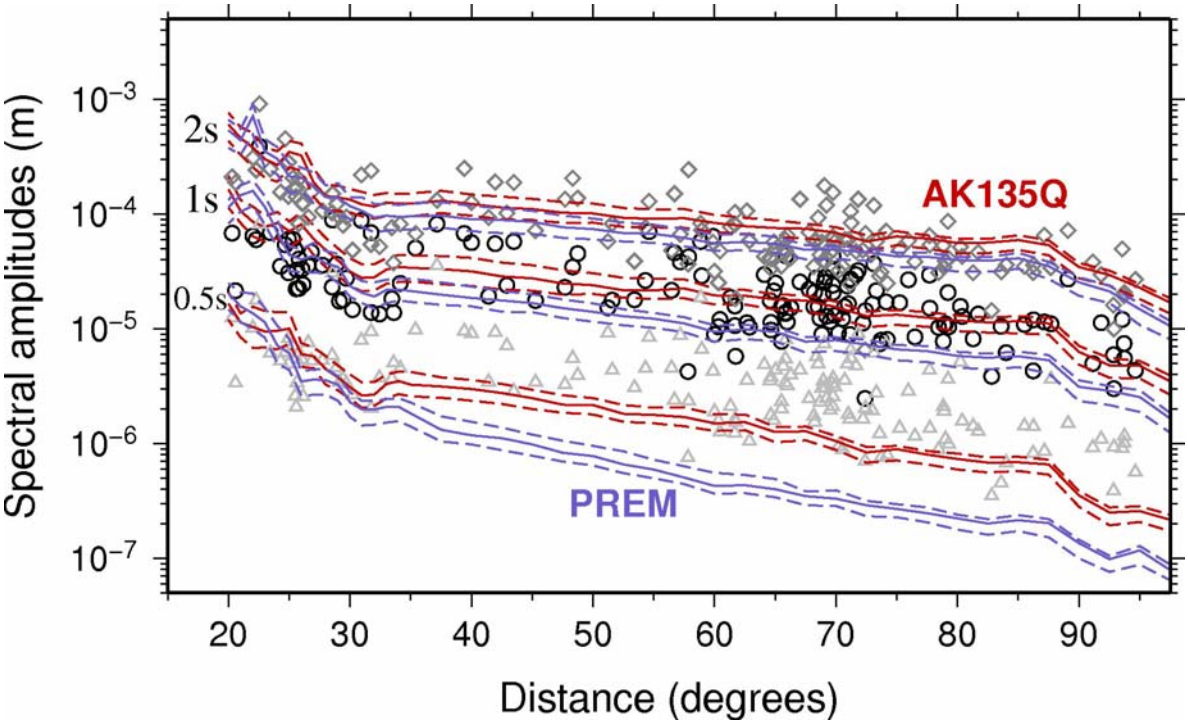

Fig. 2.6: Velocity spectral amplitudes at 2 Hz (0.5 s, light gray triangles), 1 Hz (1 s, black circles) and 0.5 Hz (2 s, gray diamonds) for the M_W = 7.9 Wenchuan earthquake of 2008 May 12 superimposed to the theoretical spectral amplitude decay functions for the same frequencies for the AK135Q model (median, 25th and 75th percentile in solid and dashed red lines, respectively) and the PREM model (median, 25th and 75th percentile in solid and dashed violet lines, respectively). An arbitrary offset has been added to the theoretical curves to make easier the comparison with the real data.

The limit of 1 Hz in the integration means that, at the present time, the proposed procedure is applicable to earthquakes with a M_W greater than about 5.5, but it does not limit the energy determination, since strong to great earthquakes have usually corner frequencies falling inside the frequency band where the correction is applied. In fact, the corner frequency f_c is expected to be < 1 Hz (as shown in the inset of Fig. 2.1b). Thus the missing part of the spectrum is not expected to bias significantly and systematically the E_S and M_E estimations.

Fig. 2.7 (Di Giacomo et al., 2010a) shows observed velocity spectral amplitudes versus distance for frequencies (periods) of 1 Hz (1 s) and 0.0625 Hz (16 s) for two recent earthquakes. Fig. 2.7a refers to the M_W = 6.9 North of

the Molucca Sea earthquake of 2007 July 26 and Fig. 2.7b relates to the M_W = 7.9 Wenchuan earthquake of 2008 May 12. The spectral amplitude decay functions for the same frequencies have been plotted by adding an arbitrary offset in order to ease the comparison of the observed data with the simulations. After applying the correction, one would expect that the corrected spectral amplitude values are on average independent of distance. Fig. 2.7 shows that, although individual measured data points may scatter significantly around the medians of the synthetic functions due to heterogeneities in the real Earth, the simulations are able to reproduce the average trend of the observations. In fact, the deviation of the actual Earth structure from its 1-D average for specific source–receiver paths (which may influence different frequencies in different ways), and/or the effects of the fine 3-D velocity and Q structure just below the seismic stations, the seismic source finiteness, directivity and radiation pattern, all may contribute to a different extent to the variability of the single station M_E estimates (in **Chapter 4** a quantitative assessment of such variability is discussed). Therefore, more stable event magnitude estimates necessitate analyzing and averaging observations from different distances and azimuths in order to minimize the influence of this data scatter.

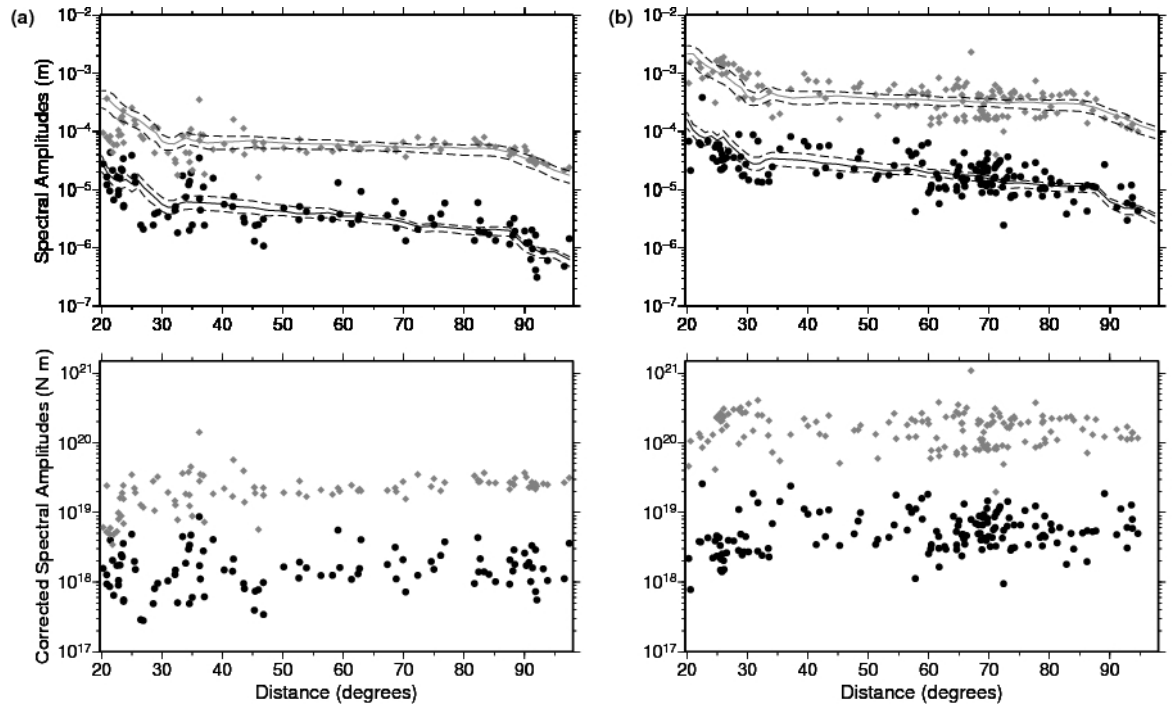

Fig. 2.7: a) The upper panel shows the observed velocity spectral amplitudes with distance from the source for frequencies of 1 Hz (black circles) and 0.0625 Hz (gray circles) for M_W = 6.9 North of the Molucca Sea earthquake of 2007; the median of the spectral amplitude decay functions at 1 Hz and 0.0625 Hz (solid black line and gray lines, respectively) are shown together with their corresponding 15th and 75th percentiles and have been shifted by an arbitrary offset in order to make easier the comparison with the real data. The lower panel shows the corresponding displacement spectral values after applying the correction at each station and scaling them to seismic moment. b) The same as for Fig. 2.7a, but for M_W = 7.9 Wenchuan earthquake of 2008 May 12.

2.4 Procedure to rapidly calculate $M_{E(GFZ)}$

As the spectral amplitude decay functions shown before are available in tabulated form, a prompt correction for the propagation effects of the real spectra can be performed. This step, of course, can be accomplished once a location is available. Then, an estimation of $\left|\hat{\dot{M}}(f)\right|$ at the single station, located at a given distance Δ, is obtained simply from the ratio between the observed velocity spectral amplitude $\hat{u}(f)$ and the corresponding value of the spectral amplitude decay function at a given frequency f. Subsequently, E_S is computed using Eq. (18).

The right side of Eq. (18) (in brackets outside the integral, having the unit of s^3/Nm and hereinafter called k) depends on the properties of the medium surrounding the source volume and could also be rewritten in terms of the S to P wave energy ratio $q = 1.5(\alpha/\beta)^5$ (which holds under the point source condition, see, e.g., Venkataraman and Kanamori, 2004a), and replacing α or β accordingly. The Earth (and especially the Earth's crust) is a heterogeneous medium, both vertically and laterally. Accordingly, k may vary over local and regional scales and with depth. This may be a source of uncertainty in the energy estimation. Being interested in calculating M_E in a rapid way for global earthquakes with source depths $h < 70$ km, only vertical heterogeneities by using the model AK135Q are accounted for. For sake of practicality, the earthquakes are separated into two groups with h shallower or deeper than 18 km, and use the respective values of α, β, and ρ given for the 1-D average structure of the AK135Q model. That is to say for events shallower than 18 km depth $\alpha = 6.8$ km/s, $\beta = 3.9$ km/s, and $\rho = 2.92$ g/cm^3 and for the deeper ones $\alpha = 8.0355$ km/s, $\beta = 4.4839$ km/s, and $\rho = 3.641$ g/cm^3, respectively. The 18 km boundary has been chosen because changes in depth above and below it do not introduce very large discrepancies in the M_E estimates. Indeed, even in the worst case scenario of a wrong hypocenter depth calculation by the near- or real-time location procedure, the use of the corresponding depth values of α, β, and ρ in Eq. (18) for either $h < 18$ km or 18 km $\leq h < 70$ km would result in M_E values that are biased by not more than ±0.25 m.u., which is still acceptable for rapid response purposes. By using the values of α, β, and ρ in the AK135Q model for very shallow earthquakes ($h \leq 10$ km) would yield a much larger M_E (up to about ~0.6 m.u.).

To make this procedure suitable for implementation in rapid response systems and to take into account the effect of the rupture duration, E_S and M_E

are computed starting with a 4 s window length after the first *P*-wave arrival, and increasing it continuously (time-variable cumulative energy windows) until, according to Bormann and Saul (2008), the normalized envelope of the high-frequency velocity amplitude falls below the threshold of 0.4. This allows avoiding the time window saturation effect in magnitude determination (Bormann et al., 2007). The duration obtained by using this technique is similar to the one of Lomax and Michelini (2009a) and is used just to constrain the final time-window length of the single station M_E computation. Obviously, the time-window considered is extended until the *S*-wave arrival if the rupture lasts for several minutes (like for the great 26 December 2004 Sumatra earthquake). Fig. 2.8 illustrates how the procedure works at the single station. For the rapid procedure, at least 3 station estimates of M_E before computing the first arithmetic event average are required. This means that first alarm magnitudes could also be provided about 7 min after earthquake origin time (OT) using stations between 20° and 30°. When more than 8 station estimates become available, the final M_E value is taken as the 25% truncated mean (e.g., Bormann and Saul, 2008) of the single station estimates. The truncated mean is advisable especially in an automatic procedure since it excludes outliers that may deviate significantly from the average.

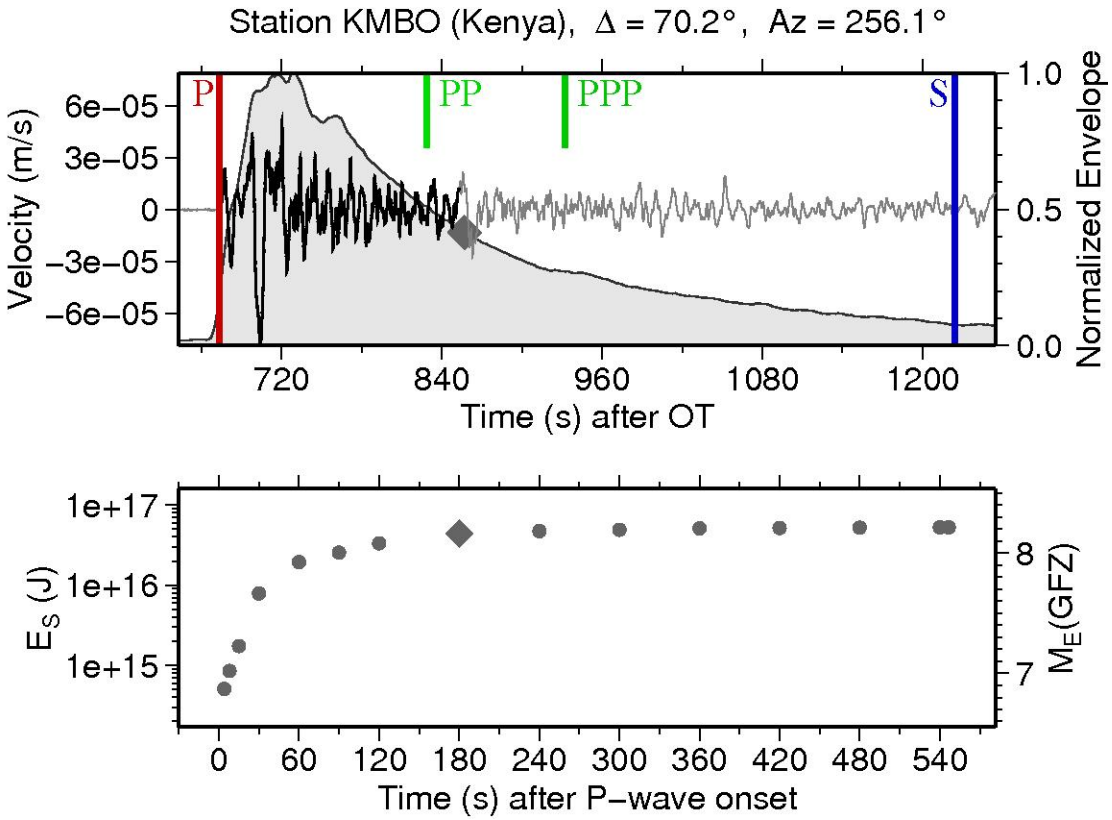

Fig. 2.8: Upper panel: vertical component velocity recording of the M_W = 7.9 12 May 2008 Wenchuan earthquake recorded at the station KMBO (Kenya). The theoretical *P*-, *PP*-, *PPP*- and S-wave arrival times have been also marked. The gray shaded area represents the envelope of high-frequency velocity amplitudes used to constrain the overall rupture time duration (Bormann and Saul, 2008), and the diamond at the end of the black record trace mark the end of the time window after the *P*-wave onset for which the final $M_{E(GFZ)}$ single station value is calculated. Thus, the full rupture duration is included in the E_S calculation. If, however, the rupture duration lasts for several minutes (as for the great 26 December 2004 Sumatra earthquake), the entire *S-P* window should be considered. Lower panel: E_S (left y-axis) and M_E (right y-axis) values for different cumulative *P*-waves windows. The diamond mark the end of the *P*-wave window that has been used for the single station M_E estimate.

To evaluate the amount of time needed by this procedure to provide a stable M_E in a real- or near-real time implementation, Fig. 2.9 shows the M_E determinations at different times after OT for the great 26 December 2004 Sumatra earthquake (Fig. 2.9a) and for the 12 May 2008 Wenchuan earthquake (Fig. 2.9b). In the exceptional case of the 2004 Sumatra earthquake, for which the rupture duration was about 500 s (Ni et al., 2005), this procedure could have yielded a stable M_E already some 15 min after OT (Fig. 2.9a, right panel), since the major energy release occurred within the first

250 s of the rupture process (Choy and Boatwright, 2007). For the case of the Wenchuan earthquake, instead, using *P*-wave time windows of 180 s, more stations (24) could have been used already 10 min after OT, and a stable M_E could have been released. Noticeably, in both cases the preliminary (alarm) $M_{E(GFZ)}$ available after 10 min are very close to the final values obtained by using all available stations. Of course, the time performance of this approach depends on the station availability with respect to the earthquake location. However, the worldwide station deployment is becoming increasingly dense, especially in areas for which a lack of instrumentation was still common a few years ago. Therefore, this procedure could yield in the near future rapid M_E estimates within 10 min after OT also for great ($M_W \geq 8$) earthquakes.

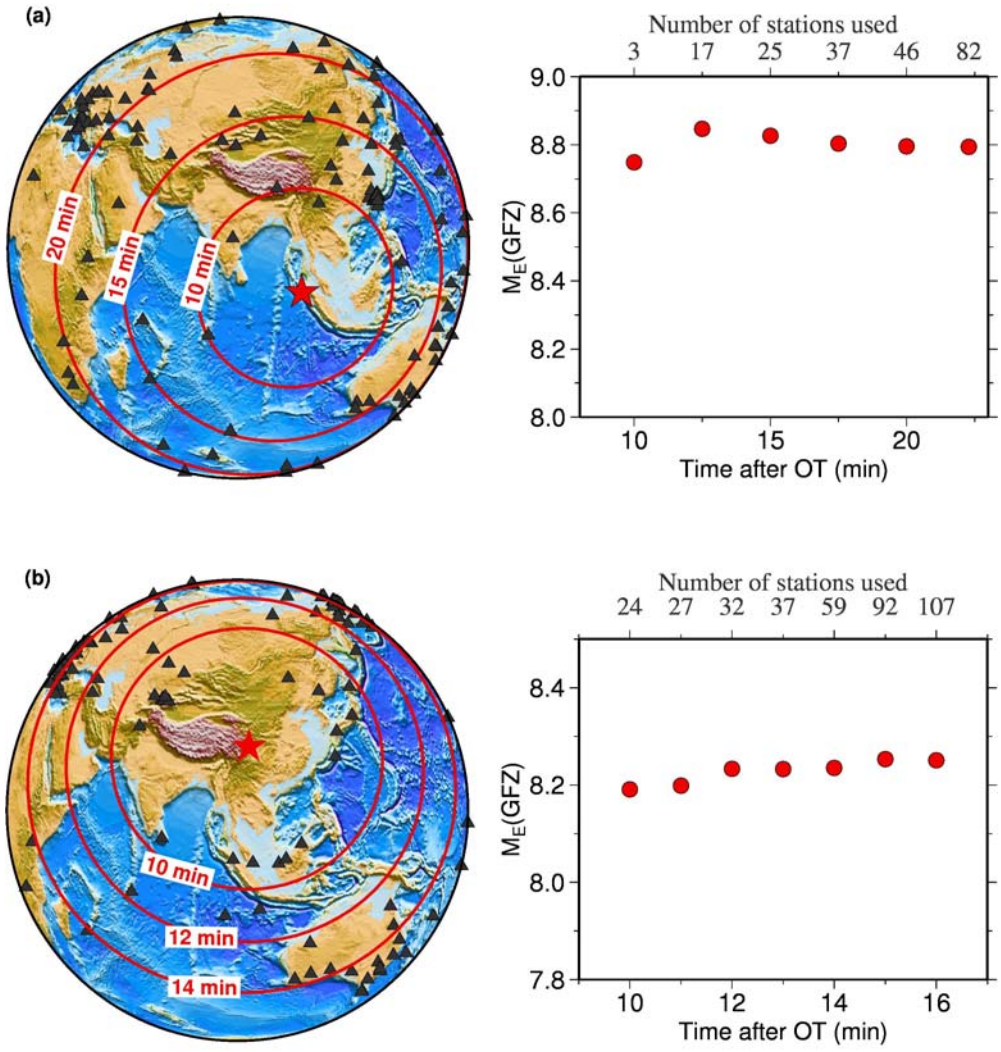

Fig. 2.9: a) Left: Map showing the location of the 26 December 2004 Sumatra earthquake (red star), the broadband stations used to calculate M_E (black triangles), and the red circles represent the *S*-wave arrival after OT. Right: $M_{E(GFZ)}$ determination of the Sumatra earthquake at different time after OT. The number of stations (NS) used to compute $M_{E(GFZ)}$ are also shown; b) As for Fig. 2.9a but for the 12 May 2008 Wenchuan earthquake. Here the red circles on the map mark the time needed to record 180 s of *P*-waves.

CHAPTER 3

Comparison of different magnitude estimates

3.1 The dataset

The data set considered to test the suitability of the proposed procedure to rapidly determine M_E includes ~1000 worldwide distributed shallow earthquakes (h < 70 km) within the magnitude range $5.5 \leq M_W \leq 9.0$ [as already mentioned, the focus of the thesis has been given to shallow earthquakes for their higher damage potential with respect to deep earthquakes; however, the proposed method can be also applied to deep earthquakes by calculating the spectral amplitude decay functions for different simulation depths]. They occurred between March 1990 and December 2008. Table A1 lists the source parameters for the analyzed events. For each earthquake, the vertical component of the broadband recordings provided by permanent stations belonging to either a global (IRIS/IDA, IRIS/USGS, GEOFON, GEOSCOPE) or a regional network have been analyzed. Of course, the number of stations available and used in the analysis is much larger both for large earthquakes and for those that occurred over the last few years, as the global networks have been enlarged. After removing stations with poor signal-to-noise ratio (SNR), a total of about 48,000 single stations M_E determinations have been obtained. Given the size of the data set considered, also for each earthquake magnitude estimation, the different source-receiver propagation paths sample a large volume of the Earth's medium.

The analyzed earthquakes have been grouped according to their Global Centroid Moment Tensor (GCMT database, http://www.globalcmt.org) fault plane solutions using the classification given by Zoback (1992). Fig. 3.1 shows their geographical distribution. Table 2 lists the number of earthquakes for each class of source geometry. The dataset is strongly dominated by thrust and strike-slip earthquakes. Although no specific corrections for the different radiation patterns are applied in the method here proposed, such a classification will be useful when discussing the magnitude comparisons, especially with regard to the M_E from USGS. Indeed, as already mentioned, USGS calculates M_E on a routine basis using the procedure of Boatwright and Choy (1986) by requiring accurate knowledge of depth and fault plane solution in order to apply the correction for the specific radiation pattern.

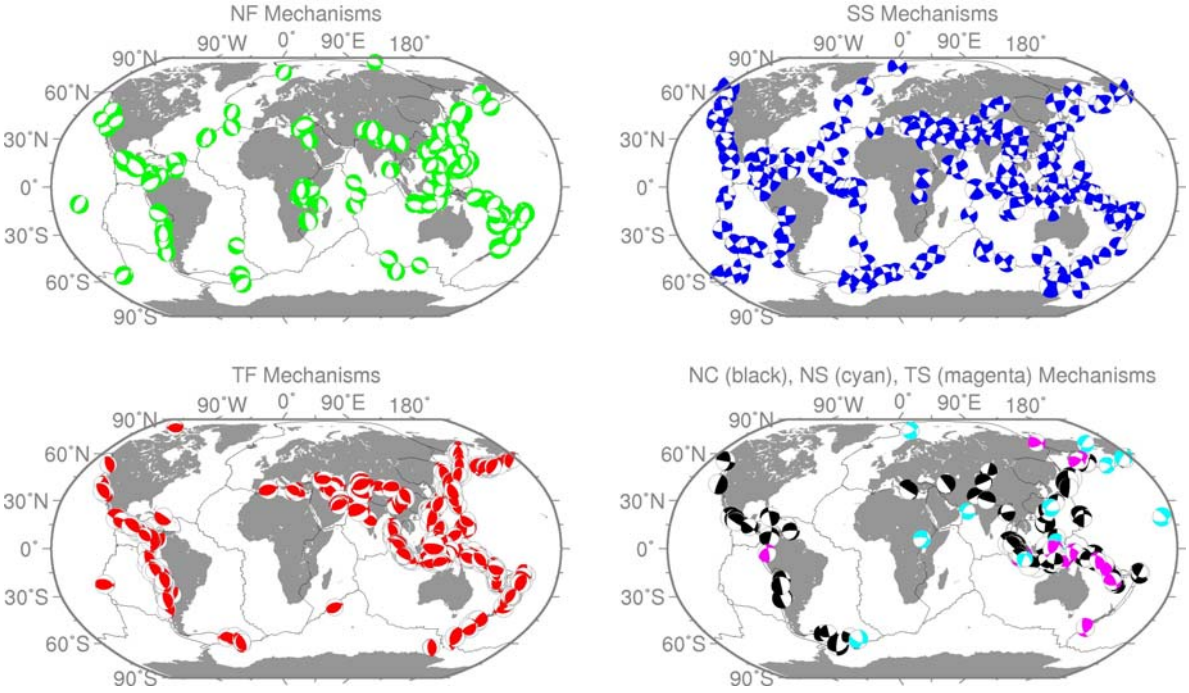

Fig. 3.1: Maps showing the distribution of the earthquakes and their types according to the classification of Zoback (1992). Normal faulting (NF) solutions are plotted in green, strike-slip (SS) solutions in blue, thrust (TF) solutions in red, not classified (NC) solutions in black, normal with strike-slip component (NS) solutions in cyan, and thrust with strike-slip component (TS) solutions in magenta. The plate tectonic boundaries have been plotted according to Bird (2003).

Table 2: Summary of the grouping of the focal solutions for the analyzed dataset using the classification of Zoback (1992).

Focal Mechanism Type	Thrust (TF)	Strike-slip (SS)	Normal (NF)	Not Classified (NC)	Thrust with strike-slip component (TS)	Normal with strike-slip component (NS)
Number of earthquakes	415	326	135	87	14	13

3.2 Comparisons of M_W and M_E

For large earthquakes, M_W from the GCMT project is commonly used as the reference for any other magnitude. $M_{W(GCMT)}$ is obtained from the inversion of very long-period waveforms of *S* and surface-waves, which are necessary to get an accurate determination of the seismic moment M_0. However, the drawback of analyzing very long periods is that $M_{W(GCMT)}$ is usually not available within less than one hour after OT. In contrast, M_W estimations of the NEIC/USGS (Sipkin, 1994), based on broadband *P*-wave records, are provided much sooner and are used by many agencies (e.g., WAPMERR, http://www.wapmerr.org/) to rapidly evaluate the earthquake's impact. According to the analyzed dataset, $M_{W(USGS)}$ and $M_{W(GCMT)}$ differ by only ±0.2 m.u. for about the 90% of the data, with the tendency, however, of $M_{W(GCMT)}$ to be generally larger than $M_{W(USGS)}$, especially for $M_W > 8$.

In Fig. 3.2 the rapid $M_{E(GFZ)}$ determinations with the $M_{W(GCMT)}$ and the $M_{W(\mathrm{USGS})}$ are compared. For some earthquakes $M_{W(USGS)}$ is not available in the SOPAR database (http://neic.usgs.gov/neis/sopar/). The difference between $M_{W(GCMT)}$ and $M_{E(GFZ)}$ is on average close to zero m.u. for SS (with a Standard

Deviation S.D. = 0.23), TF (S.D. = 0.24), and NC (S.D. = 0.28) mechanisms and less than -0.15 for NF (S.D. = 0.21), NS (S.D. = 0.17), and TS (S.D. = 0.20) mechanisms. In contrast, the average differences between $M_{W(USGS)}$ and $M_{E(GFZ)}$ are slightly larger, with a maximum of -0.23 and -0.20 m.u. for TS (S.D. = 0.21) and NF (S.D. = 0.21) mechanisms, respectively. In the absence of any *a priori* source mechanism-dependent correction applied to the GFZ measured E_S values, any systematic trend in the differences between M_W and $M_{E(GFZ)}$ due to the focal mechanism type is not observed. This agrees also with Schweitzer and Kværna (1999), who investigated the influence of source radiation patterns on globally observed short-period magnitude estimates m_b. They concluded that the effect of the source radiation pattern on the amplitudes used for m_b estimation on a global scale is relatively small compared to effects from other factors and much smaller than theoretically expected on the basis of standard source and Earth models. Thus, differences between corrected and uncorrected m_b event magnitudes were always within ±0.15 m.u.

The comparisons between $M_{W(GCMT)}$ and $M_{E(USGS)}$, and $M_{E(USGS)}$ with $M_{E(GFZ)}$ are shown in Fig. 3.3a and 3.3b, respectively. For some earthquakes $M_{E(USGS)}$ is not available in the SOPAR database. The average difference $M_{W(GCMT)} - M_{E(USGS)}$ is ~0.27 m.u. (S.D. = 0.23), ~0.22 m.u. (S.D. = 0.34), and ~0.18 m.u. (S.D. = 0.24) for TF, NC and NF events, respectively. However, the most important feature of Fig. 3.3a is that $M_{E(USGS)}$ for SS earthquakes only is generally larger (on average ~0.26 m.u., S.D. = 0.30) than $M_{W(GCMT)}$, suggesting a significant dependence of $M_{E(USGS)}$ on the focal mechanism corrections for SS events. As shown in Fig. 3.2, this is not the case for the uncorrected $M_{E(GFZ)}$ estimates, which scale more linear and with less scatter than $M_{E(USGS)}$ with $M_{W(GCMT)}$. The differences between $M_{E(USGS)}$ and $M_{E(GFZ)}$ are

within ± 0.4 m.u for 67% of the analyzed events. On average, $M_{E(USGS)} - M_{E(GFZ)}$ is 0.25 m.u. for SS (S.D. = 0.32) events and within -0.30 (NF mechanisms, S.D. = 0.20) and -0.15 m.u. (TS mechanisms, S.D. = 0.25) for the other types of mechanism.

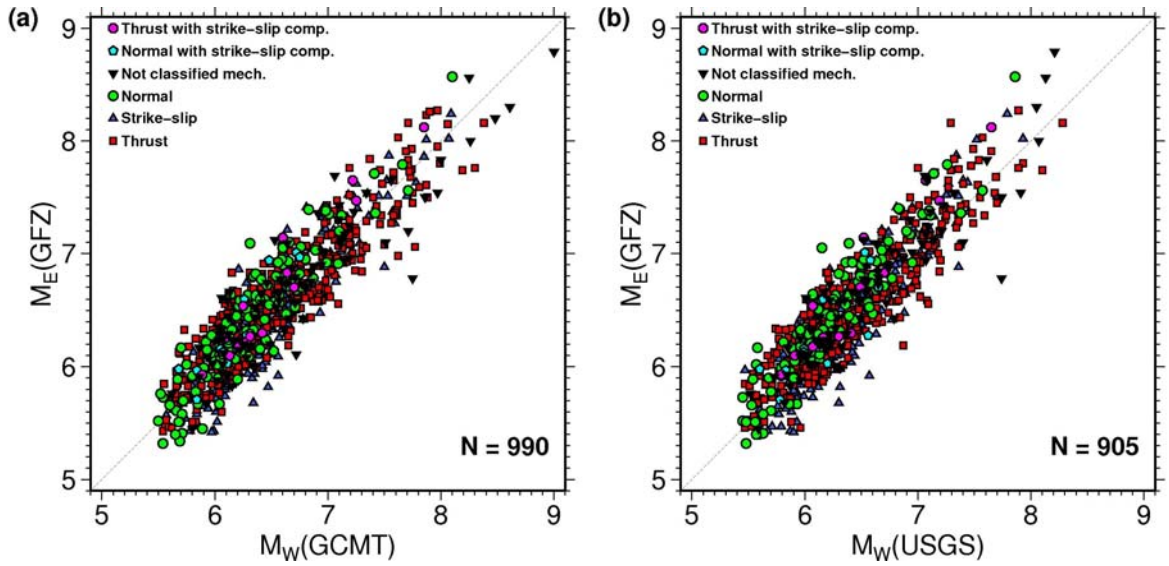

Fig. 3.2: Comparison of a) $M_{W(GCMT)}$ with $M_{E(GFZ)}$ for 990 events, and b) $M_{W(USGS)}$ with $M_{E(GFZ)}$ for 805 events. Different symbols represent the type of mechanism. The 1:1 lines are also plotted. Modified from Di Giacomo et al. (2010b) and including data from year 2008.

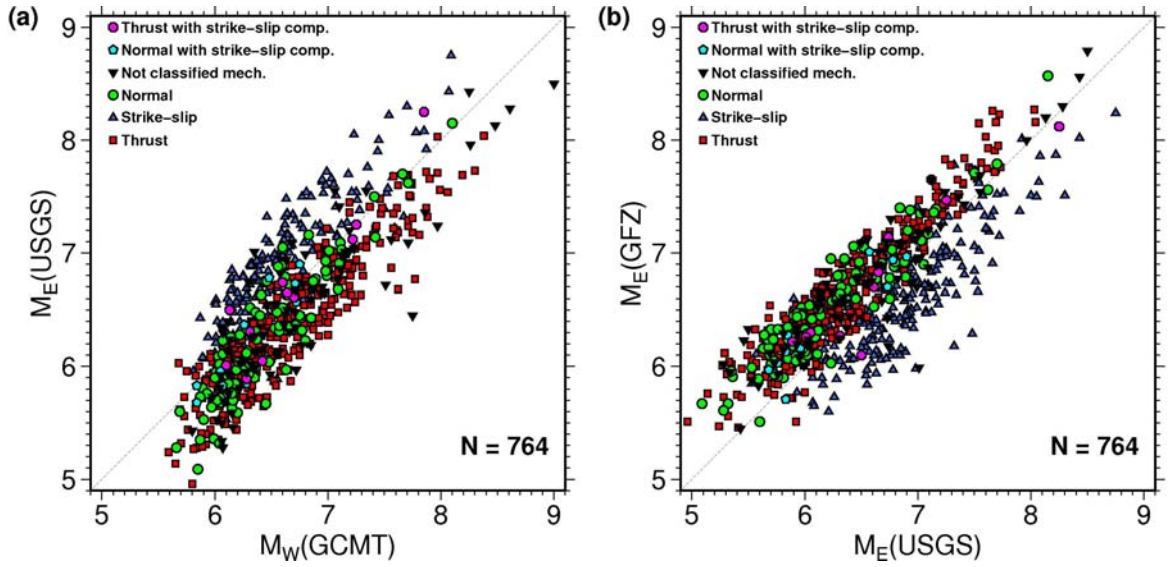

Fig. 3.3: Comparison of a) $M_{W(GCMT)}$ with $M_{E(USGS)}$ and b) $M_{E(USGS)}$ with $M_{E(GFZ)}$ for a total of 764 earthquakes. Different symbols represent the type of mechanism. The 1:1 lines are also plotted. Modified from Di Giacomo et al. (2010b) and including data from year 2008.

Previous works investigated the influence of the source geometry on E_S estimations. Newman and Okal (1998) modified the method of Boatwright and Choy (1986) to make it suitable for implementation in a real-time procedure for the discrimination of tsunami earthquakes by means of the Θ parameter. Analyzing a dataset of 52 earthquakes, they found that their E_S values for the 5 SS events included in their dataset were much smaller than the ones from USGS (up to 1.4 order of magnitude), and also that their E_S values were generally larger for all the other types of earthquakes. The large discrepancies for the SS events were attributed by Newman and Okal (1998) to the over-correction of the energy flux by the USGS when using, according to theory, small values for the radiation pattern correction, whereas the heterogeneities of the real Earth allow the high frequency content to find its way into the seismograms along non-geometrical paths. This is in agreement with the findings and interpretation of mechanism-dependent m_b corrections by Schweitzer and Kværna (1999). More recently, Pérez-Campos and Beroza (2001) extended the method of Boatwright and Choy (1986) in order to include the uncertainties in the factors involved in the E_S determination (e.g., focal mechanism, attenuation, spectral fall off, etc.). They analyzed 204 earthquakes (58 SS, 101 TF, and 45 NF earthquakes) and found their E_S estimates to be generally smaller than the USGS estimates for all mechanism types, but with the SS earthquakes showing the largest differences. However, Pérez-Campos and Beroza (2001) confirmed the persistence of a larger apparent stress drop for the strike-slip earthquakes with respect to the other type of events, which may result in slightly larger M_E values for such events.

Other reasons than source mechanism-corrections for such discrepancies may be differences in the methodologies when correcting the spectra for attenuation. Although further studies are needed to investigate the

role of the focal mechanism on E_S estimates, the consistency of the results also with some previous studies confirm that the rapid M_E procedure is a suitable contribution to the assessment of an earthquake's damage potential. Moreover, one must keep in mind that the original magnitude concept — to which any classical magnitude scale (such as m_B and M_S) is based and the modern ones (M_W and M_E) linked to them — does not take into account specific corrections for the source mechanism.

However, regardless of the discrepancies between $M_{E(USGS)}$ and $M_{E(GFZ)}$, Figs. 3.2 and 3.3 show that M_W and M_E can be significantly different, as already highlighted by several authors (e.g., Purcaru and Berckhemer, 1978; Choy and Kirby, 2004). As M_W provides information about the static and M_E about the dynamic properties of the seismic source, respectively, they should be used jointly for a better assessment both of the tsunami and shaking potential of large earthquakes soon after their occurrence. This point is emphasized by the following representative examples.

3.2.1 Representative case studies

In this section pairs of earthquakes in different seismo-tectonic regions are considered. These earthquakes have similar locations within the considered area, and, for each pair, the analysis results at one of the recording stations are shown, in order to illustrate the importance of characterizing an earthquake by both its M_W and M_E.

1) The 1991-04-22 and the 1992-09-02 Central America earthquakes

Two significant earthquakes occurred on 22 April 1991 and 2 September 1992 in Central America. They are better known as the Costa Rica

earthquake and the Nicaragua earthquake, respectively (see Fig. 3.4). The distance between the two earthquake epicenters is about 500 km, and their seismic moments M_0 are nearly identical, with $M_{W(GCMT)}$ = 7.6 for both earthquakes. As these events occurred in the early 1990s, not many broadband recordings are available of that time. Moreover, the SNR was not sufficient for half of the stations that recorded the Nicaragua earthquake. Nevertheless, three seismic stations that recorded both earthquakes have been used (see Fig. 3.4). In Fig. 3.5 are shown, from the top to the bottom panels, the *S*-*P* windows and their high frequency envelopes (Bormann and Saul, 2008), the time-frequency analyses via the *S-transforms* (Stockwell et al., 1996; Parolai, 2009) of the windows used to include the rupture duration, as well as the E_S (left y-axis) and M_E values (right y-axis) for cumulative *P*-wave windows at the station CCM for both earthquakes. Despite nearly identical travel paths of only about 10% difference in length to station CCM, the records of both earthquakes differ strikingly in their more short-period frequency content. The time-frequency analysis — which allows a better description of the information provided by the seismic recordings before applying any correction to the data — reveals that for the Costa Rica event the major contributions to seismic energy come from two distinct energy pulses peaked around ~0.1 Hz and 0.04-0.05 Hz, respectively, which are a few seconds apart from each other. These two pulses may be associated with the two main rupture patches identified by Goes et al. (1993), with the first being smaller and the second being larger. However, according to the *S-transform* plot, important burst-like contributions to the energy release come also from frequencies higher than 0.1 Hz. Thus, the Costa Rica example illustrates the usefulness of the time-frequency analysis in quantifying important details about the source process, which would not be as obvious from the time-domain analysis alone.

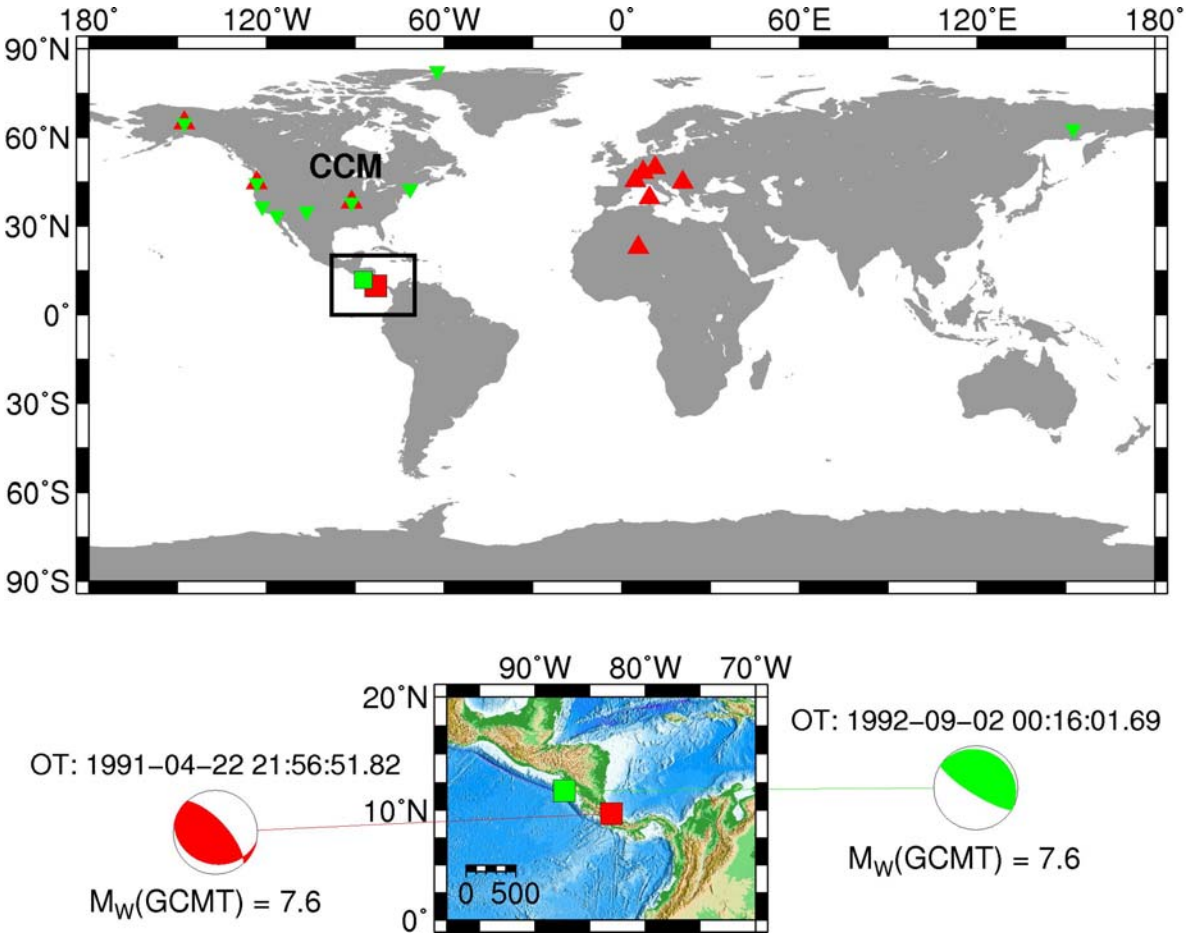

Fig. 3.4: The upper map shows the locations of the two Central America earthquakes and the stations used to calculate $M_{E(GFZ)}$. The red triangles represent the stations used for the earthquake of 22 April 1991, and the inverted green triangles for the event of 2 September 1992. The station CCM will be considered in the comparison of Fig. 3.5. The box delimitates the area shown enlarged in the lower map together with the GCMT fault plane solutions and related M_W.

The Nicaragua earthquake is probably one of the best examples of a slow earthquake generating large tsunamis (e.g., Kanamori and Kikuchi, 1993). This earthquake was significantly depleted in its high frequency content. Indeed, the energy contributions come mainly from below 0.1 Hz and are spread over a longer rupture duration as compared to the Costa Rica event. Yet, the low-frequency *S-transform* amplitudes are comparable for both events, as one would expect from their identical M_W. However, their differences in the observed high-frequency amplitudes are translated into

significantly different values of M_E, namely $M_{E(\mathrm{GFZ})}$ 7.39 and 6.98, or $M_{E(USGS)}$ 7.4 and 6.68 for the Costa Rica and Nicaragua earthquake, respectively.

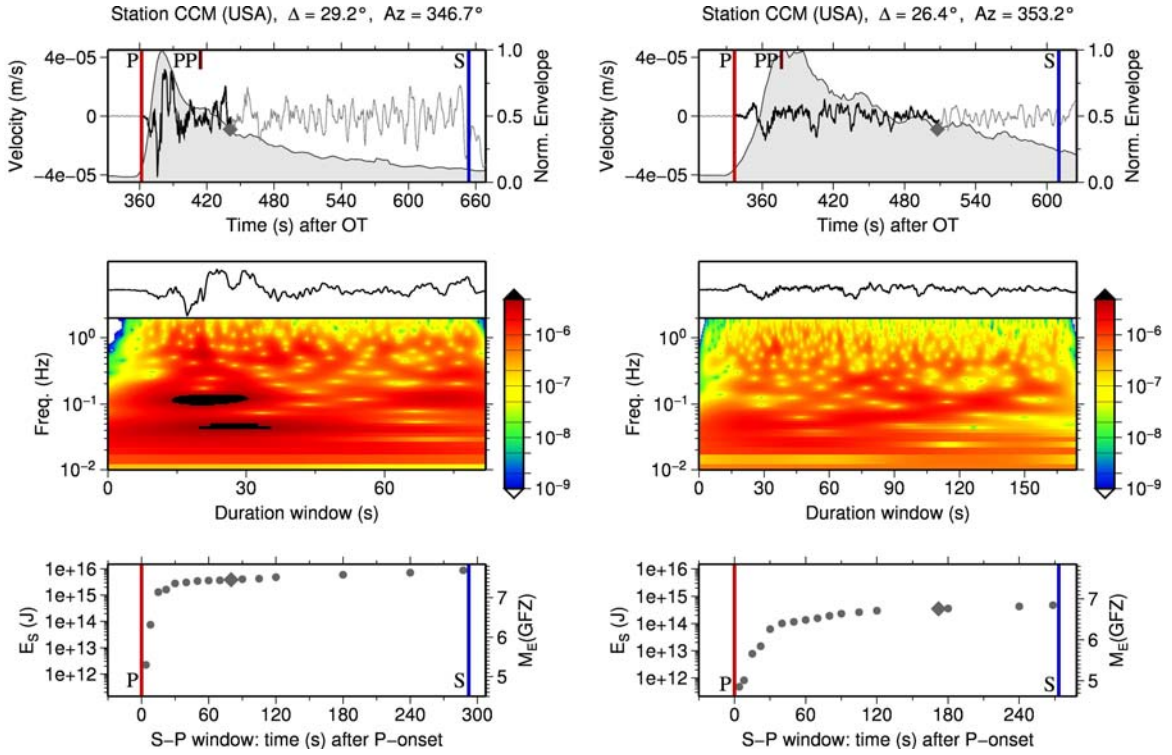

Fig. 3.5: The panels on the left refer to the Costa Rica earthquake of 22 April 1991 and the panels on the right to the Nicaragua earthquake of 02 September 1992. Upper panels: *S-P* time windows of the vertical component velocity seismograms recorded at the station INCN (Korea), with the duration windows marked by the black record trace. Also plotted are the theoretical arrival times of the *P*-, *PP*-, and *S*- phases; the gray shaded area represents the envelope of high-frequency velocity amplitudes used to constrain the overall rupture time duration (Bormann and Saul, 2008), and the diamonds at the end of the black record trace mark the end of the time window after the *P*-wave onset for which the final $M_{E(GFZ)}$ single station value is calculated. Middle panels: time-frequency analysis via the *S-transform* (Stockwell et al., 1996; Parolai, 2009) calculated over the *P*-wave duration window (black record traces in the upper panels that are also shown enlarged just above each middle panel); the colour scales represent the amplitude of the *S-transform* in m/s (see text for details). Lower panels: E_S and M_E values for different cumulative *P*-wave windows. The diamonds mark the end of the *P*-wave windows that have been used for the single station $M_{E(GFZ)}$ estimates. All the panels have the same scale values.

2) The 2007-09-13 and the 2007-10-24 Southern Sumatra earthquakes

In September-October 2007, the Sumatra arc was affected by a number of moderate to major events after the great Bengkulu earthquake of 12 September 2007. Here two earthquakes that occurred in Southern Sumatra

with similar GCMT moment magnitudes are considered, namely 7.0 for the 2007-09-13 and 6.8 for the 2007-10-24 earthquake, respectively. Their epicenter locations differed by about 250 km. Fig. 3.6 shows in the upper map the distribution of stations used in the analysis for both earthquakes (28 are in common), and next to the map cut-out below their almost identical GCMT fault plane solutions. Fig. 3.7 compares the records and analysis results for the station GNI, which is further away from the other earthquakes (65.4° and 67.6°, respectively) in the examples of Fig. 3.5 and 3.9. Despite their similarity in focal mechanism and seismic moment the two earthquakes differ in their M_E by about 0.7 m.u. and accordingly in their energy release by more than a factor of 10 ($M_{E(GFZ)}$ 7.38 and 6.64 or $M_{E(USGS)}$ 6.96 and 6.20 for the 2007-09-13 and the 2007-10-24 event, respectively). The time-frequency analyses show that the two events have similar low frequency ($f < 0.1$ Hz) amplitudes (consistent with the similar M_0 and M_W), but the high-frequency part of the spectra are very different. The first earthquake has much larger spectral amplitudes at frequencies between 0.1 and 0.3 Hz than the second one. This explains the significant differences in the equally scaled recordings. Moreover, the energy released by the first event is dominated by three energy pulses. The first one, lasting for about 20 s, arrives about 15 seconds after the first *P*-wave onset with dominating frequencies between 0.1 and 0.2 Hz. Soon after, a short second pulse (about 5 second long) and a third pulse between ~47 and 70 seconds after the first *P*-wave onset arrive, both with f ~0.3 Hz (unfortunately, due to the lack of studies regarding the rupture process of this event, a link between these energy pulses with the rupture process, as discussed in the case of the Costa Rica event, cannot be yet made).

In contrast, the second earthquake radiates its energy more homogeneously all over the rupture time, with smaller high frequency

amplitudes. Thus, this example illustrates also the large range of variability in the energy release by earthquakes with very similar mechanisms and occurring even in the same seismo-tectonic environment.

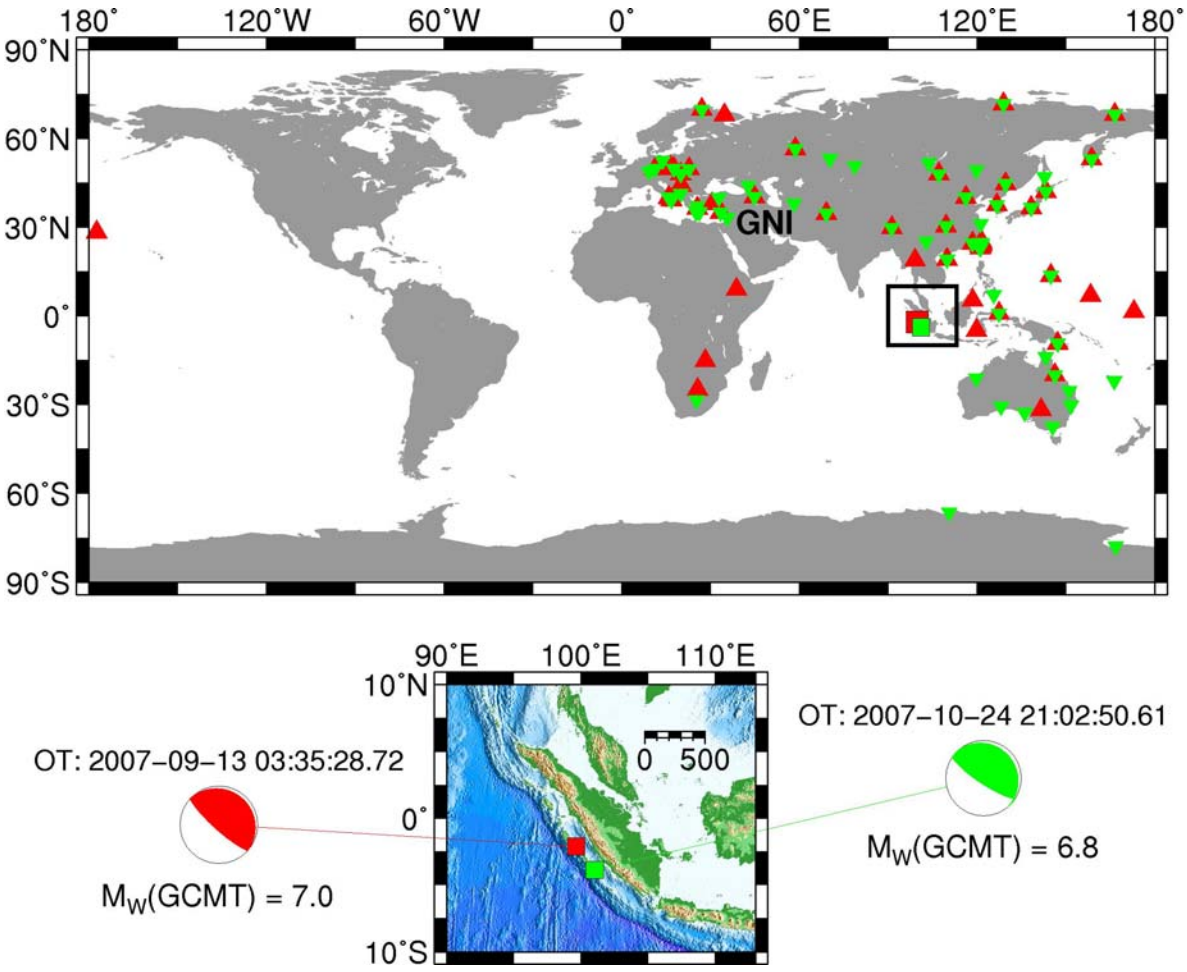

Fig. 3.6: The upper map shows the location of the two analyzed Southern Sumatra earthquakes and the stations used to calculate $M_{E(GFZ)}$. The red triangles relate to stations used for the earthquake on 13 September 2007, and the inverted green triangles to stations used for the event on 24 October 2007. The station GNI will be considered in the comparison of Fig. 3.7. The box delimitates the area shown enlarged in the lower map together with the GCMT fault plane solutions and related M_W.

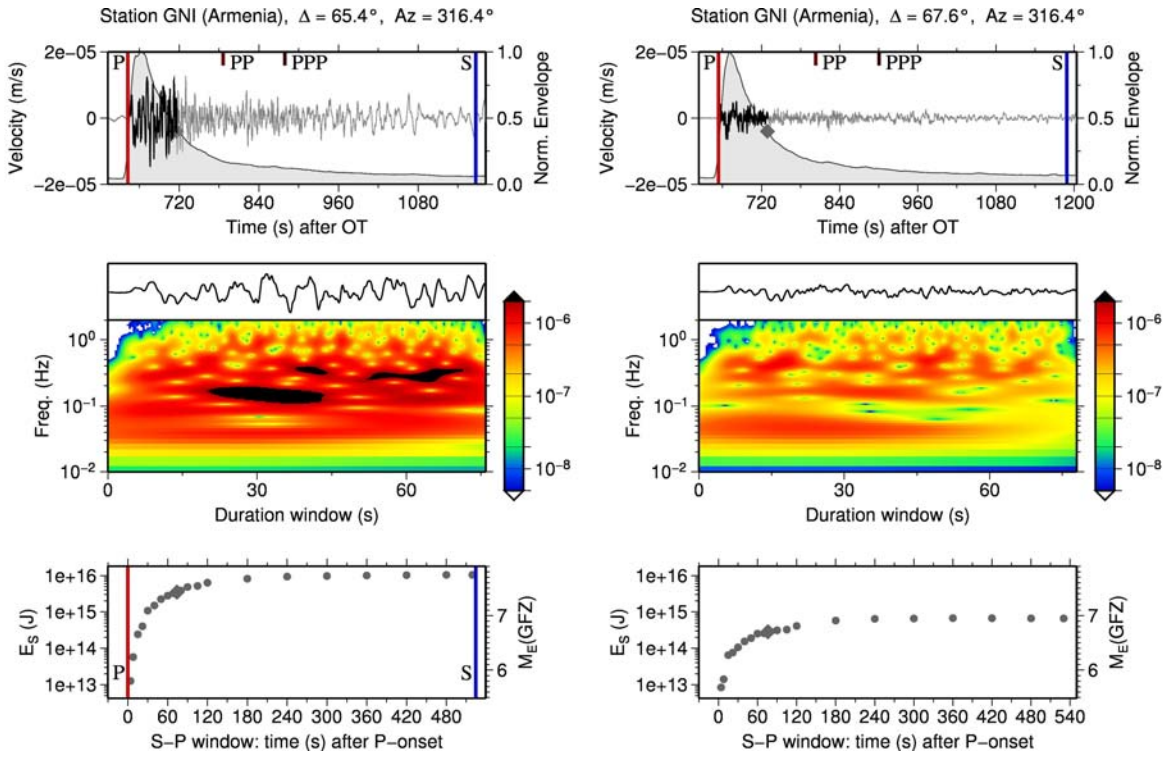

Fig. 3.7: The same as for Fig. 3.5 at the station GNI (Armenia). The panels on the left refer to the Sumatra earthquake that occurred on 13 September 2007, and the panels on the right to the other Sumatra earthquake on 24 October 2007. In the uppermost panels also the theoretical PPP arrivals are marked.

3) The 2006-11-15 and the 2007-01-13 Kuril islands earthquakes

These two recent great earthquakes represent an extraordinary example since they occurred very close in space and time and show a significant difference in the observed short-period body-wave amplitudes despite of their similarity in seismic moment (Ammon et al., 2008). $M_{W(GCMT)}$ is equal to 8.3 for the 2006-11-15 event and 8.1 for the 2007-01-13 event, but the high frequency part of the energy release of the latter was higher. This is confirmed by the different M_E values for the 2006 and 2007 earthquake: $M_{E(GFZ)}$ 7.76 and 8.57, and $M_{E(USGS)}$ 7.73 and 8.15, respectively. For both earthquakes, a large number of seismic stations has been used to compute $M_{E(GFZ)}$, and 82 of them are in common (see Fig. 3.8), so that the redundancy of the information provided by the observations is very high in both cases. Hence, since the

locations of these two earthquakes differ by only about 100 km, the paths from the source to receivers at teleseismic distances are practically the same. Therefore, it is reasonable to assume that differences in the observed short period body-wave amplitudes are mainly due to different source characteristics. In Fig. 3.9, the results of the analyses at station INCN are shown. All results underline the different high-frequency radiation content of these two earthquakes. The *S-transform* show significant differences for these two events. The 2007-01-13 earthquake (right-hand panels in Fig. 3.9) radiated a large amount of energy at ~0.1 Hz just after the *P*-wave arrival (first 15-20 s) and important contributions to the total energy release come also from successive arrivals with higher dominant frequencies between 0.2 and 0.4 Hz. In contrast, the 2006-11-15 earthquake (left-hand panels in Fig. 3.9) radiated seismic energy mainly at lower frequencies (~0.1 and ~0.03 Hz) which is spread over a longer time span. Furthermore, in agreement with its larger seismic moment, the low frequency content around 0.03 Hz is larger than the 2007 event, whereas the high-frequency content for $f > 0.1$ Hz is much smaller for the 2006 than for the 2007earthquake. The same is observed on other station records that have been used in common for both events. This highlights that M_W alone can not identify and quantify differences in source complexity and energy radiation and calls, therefore, for the need of determining and considering M_W and M_E together. These findings confirm the results of Ammon et al. (2008), who determined larger moment rate amplitudes in the medium frequency band up to 1 Hz for the 2007 earthquake than for the 2006 event, despite the larger seismic moment of the latter.

Localities in Japan and Russia, which have been affected by this pair of earthquakes, were at about the same distance from the respective epicenters. But according to the NEIC felt reports about these two earthquakes

(http://earthquake.usgs.gov/regional/world/historical.php), the 2006 earthquake was only slightly felt at some places in Russia and Japan, whereas the shaking due to the 2007 earthquake was much more severe with a maximum intensity of VI in several Russian localities. In contrast, the event with the lower shaking intensity generated a tsunami with a maximum measured tsunami wave height of 176 cm, whereas a much smaller tsunami was generated by the 2007 earthquake (maximum measured tsunami wave height 37 cm). Such differences in ground shaking and tsunami generation can be easily explained by considering the respective differences $M_{W(GCMT)}$-$M_{E(GFZ)}$ for the 2006 and 2007 events, which are about +0.5 and -0.4 m.u., respectively

Since for this pair of recent great earthquakes a lot of common station recordings are available and these are representative of the current state of the global broadband station deployment, in Fig. 3.10 their $M_{E(GFZ)}$ residual (being the difference between the single station M_E and the event average M_E) distributions is shown. The propagation paths to stations in the teleseismic range are about the same for both events and a very similar distribution of the residuals for these two events is observed. This hints that, despite the different source mechanism of these two earthquakes, the influence of the real Earth heterogeneities with respect to the model (discussed in **Chapter 4**) is playing a major role in the residual distributions. In fact, both earthquakes, in general, have negative residuals for stations located in North America (especially Canada and USA) and positive for stations located in Europe. Therefore, it is very important to use globally distributed stations in order to minimize these effects on event M_E estimates, and, at the other hand, this example shows that fault plane geometry effects play a minor role in average M_E estimates.

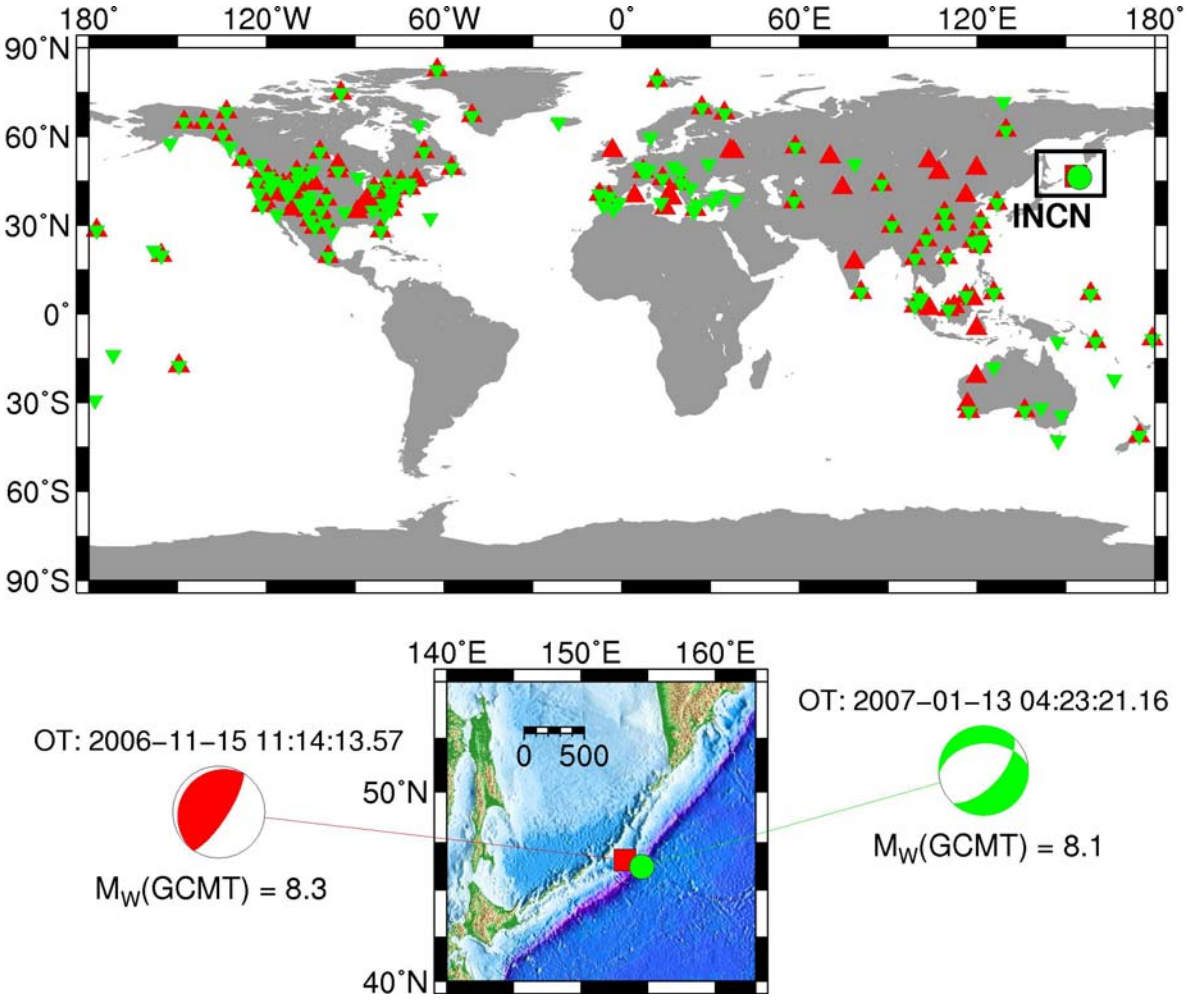

Fig. 3.8: Map showing the location of the two Kuril islands earthquakes and the stations used to calculate the final $M_{E(GFZ)}$. The red triangles represent the stations used for the earthquake of 15 November 2006, and the inverted green triangles for the event of 13 January 2007. The station INCN will be considered in the comparison of Fig. 3.9. The box delimitates the area shown enlarged in the middle together with the GCMT fault plane solutions and related M_W.

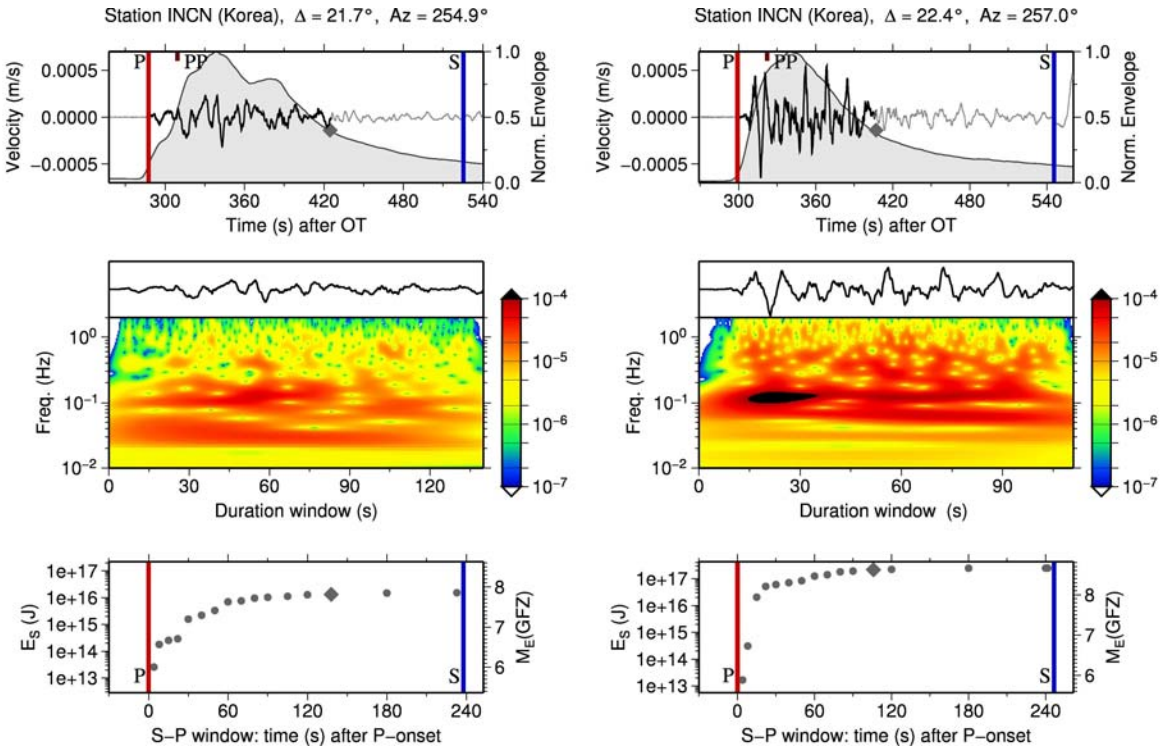

Fig. 3.9: The same as for Fig. 3.5 at the station INCN (Korea). The panels on the left refer to the Kuril islands earthquake of 15 November 2006, and the panels on the right to the close-by earthquake of 13 January 2007.

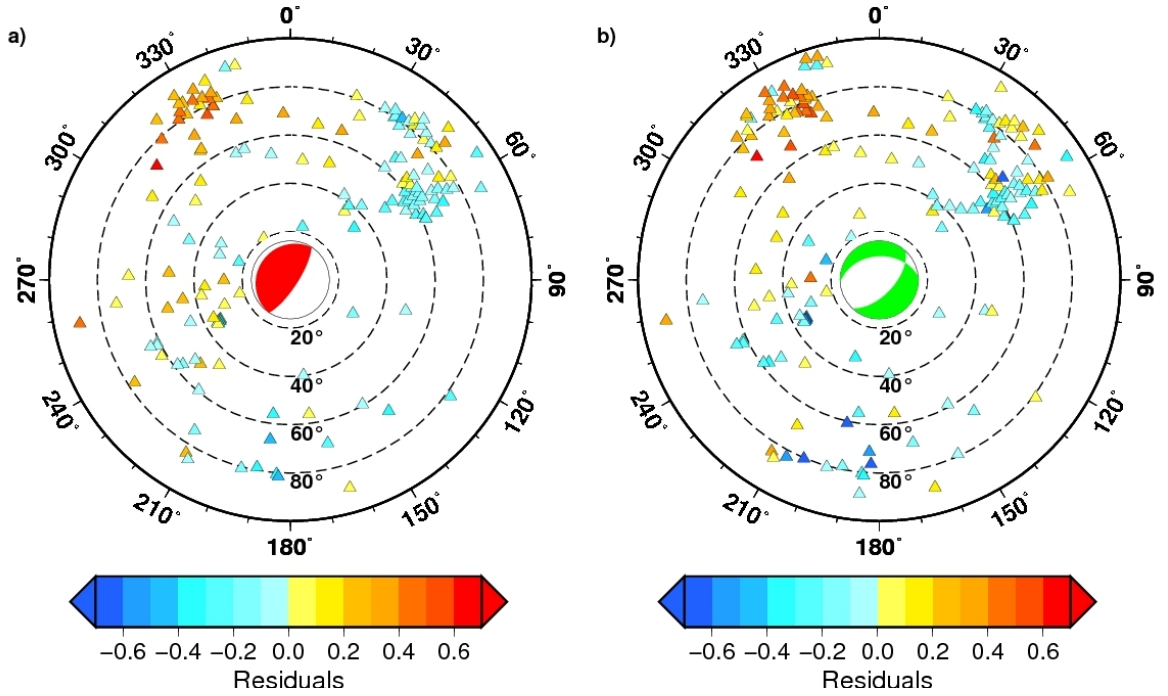

Fig. 3.10: Plots in polar projection of the residuals of $M_{E(GFZ)}$ for the 2006-11-15 and 2007-01-13 Kuril islands earthquakes. The corresponding fault plane solutions are plotted in the center of the diagrams. The dashed circles represent the distance from the source in degrees.

3.3 Comparisons of M_E and classical magnitude estimates

In this section the computation of the classical magnitude estimates M_S, m_B and m_b are briefly described and, then, compared with $M_{E(GFZ)}$ and $M_{E(USGS)}$.

Since the surface-waves have the largest amplitudes in teleseismic records for shallow earthquakes, Gutenberg (1945a) considered these waves to introduce M_S so that to calculate the magnitude for global earthquakes. Since then the computation of M_S evolved and at the present time, according to IASPEI (2005), is obtained from:

$$M_S = \log(A/T) + 1.66\log\Delta + 0.3 \qquad (19)$$

where A = vertical-component ground displacement in nm measured from the maximum surface-wave trace amplitude having a period T between 18 s and 22 s, and $20° \le \Delta \le 160°$. M_S (at 20 s) can be computed only for shallow earthquakes ($h < 70$ km) and usually scatter rather well with M_W but suffer of saturation for earthquakes with M_W larger than ~8.5.

Even the broadband body-wave magnitude m_B, applicable also to deep earthquakes, was introduced by Gutenberg (1945b and c). Usually it is computed considering the vertical component of P-wave according to:

$$m_B = \log(A/T)_{max} + Q(\Delta, h) - 3.0 \qquad (20)$$

where $(A/T)_{max} = (V_{max}/2\pi)$, with V_{max} = ground velocity in nm/s associated with the maximum trace-amplitude in the entire P-phase train as recorded on a vertical-component seismogram that is proportional to velocity at least in the period-range 0.2 s < T < 30 s, and $Q(\Delta, h)$ are the calibration functions (Gutenberg and Richter, 1956a) to account for the attenuation [frequency-independent, even if the frequency-dependent attenuation is in reality significant especially for P-waves with $T < 4$ s, as shown in Fig. 2.5] of the

amplitudes recorded in the distance range $20° \leq \Delta \leq 100°$. While m_B suffer of saturation at about $M_W = 8$, it can be used as a proxy of the energy radiated by an earthquake since it is obtained from velocity recordings by considering amplitudes in a broad range of periods (see Bormann and Saul, 2008).

The short-period body-wave magnitude m_b has been introduced after the global deployment of the World-Wide Standard Seismograph System (WWSSN) in the 1960s. It is obtained from Eq. (20) but with A_{max} measurements on narrow-band short-period records at periods < 3 s (mostly around 1 s) instead of true $(A/T)_{max}$ in a wide period range as for m_B. It must also be reminded that the $Q(\Delta, h)$ functions were obtained by analyzing mostly medium- to long-period but not short-periods body-wave amplitudes. This results in a systematic underestimation of m_b of the earthquake "*size*" even of several magnitude units and an early saturation for M_W larger than about ~6.5. This notwithstanding, m_b has its own merit since 1) it is useful for further emphasizing the short-period characteristics of an earthquake and 2) it has been calculated since many decades and also nowadays is the most frequently determined teleseismic magnitude.

In the following, the magnitude estimates M_S from the USGS, m_B from the GFZ (courtesy of J. Saul) and m_b from the USGS are compared with $M_{E(GFZ)}$ and $M_{E(USGS)}$ (Fig. 3.11, 3.12, and 3.13, respectively). Even in these comparisons the fault plane solution classification of Zoback (1992) is adopted as previously done in Fig. 3.2 and 3.3 for the M_W - M_E comparisons.

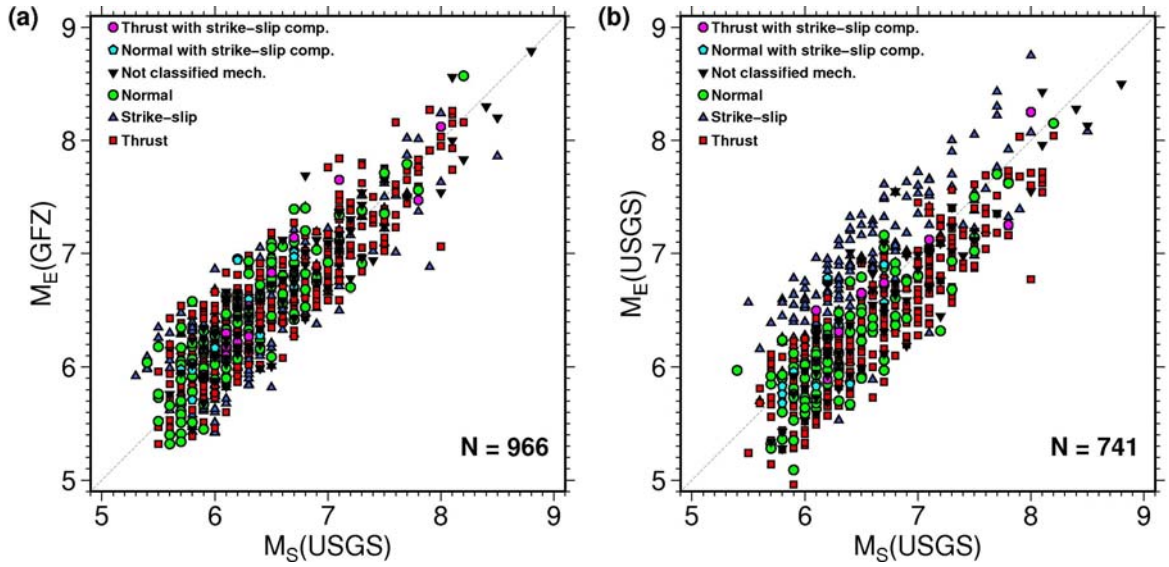

Fig. 3.11: Comparison of a) $M_{S(USGS)}$ with $M_{E(GFZ)}$ and b) $M_{S(USGS)}$ with $M_{E(USGS)}$ for a total of 966 and 764 earthquakes, respectively. Different symbols represent the type of mechanism. The 1:1 lines are also plotted.

The average difference M_S — $M_{E(GFZ)}$ spans between -0.04 m.u (S.D. = 0.3) for SS and -0.2 m.u. (S.D. = 0.21) for NS earthquakes, whereas the average difference M_S — $M_{E(USGS)}$ spans between 0.22 for TF (S.D. = 0.27) and -0.28 for SS (S.D. = 0.36) mechanisms.

Less scattered is the distribution $m_{B(GFZ)}$ — $M_{E(GFZ)}$, where the maximum and minimum average differences span between 0.27 (S.D. = 0.18) for NF and 0.13 (S.D. = 0.19) for SS mechanisms, respectively. On the other hand, the comparison $m_{B(GFZ)}$ — $M_{E(USGS)}$ is characterized, generally speaking, by two distinct clusters: one composed by SS earthquakes and another by all the other types. Indeed, the SS are generally larger than $m_{B(GFZ)}$, with an average difference $m_{B(GFZ)}$ — $M_{E(USGS)}$ of -0.15 (S.D. = 0.33), whereas the average difference is 0.50 (S.D. = 0.24) considering all the other types of mechanisms.

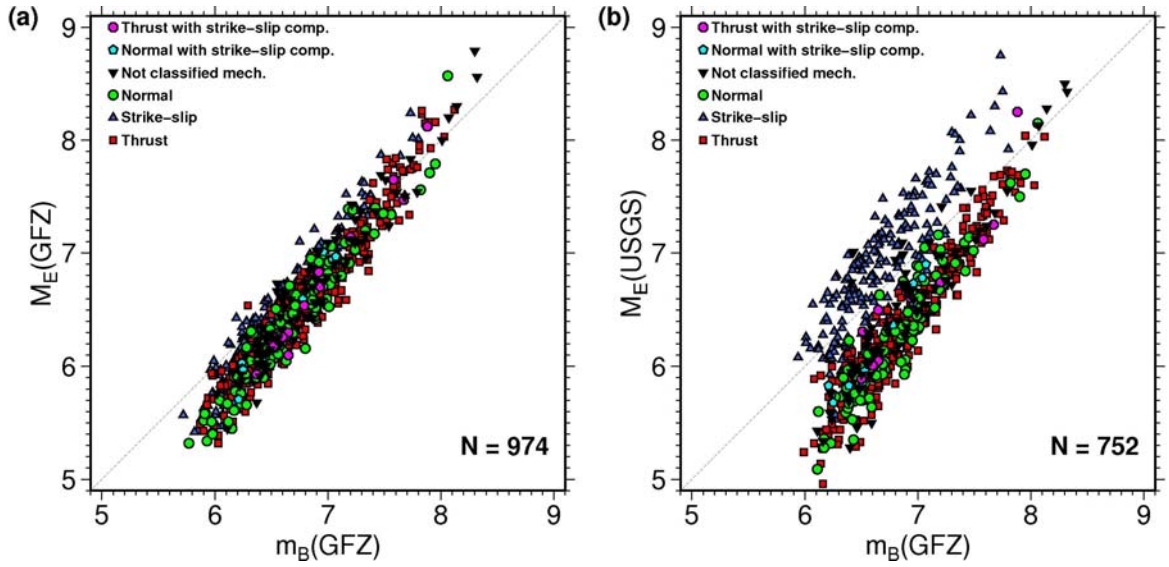

Fig. 3.12: Comparison of a) $m_{B(GFZ)}$ with $M_{E(GFZ)}$ and b) $m_{B(GFZ)}$ with $M_{E(USGS)}$ for a total of 974 and 752 earthquakes, respectively. Different symbols represent the type of mechanism. The 1:1 lines are also plotted.

The average difference m_b— $M_{E(GFZ)}$ spans between -0.4 (S.D. = 0.29) for NF and -0.61 for NC mechanisms, and between -0.14 (S.D. = 0.29) for NF and -0.85 for SS mechanisms for the average difference m_b— $M_{E(USGS)}$.

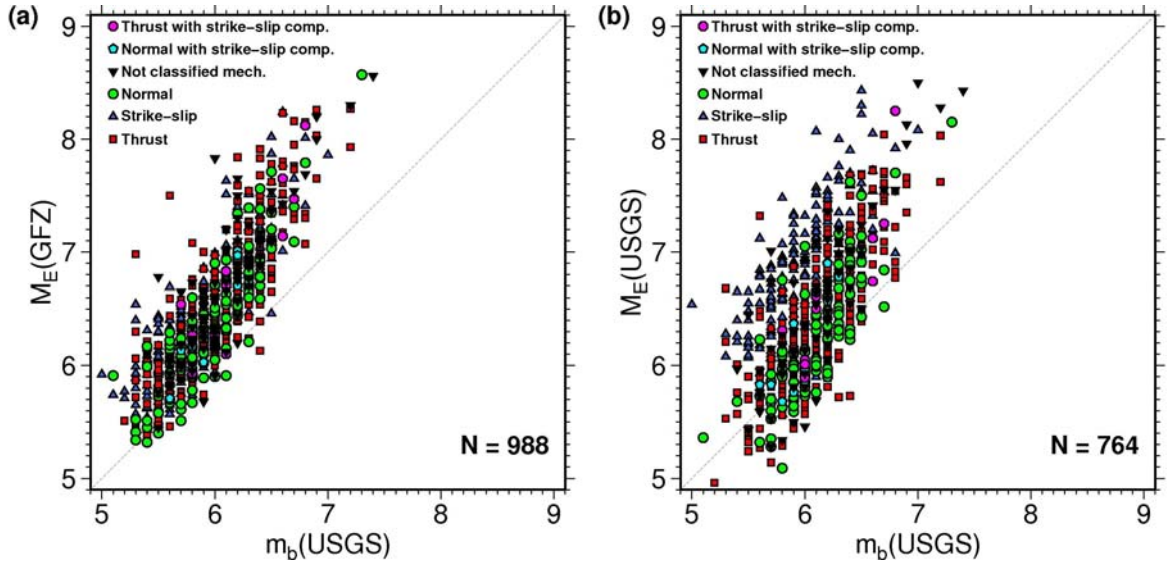

Fig. 3.13: Comparison of a) $m_{b(USGS)}$ with $M_{E(GFZ)}$ and b) $m_{b(USGS)}$ with $M_{E(USGS)}$ for a total of 988 and 764 earthquakes, respectively. Different symbols represent the type of mechanism. The 1:1 lines are also plotted.

As general result of these comparisons, it can be clearly seen that the rapid $M_{E(GFZ)}$ estimations do not show any clear tendency with the different fault plane groups. These findings are in good agreement with the ones already discussed in the M_W - $M_{E(GFZ)}$ comparisons of Fig. 3.2 and 3.3b. In contrast, $M_{E(USGS)}$ shows a clear tendency for SS earthquakes to be generally larger than all the other types of earthquakes. As previously mentioned, such dependence on source geometry does not belong to the magnitude concept, and, as endorsed by these comparisons with the classical magnitude scales, the effect on M_E estimates of theoretically based radiation pattern corrections must be further investigated.

3.4. Magnitude characteristics of tsunami and tsunamigenic earthquakes

For large earthquakes in subduction zones, the magnitude is a primary input for tsunami early warning systems. Normally, earthquakes generating significant tsunamis are characterized by source spectra depleted in their high-frequency content with respect to the low-frequency one and such a feature can be identified by complementing the information provided by different magnitude estimates.

Kanamori (1972) first pointed out that tsunami earthquakes are depleted in their short-period (1-20 s) amplitudes compared to the tsunami excitation, and such a characteristic is translated to significantly larger M_W (as expression of the overall final displacement caused by the earthquake rupture) with respect to other magnitude scales (M_E, M_S and m_b) that are more related to the medium- to short-period content radiated by the seismic source. In this section the capabilities and limitations of using the discrepancy between the low- and high-frequency content of the seismic source (as revealed by the magnitude

characteristics) in guiding earthquake tsunami early warning systems are investigated by considering the classical magnitude scales M_S and m_b — which have played an important role in past years in the characterization of tsunami-generating earthquakes — and the modern ones M_W and M_E for 89 earthquakes (Fig. 3.14) occurred over the last ~20 years and for which the tsunami parameters are available from the NGDC/NOAA tsunami database (http://www.ngdc.noaa.gov/hazard/tsu.shtml, source and corresponding tsunami parameters listed in Table A2).

Tsunamis in the NGDC/NOAA database (validity = 4, i.e. definite tsunami) caused by an earthquake (code = 1) have been searched starting from January 1990 until December 2007, including the Samoa Islands earthquake which occurred on 29 September 2009. From the various tsunami parameters available on the NGDC/NOAA database, Table A2 includes only the maximum water height (m) and the number of runups. Of course, the impact of a tsunami (see, e.g., Lomax and Michelini, 2009a and b) is dependent on many factors (e.g., bathymetry and shape of the coastline, which may focus or defocus the tsunami wave) which here are not considered. Therefore, the maximum water height is simply used as a tool to map in a simple way the tsunami excitation when comparing different magnitude determinations. For 55 of the 89 earthquakes considered in this section, the maximum water height reported in the NGDC/NOAA database is $\leq$ 1 m, for 21 earthquakes it is between 3 and 10 m, and for 7 a maximum water height larger than 10 m is reported. As expected from earthquakes distributed along subduction zones, a large percentage of them are thrust fault types (#TF = 50), and only 13 and 10 earthquakes are SS and NF types, respectively. Important examples of tsunami earthquakes, having fault plane solutions very close to TF (as #13, #16 and #66 in Table A2), fall into the not classified (NC) group. This obviously

confirms the high tsunami potential for TF-like earthquakes (Pelayo and Wiens, 1992), but also that the tsunami potential of NF (like the 29 September 2009 Samoa earthquake) and SS (like the 14 November 1994 Mindoro earthquake, the Philippines, see Tanioka and Satake, 1996) cannot be ruled out. Consequently, by considering both the findings of Okal (1988), where the far-field tsunami excitation is only marginally influenced by the focal mechanism, and by considering that, despite the important progress in real- or near real-time moment tensor solution determination (see, e.g., Sipkin, 1994; Kanamori and Rivera, 2008), fault plane solutions are often not available within 15 or 30 minutes or so after the earthquake's occurrence (potentially limiting the promptness of the response of disaster management organizations), the fault plane solution type in the following discussion is not considered.

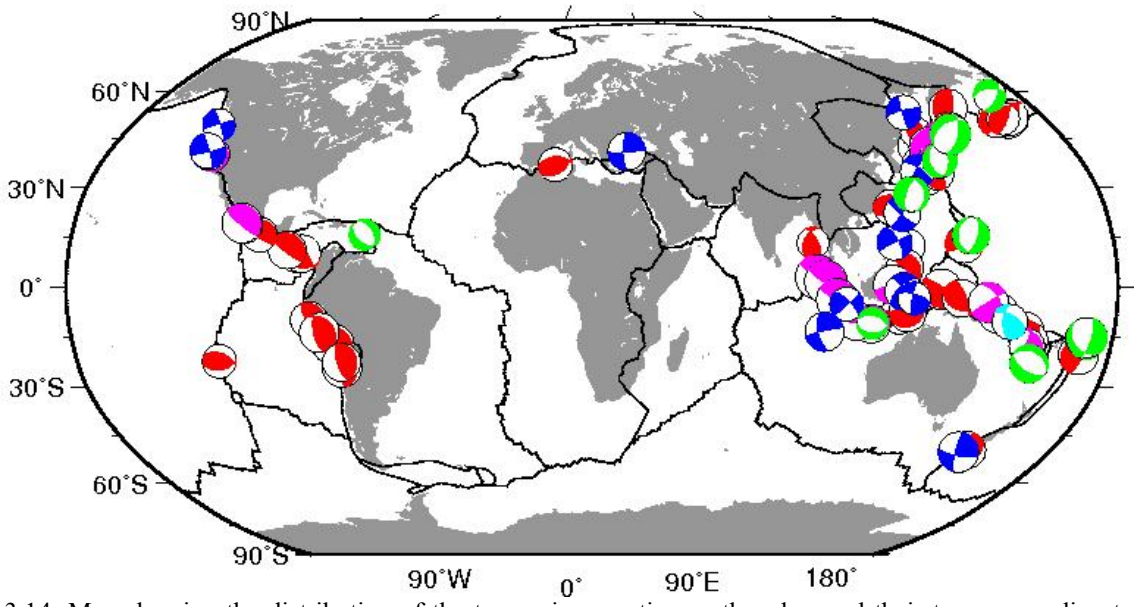

Fig. 3.14: Map showing the distribution of the tsunami-generating earthquakes and their types according to the classification of Zoback (1992). Normal-fault (NF) solutions are plotted in green, strike-slip (SS) in blue, thrust (TF) in red, not classified (NC) in magenta, and thrust with strike-slip component (TS) in cyan. The plate boundaries have been plotted according to Bird (2003).

Fig. 3.15 shows the comparisons between $M_{W(GCMT)}$ with m_b, M_S, $M_{E(USGS)}$ and $M_{E(GFZ)}$. Tsunami earthquakes are usually characterized by a significant difference between M_W and M_S (see, e.g., Pelayo and Wiens, 1992; Kanamori and Kikuchi, 1993), and such a discrepancy has been largely used in the literature to identify them. However, no quantitative threshold has been given, therefore the $M_W = M_S + 0.3$ line in Fig. 3.15b and, similarly, the $M_W = M_E + 0.3$ line in Fig. 3.15c and d are also depicted as a reference to facilitate the identification of earthquakes with significantly larger M_W than M_S and M_E, respectively. Considering the well-known 02.09.1992 Nicaragua, the 02.06.1994 Java, the 21.02.1996 Peru, and the 17.07.2006 Java tsunami earthquakes (Polet and Kanamori, 2009), identified by their ID number of Table A2 in Fig. 3.15, there is a clear difference between M_W, M_S and M_E. For example, the 1992 Nicaragua tsunami earthquake has $M_S = 7.2$ and $M_W = 7.6$. Remarkably, m_b is much smaller than normally expected for an $M_W = 7.6$ (see the Fig. 3.15a), and also M_E is several m.u. smaller than M_W. The same applies to the 1994 Java earthquake (see, e.g. Polet and Kanamori, 2000; Polet and Thio, 2003). Thus, these earthquakes show a peculiar magnitude "*fingerprint*", where, for a given M_W, the other magnitudes are several m.u. smaller.

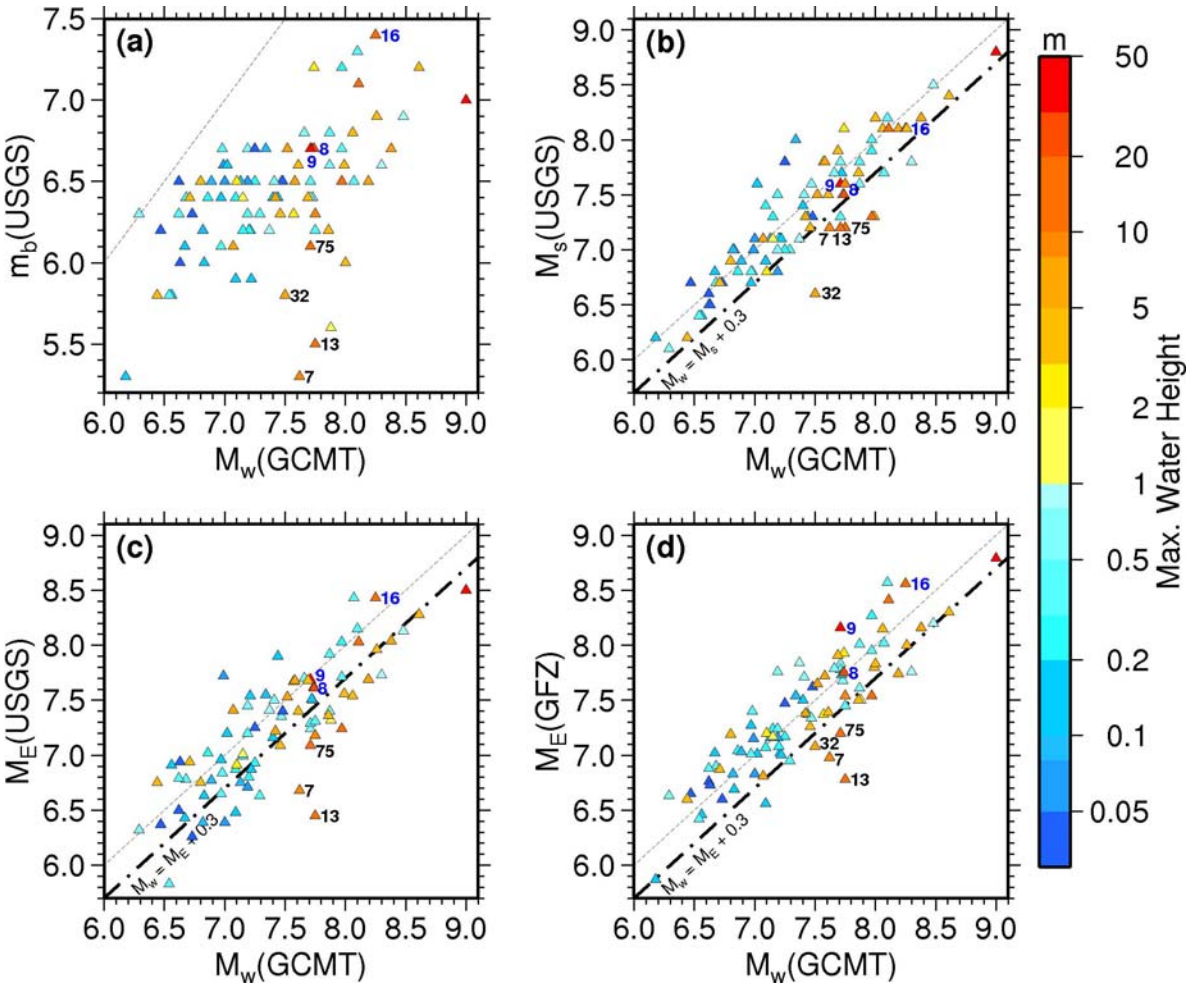

Fig. 3.15: Comparisons of $M_{W(GCMT)}$ with (a) $m_{b(USGS)}$, (b) $M_{S(USGS)}$, (c) $M_{E(USGS)}$, and (d) $M_{E(GFZ)}$. The 1:1 lines are plotted as thin-dashed line, while the $M_W = M_S + 0.3$ (Fig. 2b) and the $M_W = M_E + 0.3$ (Fig. 2c and d) are the thick-dashed-dotted lines. The ID numbers of the earthquakes discussed in the text are included (see Table A2).

Therefore, it is confirmed that known tsunami earthquakes are depleted in their high-frequency content compared to the long-period one and, accordingly, this is why procedures to identify such a feature have been developed. A popular tool for this role is the $\Theta = \log(E_S/M_0)$ parameter introduced by Newman and Okal (1998). Fig. 3.16 shows Θ as obtained from the E_S values of USGS and GFZ versus $M_{W(GCMT)}$. To better show the global trend of the Θ parameter, the values for an additional globally distributed 600 earthquakes (white circles) that are included in the dataset of Di Giacomo et

al. (2010a) are also shown. Since M_W and M_E are directly related to M_0 and E_S, respectively, differences between these two magnitudes can be easily discussed via the Θ parameter and viceversa. Newman and Okal (1998) and later Weinstein and Okal (2005) showed that Θ is an effective tool for identifying the "slow" earthquakes (events with low values of rupture velocity and stress drop, anomalously large rupture durations, and, possibly, fault ruptures propagating into the ocean floor sedimentary cover, Kanamori and Kikuchi, 1993; Polet and Kanamori, 2000), since they should have a much lower Θ than expected from a global average. The best examples in this sense are the 1992 Nicaragua and the 1994 and 2006 Java earthquakes, for which Θ (and equivalently the difference between M_W and M_E) could be successfully used to identify the very high tsunami-generating potential of such earthquakes. Fig. 3.15 and Fig. 3.16 show also that, as expected, the tsunami excitation tends to increase for larger values of M_W (even if a large scatter exists).

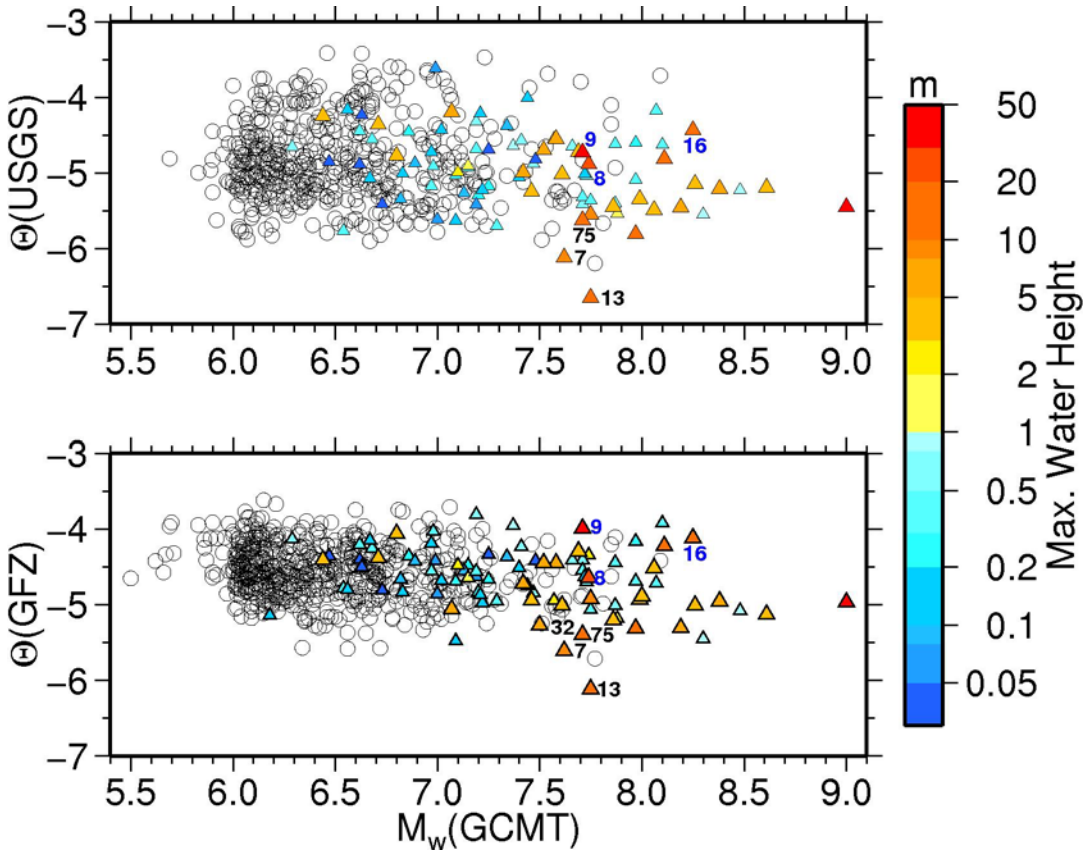

Fig. 3.16: The Θ parameter obtained by considering E_S from the USGS (upper panel) and the GFZ (lower panel) versus $M_{W(GCMT)}$. The white circles are 600 additional values of Θ from globally distributed earthquakes. M_0 is taken from the GCMT database.

In contrast, earthquakes not generating anomalously large tsunamis should be characterized by a not-so-marked discrepancy between M_W and the medium-period magnitude estimates. This is the case for many of them as found by inspecting Fig. 3.15b, c and d, where both M_S and M_E scale well with M_W for many earthquakes.

However, Fig. 3.15 and 3.16 also point out that there are earthquakes generating significant and also damaging tsunamis without showing a large difference between M_W and the other magnitudes. This is opposite to what is expected by tsunami earthquakes in the *"classical"* sense. As representative cases, three of these earthquakes are indicated by their ID number of Table A2

(#8, #9 and #16) and in blue in Fig. 3.15 and 3.16 and discussed in the following.

A striking example is the M_W = 7.71 1993 Hokkaido (#9 in Table A2) earthquake, for which M_S is only 0.1 m.u. less than M_W, and M_E is about the same or slightly larger than M_W. In any case, the tsunami following this event (Satake and Tanioka, 1995) was devastating, with a death toll and total damage of 230 and 1.2 billion U.S. dollars, respectively. The tsunami waves were well recorded not only in Japan, but also in Korea and some localities in Russia, as shown in Fig. 3.17.

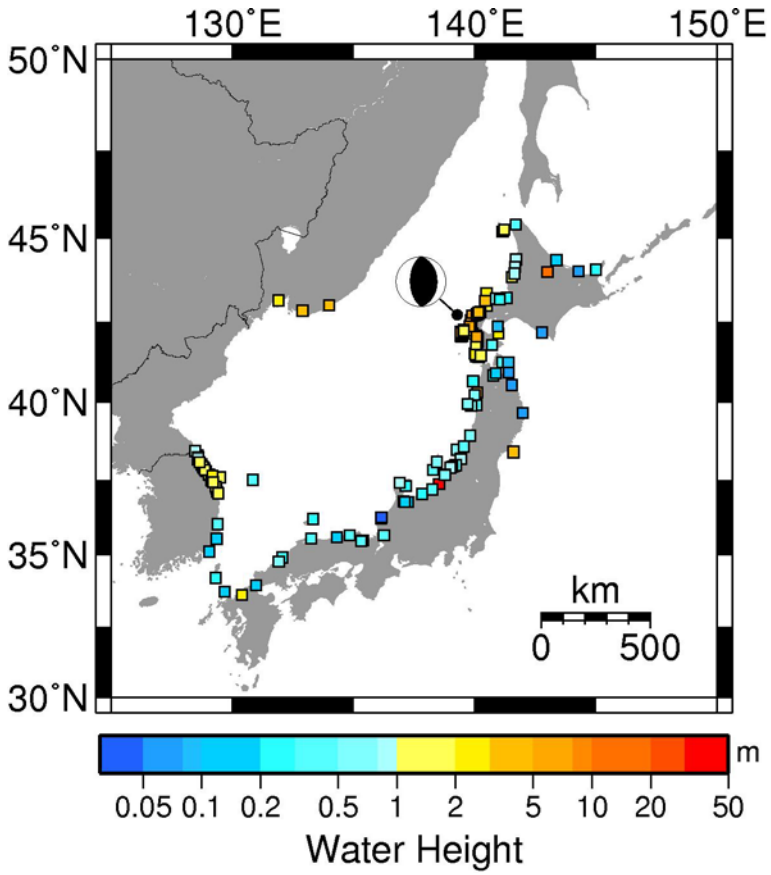

Fig. 3.17: Maximum water height (mainly tide gauges and water height measurements, http://www.ngdc.noaa.gov/hazard/tsu.shtml) resulting from the 1993 Hokkaido earthquake (#9 in Table A2). The GCMT fault plane solution is also plotted.

Similar observations can be done for the M_W = 8.25 1994 Kuril Islands earthquake (#16 in Table A2), which also shows a larger M_E than M_W, a high m_b of 7.4, and an M_S only ~0.15 m.u. less than M_W. The tsunami created serious problems in many localities in Russia, where the water height ranged between 1.5 m and 8 m, and it was also measured by tide gauges located at Hawaii and the west coast of the USA. Similar magnitude comparisons apply to the M_W = 7.74 1992 Flores Region earthquake (#8 in Table A2), where the death toll was 2500, with a total damage bill of 100 Million U.S. dollars, although the anomalously large tsunami in some localities was due to landslides/slumps caused by the earthquake (Hydayat et al., 1995; Imamura et al., 1995).

In summary, the magnitude characteristics of recent tsunami earthquakes, as defined by Kanamori (1972) and more recently by Polet and Kanamori (2009), reflect their depletion in their high-frequency content since they show significantly larger M_W than other magnitude estimates more closely related to the medium- and short-period content radiated by the seismic source. The best examples in that sense are the 1992 Nicaragua earthquake, and the two Java earthquakes that occurred in 1994 and 2006.

Such earthquakes with very high tsunami-generating potential both at local and at regional/teleseismic scales can be successfully identified in near or real-time by using different approaches. For example, by considering together the information given by the rapid determination of M_W and/or proxies of it (Okal and Talandier, 1989; Sipkin, 1994; Tsuboi et al., 1995; Kanamori and Rivera, 2008; Bormann and Saul, 2008 and 2009b; Lomax and Michelini, 2009a) along with the Θ parameter and the rupture duration (Lomax and Michelini, 2009b, who has shown the importance of quantifying anomalous rupture durations in tsunami warning) a clearer picture of the source

characteristics could arise, and, therefore, help tsunami warning systems in issuing alarms.

However, even if many earthquakes exciting very small tsunamis show similar values of M_W and M_E and also of M_S (see Fig. 3.15), examples of earthquakes generating large tsunamis that are characterized by high-frequency radiation (as revealed by high values of M_E and M_S) exist. Therefore, in the evaluation of an earthquake's tsunami-generating potential in early warning systems, the possibility that events characterized by high-frequency radiation may generate tsunamis — potentially having a large impact at local and possibly also regional scales — cannot be ruled out. As a consequence, tsunami early warning systems may risk underestimating an earthquake's tsunami-generating potential, if their methods are based only on the detection of the peculiar magnitude "*fingerprint*" (source characteristics) of tsunami earthquakes, as recently proposed by Kuenza and Soon-Hoe (2010).

Therefore, for tsunami warning systems, it is fundamental to rapidly determine the earthquake magnitude to evaluate its tsunami potential (especially for major and great events). However, in addition to seismological information, the use of off-shore data would be necessary to enhance a warning system's performance, and possibly decrease the number of false alarms.

CHAPTER 4

Intra-station and inter-station variability analyses on M_E estimations

4.1 M_E residual distribution

In the computation of the earthquake magnitude using data from the teleseismic distance range, the correction for propagation effects applied to the recorded seismograms are assumed to be valid on a global scale. Such approximations are normally satisfied since the periods (wavelengths) considered in the teleseismic seismograms should not be significantly affected by the presence of small scale heterogeneities characterizing the Earth's structure. This is particularly the case for the M_W and procedures to obtain moment tensor solutions (e.g., Dziewonski et al., 1981; Sipkin, 1994; Kanamori and Rivera, 2008) since they are computed by considering the long and very long periods of seismograms. However, the influence of heterogeneities along the propagation paths and local effects may be not negligible when considering magnitude scales (like M_E) related to the medium- and short-period content of the source spectrum. (Note: in this chapter with M_E is intended $M_{E(GFZ)}$).

Owing to the dense sampling of a large volume of the Earth's interior by different source-receiver paths offered by the dataset considered in this thesis (Fig. 3.1), it is possible to assess the influence on the M_E estimates of the propagation and local effects not accounted for by the average 1-D model AK135Q (Fig. 2.3). Here local effects are denoted as those related to the differences between the model AK135Q and the real Earth properties over a depth range corresponding to a vertical or nearly vertical propagation of the

seismic rays arriving at a given station from teleseismic distances. To show the extent of the variability of the real data, Fig. 4.1 compares the theoretical spectral amplitude decay functions for 1 Hz (1 s, black lines) and 0.0625 Hz (16 s, gray lines) with the real spectral amplitudes at the same frequencies for 11 earthquakes with M_W between 6.50 and 6.52. Although the theoretical curves are able to capture the overall trend in the data with distance, a significant scatter affects the distribution of the observations for each considered frequency.

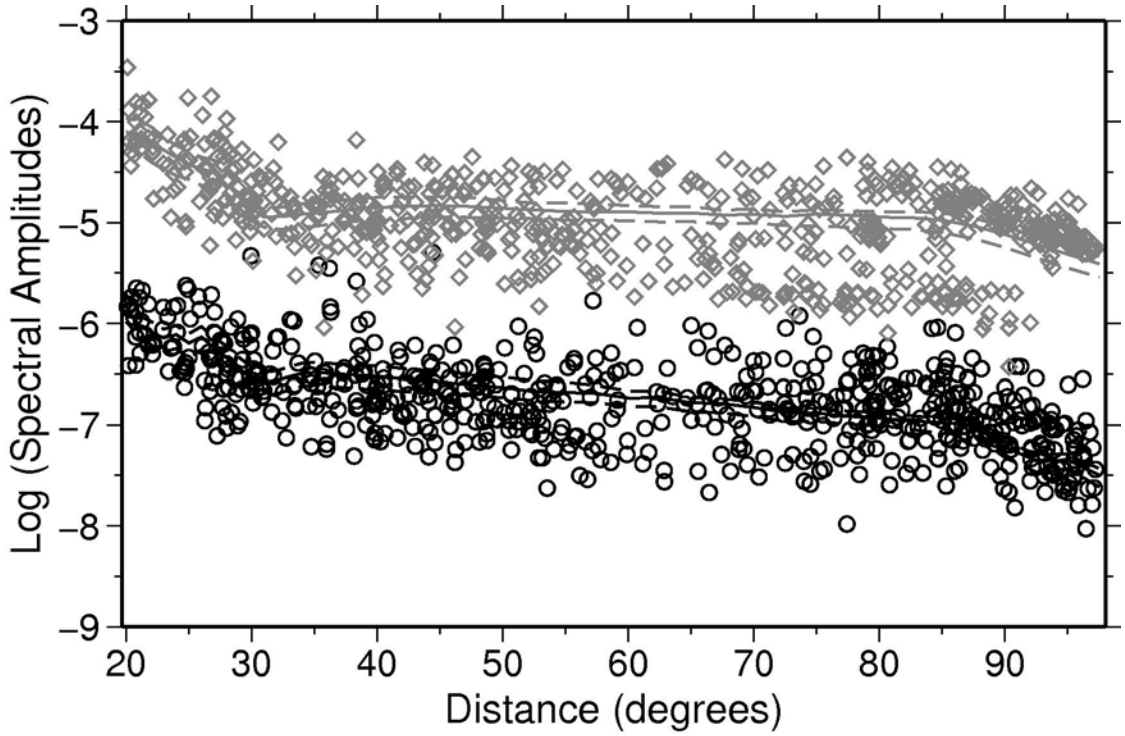

Fig. 4.1: Observed spectral amplitudes as a function of distance for frequencies of 1 Hz (black circles) and 0.0625 Hz (gray diamonds), considering 11 earthquakes of magnitude $6.50 \leq M_W \leq 6.52$. The median of the theoretical spectral amplitude decay functions at 1 Hz and 0.0625 Hz are the solid black and gray lines, respectively, along with their corresponding 15^{th} and 75^{th} percentiles (dashed lines).

In this chapter the contribution of local effects to such a scatter (reflected in the variability of the single station M_E estimates) is quantified and separated from the contribution associated with all the other sources of

variability, such as source characteristics (e.g., radiation pattern and directivity effects) and propagation effects (e.g., significant deviation of the real Earth structure from the adopted average model for attenuation and velocity). The magnitude residuals (difference between the single station M_E and the event average M_E) are used to accomplish this task.

The dataset consists of about 48,000 single stations M_E estimates computed from the recordings of 476 seismic stations deployed worldwide. For 26% of the stations considered, recordings for less than 20 earthquakes are available. For 25% of stations, between 21 and 70 of the selected earthquakes were recorded while, for the remaining ~49%, more than 70 earthquakes can be analyzed. Finally, in the considered data set, there are a few stations (CHTO, YAK, BJT, KMI and HIA) that recorded nearly 500 of the selected earthquakes.

Fig. 4.2 shows the M_E station residuals for different distance ranges. For each distance range (10° wide with an overlap of 5°) the average value ± one standard deviation is also reported in each subplot. The standard deviations range from 0.270 for distances between 50° and 60° to 0.328 for distances between 20° and 30°. The largest values are observed over the two shortest distance ranges (20°-30° and 25°-35°), corresponding to rays traveling mainly through the most heterogeneous part of the Earth, that is the transition zone and upper mantle. However, the use of stations between 20° and 30° does not introduce any bias in the final M_E estimations.

In the following, the different contributions to the observed variability of the residuals are quantified by exploiting the size of the analyzed data set and the distribution of the considered stations and hypocenters, which allowed to sample a large portion of the Earth's volume when looking at different source-to-receiver propagation paths.

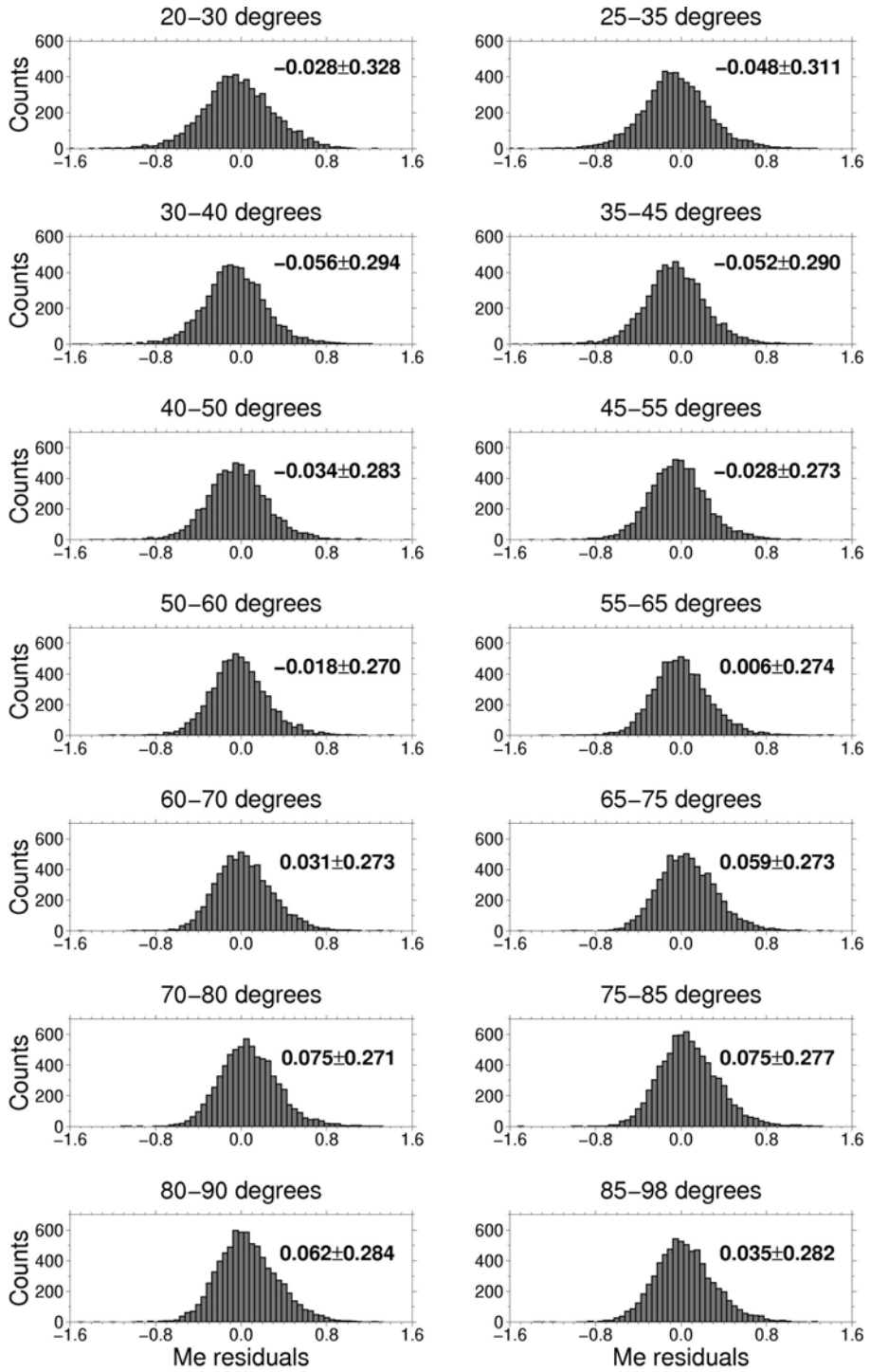

Fig. 4.2: Distributions of residuals for the complete dataset as a function of distance. In each subplot, the average ± one standard deviation is also reported. See text for details.

4.2 Inter-station and intra-station components of variance on M_E estimates

A mixed model (Brillinger and Preisler, 1985; Abrahamson and Youngs, 1992) is considered to describe the residual distribution between the average event-magnitude and the single-station magnitude. In particular, the residuals are separated into fixed and random-effect components as follows:

$$M_{ij} - M_i = M_{ij} - \frac{1}{N_i}\sum_{j=1}^{N_i} M_{ij} = \delta_{ij} = \eta_i + \varepsilon_{ij}\,, \qquad (21)$$

where M_{ij} is the magnitude estimate at station j for event i, M_i is the average magnitude computed for event i, N_i is the number of the stations that recorded event i, δ_{ij} are the residuals, η_i represents the inter-station variations (station-to-station component of error) and ε_{ij} represents the intra-station variations (record-to-record component of error). The distributions of error η_i and ε_{ij} are assumed to be independent and normally distributed with variances σ^2 and τ^2, respectively. The inter-station error η_i takes on a specific value for each station and accounts for the correlation between magnitude values estimated for different earthquakes at the same station. It describes a sort of site effect that can be due to either to significant deviations between the uppermost part of the Earth structure beneath a given station and the global model AK135Q used in the numerical simulations of Green's functions and/or to instrumental problems (e.g. incorrect calibration function). On the other hand, the intra-station error ε_{ij} takes on a specific value for each source-to-station path and includes both propagation effects (e.g. lateral variation in the seismic velocity and attenuation not considered in the global model used for computing the Green's function) and source effects (e.g. radiation pattern effects). A maximum likelihood approach (Abrahamson and Youngs, 1992) is applied to

determine the distribution of errors for the problem described by equation (21).

4.2.1 Results

Fig. 4.3 shows the residual distribution δ (top), the inter-station η (middle) and intra-station ε (bottom) error distributions, as well as their histogram distributions. Although the intra-station component of variance (τ^2 = 0.240) is the dominant one, the inter-station variability (σ^2 = 0.159) is not negligible. In the following the results regarding the inter-station variability are discussed first and followed by the intra-station component of variability.

1) Inter-station distribution of error

The middle panel of Fig. 4.3 shows that, although the errors for a few stations (e.g. KHC, GRGR, SUW, and LZH, as indicated also in the figure) exceed 0.5 m.u., most of the stations (~78%) show inter-station errors in the range $-0.2 \leq \eta \leq 0.2$ (their geographical distribution is shown in Fig. 4.4, bottom). This result confirms how the global velocity and attenuation models (AK135Q, Fig. 2.3) used to compute the Green's functions provide a reasonable average description of the propagation effects in the uppermost part of lithosphere, where the seismic rays reaching a given station are propagating almost vertically. The remaining ~22% of the stations with inter-station errors larger than 0.2 in absolute value are plotted in the upper map of Fig. 4.4. Apart from potential instrumental issues, overestimation (positive error) is due to a correction that overestimates the attenuation over the last part of propagation, whereas for the underestimation case (negative error) the opposite is true. The station showing the largest positive error is KHC, installed in the Czech

Republic, while the largest negative error is obtained for station LZH, installed in China. It is worth noting that for these stations large values of the residuals are observed systematically, regardless of the source position and strength, while neighboring stations, available at least for KHC, do not show such large values. Consequently, such large inter-station errors are most probably due to instrumental problems (e.g. miss-calibration).

Most of the stations with inter-station errors greater than 0.2 (Fig. 4.4, top) are located in the Europe/Mediterranean area, in Indonesia and in the Pacific and Atlantic oceans, whereas the main patterns of negative inter-station errors are located in Australia and the USA. Since the inter-station errors, apart from instrumental errors, are related to propagation effects in the lithospheric layers below the stations, large absolute values of η for group of stations could hint at significant deviations between local/regional lithospheric structure and the global AK135Q model. Although a direct comparison with lateral variations in *P*-wave velocity imaged by teleseismic tomography is not straightforward, a fair consistency between patterns of positive and negative inter-station errors with anomalies in the crust and upper mantle is found. For example, the inter-station distribution for North-America (Figs. 4.4) shows a cluster of station with negative errors (i.e. single station magnitudes less than the average magnitude) in the western United States in an area encompassing California, the Great Basin, the High Lava Plains, and the Yellowstone-Snake River plain hotspot, whereas positive errors are obtained for the Cascade region and in the central-southern United States. These patterns fit, to a first-order approximation, the velocity anomalies shown by Burdick et al. (2009). Similarly, in Europe a fairly good agreement between the distribution of positive and negative inter-station errors and the lateral variations in the

lithosphere imaged by *P*-wave tomography are observed (Koulakov et al., 2009).

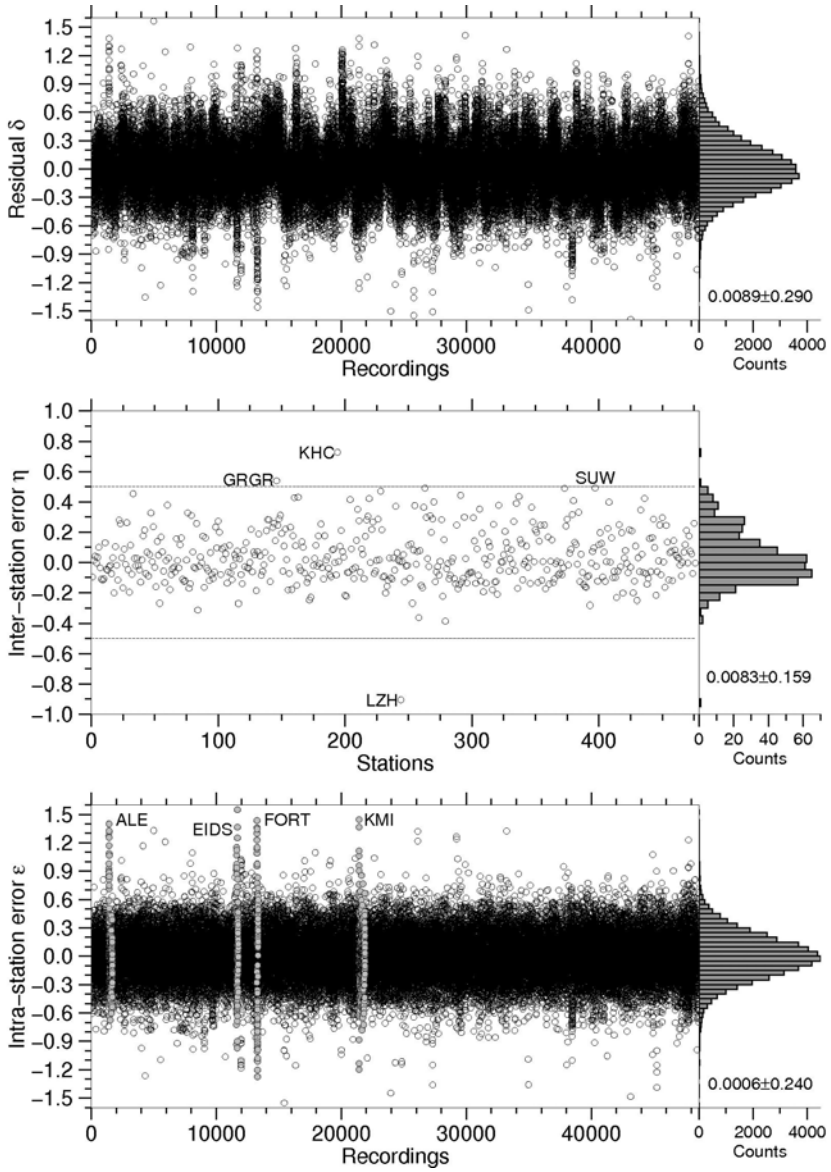

Fig. 4.3: Top: residual distribution δ_{ij}; middle: inter-station errors η_i, with the names referring to the four stations discussed in the text with larger inter-station errors; bottom: intra-station errors ε_{ij}, with the gray circles and corresponding names marking the stations with large values of intra-station errors. As a representative example for these stations, ALE is discussed later. For each panel, the histogram distributions and the mean ± one standard deviation are also shown. The x-axes are sorted by station name.

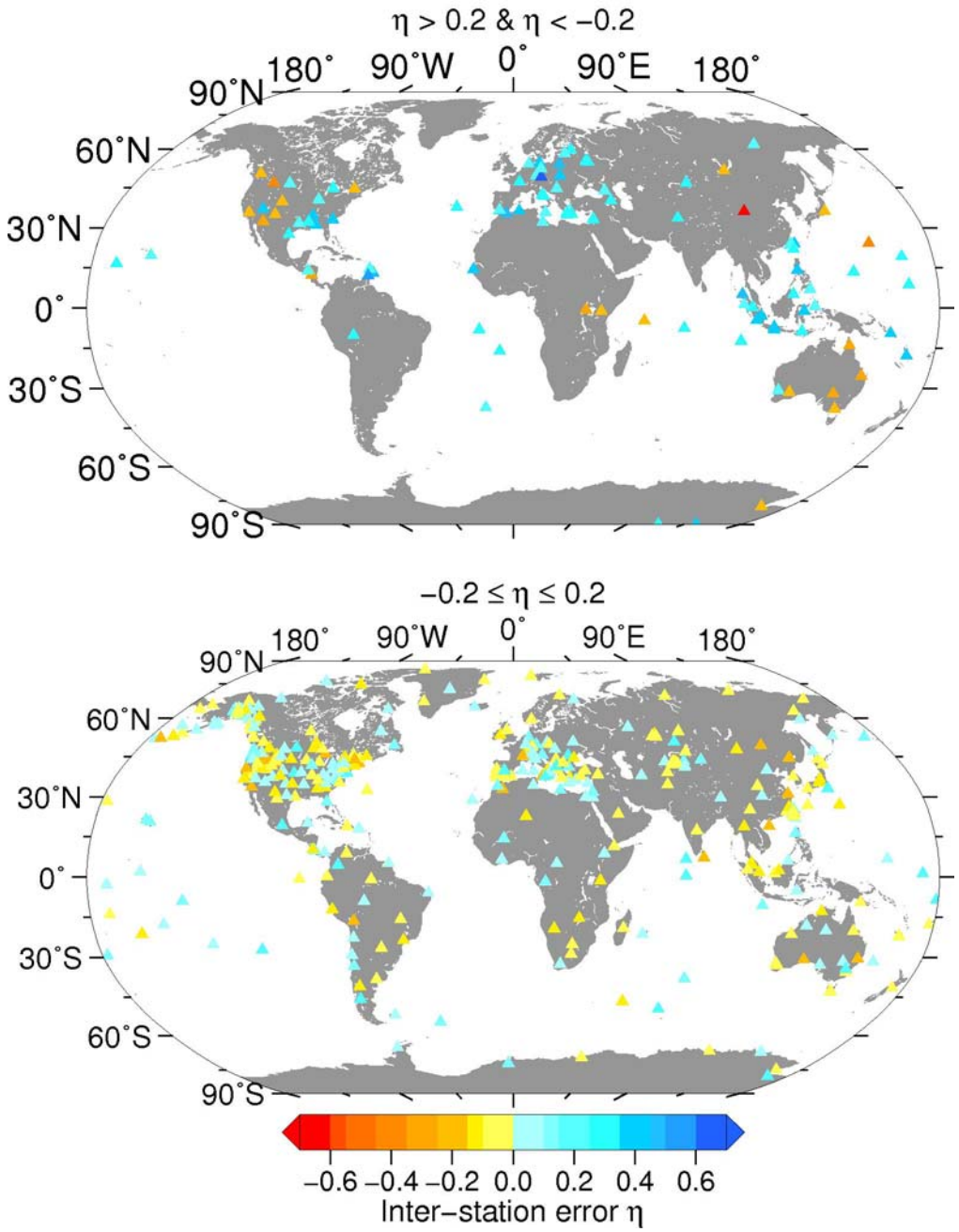

Fig. 4.4: Maps of the inter-station errors for the 476 station used in the regression analysis. Top: stations with absolute inter-station errors larger than 0.2 m.u. Bottom: inter-station errors within the range ±0.2 m.u.

Considering, however, that the velocity and attenuation models may be obtained using period ranges and wave types significantly different from the *P*-waves period range (1 to ~80 s) considered in this thesis, these kinds of

comparisons are left out in order to avoid an over-interpretation of such results.

2) Intra-station distribution of error

The standard deviation of the intra-station distribution of errors is 0.24 (Fig. 4.3, bottom panel). Removing the inter-station errors from the residual distribution leads to a reduction of the variance with respect to the residual distribution shown in Fig. 4.2. This is shown in Fig. 4.5, where the intra-station errors are computed over different distance ranges as in Fig. 4.2, with a reduction of the dispersion observed over all distance ranges.

Some stations still present few recordings with large errors clustered in time. Fig. 4.6 exemplifies the case of station ALE, whose recordings are marked in gray in Fig. 4.3 (bottom panel). The large errors correspond to earthquakes recorded between 1990 and 1993 while, after this date, the average intra-station error is almost zero. Since the dependence on time of the residuals is averaged out when computing the inter-station error, this affects the intra-station error distribution. Similar behavior is also observed at a few other stations (EIDS, FORT, KMI) indicated in Fig. 4.3.

The intra-station variability can be related to propagation or source effects. Regarding the dependence on source, Fig. 4.7 shows the intra-station residuals versus distance for the entire dataset divided into their different fault plane solution groups of Zoback (1992). The average and standard deviation of the intra-station error distributions for the different groups are very similar, suggesting that the magnitude estimates are not strongly affected, on average, by the source mechanism. This is also confirmed in Fig. 4.8, where the distribution of the intra-station errors for two stations, CHTO in Thailand and BJT in China, that recorded a large number of earthquakes, do not show any

significant trend with respect to the different fault mechanism groups. That is, the trend in the intra-station errors with both distance and backazimuth are independent of the focal mechanism. The observed scatter (similar for the different mechanisms) is related to the different propagation distances, suggesting that rays travelling at different mantle depths cross different lateral heterogeneities. This confirms the findings of Fig. 3.10 for the example of the recent great doublet in the Kuril islands that the source mechanism does not play a dominant role in the residual pattern when the average magnitude is computed over a broad range of azimuths and distances. In this sense, directivity effects, which according to Venkataraman and Kanamori (2004a) may influence single station estimates of E_S by a factor of 2-3 (that is to say 0.2-0.3 m.u.) and even more in some case, are expected to be averaged out. Moreover, considering also the fact that the distribution of intra-station errors does not show any dependence on magnitude (not shown here), the intra-station errors are, therefore, discussed in terms of path distributions only.

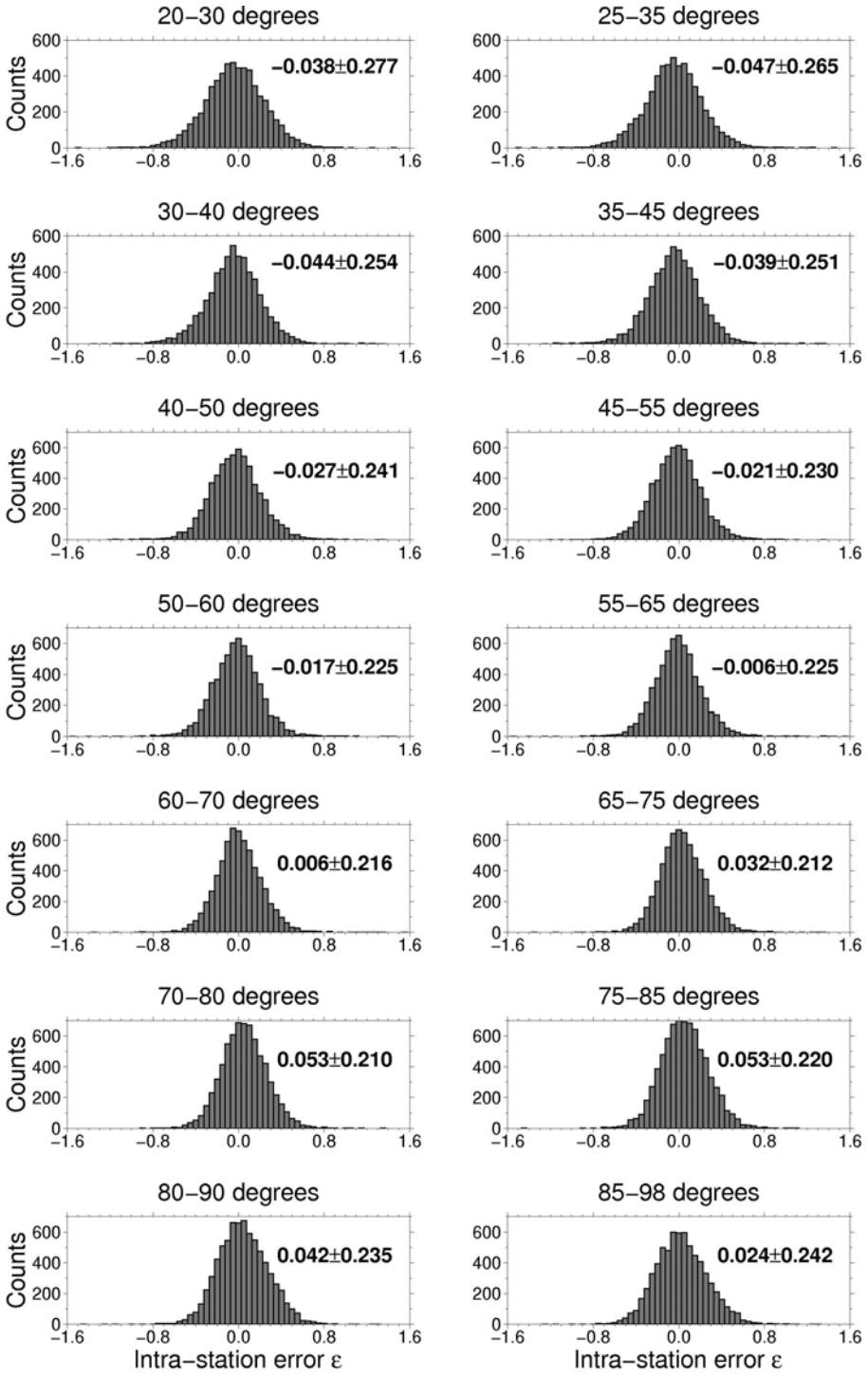

Fig. 4.5: Intra-station distributions for different distance ranges as in Fig. 4.2. In each subplot, the average ± one standard deviation is also reported.

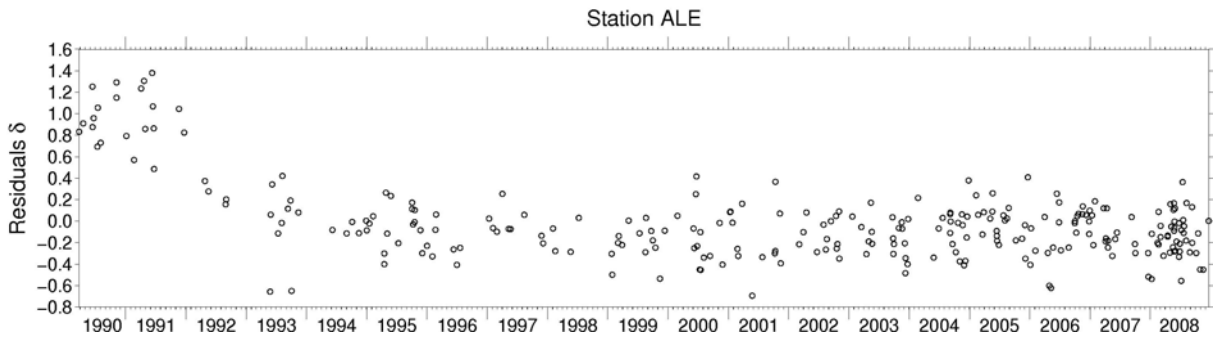

Fig. 4.6: Temporal distribution of the M_E residuals δ at station ALE (Canada).

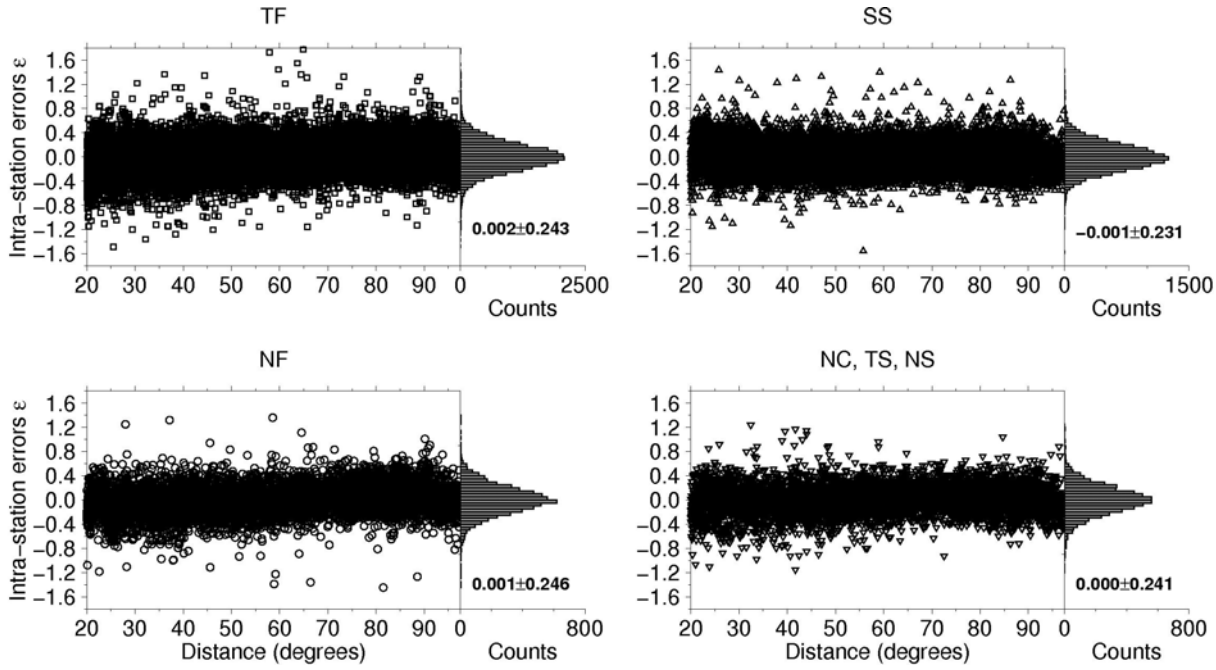

Fig. 4.7: Intra-station errors versus distance, grouped into the fault plane solution classes of Zoback (1992). TF identifies thrust, SS strike-slip, NF normal fault, NC not classified, TS thrust with strike-slip component, and NS normal with strike-slip component earthquakes, respectively. In each subplot, the average ± one standard deviation is also reported.

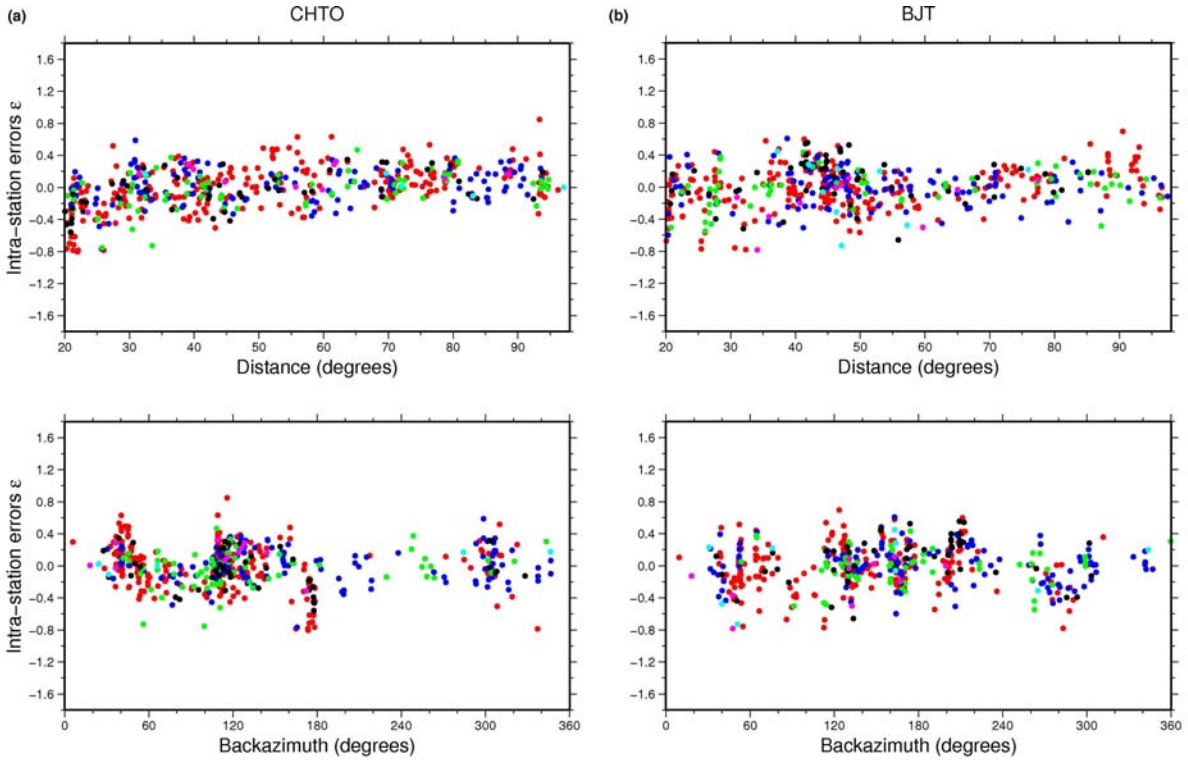

Fig. 4.8: a) Intra-station errors for station CHTO, plotted using the fault plane solution groups of Zoback (1992). The upper panel shows the intra-station error distribution versus distance, the lower one versus backazimuth. The red points refer to TF, green to NF, blue to SS, black to NC, magenta to TS and cyan to NS earthquakes, respectively. b) The same as for a) but for station BJT.

Fig. 4.9a shows the intra-station errors for station CHTO for the different travel paths. On the one hand, for earthquakes occurring in an area that ranges from Hokkaido (Japan) in the south to the Kuril and Aleutian islands in the north, the intra-station error is generally positive (only 7 negative values over 50 rays) spanning between -0.27 and 0.63. A similar pattern is found for the ray paths coming from the South Pacific Ocean, in the South-East quadrant of Fig. 4.9a. On the other hand, a clear cluster of negative intra-station error values is observed for earthquakes occurring in the Philippines Sea-Mariana islands region. For rays arriving at station CHTO from the Indian Ocean, Eurasian plate and Africa, more data are necessary before patterns in the intra-station error distributions can be identified.

In Fig. 4.9b, the propagation paths for 26 earthquakes that occurred in the Kuril islands-Japan area (latitude between 30.6°N and 52.1°N, longitude between 131°E and 150°E) are considered both at station BFO in Germany and TUC in the United States. The differences in epicentral distances for these earthquakes to the BFO and TUC locations span between 1° and 12°. Noticeably, the rays travelling to BFO have nearly zero or positive intra-station errors ($-0.007 < \varepsilon < 0.67$), whereas for the same earthquakes, rays arriving at TUC generally show negative values ($-0.32 < \varepsilon < -0.03$, with only one event having a relatively large positive ε of 0.29). As already mentioned, this outcome confirms the result of Fig. 3.10 for the great Kuril islands doublet. The most probable cause for the distinct intra-station patterns of Fig. 4.9b lies in the difference in the cumulative propagation attenuation for rays travelling mostly along continental (station BFO) or oceanic (station TUC) paths.

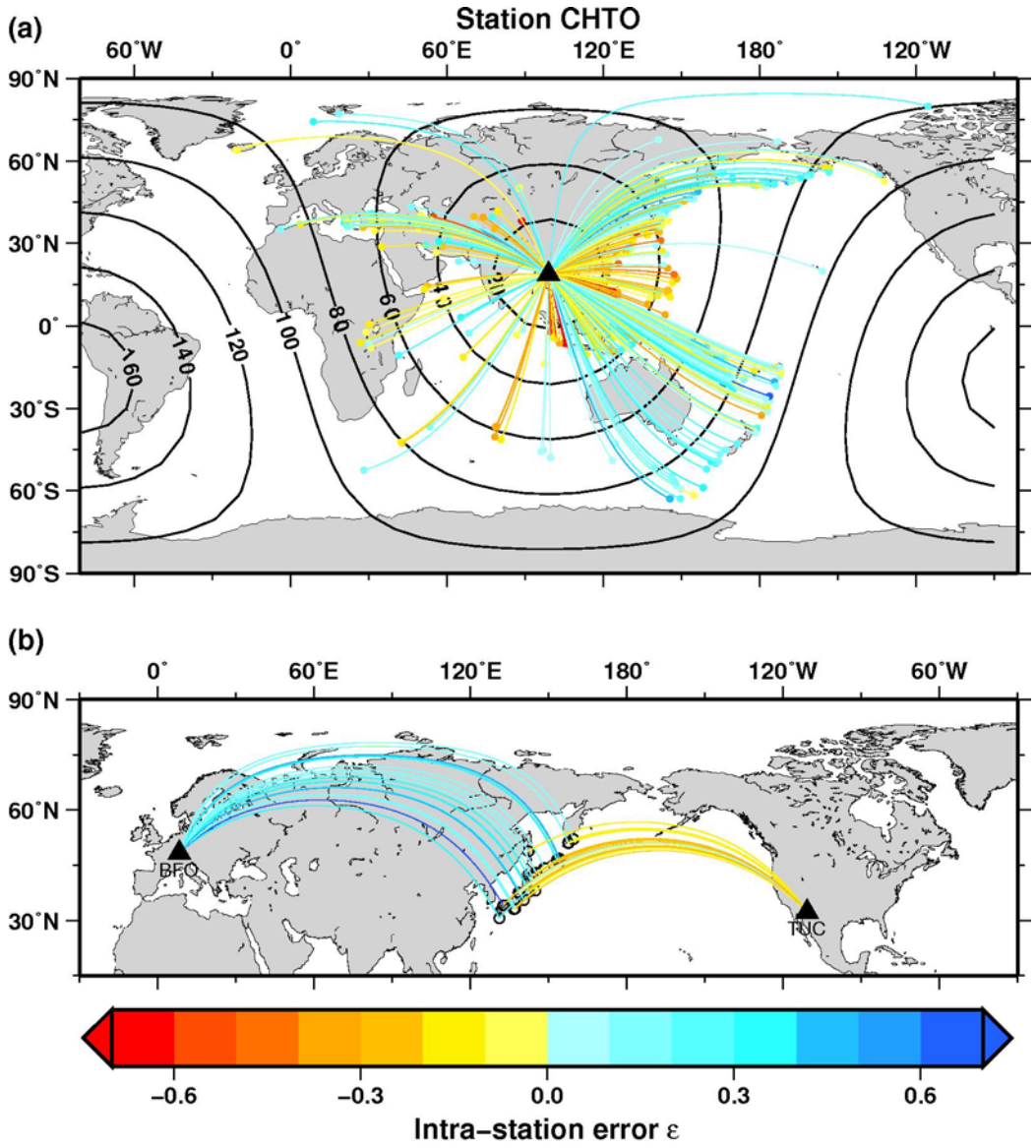

Fig. 4.9: a) Intra-station errors for about 500 earthquakes recorded at station CHTO (black triangle). b) Intra-station errors for 26 earthquakes that occurred in the Kuril islands-Japan region and were recorded by stations BFO (Germany) and TUC (USA).

4.3 Summary of the inter- and intra-station errors

The station-to-station (inter-station) and the record-to-record (intra-station) components of variability affecting the M_E estimations have been quantified by performing a regression analysis on the magnitude residuals resulting from the approach here presented. Bearing in mind that the

correction for the various propagation effects of the *P*-wave signals in the frequency band 12.4 mHz – 1 Hz is performed by using theoretical spectral amplitude decay functions based on the average global model AK135Q, the results can be summarized as follows:

1. The inter-station errors range within ±0.2 m.u. for most (78%) of the analyzed stations and the variance of their distribution is 0.159. This suggests that the 1-D model AK135Q provided a good average description of the propagation effects in the uppermost part of the lithosphere. For only a few stations, the inter-station error exceeds 0.5 m.u. in absolute value, which may result not only from the effect of the shallow structure but most probably also from miss-calibration effects. The geographical distribution of the relatively large positive and negative inter-station errors can be reasonably well explained by considering the shallow velocity structure anomalies observed by different authors (as discussed for North America and Europe).
2. The variance of the intra-station distribution of error is 0.24 and is the largest component of variability affecting the M_E estimates. It is generally independent of fault plane geometry as the intra-station error distributions for different fault plane solution groups do not show any significant trend with distance and backazimuth. On the other hand, the intra-station errors are not random with respect to the travel paths, and the inter-station error may vary significantly at a given station for rays coming from different seismogenic areas. Moreover, oceanic and continental paths may show distinct inter-station error patterns for the same earthquakes.

Large intra-station errors at a few stations are also due to important temporal variations in the original residuals distribution. This may be due to

instrumental problems during particular time periods, hence the residuals themselves could be used as simple and quick indicators to detect such problems. With the increasing number of stations deployed worldwide and, as a result, the increasing availability of seismic data, the outcomes of this study can be used in the future to improve M_E estimates by applying sets of coefficients empirically determined to account for the heterogeneities of the real Earth. Such heterogeneities may significantly influence the medium-to-short period teleseismic *P*-wave signals and are not considered in the theoretical calculations of Green's functions used to correct the recorded data for geometrical spreading and anelastic attenuation given the 1-D average global model AK135Q.

CHAPTER 5

Conclusions and outlook

The thesis has focused on the determination of the energy magnitude M_E for application to rapid response purposes. Indeed, despite the importance of this magnitude scale in the evaluation of an earthquake's damage potential, the use of M_E in this sense has been limited (if not absent) since a procedure to rapidly calculate it was missing.

A rapid and robust procedure to calculate M_E in a short time after OT using *P*-waves of teleseismic seismograms in the distance range 20°-98° has been presented. The correction for the propagation path effects is accomplished by applying pre-calculated spectral amplitude decay functions for different frequencies, that have been computed using numerical simulations of Green's functions based on the reference Earth model AK135Q. The calculation of M_E is performed using time-variable cumulative energy windows in order to avoid the problem of the time window saturation effect in magnitude determination. Being the spectral amplitude decay functions available in a tabulated form similarly to the $Q(\Delta, h)$ functions for computing m_B, the proposed procedure to determine M_E can be easily implemented in rapid response systems. Indeed, it has been shown that this approach would allow determinations of M_E within minutes of the first *P*-wave arrival, even for great earthquakes with very long rupture duration, such as the 26 December, 2004 Sumatra earthquake.

It has been shown, then, that the moment magnitude M_W alone brings only limited information about the source characteristics. A better evaluation

of an earthquake's damage potential (both in terms of shaking and tsunami) would benefit by the joint use of the information provided by M_W and M_E. This has been highlighted by the comparisons of M_W and M_E for a large global dataset. These two modern non-saturating magnitude scales may differ of several magnitude units since they reflect different aspects of the seismic source properties. Indeed, M_W better represents the static properties of the source (e.g., the overall final displacement and rupture area), which are fundamental for assessing the earthquake's tsunamigenic potential, whereas M_E is more suitable to quantify the fraction of energy involved in the rupture process that is transformed into seismic waves. To further stress this point, representative examples of close-by pair of earthquakes with similar M_W but very different M_E have been analyzed in different seismotectonic regions. Since the propagation paths for the respective event pairs are almost identical, the differences in the observed spectral contents can be attributed mainly to differences in source dynamics, and it has been shown that M_E is sensitive to the relative amount of more high-frequency energy radiated by the seismic source, in contrast to M_W, that is controlled by the asymptotic low-frequency amplitudes only. Moreover, it has also been shown that even earthquakes with very similar focal mechanism and seismic moment occurring in the same seismo-tectonic area may radiate significantly different amounts of seismic energy. This highlights the need to introduce joint rapid routine measurements of both M_W and M_E in global seismic monitoring practice. In addition, it has been shown the usefulness of rapid M_E determinations as complement to M_W for tsunami early warning systems, although, beside the seismological information, the use of off-shore data would be necessary to enhance a tsunami warning system's performance, and possibly decrease the number of false alarms.

Since the proposed procedure is intended to work without knowledge of the source geometry (usually available several minutes or hours after OT), the earthquakes have been classified by their GCMT fault plane solutions according to Zoback (1992). This step has been performed in order to discuss possible effects of the focal mechanism on the M_E determinations. It has been shown that the rapid $M_{E(GFZ)}$ does not show any clear trend with the different fault plane solution groups both for the comparisons with M_W as well as for the classical M_S, m_B and m_b scales. This is not the case for the M_E routinely determined by the USGS, which apply focal-specific corrections (Boatwright and Choy, 1986). Indeed, for strike-slip earthquakes $M_{E(USGS)}$ is almost systematically larger than the other types of mechanisms, as shown both for the comparisons with M_W and the classical magnitude scales. This suggests that $M_{E(USGS)}$ strongly depend on focal mechanism corrections for strike-slip earthquakes. This has already been noted by previous studies. In this context it has to be stressed that none of the classical magnitude procedures, to which also M_W and M_E have been scaled (see Bormann et al., 2009), foresees a priori corrections of the measured amplitudes depending on the source mechanism. This may explain why the uncorrected $M_{E(GFZ)}$ values scale more linear and with less scatter than $M_{E(USGS)}$ with $M_{W(GCMT)}$.

The final part of the thesis investigated and quantified the influence of propagation and site effects on the variability of the single station $M_{E(GFZ)}$ estimations. This has been done by exploiting the redundancy of the information provided by the analyzed dataset (~48000 single station M_E determinations from ~1000 earthquakes globally distributed recorded at 476 seismic station, for which the different source-receiver paths sample a large volume of the Earth's interior) by performing a regression analysis on the

magnitude residuals. The station-to-station (inter-station) error range within ±0.2 m.u. for most (78%) of the analyzed stations and the variance of their distribution is 0.159. This suggests that the model AK135Q allows for a good average description of the propagation effects in the uppermost part of the lithosphere. Only for a few stations, the inter-station error exceeds 0.5 magnitude units in absolute value (most probably due to miss-calibration effects). The record-to-record (intra-station) errors are the largest component of variability affecting the M_E estimates. It is substantially independent on the fault plane geometry but is not random with respect to the travel paths, since the inter-station errors may vary significantly at a given station for rays coming from different seismogenic areas. In the future the M_E estimates may be improved by applying sets of coefficients empirically determined to account for the heterogeneities of the real Earth (which may significantly influence the medium-to-short period teleseismic *P*-wave signals) not considered in the theoretical calculations of Green's functions used to correct the recorded data for geometrical spreading and anelastic attenuation given the average global model AK135Q.

Future works have to be focused on the comparison of the teleseismic estimations of M_E with the analysis of local/regional data. This is a fundamental task in order to ultimately demonstrate the superiority of M_E in the evaluation of the shaking potential of an earthquake. One of the regions where it is possible to retrieve and analyze enough data both in the teleseismic and local/regional distance range is the seismogenic area of the Japan arc. Fig. 5.1 considers the interesting example of three earthquakes occurring in the south of Japan: the M_W = 6.65 Tottori strike-slip earthquake of 2000 October 6, the M_W = 6.70 Kyushu thrust earthquake of 1996 October 19, and the M_W =

6.80 Geiyo normal-fault earthquake of 2001 March 24. These earthquakes are very compact in space (the maximum inter-epicentral distance is distance is ~420 km between the 1996 Kyushu and 2000 Tottori earthquakes), therefore the difference in the travel path to common stations is negligible, and also they have very similar M_W and are representative of the main three groups of fault plane solutions (TF, SS, and NF). The map in Fig. 5.1 shows the earthquake locations (along with their beach-ball representations in the inset) with the respective locations of the stations used to obtain $M_{E(GFZ)}$, and, in the lower panels, the spectral amplitudes decay for four representative frequencies. It is worth noting as for 1 Hz the observed amplitudes relative to the Geiyo earthquake are in general larger than the one of the Tottori and Kyushu earthquakes, and also that the amplitudes for all the considered frequencies relative to the Tottori earthquake are in general below the spectral amplitude of the Geiyo and Kyushu earthquakes. These mutual differences in the teleseismic spectral amplitudes are, however, not extremely large and they are translated in $M_{E(GFZ)}$ = 6.74, 6.76 and 6.95 for the Tottori, Kyushu and Geiyo earthquakes, respectively. The respective $M_{E(USGS)}$ values are 7.37, 6.61 and 6.23. Thus, the larger $M_{E(USGS)}$ value is obtained for the Tottori strike-slip earthquake and the smaller value for the Geiyo normal-fault earthquake. This confirms the outcomes of the magnitude comparisons that $M_{E(USGS)}$ is generally larger for SS events with respect to the other mechanism types.

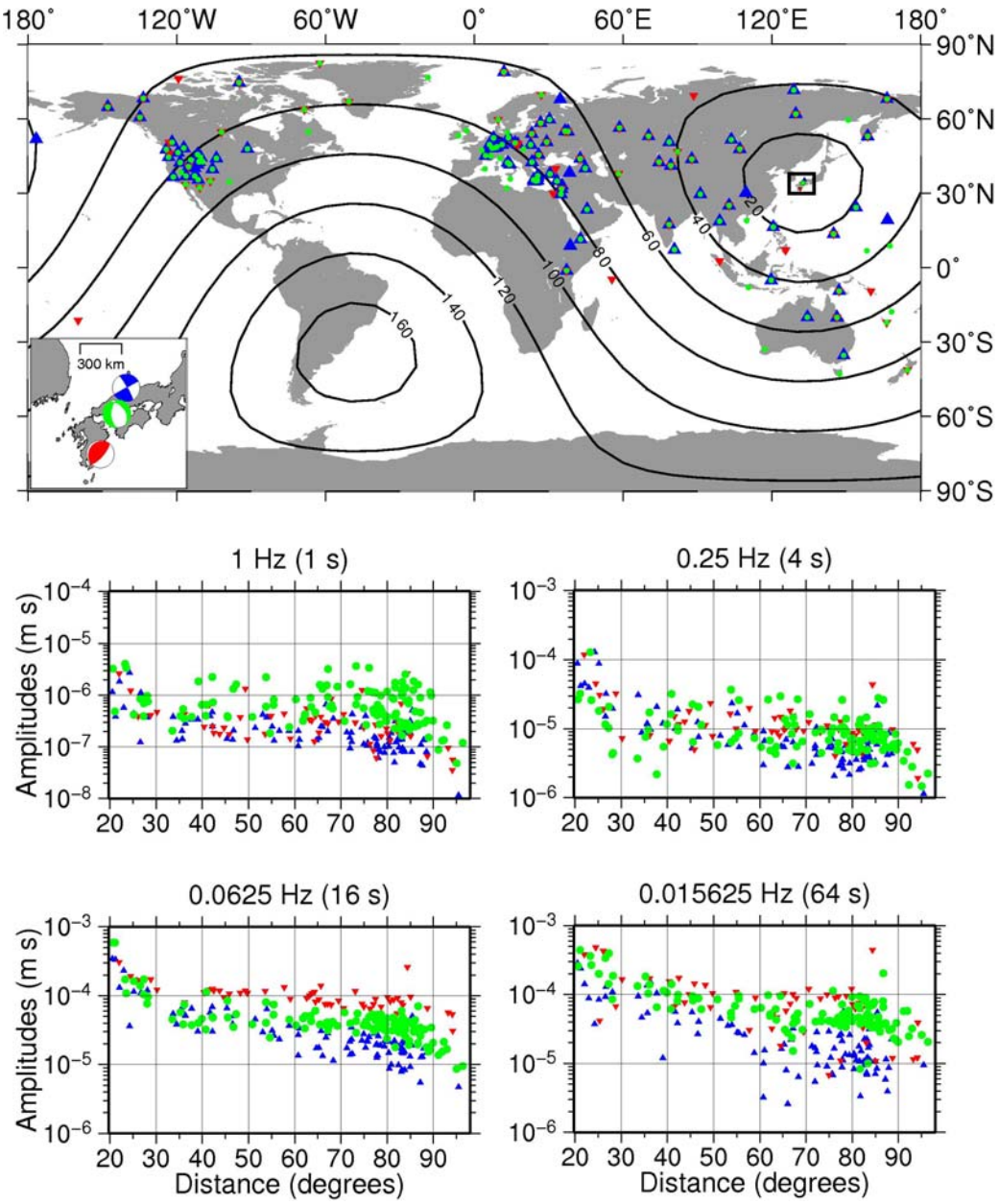

Fig. 5.1: Top: Global distributions of seismic stations which recorded the M_W = 6.65 Tottori 2000 strike-slip earthquake, the M_W = 6.70 1996 Kyushu thrust earthquake and the M_W = 6.80 Geiyo 2001 normal-fault earthquake (the inset shows their GCMT fault plane solutions). The solid curves represent the distance in degrees from the Geiyo 2001 earthquake. Bottom: Spectral amplitudes measured at different frequencies (periods) at different seismic stations between $20° \leq \Delta < 98°$ epicentral distance. The color of the beach-ball representations in the global map corresponds with the symbol color of the recording stations and the measured spectral amplitudes: blue triangles – Tottori 2000 strike-slip earthquake; red inverted triangles – 1996 Kyushu thrust earthquake; green circles – Geiyo 2001 normal-fault earthquake. There is no obvious and unique mechanism-dependent trend in the level of plotted spectral amplitudes.

However, the analysis of local/regional data (K- and KiK-net) via the Generalized Inversion Technique performed by Oth et al. (2010) shows that

the source spectral shapes of these earthquakes agree rather well with the $M_{E(GFZ)}$ results. Indeed, Fig 5.2 shows that the source spectral shape of the Geiyo earthquake is slightly larger than the ones of the Kyushu and Tottori, and also that the Kyushu earthquake is comparable with the source shape of the Tottori earthquake.

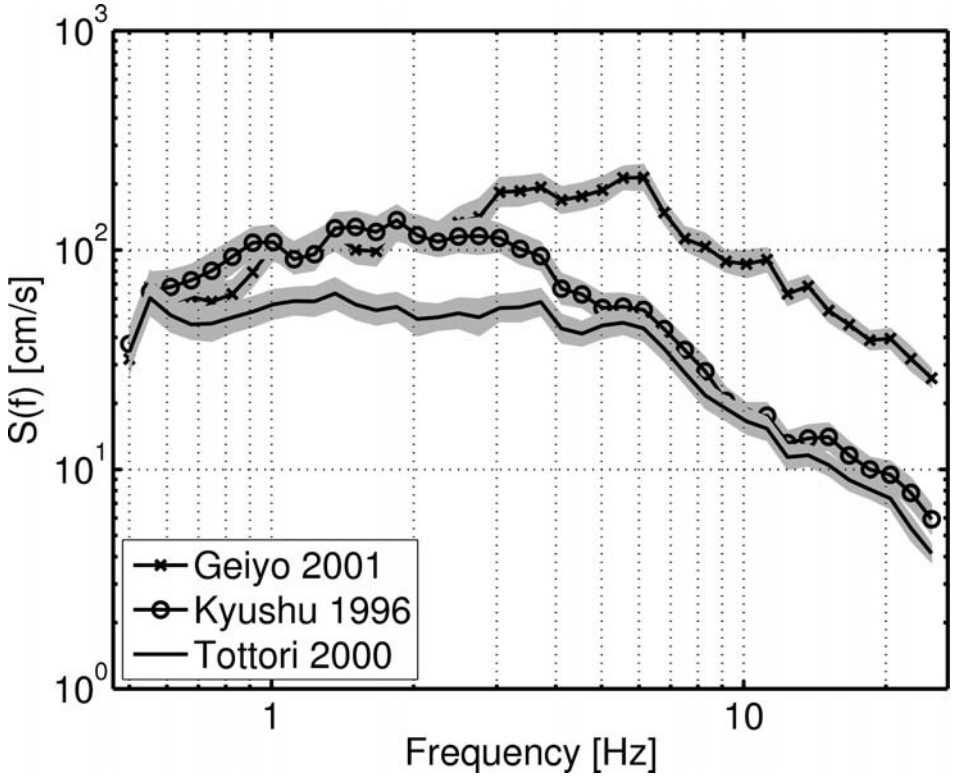

Fig. 5.2: Acceleration source contribution for the three Japanese earthquakes of Fig. 5.1 obtained from inversion of local/regional data. Courtesy of A. Oth.

These comparisons of teleseismic and local/regional data will help in clarifying the effects of theoretically-based radiation pattern corrections on M_E estimates and will be also fundamental for establishing M_E as one of reference magnitudes in applications relevant for seismic hazard studies, ShakeMap and loss estimations.

References

Abe, K. (1981). Magnitudes of large shallow earthquakes from 1904 to 1980, *Phys. Earth Planet. Interiors* **27**, 72-92.

Abercrombie, R. E. (1995). Earthquake source scaling relationships from -1 to 5 M_L using seismograms recorded at 22.5 km depth, *J. Geophys Res.* **100**, 24,015-24,036.

Abrahamson, N. A., and R. R. Youngs (1992). A stable algorithm for regression analyses using the random effect model, *Bull. Seism. Soc. Am.* **82**(1), 505-510.

Aki, K. (1966). Generation and propagation of *G* waves from the Niigata earthquake of June 16, 1964, part 2: Estimation of earthquake moment, released energy, and stress-strain drop from the *G* wave spectrum, *Bull. Earthq. Res. Inst. Tokyo Univ.* **44**, 73-88.

Aki, K. (1967). Scaling law of seismic spectrum, *J. Geophys. Res.* **72**, 1217-1231.

Aki, K., and P. Richards (1980). Quantitative Seismology. Theory and Methods, *Freeman*, *San Francisco*, *CA*, 932 pp.

Ammon, C. J., H. Kanamori, and T. Lay (2008). A great earthquake doublet and seismic stress transfer cycle in the central Kuril islands, *Nature* **451**, 561-65, doi:10.1038/nature06521.

Beresnev, I. (2009). The reality of the scaling law of earthquake-source spectra?, *J. Seismology* **13**, 433-436, DOI 10.1007/s10950-008-9136-9.

Bird, P. (2003). An updated digital model of plate boundaries, *Geochem. Geophys. Geosyst.* **4**(3), 1027, doi:10.1029/2001GC000252.

Boatwright, J., and J. B. Fletcher (1984). The partition of radiated energy between P and S waves, *Bull. Seism. Soc. Am.* **74**(2), 361-376.

Boatwright, J., and G. L. Choy (1986). Teleseismic estimates of the energy radiated by shallow earthquakes, *J. Geophys. Res.* **91**, 2095-2112.

Bormann, P., M. Baumbach, M. Bock, H. Grosser, G. L. Choy, and J. Boatwright (2002). Seismic sources and source parameters, in: Bormann, P. (ed), in *IASPEI New Manual Seismological Observatory Practice*, *GeoForschungsZentrum Potsdam*, Vol. **1**, Chapter 3, 94 pp.

Bormann, P., R. Liu, X. Ren, R. Gutdeutsch, D. Kaiser, and S. Castellaro (2007). Chinese National Network magnitudes, their relation to NEIC Magnitudes, and recommendations for new IASPEI magnitude standards, *Bull. Seism. Soc. Am.* **97**, 114-127, doi:10.1785/0120060078.

Bormann, P., and J. Saul (2008). The new IASPEI standard broadband magnitude m_B, *Seismol. Res. Lett.* **79**(5), 699-706.

Bormann, P., and J. Saul (2009a). Earthquake magnitude, in *Encyclopedia of Complexity and Systems Science*, ed. R. Meyers, *Springer, Heidelberg-New York*, Vol. **3,** 2473-2496.

Bormann, P., and J. Saul (2009b). A fast, non-saturating magnitude estimator for great earthquakes, *Seism. Res. Lett.* **80**(5), 808-816; doi: 10.1785/gssrl.80.5.808.

Bormann P, R. Liu, Z. Xu, K. Ren, L. Zhang, and S. Wendt (2009). First application of the new IASPEI teleseismic magnitude standards to data of the China National Seismographic Network, *Bull. Seism. Soc. Am.* **99**(3), 1868-1891, doi: 10.1785/0120080010.

Bormann, P., and D. Di Giacomo (2010). The moment magnitude M_w and the energy magnitude M_e: common roots and differences, submitted to *Journal of Seismology*.

Brillinger, D. R., and H. K. Preisler (1985). Further analysis of the Joyner-Boore attenuation data, *Bull. Seism. Soc. Am.* **75**(2), 611-614.

Brune, J. N. (1970). Tectonic stress and the spectra of shear waves from earthquakes, *J. Geophys. Res.* **75**, 4997-5009.

Burdick, S., R. D. van der Hilst, F. L. Vernon, V. Martynov, T. Cox, J. Eakins, T. Mulder, L. Astiz, and G. L. Pavlis (2009). Model Update December 2008: Upper Mantle Heterogeneity beneath North America from P-wave Travel

Time Tomography with Global and USArray Transportable Array Data, *Seism. Res. Lett.* **80**(4), 638-645, doi: 10.1785/gssrl.80.4.638

Choy, G. L., and J. Boatwright (1995). Global patterns of radiated seismic energy and apparent stress, *J. Geophys. Res.* **100**, 18,205-18,228.

Choy, G. L., and S. Kirby (2004). Apparent stress, fault maturity and seismic hazard for normal-fault earthquakes at subduction zones, *Geophys. J. Int.* **159**, 991-1012.

Choy, G. L., A. McGarr, S. H. Kirby, and J. Boatwirght (2006). An overview of the global variability in radiated energy and apparent stress, in Abercrombie, R., A. McGarr, and H. Kanamori (eds): *Radiated energy and the physics of earthquake faulting*, *AGU Geophys. Monogr. Ser.* **170**, 43-57.

Choy, G. L, and J. Boatwright (2007). The energy radiated by the 26 December 2004 Sumatra-Andaman earthquake estimated from 10-minute P-wave windows, *Bull. Seism. Soc. Am.* **97**(1), S18-S24.

Di Bona, M., and A. Rovelli (1988). Effects of bandwidth limitation on stress drop estimated from integrals of the ground motion, *Bull. Seism. Soc. Am.* **78**, 1818-1825.

Di Giacomo, D., H. Grosser, S. Parolai, P. Bormann, and R. Wang (2008). Rapid determination of Me for strong to great shallow earthquakes, *Geophys. Res. Lett.* **35**, L10308, doi:10.1029/2008GL033505.

Di Giacomo, D., S. Parolai, P. Bormann, H. Grosser, J. Saul, R. Wang, and J. Zschau (2010a). Suitability of rapid energy magnitude estimations for emergency response purposes, *Geophys. J. Int.*, **180***,* 361-374, doi: 10.1111/j.1365-246X.2009.04416.x.

Di Giacomo, D., S. Parolai, P. Bormann, H. Grosser, J. Saul, R. Wang, and J. Zschau (2010b). Erratum to "Suitability of rapid energy magnitude estimations for emergency response purposes", *Geophys. J. Int.*, in press.

Di Giacomo, D., and S. Parolai (2010). Is the detection of earthquakes depleted in their high frequency content sufficient for tsunami warning systems?, submitted to *Natural Hazards*.

Di Giacomo, D., D. Bindi, S. Parolai, and A. Oth (2010). Residual analysis of teleseismic P-wave energy magnitude estimates: inter- and intra-station variability, submitted to *Phys. Earth Planet. Interiors*.

Duda, S. J., and T. B. Yanovskaya (1993). Spectral amplitude-distance curves for P-waves: effects of velocity and Q-distribution, *Tectonophysics* **217**, 255-265.

Dziewonski, A. M., and D. L. Anderson (1981). Preliminary reference Earth model, *Phys. Earth Planet. Interiors* **25**, 297-356.

Dziewonski, A. M., T. A. Chou, and J. H. Woodhouse (1981). Determination of earthquake source parameters from waveform data for studies of global and regional seismicity, *J. Geophys. Res.* **86**, B4, 2825-2852.

Gilbert, F., and G. Backus (1968). Elastic-gravitational vibrations of a radially stratified sphere, in *Dynamics of Stratified Solids*, ed. G. Hermann, *Am. Soc. Mech. Eng.*, New York, NY, 82–95.

Goes, S. D. B., A. A. Velasco, S. Y. Schwartz, and T. Lay (1993). The April 22, 1991, Valle de la Estrella, Costa Rica (Mw = 7.7) earthquake and its tectonic implications: a broadband seismic study, *J. Geophys. Res.* **98**, B5, 8127-8142.

Gutenberg, B. (1945a). Amplitude of surface waves and magnitude of shallow earthquakes, *Bull. Seism. Soc. Am.* **35**, 3-12.

Gutenberg, B. (1945b). Amplitudes of P, PP, and S and magnitude of shallow earthquakes, *Bull. Seism. Soc. Am.* **35**, 57-69.

Gutenberg, B. (1945c). Magnitude determination of deep-focus earthquakes, *Bull. Seism. Soc. Am*. **35**, 117-130.

Gutenberg, B., and C. F. Richter (1956a). Magnitude and energy of earthquakes, *Annali di Geofisica* **9**, 1-15.

Gutenberg, B., and C. F. Richter (1956b). Earthquake magnitude, intensity, energy and acceleration, *Bull. Seism. Soc. Am.* **46**, 105-145.

Grosser, H., M. Baumbach, H. Berkhemer, B. Baier, A. Karahan, H. Schelle, F. Krüger, A. Paulat, G. Michel, R. Demirtas, S. Gencoglu, and R. Yilmaz (1998). The Erzincan (Turkey) earthquake (M_S 6.8) of March 13, 1992 and ist aftershock sequence, *Pure Appl. Geoph.* **152**(3), 465-505.

Hanks, C., and H. Kanamori (1979). A moment magnitude scale, *J. Geophys. Res.* **84**, 2348-2350.

Haskell, N. A. (1964). Total energy and energy spectral density of elastic wave radiation from propagating faults, *Bull. Seism. Soc. Am.* **54**(6), 1811-1841.

Houston, H., and H. Kanamori (1986). Source spectra of great earthquakes: teleseismic constraints on rupture process and strong motion, *Bull. Seism. Soc. Am*. **76**(1), 19-42

Hydayat, D., J. S. Barker, and K. Satake (1995). Modelling the seismic source and tsunami generation of the December 12, 1992 Flores Island, Indonesia, earthquake, *Pure Appl. Geoph.* **144**(3/4), 537-554.

IASPEI, (2005). Summary of Magnitude Working Group recommendations on standard procedures for determining earthquake magnitudes from digital data, http://www.iaspei.org/commissions/CSOI.html

Ide, S., and G. C Beroza (2001). Does apparent stress vary with earthquake size? *Geophys. Res. Lett.* ***28***(17), 3349-3352.

Imamura, F., E. Gica, T. Takahashi, and N. Shuto (1995). Numerical simulation of the 1992 Flores tsunami: interpretation of tsunami phenomena in Northeastern Flores Island and damage at Babi Island, *Pure Appl. Geoph.* **144**(3/4), 555-568.

Kanamori, H. (1972). Mechanism of tsunami earthquakes, *Phys. Earth Planet. Interiors* **6**, 346-359.

Kanamori, H. (1977). The energy release in great earthquakes, *J. Geophys. Res*. **82**, 2981-2987.

Kanamori, H. (1983). Magnitude scale and quantification of earthquakes, *Tectonophysics* **93**, 185-199.

Kanamori, H., and E. E. Brodsky (2004). The physics of earthquakes, *Rep. Prog. Phys.* **67**, 1429-1496, doi: 10.1088/0034-4885/67/8/R03.

Kanamori, H., and M. Kikuchi (1993). The 1992 Nicaragua earthquake: a slow tsunami earthquake associated with subducted sediments, *Nature* **361**, 714-716.

Kanamori, H., and L. Rivera (2008). Source inversion of W phase: speeding up seismic tsunami warning, *Geophys. J. Int*. **175**, 222-238.

Kennett, B. L. N., E. R. Engdahl, and R. Buland (1995). Constraints on seismic velocities in the Earth from traveltimes, *Geophys. J. Int*. **122**, 108-124.

Knopoff, L. (1958). Energy release in earthquakes, *Geophys. J.* **1,** 44-52.

Koulakov, I., M. K. Kaban, M. Tesauro, and S. Cloetingh (2009). *P*- and *S*-velocity anomalies in the upper mantle beneath Europe from tomographic inversion of ISC data, *Geophys. J. Int.* **179**, 345-366, doi: 10.1111/j.1365-246X.2009.04279.x.

Kuenza, K., and C. Soon-Hoe (2010). Anatomy of the 17 July 2006 Java earthquake reveals its tsunamigenic nature, *Seism. Res. Lett.* **81**(1), 99-112, doi: 10.1785/gssrl.81.1.99.

Lomax, A., A. Michelini and A. Piatanesi (2007). An energy-duration procedure for rapid and accurate determination of earthquake magnitude and tsunamigenic potential, *Geophys. J. Int*. **170**, 1195-1209, doi: 10.1111/j.1365-246X.2007.03469.x.

Lomax, A., and A. Michelini (2009a). M_{wpd}: a duration-amplitude procedure for rapid determination of earthquake magnitude and tsunamigenic potential from *P* waveforms, *Geophys. J. Int*. **176**, 200-214, doi: 10.1111/j.1365-246X.2008.03974.x.

Lomax, A., and A. Michelini (2009b). Tsunami early warning using earthquake rupture duration, *Geophys. Res. Lett.* **36**, L09306, doi: 10.1029/2009GL037223.

Montagner, J.-P., and B. L. N. Kennett (1996). How to reconcile body-wave and normal-mode reference Earth models?, *Geophys. J. Int.* **125**, 229-248.

Newman, A. V., and E. A. Okal (1998). Teleseismic estimates of radiated seismic energy: the E/M_0 discriminant for tsunami earthquakes, *J. Geophys. Res.* **103***,* B11, 26,885-26,898.

Ni, S., H. Kanamori, and D. Helmberger (2005). Energy radiation from the Sumatra earthquake, *Nature* **434**, 582.

Okal, E. A. (1988). Seismic parameters controlling far-field tsunami amplitudes: a review, *Natural Hazards* **1**, 67-96.

Okal, E. A., and J. Talandier (1989). *Mm*: a variable-period mantle magnitude, *J. Geophys. Res.* **94***,* B4, 4169-4193.

Orowan, E. (1960). Mechanisms of seimic faulting in rock deformation: a symposium, *Geol. Soc. Am. Mem.* **79**, 323-345.

Oth, A., D. Bindi, S. Parolai, and D. Di Giacomo (2010). Spectral analysis of K- and KiK-net data in Japan II – On attenuation characteristics, source parameters and site response of borehole and surface stations, submitted to *Bull. Seism. Soc. Am.*

Parolai, S., D. Bindi, E. Durukal, H. Grosser, C. Milkereit (2007). Source parameter and seismic moment-magnitude scaling for northwestern Turkey, *Bull. Seim. Soc. Am.* **97**(2), 655-660.

Parolai, S. (2009). Denoising of seismograms using the *S* transform, *Bull. Seism. Soc. Am.* **99**(1)*,* 226-234, doi:10.1785/0120080001.

Pelayo, A. M., and D. A. Wiens (1992). Tsunami earthquakes: thrust-faulting events in the accretionary wedge, *J. Geophys. Res.* **97***,* B11, 15,321-15,337.

Pérez-Campos, X., and G. C. Beroza (2001). An apparent mechanism dependence of radiated seismic energy, *J. Geophys. Res.* **106***,* B6, 11,127-11,136.

Polet, J., and H. Kanamori (2000). Shallow subduction zone earthquakes and their tsunamigenic potential, *Geophys. J. Int.* **142**, 684-702.

Polet, J., and H. K. Thio (2003). The 1994 Java tsunami earthquake and its "normal" aftershocks, *Geophys. Res. Lett.* **30**(9), 1474, doi:10.1029/2002GL016806.

Polet, J., and H. Kanamori (2009). Tsunami earthquakes, in *Encyclopedia on Complexity and Systems Science*, *10*, Meyers, R. A. (Ed.), Springer, 9577-9592.

Purcaru G., and H. Berckhemer (1978). A magnitude scale for very large earthquakes, *Tectonophysics* **49**, 189-198.

Richeter, C. F., (1935). An instrumental earthquake magnitude scale, *Bull. Seism. Soc. Am.* **25**(1), 1-32.

Rudnicki, J. W., and L. B. Freund (1981). On energy radiation from seismic sources, *Bull. Seism. Soc. Am.* **71**(3), 583-595.

Satake, K., and Y. Tanioka, (1995). Tsunami generation of the 1993 Hokkaido Nansei-Oki earthquake, *Pure Appl. Geoph.* **145**(3/4), 803-821.

Savage, J. C., and M. D. Wood (1971). The relation between apparent stress and stress drop, *Bull. Seism. Soc. Am.* **61**, 1381-1388.

Schweitzer, J., and T. Kværna (1999). Influence of source radiation patterns on globally observed short-period magnitude estimates (mb), *Bull. Seism. Soc. Am.* **89**(2), 342-347.

Singh, S. K., and M. Ordaz (1994). Seismic energy release in Mexican subduction zone earthquakes, *Bull. Seism. Soc. Am.* **84**(5), 1533-1550.

Sipkin, S. A. (1994). Rapid determination of global moment-tensor solutions, *Geophys. Res. Lett.* **21**, 1667-1670.

Stockwell, R. G., L. Mansinha, and R. P. Lowe (1996). Localization of the complex spectrum: the *S* transform, *IEEE Trans. Signal Process.* **44**, 998-1001.

Tanioka, Y., and K. Satake (1996). Tsunami generation by horizontal displacement of ocean bottom, *Geophys. Res. Lett.* **23**(8), 861-864.

Tsuboi, S., K. Abe, K. Takano, and Y. Yamanaka (1995). Rapid determination of *Mw* from broadband *P* waveforms, *Bull. Seism. Soc. Am.* **85**(2), 606-613.

Vassiliou, M. S., and H. Kanamori (1982). The energy release in earthquakes, *Bull. Seism. Soc. Am.* **72**(2), 371-387.

Venkataraman, A., and H. Kanamori (2004a). Effect of directivity on estimates of radiated seismic energy, *J. Geophys. Res.* **109**, B04301, doi:10.1029/2003JB002548.

Venkataraman, A., and H. Kanamori (2004b). Observational constraints on the fracture energy of subduction zone earthquakes, *J. Geophys. Res.* **109**, B04301, doi: 0431.01029JB002549.

Wang, R. (1999). A simple orthonormalization method for stable and efficient computation of Green's functions, *Bull. Seism. Soc. Am.* **89**(3), 733-741.

Weinstein, S. A., and E. A. Okal (2005). The mantle wave magnitude M_m and the slowness parameter Θ: Five years of real-time use in the context of tsunami warning, *Bull. Seism. Soc. Am.* **95**(3), 779-799; doi: 10.1785/0120040112

Wyss, M. (1968). Observation and interpretation of tectonic strain release mechanisms, *Ph.D. Thesis*, California Institute of Technology, Pasadena.

Zoback, M. L. (1992). First- and second-order patterns of stress in the lithosphere: the World Stress Map project, *J. Geophys. Res.* **97**, B8, 11,703-11,728.

TABLE A1: List of source and magnitude parameters of the analyzed earthquakes

ID-Nr	Origin time	Long.	Lat.	h(km)	Mw(USGS)	Mw(GCMT)	Mec.	Me(USGS)	Me(GFZ)	REGION
#1	1990-03-03 12:16:27.96	175.163	-22.122	33.0	7.34	7.59	SS	7.22	7.27	SOUTH-OF-FIJI-ISLANDS
#2	1990-03-05 16:38:12.57	168.063	-18.318	33.0	7.08	6.95	TF	6.48	6.59	VANUATU-ISLANDS
#3	1990-03-25 13:22:55.60	-84.808	9.919	19.0	na	7.29	TF	6.63	6.95	COSTA-RICA
#4	1990-04-05 21:12:35.55	147.596	15.125	32.0	7.14	7.41	NF	7.50	7.71	MARIANA-ISLANDS-REGION
#5	1990-04-18 13:39:19.01	122.857	1.186	28.0	7.36	7.61	TF	7.20	7.34	MINAHASSA-PENINSULA
#6	1990-05-20 02:22:01.62	32.145	5.121	7.0	7.18	7.08	SS	7.16	7.16	SUDAN
#7	1990-05-29 18:31:12.29	-153.569	56.956	33.0	na	6.06	NCL	5.34	5.95	KODIAK-ISLAND-REGION
#8	1990-06-14 07:40:56.21	121.899	11.760	15.0	6.97	7.05	SS	na	6.92	PANAY,-PHILIPPINES
#9	1990-06-14 12:47:28.82	85.076	47.869	54.0	6.56	6.59	SS	6.77	7.10	KAZAKH-XINJIANG-BORDER
#10	1990-06-20 21:00:09.98	49.409	36.957	10.0	7.29	7.35	SS	7.76	7.53	WESTERN-IRAN
#11	1990-07-09 15:11:20.38	31.654	5.395	10.0	6.56	6.28	NS	5.85	6.28	SUDAN
#12	1990-07-14 05:54:25.49	-17.376	0.003	10.0	6.47	6.56	SS	6.98	6.79	N-OF-ASCENSION-ISLAND
#13	1990-07-16 07:26:34.61	121.172	15.679	25.0	na	7.67	SS	7.32	7.78	LUZON,-PHILIPPINES
#14	1990-08-03 09:15:06.15	84.961	47.963	19.0	6.17	6.13	NCL	6.24	6.66	KAZAKH-XINJIANG-BORDER
#15	1990-10-15 01:35:44.56	92.249	-2.211	34.0	6.74	6.69	SS	7.34	6.63	SOUTHWEST-OF-SUMATERA
#16	1990-11-06 18:45:52.23	55.462	28.251	25.0	6.42	6.55	TF	6.10	6.61	SOUTHERN-IRAN
#17	1990-11-06 20:14:29.74	169.871	53.452	32.0	7.04	7.11	NCL	6.86	7.09	KOMANDORSKY-ISLANDS-REG.
#18	1990-11-15 02:34:32.40	97.457	3.908	56.0	6.55	6.65	SS	6.43	6.55	NORTHERN-SUMATERA
#19	1991-01-05 14:57:11.59	95.901	23.613	20.0	6.85	6.93	SS	7.25	7.04	BURMA
#20	1991-02-21 02:35:34.05	-175.450	58.427	10.0	6.50	6.62	NF	6.79	6.88	BERING-SEA
#21	1991-03-08 11:36:28.43	167.023	60.904	33.0	6.53	6.60	TF	6.40	6.58	EASTERN-SIBERIA
#22	1991-04-05 04:19:49.52	-77.094	-5.982	33.0	6.90	6.91	TF	7.05	7.12	NORTHERN-PERU
#23	1991-04-06 14:34:20.70	-175.521	-15.008	14.0	6.63	6.63	SS	7.48	6.29	TONGA-ISLANDS
#24	1991-04-22 21:56:51.82	-83.073	9.685	10.0	7.29	7.61	TF	7.40	7.39	COSTA-RICA
#25	1991-04-29 09:12:48.10	43.673	42.453	10.0	na	6.95	TF	6.50	6.97	WESTERN-CAUCASUS
#26	1991-06-10 17:35:49.48	-45.368	23.771	10.0	6.42	6.28	SS	6.48	6.74	NORTH-ATLANTIC-RIDGE
#27	1991-06-15 00:59:20.31	44.009	42.461	10.0	6.05	6.25	TF	5.93	6.54	WESTERN-CAUCASUS
#28	1991-06-20 05:18:52.51	122.787	1.196	33.0	7.40	7.51	NCL	6.72	7.10	MINAHASSA-PENINSULA
#29	1991-06-22 00:30:26.48	-108.549	23.915	10.0	na	6.13	SS	na	6.43	GULF-OF-CALIFORNIA
#30	1991-08-08 02:09:44.71	122.631	0.972	33.0	6.68	6.58	TF	5.96	6.40	MINAHASSA-PENINSULA
#31	1991-08-17 19:29:40.00	-124.348	40.235	12.0	6.28	6.12	TF	6.13	6.40	NR-NORTHERN-CALIF.-COAST
#32	1991-08-17 22:17:14.68	-125.397	41.821	10.0	6.84	7.03	SS	7.66	6.91	OFF-N-CALIFORNIA-COAST
#33	1991-10-14 15:58:12.79	158.442	-9.094	33.0	7.14	7.20	TF	6.80	7.08	SOLOMON-ISLANDS
#34	1991-11-19 22:28:51.09	-77.442	4.554	21.0	7.07	7.18	TF	6.90	7.08	NEAR-W-COAST-OF-COLOMBIA
#35	1991-12-22 08:43:13.41	151.021	45.533	26.0	7.49	7.56	TF	6.87	7.27	KURIL-ISLANDS
#36	1991-12-27 04:05:58.24	-25.266	-56.032	33.0	7.11	7.12	NF	na	7.34	SOUTH-SANDWICH-ISLANDS
#37	1991-12-28 00:52:10.16	-24.614	-56.102	33.0	6.50	6.60	NF	7.05	6.90	SOUTH-SANDWICH-ISLANDS
#38	1992-04-23 04:50:23.22	-116.318	33.961	10.0	6.19	6.15	SS	6.17	6.15	SOUTHERN-CALIFORNIA
#39	1992-04-23 14:18:35.15	98.904	22.437	31.0	na	6.07	SS	6.06	6.13	BURMA-CHINA-BORDER-REG.
#40	1992-04-24 07:07:23.91	66.065	27.550	33.0	6.16	6.00	SS	6.12	6.20	PAKISTAN
#41	1992-04-25 18:06:04.21	-124.316	40.368	15.0	7.07	7.15	NCL	7.01	7.17	NR-NORTHERN-CALIF.-COAST
#42	1992-05-15 07:05:05.34	147.572	-6.075	50.0	7.19	7.21	TF	6.88	7.19	E-PAPUA-NEW-GUINEA-REG.
#43	1992-05-17 09:49:19.11	126.645	7.239	33.0	7.03	7.06	TF	6.78	6.98	MINDANAO,-PHILIPPINES
#44	1992-05-20 12:20:32.85	71.317	33.377	33.0	6.22	6.04	NCL	5.81	6.29	PAKISTAN
#45	1992-05-25 16:55:04.17	-77.872	19.613	33.0	na	6.80	NCL	6.99	6.70	CUBA-REGION
#46	1992-05-27 05:13:38.81	165.239	-11.122	33.0	6.95	6.99	NF	6.80	6.92	SANTA-CRUZ-ISLANDS
#47	1992-06-02 21:05:09.50	92.920	-15.960	10.0	na	6.20	SS	na	6.45	SOUTH-INDIAN-OCEAN
#48	1992-06-15 02:48:56.25	95.932	24.027	16.0	6.26	6.26	SS	6.29	6.48	BURMA
#49	1992-06-21 17:43:08.84	176.861	-37.689	33.0	6.13	6.21	NF	5.97	6.52	N-ISLAND,-NEW-ZEALAND
#50	1992-06-28 11:57:34.12	-116.436	34.201	5.0	7.15	7.28	SS	7.38	7.09	SOUTHERN-CALIFORNIA
#51	1992-07-20 07:46:46.74	5.523	78.562	10.0	6.60	6.68	SS	7.07	6.49	SVALBARD-REGION
#52	1992-08-07 18:19:20.44	-142.846	57.589	10.0	6.83	6.76	SS	7.25	6.97	GULF-OF-ALASKA
#53	1992-08-19 02:04:37.41	73.575	42.142	22.0	7.24	7.19	TF	6.91	7.30	KIRGHIZ-SSR

#54	1992-08-28	18:18:46.44	-13.562	-0.965	10.0	6.84	6.80	SS	7.35	6.96	N-OF-ASCENSION-ISLAND
#55	1992-09-02	00:16:01.69	-87.340	11.742	15.0	na	7.62	TF	6.68	6.98	NEAR-COAST-OF-NICARAGUA
#56	1992-09-11	03:57:26.50	26.651	-6.087	10.0	6.39	6.31	NF	6.52	7.09	ZAIRE-REPUBLIC
#57	1992-09-26	22:15:57.51	129.118	1.289	26.0	6.65	6.54	SS	6.91	6.50	HALMAHERA
#58	1992-10-18	15:11:59.11	-76.862	7.075	10.0	7.22	7.10	NCL	7.41	7.43	NORTHERN-COLOMBIA
#59	1992-12-12	05:29:26.35	121.896	-8.480	35.0	7.36	7.74	TF	7.61	7.75	FLORES-ISLAND-REGION
#60	1992-12-20	20:52:47.28	130.393	-6.582	33.0	7.07	7.22	TS	7.12	7.65	BANDA-SEA
#61	1992-12-24	00:34:13.81	-173.128	-15.293	68.0	6.13	6.22	NCL	6.03	6.24	TONGA-ISLANDS
#62	1993-03-06	03:05:49.87	164.181	-10.972	14.0	7.09	7.08	SS	7.14	6.98	SANTA-CRUZ-ISLANDS-REG.
#63	1993-03-20	14:51:59.77	87.333	29.084	22.0	na	6.20	NF	5.59	5.89	TIBET
#64	1993-05-11	18:26:51.32	126.570	7.219	33.0	6.99	6.95	TF	6.40	6.72	MINDANAO,-PHILIPPINES
#65	1993-05-13	11:59:49.25	-160.458	55.177	32.0	6.84	6.86	TF	6.36	6.77	ALASKA-PENINSULA
#66	1993-05-15	03:12:32.72	-98.395	16.698	28.0	6.09	6.03	NCL	na	6.24	NR-GUERRERO-MEXICO-COAST
#67	1993-05-17	23:20:49.22	-117.775	37.171	7.0	6.07	6.11	NF	5.90	6.18	CALIFORNIA-NEVADA-BORDER
#68	1993-05-25	23:16:43.44	-160.513	55.021	33.0	6.12	6.05	TF	5.81	6.45	ALASKA-PENINSULA
#69	1993-05-29	06:50:13.42	-26.476	19.072	10.0	6.35	6.31	SS	6.90	6.44	NORTH-ATLANTIC-OCEAN
#70	1993-06-06	13:23:20.86	146.595	15.823	68.0	6.47	6.41	TF	6.27	6.32	MARIANA-ISLANDS
#71	1993-07-06	02:53:03.78	-111.888	-24.601	10.0	6.30	6.34	SS	6.07	5.68	EASTER-ISLAND-REGION
#72	1993-07-12	13:17:11.96	139.197	42.851	17.0	7.29	7.71	TF	7.69	8.16	HOKKAIDO,-JAPAN-REGION
#73	1993-07-22	04:57:07.05	-71.210	6.470	19.0	6.05	6.01	NF	5.95	6.15	NORTHERN-COLOMBIA
#74	1993-08-03	12:43:05.36	34.553	28.729	10.0	6.01	6.10	NF	5.85	6.35	ARAB-REPUBLIC-OF-EGYPT
#75	1993-08-08	08:34:24.93	144.801	12.982	61.0	7.49	7.74	TF	7.62	7.93	SOUTH-OF-MARIANA-ISLANDS
#76	1993-08-20	05:06:53.85	142.743	-5.997	7.0	6.17	6.14	TF	5.92	6.54	PAPUA-NEW-GUINEA
#77	1993-09-04	21:39:33.84	122.528	-9.571	39.0	6.20	6.17	NCL	na	6.24	SAVU-SEA
#78	1993-09-10	19:12:54.62	-92.645	14.717	34.0	7.20	7.21	TF	6.63	6.94	NEAR-COAST-OF-CHIAPAS,-M
#79	1993-09-20	10:17:42.06	-29.354	0.750	10.0	6.24	6.10	SS	na	6.11	CENTRAL-MID-ATLANTIC-RID
#80	1993-09-26	03:31:14.63	138.222	9.997	33.0	6.24	6.26	NF	6.04	6.31	WEST-CAROLINE-ISLANDS
#81	1993-09-27	13:37:32.97	-51.621	-53.651	33.0	6.54	6.57	NCL	na	6.66	SOUTH-ATLANTIC-OCEAN
#82	1993-09-29	22:25:48.62	76.451	18.066	6.0	6.12	6.16	TF	6.11	6.67	INDIA
#83	1993-10-02	08:42:32.71	88.663	38.190	16.0	6.01	6.08	TF	6.00	6.60	SOUTHERN-XINJIANG,-CHINA
#84	1993-10-13	02:06:00.34	146.020	-5.889	24.0	6.54	6.87	NCL	6.69	6.89	EAST-PAPUA-NEW-GUINEA-RE
#85	1993-11-13	01:18:04.18	158.647	51.934	34.0	6.99	7.00	TF	6.39	6.83	NEAR-EAST-COAST-OF-KAMCH
#86	1993-12-29	07:48:14.20	169.789	-20.230	33.0	6.33	6.98	SS	7.05	6.65	VANUATU-ISLANDS
#87	1994-01-17	12:30:55.39	-118.537	34.213	18.0	6.65	6.65	TF	6.43	6.76	SOUTHERN-CALIFORNIA
#88	1994-02-05	23:34:09.97	30.037	0.593	10.0	6.13	6.15	NF	5.63	6.16	UGANDA
#89	1994-02-12	04:16:26.89	-128.798	-10.786	10.0	6.60	6.62	NF	6.33	6.80	SOUTH-PACIFIC-OCEAN
#90	1994-02-15	17:07:43.80	104.302	-4.967	15.0	6.60	6.83	SS	6.63	6.69	SOUTHERN-SUMATERA
#91	1994-02-26	02:31:11.09	60.549	30.897	12.0	5.91	6.03	TF	5.81	6.21	IRAN
#92	1994-03-14	04:30:15.75	-23.569	-1.278	10.0	6.98	7.01	SS	7.20	6.96	CENTRAL-MID-ATLANTIC-RID
#93	1994-06-02	18:17:34.02	112.835	-10.477	39.0	7.74	7.75	NCL	6.45	6.78	SOUTH-OF-JAVA
#94	1994-06-04	00:57:50.66	113.366	-10.777	33.0	6.15	6.44	NF	6.75	6.60	SOUTH-OF-JAVA
#95	1994-06-06	20:47:40.53	-76.057	2.917	9.0	6.68	6.78	SS	7.22	7.05	COLOMBIA
#96	1994-06-15	09:22:57.22	113.660	-10.335	33.0	6.15	6.03	NF	6.09	6.26	SOUTH-OF-JAVA
#97	1994-06-18	03:25:15.83	171.658	-42.963	33.0	6.68	6.71	SS	6.30	6.50	SOUTH-ISLAND,-NEW-ZEALAN
#98	1994-07-13	02:35:56.02	167.518	-16.620	33.0	7.07	7.15	NCL	6.98	6.94	VANUATU-ISLANDS
#99	1994-09-01	15:15:53.08	-125.680	40.402	10.0	7.03	6.99	SS	7.72	7.15	OFF-COAST-OF-NORTHERN-CA
#100	1994-09-13	10:01:32.09	-76.678	7.054	33.0	6.01	6.02	SS	5.70	5.99	NORTHERN-COLOMBIA
#101	1994-09-16	06:20:18.74	118.711	22.528	12.0	6.72	6.66	NF	6.72	7.10	TAIWAN-REGION
#102	1994-09-23	07:59:38.92	148.537	-3.379	15.0	5.96	6.02	SS	6.40	5.96	BISMARCK-SEA
#103	1994-10-04	13:22:55.84	147.321	43.773	33.0	8.13	8.25	NCL	8.43	8.56	KURIL-ISLANDS
#104	1994-10-09	07:55:39.58	147.916	43.905	23.0	7.11	7.25	TF	6.93	7.17	KURIL-ISLANDS
#105	1994-11-14	19:15:30.66	121.067	13.525	33.0	6.94	7.07	SS	7.41	6.81	MINDORO,-PHILIPPINE-ISLA
#106	1994-12-28	12:19:23.03	143.419	40.525	33.0	7.69	7.73	TF	7.50	7.68	OFF-EAST-COAST-OF-HONSHU
#107	1995-01-01	06:59:55.95	143.549	40.701	10.0	6.46	6.41	NCL	6.15	6.65	OFF-EAST-COAST-OF-HONSHU
#108	1995-01-16	20:46:52.12	135.018	34.583	16.0	6.77	6.86	SS	7.02	7.04	NEAR-S.-COAST-OF-SOUTHER
#109	1995-01-19	15:05:03.41	-72.916	5.050	18.0	6.49	6.50	TF	6.54	6.82	COLOMBIA

#110	1995-02-05	22:51:05.14	178.752	-37.759	59.0	6.93	7.11	NF	7.09	7.17	OFF-E.-COAST-OF-N.-ISLAN
#111	1995-02-08	18:40:25.38	-76.622	4.104	69.0	6.35	6.34	NF	6.29	6.80	COLOMBIA
#112	1995-03-06	18:43:40.15	118.226	2.690	33.0	6.03	6.04	TF	5.73	5.87	CELEBES-SEA
#113	1995-03-08	03:45:58.69	-59.559	16.562	15.0	6.07	6.14	NF	6.26	6.64	LEEWARD-ISLANDS
#114	1995-04-07	22:06:56.89	-173.529	-15.199	31.0	7.32	7.34	NCL	7.55	7.54	TONGA-ISLANDS
#115	1995-04-17	07:14:35.22	-38.576	33.763	10.0	6.15	6.11	SS	6.60	6.27	NORTH-ATLANTIC-RIDGE
#116	1995-04-17	23:28:06.89	151.283	45.928	34.0	6.63	6.72	TF	6.17	6.52	KURIL-ISLANDS
#117	1995-04-21	00:34:46.09	125.580	12.059	23.0	7.07	7.15	TF	6.99	7.24	SAMAR,-PHILIPPINE-ISLAND
#118	1995-04-27	12:44:41.20	-85.031	1.297	10.0	6.09	6.16	SS	6.28	5.89	OFF-COAST-OF-ECUADOR
#119	1995-05-05	03:53:45.05	125.297	12.626	33.0	6.99	7.04	TF	6.81	6.86	SAMAR,-PHILIPPINE-ISLAND
#120	1995-05-14	11:33:18.87	125.127	-8.378	33.0	6.47	6.85	NF	6.43	6.75	TIMOR
#121	1995-05-16	20:12:44.22	169.900	-23.008	33.0	7.26	7.66	NF	7.70	7.79	LOYALTY-ISLANDS-REGION
#122	1995-05-23	22:10:11.84	-3.361	-55.945	10.0	6.55	6.71	SS	na	6.54	SOUTH-ATLANTIC-RIDGE
#123	1995-05-27	13:03:52.65	142.827	52.629	33.0	7.02	7.02	SS	7.20	7.01	SAKHALIN-ISLAND
#124	1995-06-14	11:11:47.40	-88.360	12.128	39.0	na	6.52	NF	na	6.14	OFF-COAST-OF-CENTRAL-AME
#125	1995-06-21	15:28:51.71	154.766	-61.673	10.0	6.63	6.68	SS	7.12	6.69	BALLENY-ISLANDS-REGION
#126	1995-07-03	19:50:50.62	-177.589	-29.211	33.0	7.13	7.13	TF	6.76	7.05	KERMADEC-ISLANDS
#127	1995-07-11	21:46:39.78	99.196	21.966	13.0	6.74	6.79	SS	7.09	6.72	BURMA-CHINA-BORDER-REGIO
#128	1995-07-30	05:11:23.63	-70.294	-23.340	47.0	7.93	7.99	TF	7.56	7.80	NEAR-COAST-OF-NORTHERN-C
#129	1995-08-07	19:44:25.43	143.770	4.041	10.0	6.10	6.14	SS	na	6.29	CAROLINE-ISLANDS-REGION
#130	1995-08-16	10:27:28.63	154.178	-5.799	16.0	7.54	7.71	TF	7.24	7.83	SOLOMON-ISLANDS
#131	1995-08-18	02:16:25.99	-28.832	-55.934	36.0	6.19	6.16	SS	6.22	6.34	SOUTH-SANDWICH-ISLANDS-R
#132	1995-09-14	14:04:31.43	-98.597	16.779	21.0	7.36	7.34	TF	7.12	7.29	NEAR-COAST-OF-GUERRERO,
#133	1995-10-03	01:51:23.90	-77.881	-2.750	27.0	6.79	6.99	TF	6.91	6.99	PERU-ECUADOR-BORDER-REGI
#134	1995-10-03	12:44:58.09	-77.851	-2.778	33.0	6.41	6.42	TS	6.05	6.30	PERU-ECUADOR-BORDER-REGI
#135	1995-10-09	15:35:53.91	-104.205	19.055	49.0	7.91	7.97	NCL	7.24	7.54	NEAR-COAST-OF-JALISCO,-M
#136	1995-10-13	15:22:23.45	158.280	-59.014	10.0	6.01	6.08	TF	na	6.14	MACQUARIE-ISLANDS-REGION
#137	1995-10-18	10:37:26.38	130.175	27.929	27.0	6.90	7.10	NF	6.91	7.20	RYUKYU-ISLANDS
#138	1995-10-19	02:41:36.19	130.148	28.094	31.0	6.63	6.72	NF	6.37	6.68	RYUKYU-ISLANDS
#139	1995-10-23	22:46:50.81	102.227	26.003	10.0	6.12	6.16	SS	6.48	6.44	Szechwan-Province,-China
#140	1995-11-22	04:15:11.94	34.799	28.826	10.0	7.06	7.17	SS	7.27	7.32	ARAB-REPUBLIC-OF-EGYPT
#141	1995-11-24	06:18:56.47	171.793	-42.984	10.0	6.13	6.10	SS	na	6.32	SOUTH-ISLAND,-NEW-ZEALAN
#142	1995-12-01	05:20:28.83	-104.000	10.160	67.0	6.57	6.56	SS	6.54	5.92	Off-Coast-Of-Mexico
#143	1995-12-03	18:01:08.99	149.300	44.663	22.0	7.55	7.88	TF	7.32	7.50	Kurile-Islands
#144	1995-12-05	06:32:06.10	124.670	-9.027	22.0	6.33	6.36	SS	na	6.40	Timor
#145	1996-01-01	08:05:10.83	119.931	0.729	33.0	7.74	7.86	NCL	7.36	7.50	MINAHASSA-PENINSULA
#146	1996-02-03	11:14:20.12	100.276	27.291	10.0	6.15	6.60	NF	6.52	7.05	YUNNAN-PROVINCE,-CHINA
#147	1996-02-07	21:36:46.30	149.892	45.324	33.0	7.05	7.14	TF	6.64	6.95	KURIL-ISLANDS
#148	1996-02-12	09:08:07.99	118.670	-11.044	33.0	6.01	6.04	NF	5.93	6.07	SOUTH-OF-SUMBAWA-ISLAND
#149	1996-02-17	05:59:30.55	136.952	-0.891	33.0	8.10	8.19	TF	7.69	7.74	WEST-IRIAN-REGION
#150	1996-02-18	02:25:33.35	136.464	-1.336	33.0	6.01	6.36	SS	6.61	6.39	WEST-IRIAN-REGION
#151	1996-02-21	12:51:01.30	-79.587	-9.593	10.0	7.38	7.50	TF	na	7.08	OFF-COAST-OF-NORTHERN-PE
#152	1996-02-25	03:08:15.87	-98.070	15.978	33.0	7.09	7.09	TF	6.48	6.56	OAXACA,-MEXICO
#153	1996-04-27	08:40:41.85	-79.341	2.368	10.0	6.12	6.06	TF	na	6.02	SOUTH-OF-PANAMA
#154	1996-04-29	14:40:41.09	154.999	-6.518	44.0	7.16	7.19	TF	6.87	7.09	SOLOMON-ISLANDS
#155	1996-06-02	02:52:09.55	-42.254	10.797	10.0	6.81	6.92	SS	7.02	7.06	NORTH-ATLANTIC-RIDGE
#156	1996-06-06	17:35:38.19	80.666	-41.329	20.0	6.28	6.19	SS	6.55	5.97	MID-INDIAN-RISE
#157	1996-06-10	04:03:35.48	-177.632	51.564	33.0	7.53	7.87	TF	7.40	7.61	ANDREANOF-ISLANDS,-ALEUT
#158	1996-06-10	15:24:56.00	-176.847	51.478	26.0	7.18	7.22	TF	6.87	7.00	ANDREANOF-ISLANDS,-ALEUT
#159	1996-06-11	18:22:55.73	125.154	12.614	33.0	6.94	7.06	TF	6.60	6.81	SAMAR,-PHILIPPINE-ISLAND
#160	1996-06-14	15:04:40.74	125.055	12.811	29.0	6.07	6.07	NF	6.23	6.03	SAMAR,-PHILIPPINE-ISLAND
#161	1996-06-22	00:32:13.47	8.800	-53.774	10.0	6.36	6.39	SS	na	6.56	BOUVET-ISLAND-REGION
#162	1996-06-30	11:32:35.84	159.812	51.726	33.0	6.03	6.03	TF	na	6.02	OFF-EAST-COAST-OF-KAMCHA
#163	1996-07-20	00:00:41.88	27.103	36.147	33.0	5.93	6.18	NF	5.85	6.07	DODECANESE-ISLANDS
#164	1996-07-22	14:19:35.77	120.450	1.000	33.0	6.94	6.97	TF	6.54	6.69	MINAHASSA-PENINSULA
#165	1996-08-05	02:08:58.25	-173.126	-15.267	41.0	6.60	6.63	NF	5.97	6.47	TONGA-ISLANDS

#166	1996-09-05	08:14:14.48	-113.436	-22.118	10.0	6.70	6.82	TF	6.39	6.83	EASTER-ISLAND-REGION
#167	1996-09-20	04:10:27.68	126.284	9.463	33.0	6.42	6.52	TF	5.87	6.39	MINDANAO,-PHILIPPINE-ISL
#168	1996-10-01	15:50:23.66	58.066	12.434	10.0	6.21	6.40	SS	6.64	6.38	ARABIAN-SEA
#169	1996-10-06	20:13:09.18	-127.880	49.047	10.0	5.99	6.16	SS	6.68	6.24	VANCOUVER-ISLAND-REGION
#170	1996-10-09	13:10:52.13	32.126	34.556	33.0	6.75	6.78	SS	6.84	6.98	CYPRUS
#171	1996-10-24	19:31:53.93	-173.229	66.986	20.0	5.99	6.05	NS	5.96	6.16	NEAR-N.-COAST-OF-EASTERN
#172	1996-11-12	16:59:44.03	-75.675	-14.993	33.0	7.47	7.71	TF	7.29	7.78	NEAR-COAST-OF-PERU
#173	1996-11-19	10:44:46.06	78.133	35.345	33.0	6.87	6.85	SS	7.09	6.71	EASTERN-KASHMIR
#174	1996-12-03	12:56:56.92	-172.275	-18.351	33.0	6.09	6.12	TF	6.25	6.54	TONGA-ISLANDS-REGION
#175	1996-12-09	03:54:16.31	107.489	-7.936	51.0	5.99	6.03	TF	5.35	6.02	JAVA
#176	1996-12-09	11:28:48.61	-42.855	29.850	10.0	5.90	6.00	NF	5.69	6.10	NORTH-ATLANTIC-RIDGE
#177	1996-12-10	08:36:18.70	-30.039	0.870	10.0	6.56	6.62	SS	6.95	6.64	CENTRAL-MID-ATLANTIC-RID
#178	1997-01-11	20:28:26.02	-102.756	18.219	33.0	7.14	7.12	NCL	6.98	7.12	MICHOACAN,-MEXICO
#179	1997-01-17	15:53:13.43	129.953	28.814	33.0	6.19	6.22	NCL	5.81	6.15	RYUKYU-ISLANDS
#180	1997-02-04	10:37:47.14	57.291	37.661	10.0	6.46	6.48	SS	7.09	6.70	IRAN-USSR-BORDER-REGION
#181	1997-02-09	12:32:36.29	-76.276	-14.486	33.0	5.96	6.09	TF	5.72	6.00	NEAR-COAST-OF-PERU
#182	1997-02-27	21:08:02.36	68.208	29.976	33.0	7.00	7.08	TF	6.70	6.96	PAKISTAN
#183	1997-02-28	12:57:18.64	48.050	38.075	10.0	5.93	6.09	SS	na	6.37	N.W.-IRAN-USSR-BORDER-RE
#184	1997-03-11	19:22:00.13	127.647	7.742	10.0	6.84	6.83	NF	7.16	7.39	PHILIPPINE-ISLANDS-REGIO
#185	1997-04-02	06:14:31.09	-60.942	11.412	45.0	6.05	6.05	SS	na	6.26	WINDWARD-ISLANDS
#186	1997-04-21	12:02:26.43	166.676	-12.584	33.0	7.65	7.69	TF	7.68	7.91	SANTA-CRUZ-ISLANDS
#187	1997-04-22	09:31:23.25	-60.892	11.112	5.0	6.70	6.64	NF	6.63	6.71	WINDWARD-ISLANDS
#188	1997-04-28	12:07:37.83	42.686	-42.504	10.0	6.52	6.71	SS	na	6.52	PRINCE-EDWARD-ISLANDS-RE
#189	1997-05-01	11:37:36.15	-107.350	18.993	33.0	6.89	6.89	SS	7.24	6.65	OFF-COAST-OF-JALISCO,-ME
#190	1997-05-10	07:57:29.72	59.809	33.825	10.0	7.25	7.18	SS	7.70	7.52	IRAN
#191	1997-05-22	13:21:36.35	121.336	18.915	34.0	5.96	6.02	TF	5.81	6.18	LUZON,-PHILIPPINE-ISLAND
#192	1997-05-29	17:02:38.74	-102.511	-35.964	10.0	6.37	6.45	SS	na	6.41	SOUTHERN-PACIFIC-OCEAN
#193	1997-06-10	21:53:55.02	-108.135	-35.815	10.0	6.50	6.51	SS	6.96	6.34	EASTER-ISLAND-CORDILLERA
#194	1997-07-09	19:24:13.17	-63.486	10.598	20.0	6.88	6.93	SS	6.43	6.48	NEAR-COAST-OF-VENEZUELA
#195	1997-07-19	14:22:08.75	-98.216	16.333	33.0	6.87	6.65	TF	5.97	6.19	NEAR-COAST-OF-GUERRERO,
#196	1997-07-20	00:30:20.99	-167.484	52.562	14.0	6.05	6.04	TF	5.65	6.09	FOX-ISLANDS,-ALEUTIAN-IS
#197	1997-07-25	06:47:02.67	-71.906	-30.462	33.0	6.20	6.04	TF	na	5.96	NEAR-COAST-OF-CENTRAL-CH
#198	1997-08-10	09:20:30.98	124.329	-16.013	10.0	6.22	6.21	SS	6.61	6.86	WESTERN-AUSTRALIA
#199	1997-08-13	04:45:04.86	125.770	25.030	55.0	6.12	6.11	TF	5.68	6.43	SOUTHWESTERN-RYUKYU-ISLA
#200	1997-09-03	06:22:44.28	-128.989	-55.190	10.0	5.99	6.09	SS	na	5.74	SOUTH-PACIFIC-CORDILLERA
#201	1997-09-20	16:11:32.15	-177.624	-28.683	30.0	6.90	6.96	TF	6.48	6.92	KERMADEC-ISLANDS-REGION
#202	1997-10-15	01:03:33.46	-71.220	-30.933	58.0	7.06	7.06	NCL	7.55	7.69	NEAR-COAST-OF-CENTRAL-CH
#203	1997-11-08	10:02:52.61	87.325	35.069	33.0	7.36	7.50	SS	7.39	6.88	TIBET
#204	1997-11-18	13:07:41.73	20.656	37.570	33.0	6.35	6.57	NCL	6.14	6.59	IONIAN-SEA
#205	1997-11-21	11:23:06.31	92.702	22.212	54.0	6.05	6.06	NCL	5.50	6.33	INDIA-BANGLADESH-BORDER
#206	1997-11-25	12:14:33.63	122.536	1.241	24.0	6.98	7.01	TF	6.85	6.96	MINAHASSA-PENINSULA
#207	1997-12-05	11:26:54.69	162.035	54.841	33.0	7.68	7.75	TF	7.18	7.54	NEAR-EAST-COAST-OF-KAMCH
#208	1997-12-27	20:11:10.50	-3.720	-55.970	10.0	na	6.15	SS	na	5.92	SOUTH-ATLANTIC-RIDGE
#209	1998-01-03	06:10:08.38	-16.191	-35.474	10.0	6.15	6.24	SS	na	5.99	SOUTH-ATLANTIC-RIDGE
#210	1998-01-10	04:54:25.39	-72.074	-12.029	33.0	6.38	6.15	TF	6.07	6.24	PERU
#211	1998-01-30	12:16:08.69	-70.207	-23.913	42.0	6.96	7.03	TF	6.55	7.18	NEAR-COAST-OF-NORTHERN-C
#212	1998-02-03	03:02:00.24	-96.298	15.883	33.0	6.33	6.31	TF	6.13	6.34	NEAR-COAST-OF-OAXACA,-ME
#213	1998-02-16	23:53:19.72	-33.677	52.718	10.0	6.63	6.71	SS	7.29	6.73	NORTH-ATLANTIC-OCEAN
#214	1998-02-19	14:14:51.19	129.082	-4.476	33.0	6.43	6.49	TF	6.71	6.68	BANDA-SEA
#215	1998-03-20	21:08:08.53	163.107	-50.008	10.0	6.65	6.68	SS	na	6.60	AUCKLAND-ISLANDS-REGION
#216	1998-03-22	01:08:57.48	66.245	-11.430	10.0	5.88	6.05	NF	5.68	6.17	MID-INDIAN-RISE
#217	1998-03-25	03:12:25.07	149.527	-62.877	10.0	7.79	8.09	SS	8.75	8.24	BALLENY-ISLANDS-REGION
#218	1998-03-29	07:14:58.98	-17.932	-0.239	10.0	5.99	6.08	SS	6.16	6.30	NORTH-OF-ASCENSION-ISLAN
#219	1998-05-03	23:30:21.91	125.308	22.306	33.0	7.45	7.44	SS	7.90	7.37	SOUTHEAST-OF-TAIWAN
#220	1998-05-21	05:34:25.50	119.584	0.207	33.0	6.63	6.61	SS	7.12	6.83	MINAHASSA-PENINSULA
#221	1998-05-22	04:48:50.44	-65.431	-17.731	24.0	6.57	6.55	SS	5.89	6.40	BOLIVIA

#222	1998-05-30	06:22:28.95	70.110	37.106	33.0	6.52	6.53	SS	6.99	6.52	AFGHANISTAN-USSR-BORDER
#223	1998-06-18	04:17:54.98	-13.894	-11.572	10.0	6.17	6.22	SS	6.40	6.06	ASCENSION-ISLAND-REGION
#224	1998-06-27	13:55:52.08	35.307	36.878	33.0	6.19	6.25	SS	6.57	6.24	TURKEY
#225	1998-07-09	05:19:07.30	-28.626	38.650	10.0	6.13	6.13	SS	6.54	6.17	AZORES-ISLANDS
#226	1998-07-17	08:49:13.28	141.926	-2.961	10.0	6.98	6.98	TF	6.65	6.76	NEAR-N-COAST-OF-PAPUA-NE
#227	1998-07-29	18:00:29.99	138.901	-2.693	33.0	6.49	6.66	NCL	6.31	6.43	WEST-IRIAN
#228	1998-08-04	18:59:20.10	-80.393	-0.593	33.0	7.02	7.14	TF	6.86	6.92	NEAR-COAST-OF-ECUADOR
#229	1998-08-30	01:48:08.76	148.133	17.092	33.0	6.22	6.29	NF	6.14	6.45	MARIANA-ISLANDS-REGION
#230	1998-11-09	05:30:14.40	129.022	-6.954	33.0	6.49	6.70	TS	6.61	6.70	BANDA-SEA
#231	1998-11-09	05:38:44.22	128.946	-6.920	33.0	6.94	7.00	TF	6.91	7.16	BANDA-SEA
#232	1998-11-19	15:39:19.10	125.783	22.605	10.0	6.23	6.28	SS	6.69	6.33	SOUTHEAST-OF-TAIWAN
#233	1998-11-29	14:10:31.96	124.891	-2.071	33.0	7.70	7.70	SS	8.30	7.51	CERAM-SEA
#234	1998-12-06	00:47:13.45	126.198	1.253	33.0	6.49	6.55	TF	6.61	6.81	MOLUCCA-PASSAGE
#235	1999-01-24	00:37:04.63	131.086	30.618	33.0	6.25	6.36	NF	5.99	6.34	KYUSHU,-JAPAN
#236	1999-01-25	18:19:16.87	-75.724	4.461	17.0	6.15	6.14	SS	6.39	6.48	COLOMBIA
#237	1999-01-28	08:10:05.42	-169.123	52.886	67.0	6.54	6.58	TF	6.43	6.58	FOX-ISLANDS,-ALEUTIAN-IS
#238	1999-03-04	08:52:01.90	121.937	5.397	33.0	6.93	7.06	TF	6.91	7.12	CELEBES-SEA
#239	1999-03-08	12:25:48.99	159.520	52.056	57.0	6.77	6.87	TF	6.33	6.58	OFF-EAST-COAST-OF-KAMCHA
#240	1999-03-28	19:05:11.03	79.403	30.512	15.0	6.52	6.53	NCL	6.55	7.12	TIBET-INDIA-BORDER-REGIO
#241	1999-05-06	23:00:53.12	51.880	29.501	33.0	6.09	6.20	SS	na	6.22	SOUTHERN-IRAN
#242	1999-05-16	15:25:53.81	138.217	-2.642	59.0	6.31	6.32	TF	6.40	6.69	WEST-IRIAN
#243	1999-07-11	14:14:16.53	-88.330	15.782	10.0	6.65	6.66	SS	7.00	6.74	HONDURAS
#244	1999-08-12	05:44:59.59	122.456	-1.716	33.0	6.13	6.13	SS	na	6.38	SULAWESI
#245	1999-08-17	00:01:39.13	29.864	40.748	17.0	7.36	7.57	SS	7.67	7.37	TURKEY
#246	1999-08-20	10:02:21.10	-84.159	9.044	20.0	6.74	6.88	TF	na	6.67	COSTA-RICA
#247	1999-08-21	21:51:11.47	-13.196	-58.311	10.0	6.17	6.17	SS	na	6.19	SOUTHWESTERN-ATLANTIC-OC
#248	1999-08-22	09:35:39.47	-74.756	-40.509	33.0	6.13	6.37	NF	6.24	6.58	OFF-COAST-OF-SOUTHERN-CH
#249	1999-09-20	17:47:18.49	120.982	23.772	33.0	7.42	7.62	TF	7.18	7.44	TAIWAN
#250	1999-09-30	16:31:15.69	-96.931	16.059	61.0	7.38	7.42	NF	7.14	7.36	OAXACA,-MEXICO
#251	1999-10-16	09:46:44.13	-116.271	34.594	10.0	7.10	7.12	SS	7.25	7.02	SOUTHERN-CALIFORNIA
#252	1999-11-12	16:57:19.55	31.161	40.758	10.0	7.10	7.15	SS	6.98	7.22	TURKEY
#253	1999-11-15	05:42:43.22	88.976	-1.339	10.0	6.74	6.95	SS	7.63	7.19	SOUTH-INDIAN-OCEAN
#254	1999-11-19	13:56:46.45	148.763	-6.351	33.0	6.77	7.00	TF	6.28	6.68	NEW-BRITAIN-REGION
#255	1999-11-26	13:21:15.57	168.214	-16.423	33.0	7.22	7.42	TF	7.22	7.38	VANUATU-ISLANDS
#256	1999-11-29	03:46:30.18	89.043	-1.275	10.0	6.39	6.37	SS	6.88	6.58	SOUTH-INDIAN-OCEAN
#257	1999-12-01	19:23:06.01	-82.356	17.647	10.0	6.26	6.27	SS	na	6.33	CARIBBEAN-SEA
#258	1999-12-06	23:12:33.92	-154.489	57.413	66.0	6.95	6.96	SS	6.99	7.41	KODIAK-ISLAND-REGION
#259	1999-12-10	18:38:30.10	-97.316	-36.206	10.0	6.48	6.49	SS	na	6.40	WEST-CHILE-RISE
#260	1999-12-11	18:03:36.45	119.740	15.766	33.0	7.11	7.23	NCL	7.04	7.37	LUZON,-PHILIPPINE-ISLAND
#261	1999-12-24	19:26:04.94	146.723	-56.211	10.0	6.26	6.23	SS	na	6.31	WEST-OF-MACQUARIE-ISLAND
#262	1999-12-29	13:29:19.62	165.354	-10.860	33.0	6.84	6.84	TF	6.43	6.44	SANTA-CRUZ-ISLANDS
#263	2000-01-06	10:42:25.00	-136.870	58.040	1.0	6.05	6.07	SS	6.19	6.07	SOUTHEASTERN-ALASKA
#264	2000-01-06	21:31:06.22	119.484	16.095	33.0	6.19	6.18	TF	5.81	5.93	LUZON,-PHILIPPINE-ISLAND
#265	2000-01-09	21:54:40.49	174.370	-18.823	33.0	6.44	6.39	SS	6.84	6.10	FIJI-ISLANDS-REGION
#266	2000-02-25	01:43:58.64	173.818	-19.528	33.0	6.97	7.07	SS	7.51	6.75	VANUATU-ISLANDS-REGION
#267	2000-02-26	18:24:39.22	-78.532	9.406	65.0	6.09	6.08	NF	5.97	6.04	PANAMA
#268	2000-03-05	23:57:03.17	145.637	-62.902	10.0	6.07	6.07	TF	na	6.60	SOUTH-OF-AUSTRALIA
#269	2000-05-04	04:21:16.21	123.573	-1.105	26.0	7.40	7.52	SS	7.53	7.65	SULAWESI
#270	2000-06-03	08:54:49.20	140.464	35.552	62.0	6.05	6.11	TF	na	6.11	NEAR-EAST-COAST-OF-HONSH
#271	2000-06-04	16:28:26.17	102.087	-4.721	33.0	7.65	7.85	TS	8.25	8.12	SOUTHERN-SUMATERA
#272	2000-06-07	21:46:55.90	97.238	26.856	33.0	6.21	6.32	TF	6.50	6.78	BURMA
#273	2000-06-17	15:40:41.73	-20.487	63.966	10.0	6.36	6.50	SS	6.67	6.33	ICELAND
#274	2000-06-18	14:44:13.31	97.453	-13.802	10.0	7.52	7.87	SS	7.92	8.01	SOUTH-INDIAN-OCEAN
#275	2000-06-21	00:51:46.88	-20.758	63.980	10.0	6.40	6.42	SS	6.72	6.43	ICELAND
#276	2000-06-25	06:34:42.88	131.206	31.183	10.0	5.93	6.02	TF	5.67	6.32	KYUSHU,-JAPAN
#277	2000-07-11	01:32:28.52	-154.206	57.369	44.0	6.58	6.48	NS	6.78	6.94	KODIAK-ISLAND-REGION

#278	2000-07-15	01:30:30.50	139.260	34.319	10.0	5.92	6.03	SS	na	6.17	NEAR-S.-COAST-OF-HONSHU,
#279	2000-07-16	03:21:45.53	122.043	20.253	33.0	6.37	6.36	SS	6.79	6.66	PHILIPPINE-ISLANDS-REGIO
#280	2000-08-04	21:13:02.71	142.246	48.786	10.0	6.63	6.79	TF	6.38	6.93	SAKHALIN-ISLAND
#281	2000-08-21	09:16:25.45	-45.966	-53.020	10.0	6.07	6.05	NCL	5.92	6.34	SOUTH-ATLANTIC-OCEAN
#282	2000-09-10	19:06:15.63	129.332	-1.112	33.0	6.03	6.04	NF	6.02	6.10	HALMAHERA
#283	2000-09-12	00:27:58.62	99.343	35.389	10.0	6.10	6.10	SS	6.31	6.05	QINGHAI-PROVINCE,-CHINA
#284	2000-09-28	23:23:43.35	-80.582	-0.215	23.0	6.32	6.37	TF	6.13	6.00	NEAR-COAST-OF-ECUADOR
#285	2000-10-02	02:25:31.31	30.709	-7.977	34.0	6.44	6.44	NF	6.06	6.42	LAKE-TANGANYIKA-REGION
#286	2000-10-04	16:58:44.31	166.910	-15.421	23.0	6.68	6.92	TF	6.39	6.62	VANUATU-ISLANDS
#287	2000-10-05	13:39:11.67	-40.958	31.732	10.0	5.79	6.06	NF	na	5.99	NORTH-ATLANTIC-RIDGE
#288	2000-10-21	11:35:59.13	-12.403	-47.347	10.0	5.93	6.01	SS	na	5.77	SOUTH-ATLANTIC-RIDGE
#289	2000-10-25	09:32:23.97	105.630	-6.549	38.0	6.74	6.76	TF	6.33	6.90	SUNDA-STRAIT
#290	2000-10-25	19:00:17.49	-109.458	-34.678	10.0	6.01	6.07	SS	na	5.96	EASTER-ISLAND-CORDILLERA
#291	2000-11-08	06:59:58.86	-77.829	7.042	17.0	6.51	6.50	TF	6.35	6.76	PANAMA-COLOMBIA-BORDER-R
#292	2000-11-16	04:54:56.74	152.169	-3.980	33.0	7.61	8.00	NCL	na	7.83	NEW-IRELAND-REGION
#293	2000-11-16	07:42:16.93	153.102	-5.233	30.0	7.27	7.81	TF	7.16	7.59	NEW-IRELAND-REGION
#294	2000-11-17	21:01:56.49	151.781	-5.496	33.0	7.36	7.77	TF	6.77	7.06	NEW-BRITAIN-REGION
#295	2000-11-25	18:09:11.42	49.946	40.245	50.0	6.22	6.77	NCL	6.19	6.73	EASTERN-CAUCASUS
#296	2000-11-29	10:25:13.26	-70.886	-24.869	58.0	6.31	6.28	NF	6.12	6.32	NEAR-COAST-OF-NORTHERN-C
#297	2000-12-06	17:11:06.40	54.799	39.566	30.0	6.92	6.99	TF	7.01	7.29	TURKMEN-SSR
#298	2000-12-15	16:44:47.66	31.351	38.457	10.0	5.91	5.99	NF	5.36	5.91	TURKEY
#299	2000-12-19	13:11:47.37	144.760	11.765	33.0	6.05	6.12	NF	na	6.21	SOUTH-OF-MARIANA-ISLANDS
#300	2000-12-20	16:49:43.30	154.353	-9.231	33.0	6.45	6.59	SS	na	6.33	DENTRECASTEAUX-ISLANDS-R
#301	2001-01-01	06:57:04.17	126.579	6.898	33.0	7.38	7.43	TF	7.24	7.42	MINDANAO,-PHILIPPINE-ISL
#302	2001-01-02	07:30:03.78	126.809	6.749	33.0	6.29	6.35	NCL	6.27	6.44	MINDANAO,-PHILIPPINE-ISL
#303	2001-01-10	16:02:44.23	-153.211	57.078	33.0	6.75	6.94	NCL	6.64	6.90	KODIAK-ISLAND-REGION
#304	2001-01-13	17:33:32.38	-88.660	13.049	60.0	7.57	7.71	NF	7.62	7.56	EL-SALVADOR
#305	2001-01-15	05:52:16.25	78.362	-40.344	10.0	6.35	6.33	SS	6.50	6.17	MID-INDIAN-RISE
#306	2001-01-16	13:25:09.83	101.776	-4.022	28.0	6.87	6.80	TF	6.43	6.65	SOUTHERN-SUMATERA
#307	2001-01-19	08:10:14.75	166.380	-11.662	50.0	6.31	6.25	TF	5.85	6.33	SANTA-CRUZ-ISLANDS
#308	2001-01-26	03:16:40.50	70.232	23.419	16.0	7.57	7.62	TF	7.60	8.03	INDIA
#309	2001-02-13	19:28:30.26	102.562	-4.680	36.0	7.14	7.31	TF	6.80	7.07	SOUTHERN-SUMATERA
#310	2001-02-24	07:23:48.73	126.249	1.271	35.0	7.04	7.03	TF	7.02	7.17	MOLUCCA-PASSAGE
#311	2001-02-28	18:54:32.83	-122.727	47.149	52.0	6.70	6.76	NF	6.43	7.06	WASHINGTON
#312	2001-03-06	09:17:36.08	157.271	-54.588	10.0	6.40	6.07	SS	na	6.36	MACQUARIE-ISLANDS-REGION
#313	2001-03-24	06:27:53.58	132.526	34.083	50.0	6.68	6.80	NF	6.23	6.95	SOUTHERN-HONSHU,-JAPAN
#314	2001-04-04	07:44:11.20	132.369	-5.176	33.0	6.21	6.34	SS	6.75	6.24	AROE-ISLANDS-REGION
#315	2001-04-07	23:17:37.92	-176.336	-27.554	33.0	5.99	6.16	TF	na	6.11	KERMADEC-ISLANDS-REGION
#316	2001-04-09	09:00:57.17	-73.109	-32.668	11.0	6.63	6.65	NF	6.35	6.93	OFF-COAST-OF-CENTRAL-CHI
#317	2001-04-13	15:33:53.55	-25.586	-59.723	26.0	6.12	6.19	TF	5.53	6.06	SOUTH-SANDWICH-ISLANDS-R
#318	2001-05-09	17:38:26.12	161.232	-10.318	68.0	6.20	6.22	TF	6.19	6.54	SOLOMON-ISLANDS
#319	2001-05-25	00:40:50.60	148.393	44.268	33.0	6.63	6.69	TF	6.35	6.60	KURIL-ISLANDS
#320	2001-05-29	23:37:19.49	155.037	-7.022	14.0	6.23	6.37	TF	5.95	6.27	SOLOMON-ISLANDS
#321	2001-06-05	09:00:05.38	146.388	-6.884	10.0	6.27	6.40	TF	6.10	6.54	EAST-PAPUA-NEW-GUINEA-RE
#322	2001-06-23	20:33:14.13	-73.641	-16.265	33.0	8.28	8.38	TF	8.04	8.16	NEAR-COAST-OF-PERU
#323	2001-06-26	04:18:31.38	-71.649	-17.745	24.0	6.65	6.70	TF	6.65	6.73	NEAR-COAST-OF-PERU
#324	2001-07-05	13:53:48.36	-73.987	-16.086	62.0	6.56	6.53	NF	6.34	6.58	NEAR-COAST-OF-PERU
#325	2001-07-07	09:38:43.52	-72.077	-17.543	33.0	7.48	7.60	TF	7.14	7.36	NEAR-COAST-OF-PERU
#326	2001-07-24	05:00:09.09	-69.255	-19.448	33.0	6.32	6.30	NCL	6.74	6.18	NORTHERN-CHILE
#327	2001-07-26	00:21:36.92	24.244	39.059	10.0	6.45	6.43	SS	6.94	6.51	AEGEAN-SEA
#328	2001-08-06	03:52:59.51	-123.422	-55.537	10.0	6.58	6.71	NF	na	6.74	EASTER-ISLAND-CORDILLERA
#329	2001-08-21	06:52:06.25	-179.575	-36.813	33.0	7.09	7.08	TF	7.01	7.47	EAST-OF-NORTH-ISLAND,-N.
#330	2001-09-02	02:25:54.09	82.501	0.889	10.0	6.05	6.03	SS	na	6.32	NORTH-INDIAN-OCEAN
#331	2001-10-08	18:14:26.44	160.324	52.591	48.0	6.33	6.44	TF	6.17	6.41	OFF-EAST-COAST-OF-KAMCHA
#332	2001-10-12	05:02:34.00	-132.200	52.630	20.0	5.96	6.03	TF	5.73	5.92	QUEEN-CHARLOTTE-ISLANDS
#333	2001-10-12	15:02:16.84	144.980	12.686	37.0	6.88	6.98	TF	7.09	7.35	SOUTH-OF-MARIANA-ISLANDS

#334	2001-10-19	03:28:44.46	123.907	-4.102	17.0	7.36	7.45	SS	8.00	7.51	BANDA-SEA
#335	2001-10-21	00:29:21.49	178.982	-37.137	18.0	6.52	6.62	SS	6.78	6.52	OFF-E.-COAST-OF-N.-ISLAN
#336	2001-10-31	09:10:20.00	150.196	-5.912	33.0	6.81	6.92	TF	6.27	6.58	NEW-BRITAIN-REGION
#337	2001-11-09	00:47:55.02	-82.300	9.643	10.0	6.03	6.03	TF	6.05	6.39	PANAMA-COSTA-RICA-BORDER
#338	2001-11-14	09:26:10.01	90.541	35.946	10.0	7.44	7.78	SS	8.07	7.63	QINGHAI-PROVINCE,-CHINA
#339	2001-11-15	01:03:06.06	-15.578	-1.587	10.0	6.25	6.27	SS	6.26	6.08	NORTH-OF-ASCENSION-ISLAN
#340	2001-11-22	23:22:20.44	178.019	-16.255	10.0	6.31	6.29	SS	na	6.30	FIJI-ISLANDS
#341	2001-12-12	14:02:35.04	124.688	-42.813	10.0	7.05	7.05	SS	7.61	7.21	SOUTH-OF-AUSTRALIA
#342	2001-12-23	22:52:54.33	159.530	-9.613	16.0	6.72	6.81	TF	6.79	7.07	SOLOMON-ISLANDS
#343	2002-01-02	17:22:48.76	167.856	-17.600	21.0	7.09	7.19	NCL	7.20	7.24	VANUATU-ISLANDS
#344	2002-01-03	10:17:36.30	168.004	-17.664	10.0	6.41	6.60	TF	6.16	6.71	VANUATU-ISLANDS
#345	2002-01-10	11:14:56.93	142.427	-3.212	11.0	6.60	6.70	TF	6.63	6.82	NEAR-N-COAST-OF-PAPUA-NE
#346	2002-01-15	07:12:58.03	105.205	-6.314	10.0	6.05	6.06	SS	na	6.42	SUNDA-STRAIT
#347	2002-02-03	07:11:28.41	31.271	38.573	5.0	6.19	6.45	NF	5.67	6.24	TURKEY
#348	2002-03-05	21:16:09.13	124.249	6.033	31.0	7.21	7.46	TF	7.09	7.26	MINDANAO,-PHILIPPINE-ISL
#349	2002-03-25	14:56:33.82	69.315	36.062	8.0	5.99	6.07	TF	6.17	6.46	HINDU-KUSH-REGION
#350	2002-03-31	06:52:50.49	122.179	24.279	33.0	7.09	7.09	TF	6.87	7.07	TAIWAN-REGION
#351	2002-04-11	21:56:56.39	167.687	-14.392	10.0	6.12	6.09	TF	6.20	6.56	VANUATU-ISLANDS
#352	2002-04-18	05:02:46.19	-100.865	16.985	25.0	6.03	6.72	NCL	5.97	6.11	NEAR-COAST-OF-GUERRERO,
#353	2002-04-18	16:08:36.78	-70.586	-27.535	62.0	6.65	6.56	SS	6.45	6.84	NEAR-COAST-OF-NORTHERN-C
#354	2002-05-14	16:56:10.42	78.932	-36.518	10.0	6.10	6.21	SS	na	6.07	MID-INDIAN-RISE
#355	2002-06-13	01:27:19.47	99.751	-47.801	10.0	6.48	6.53	SS	na	6.41	SOUTHEAST-INDIAN-RISE
#356	2002-06-17	21:26:22.92	166.383	-12.592	33.0	6.60	6.70	TF	6.14	6.65	SANTA-CRUZ-ISLANDS
#357	2002-06-18	13:56:22.83	-71.124	-30.805	54.0	6.55	6.42	TF	6.32	6.82	NEAR-COAST-OF-CENTRAL-CH
#358	2002-06-22	02:58:21.30	49.047	35.626	10.0	6.49	6.50	TF	6.43	6.91	WESTERN-IRAN
#359	2002-07-03	23:00:18.47	147.336	-5.032	31.0	6.16	6.14	SS	6.67	6.06	EAST-PAPUA-NEW-GUINEA-RE
#360	2002-07-31	00:16:44.61	-82.793	7.929	10.0	6.47	6.46	SS	6.54	6.50	SOUTH-OF-PANAMA
#361	2002-08-14	13:12:39.88	136.880	7.831	10.0	6.22	6.20	TF	6.18	6.66	WEST-CAROLINE-ISLANDS
#362	2002-08-20	10:59:32.02	141.966	30.986	9.0	6.28	6.05	TF	6.01	6.21	SOUTH-OF-HONSHU,-JAPAN
#363	2002-09-08	18:44:23.71	142.945	-3.302	13.0	7.15	7.58	TF	7.68	7.72	NEAR-N-COAST-OF-PAPUA-NE
#364	2002-09-13	22:28:29.46	93.068	13.036	21.0	6.45	6.47	TF	6.37	6.65	ANDAMAN-ISLANDS-REGION
#365	2002-10-03	16:08:29.62	-108.530	23.324	10.0	6.41	6.46	SS	6.65	6.31	GULF-OF-CALIFORNIA
#366	2002-10-06	15:46:33.01	118.341	-8.197	10.0	6.21	6.22	TF	5.90	6.50	SUMBAWA-REGION,-INDONESI
#367	2002-10-10	10:50:20.57	134.297	-1.757	10.0	7.34	7.54	SS	8.22	7.87	IRIAN-JAYA-REGION,-INDON
#368	2002-10-14	14:12:43.75	142.249	41.174	61.0	6.09	6.07	TF	5.83	6.27	HOKKAIDO,-JAPAN-REGION
#369	2002-10-19	12:09:05.38	149.960	44.297	33.0	6.12	6.26	TF	na	6.11	KURIL-ISLANDS
#370	2002-10-23	11:27:19.43	-147.912	63.514	4.0	6.70	6.62	SS	7.32	6.99	CENTRAL-ALASKA
#371	2002-10-24	06:08:37.98	29.004	-1.884	11.0	6.03	6.16	NF	5.70	6.33	LAKE-TANGANYIKA-REGION
#372	2002-11-02	01:26:10.70	96.085	2.824	30.0	7.34	7.24	TF	7.04	7.23	NORTHERN-SUMATRA,-INDONE
#373	2002-11-03	22:12:41.00	-147.444	63.517	5.0	na	7.85	SS	8.08	7.86	CENTRAL-ALASKA
#374	2002-11-15	19:58:31.78	-36.404	-56.051	10.0	6.41	6.61	TF	na	6.94	SOUTH-GEORGIA-ISLAND-REG
#375	2002-11-20	21:32:30.81	74.515	35.414	33.0	5.96	6.30	NF	5.92	6.09	NORTHWESTERN-KASHMIR
#376	2002-11-26	00:48:15.04	-173.537	51.465	21.0	5.89	6.07	TF	5.83	6.22	ANDREANOF-ISLANDS,-ALEUT
#377	2002-12-11	03:49:40.19	135.123	-3.810	10.0	6.23	6.20	SS	na	6.26	IRIAN-JAYA-REGION,-INDON
#378	2003-01-16	00:53:15.72	-129.024	44.284	10.0	6.23	6.21	SS	6.21	6.05	OFF-COAST-OF-OREGON
#379	2003-01-20	08:43:06.07	160.770	-10.491	33.0	7.19	7.25	TS	7.25	7.47	SOLOMON-ISLANDS
#380	2003-01-22	02:06:34.61	-104.104	18.770	24.0	7.59	7.47	TF	7.35	7.34	NEAR-COAST-OF-JALISCO,-M
#381	2003-02-12	22:33:30.83	144.242	-3.652	10.0	6.12	6.17	TF	6.14	6.57	NEAR-N-COAST-OF-NEW-GUIN
#382	2003-02-19	03:32:36.36	-164.643	53.645	19.0	6.53	6.61	TF	6.35	6.44	UNIMAK-ISLAND-REGION,-AL
#383	2003-02-24	02:03:41.45	77.230	39.610	11.0	6.23	6.32	TF	5.69	6.54	SOUTHERN-XINJIANG,-CHINA
#384	2003-03-02	16:42:56.33	-20.879	-36.958	10.0	6.13	6.02	NF	na	6.18	SOUTHERN-MID-ATLANTIC-RI
#385	2003-03-11	07:27:32.65	153.238	-4.694	40.0	6.60	6.78	SS	6.34	6.71	NEW-IRELAND-REGION,-P.N.
#386	2003-03-12	23:41:32.92	-110.587	26.556	10.0	6.34	6.33	SS	na	6.17	GULF-OF-CALIFORNIA
#387	2003-03-17	16:36:17.31	177.978	51.272	33.0	7.02	7.02	TF	6.45	6.62	RAT-ISLANDS,-ALEUTIAN-IS
#388	2003-03-25	02:53:25.03	120.743	-8.294	33.0	6.30	6.42	NCL	6.28	6.57	FLORES-REGION,-INDONESIA
#389	2003-03-30	18:13:34.09	127.542	-3.169	33.0	6.13	6.19	NS	na	6.17	SERAM,-INDONESIA

#390	2003-04-02	03:43:11.58	-35.729	35.280	10.0	6.10	6.24	SS	na	6.06	NORTHERN-MID-ATLANTIC-RI
#391	2003-04-17	00:48:38.58	96.476	37.529	14.0	6.16	6.34	TF	6.24	6.69	QINGHAI,-CHINA
#392	2003-04-17	14:50:48.58	1.432	-54.624	10.0	6.42	6.50	SS	na	6.13	BOUVET-ISLAND-REGION
#393	2003-05-01	00:27:04.70	40.464	39.007	10.0	6.34	6.32	SS	6.88	6.38	TURKEY
#394	2003-05-05	23:04:45.67	127.954	3.715	56.0	6.12	6.06	TF	6.02	6.35	TALAUD-ISLANDS,-INDONESI
#395	2003-05-14	06:03:35.86	-58.633	18.266	42.0	6.63	6.60	SS	6.97	6.94	NORTH-ATLANTIC-OCEAN
#396	2003-05-19	16:27:10.20	-105.473	17.546	10.0	6.03	6.07	SS	na	5.96	OFF-COAST-OF-JALISCO,-ME
#397	2003-05-21	18:44:20.10	3.634	36.964	12.0	6.68	6.80	TF	6.75	7.19	NORTHERN-ALGERIA
#398	2003-05-26	09:24:33.40	141.568	38.849	68.0	7.01	6.99	TF	7.22	7.43	NEAR-EAST-COAST-OF-HONSH
#399	2003-05-26	19:23:27.94	128.855	2.354	31.0	6.72	6.93	TF	6.98	7.12	HALMAHERA,-INDONESIA
#400	2003-06-20	13:30:41.64	-71.637	-30.608	33.0	6.68	6.76	TF	6.68	6.92	NEAR-COAST-OF-CENTRAL-CH
#401	2003-07-15	20:27:50.53	68.382	-2.598	10.0	na	7.53	SS	7.57	7.51	CARLSBERG-RIDGE
#402	2003-07-25	09:37:45.84	149.694	-1.528	24.0	6.35	6.42	TF	6.59	6.77	NEW-IRELAND-REGION,-P.N.
#403	2003-08-04	04:37:20.13	-43.411	-60.532	10.0	7.08	7.56	NCL	7.12	7.65	SCOTIA-SEA
#404	2003-08-14	05:14:54.76	20.605	39.160	10.0	6.13	6.25	SS	6.80	6.40	GREECE-ALBANIA-BORDER-RE
#405	2003-08-21	12:12:49.79	167.144	-45.104	28.0	7.05	7.18	TF	6.89	7.14	SOUTH-ISLAND,-NEW-ZEALAN
#406	2003-09-06	02:08:13.81	-106.045	-4.623	10.0	6.07	6.01	SS	6.26	5.73	CENTRAL-EAST-PACIFIC-RIS
#407	2003-09-07	13:19:20.45	172.123	-22.472	33.0	6.31	6.35	NCL	7.01	5.99	SOUTHEAST-OF-LOYALTY-ISL
#408	2003-09-21	18:16:13.41	95.672	19.917	10.0	6.53	6.55	SS	6.69	6.84	MYANMAR
#409	2003-09-22	04:45:36.24	-70.673	19.777	10.0	6.39	6.41	TF	6.40	6.80	DOMINICAN-REPUBLIC-REGIO
#410	2003-09-25	19:50:06.36	143.910	41.815	27.0	8.07	8.26	NCL	7.96	8.00	HOKKAIDO,-JAPAN-REGION
#411	2003-09-27	11:33:25.08	87.813	50.038	16.0	7.27	7.25	SS	7.54	7.62	SOUTHWESTERN-SIBERIA,-RU
#412	2003-10-01	01:03:25.24	87.721	50.211	10.0	6.68	6.64	SS	7.35	7.21	SOUTHWESTERN-SIBERIA,-RU
#413	2003-10-07	04:55:28.81	-170.192	-16.526	10.0	6.19	6.13	TF	5.89	6.48	SAMOA-ISLANDS-REGION
#414	2003-10-31	01:06:28.28	142.619	37.812	10.0	6.95	6.97	NCL	6.65	7.01	OFF-EAST-COAST-OF-HONSHU
#415	2003-11-02	05:32:15.72	166.535	-45.190	10.0	6.39	6.37	TF	6.21	6.30	OFF-W.-COAST-OF-S.-ISLAN
#416	2003-11-12	00:29:45.35	126.480	1.593	33.0	6.01	6.20	TF	6.10	6.23	NORTHERN-MOLUCCA-SEA
#417	2003-11-14	04:28:33.30	172.331	-16.737	10.0	5.93	6.04	NF	5.32	5.67	VANUATU-ISLANDS-REGION
#418	2003-11-17	06:43:06.80	178.650	51.146	33.0	7.70	7.75	TF	7.31	7.45	RAT-ISLANDS,-ALEUTIAN-IS
#419	2003-11-18	17:14:22.62	125.416	12.025	35.0	6.51	6.49	TF	6.26	6.58	SAMAR,-PHILIPPINES
#420	2003-12-05	21:26:09.48	165.780	55.538	10.0	6.70	6.64	TS	6.65	6.83	KOMANDORSKIYE-OSTROVA-RE
#421	2003-12-09	12:44:01.68	-179.272	51.334	33.0	6.07	6.15	TF	5.92	6.15	ANDREANOF-ISLANDS,-ALEUT
#422	2003-12-10	04:38:11.59	121.362	23.039	10.0	6.75	6.80	TF	6.69	6.98	TAIWAN
#423	2003-12-22	19:15:56.00	-121.102	35.706	8.0	6.35	6.55	TF	6.26	6.78	CENTRAL-CALIFORNIA
#424	2003-12-26	01:56:52.44	58.311	28.995	10.0	6.48	6.58	SS	6.92	6.84	SOUTHERN-IRAN
#425	2003-12-27	16:00:59.45	169.766	-22.015	10.0	7.19	7.25	TF	6.94	7.20	SOUTHEAST-OF-LOYALTY-ISL
#426	2003-12-27	22:38:01.88	169.835	-21.672	10.0	6.65	6.70	TF	6.37	6.75	SOUTHEAST-OF-LOYALTY-ISL
#427	2004-01-03	16:23:21.02	169.683	-22.253	22.0	6.74	7.12	NF	7.03	7.11	SOUTHEAST-OF-LOYALTY-ISL
#428	2004-01-11	04:32:47.79	53.352	-36.696	5.0	6.19	6.15	TF	6.21	6.83	SOUTH-INDIAN-OCEAN
#429	2004-01-16	18:07:55.66	-37.704	7.641	10.0	6.12	6.15	SS	6.52	6.22	CENTRAL-MID-ATLANTIC-RID
#430	2004-01-28	22:15:30.70	127.400	-3.120	17.0	6.65	6.63	NCL	6.94	6.73	SERAM,-INDONESIA
#431	2004-01-29	03:52:52.30	-114.780	-50.206	10.0	6.05	6.09	SS	na	5.80	SOUTHERN-EAST-PACIFIC-RI
#432	2004-02-05	21:05:02.84	135.538	-3.615	17.0	6.77	6.95	NCL	6.70	7.02	IRIAN-JAYA-REGION,-INDON
#433	2004-02-07	02:42:35.21	135.023	-4.003	10.0	7.26	7.26	SS	7.47	7.40	IRIAN-JAYA-REGION,-INDON
#434	2004-02-08	08:58:51.80	135.339	-3.665	26.0	6.50	6.65	SS	6.52	6.38	IRIAN-JAYA-REGION,-INDON
#435	2004-02-21	02:34:42.70	-14.963	-58.425	10.0	6.55	6.59	SS	na	6.68	EAST-OF-SOUTH-SANDWICH-I
#436	2004-02-23	16:04:49.44	-175.630	-14.740	12.0	6.28	6.13	SS	6.76	6.10	SAMOA-ISLANDS-REGION
#437	2004-02-24	02:27:46.23	-3.997	35.142	10.0	6.39	6.33	SS	6.91	6.60	STRAIT-OF-GIBRALTAR
#438	2004-03-08	23:39:11.34	-43.919	10.480	10.0	5.96	6.00	SS	na	5.99	NORTHERN-MID-ATLANTIC-RI
#439	2004-04-14	01:54:09.22	162.659	55.226	51.0	6.16	6.10	TS	6.01	6.26	NEAR-EAST-COAST-OF-KAMCH
#440	2004-04-15	20:06:55.30	169.631	-19.374	10.0	6.22	6.10	NF	na	6.39	VANUATU-ISLANDS
#441	2004-04-23	01:50:30.22	122.839	-9.362	66.0	6.63	6.64	NCL	6.50	7.09	SAVU-SEA
#442	2004-05-03	04:36:50.04	-73.406	-37.695	21.0	6.55	6.61	TF	6.25	6.42	NEAR-COAST-OF-CENTRAL-CH
#443	2004-05-13	09:58:43.45	150.730	-3.584	10.0	6.19	6.32	SS	6.89	6.36	NEW-IRELAND-REGION,-P.N.
#444	2004-05-28	12:38:44.47	51.610	36.290	17.0	6.20	6.31	TF	6.12	6.83	NORTHERN-AND-CENTRAL-IRA
#445	2004-06-02	08:50:37.13	-179.447	-32.875	43.0	6.17	6.07	TF	5.83	6.08	SOUTH-OF-KERMADEC-ISLAND

#446	2004-06-09	22:52:08.80	139.615	-51.603	10.0	6.21	6.40	SS	6.93	6.48	WESTERN-INDIAN-ANTARCTIC
#447	2004-06-28	09:49:47.00	-134.250	54.800	20.0	6.79	6.78	NCL	6.73	6.43	QUEEN-CHARLOTTE-ISLANDS
#448	2004-07-16	23:58:19.04	-179.574	-65.651	10.0	6.09	6.11	SS	na	6.18	PACIFIC-ANTARCTIC-RIDGE
#449	2004-07-22	09:45:14.90	128.890	26.490	21.0	na	6.03	SS	na	6.30	RYUKYU-ISLANDS,-JAPAN
#450	2004-07-28	03:56:28.60	133.090	-0.440	13.0	na	6.47	TF	na	6.54	IRIAN-JAYA-REGION,-INDON
#451	2004-08-28	13:41:25.60	-70.525	-35.173	11.0	6.48	6.50	SS	5.90	6.60	CHILE-ARGENTINA-BORDER-R
#452	2004-09-05	10:07:07.82	136.618	33.070	14.0	7.00	7.19	TF	7.45	7.76	NEAR-S.-COAST-OF-WESTERN
#453	2004-09-05	14:57:18.61	137.071	33.184	10.0	7.32	7.37	TF	7.41	7.84	NEAR-S.-COAST-OF-HONSHU,
#454	2004-09-06	12:42:59.39	-28.976	-55.372	10.0	6.87	6.75	TF	na	6.97	SOUTH-SANDWICH-ISLANDS-R
#455	2004-09-06	23:29:35.09	137.227	33.205	10.0	6.47	6.59	TF	6.45	6.98	NEAR-S.-COAST-OF-HONSHU
#456	2004-09-07	11:53:06.11	-65.840	-28.573	22.0	6.35	6.08	TF	6.24	6.60	SANTIAGO-DEL-ESTERO-PROV
#457	2004-09-08	14:58:25.83	137.200	33.140	21.0	6.05	6.11	TF	6.23	6.47	NEAR-S.-COAST-OF-HONSHU,
#458	2004-09-19	20:26:04.10	174.027	52.205	25.0	6.10	6.21	TF	5.73	6.17	NEAR-ISLANDS,-ALEUTIAN-I
#459	2004-09-28	15:29:53.82	28.016	-52.515	10.0	6.29	6.32	SS	6.75	6.68	SOUTH-OF-AFRICA
#460	2004-10-06	22:30:56.95	134.426	-0.670	10.0	6.05	6.14	SS	na	6.28	IRIAN-JAYA-REGION,-INDON
#461	2004-10-09	21:26:53.69	-86.665	11.422	35.0	6.80	6.92	TF	6.43	6.70	NEAR-COAST-OF-NICARAGUA
#462	2004-10-20	18:32:24.57	166.612	-14.027	60.0	5.93	6.02	TF	na	5.96	VANUATU-ISLANDS
#463	2004-10-23	08:56:00.86	138.779	37.226	16.0	6.32	6.56	TF	6.50	6.87	NEAR-WEST-COAST-OF-HONSH
#464	2004-10-26	22:53:07.86	-24.679	-57.071	10.0	6.39	6.19	TF	na	6.28	SOUTH-SANDWICH-ISLANDS-R
#465	2004-11-02	10:02:12.82	-128.772	49.277	10.0	6.63	6.56	SS	6.91	6.46	VANCOUVER-ISLAND,-CANADA
#466	2004-11-08	15:55:01.15	122.542	24.104	29.0	6.20	6.27	TF	5.70	6.31	TAIWAN-REGION
#467	2004-11-11	17:34:52.05	162.208	-11.128	10.0	6.65	6.61	TF	6.11	6.70	SOLOMON-ISLANDS
#468	2004-11-11	21:26:41.15	124.868	-8.152	10.0	7.40	7.48	TF	7.40	7.62	TIMOR-REGION
#469	2004-11-15	09:06:56.56	-77.508	4.695	15.0	7.15	7.19	TF	7.36	7.52	NEAR-WEST-COAST-OF-COLOM
#470	2004-11-20	08:07:22.08	-84.172	9.602	16.0	6.39	6.38	SS	6.38	6.52	COSTA-RICA
#471	2004-11-20	22:01:45.66	-90.056	13.376	41.0	6.19	6.29	TF	5.81	6.03	NEAR-COAST-OF-GUATEMALA
#472	2004-11-21	11:41:07.76	-61.706	15.679	14.0	6.27	6.29	NF	6.32	6.63	LEEWARD-ISLANDS
#473	2004-11-22	20:26:23.90	164.721	-46.676	10.0	6.95	7.10	TF	6.84	7.39	OFF-W.-COAST-OF-S.-ISLAN
#474	2004-11-26	02:25:03.31	135.404	-3.609	10.0	6.93	7.09	NCL	6.76	7.30	IRIAN-JAYA-REGION,-INDON
#475	2004-11-28	02:35:13.41	-113.834	-26.525	10.0	6.44	6.57	SS	na	6.26	EASTER-ISLAND-REGION
#476	2004-11-28	18:32:14.13	145.119	43.006	39.0	6.98	6.97	TF	6.96	7.27	HOKKAIDO,-JAPAN-REGION
#477	2004-12-06	14:15:11.89	145.228	42.900	35.0	6.72	6.74	TF	6.79	6.96	HOKKAIDO,-JAPAN-REGION
#478	2004-12-14	23:20:13.36	-81.409	18.958	10.0	6.81	6.77	SS	7.50	7.06	NORTH-OF-HONDURAS
#479	2004-12-18	06:46:19.87	156.309	48.837	11.0	6.20	6.15	TF	5.90	6.18	EAST-OF-KURIL-ISLANDS
#480	2004-12-23	14:59:04.41	161.345	-49.312	10.0	7.93	8.07	SS	8.43	8.02	NORTH-OF-MACQUARIE-ISLAN
#481	2004-12-26	00:58:53.45	95.982	3.295	30.0	8.21	9.00	NCL	8.50	8.79	OFF-W-COAST-OF-NORTHERN
#482	2004-12-27	09:39:06.80	94.650	5.348	35.0	6.07	6.01	TF	6.07	6.25	NORTHERN-SUMATRA,-INDONE
#483	2005-01-01	06:25:44.82	92.304	5.099	12.0	6.48	6.65	SS	7.16	6.85	OFF-W-COAST-OF-NORTHERN
#484	2005-01-03	17:59:28.89	161.866	-50.659	10.0	6.03	6.04	SS	na	6.09	NORTH-OF-MACQUARIE-ISLAN
#485	2005-01-12	08:40:03.65	-21.194	-0.878	10.0	6.77	6.78	SS	6.59	6.42	CENTRAL-MID-ATLANTIC-RID
#486	2005-01-16	08:25:04.47	-176.299	-25.528	16.0	6.16	6.11	TF	6.07	6.41	SOUTH-OF-FIJI-ISLANDS
#487	2005-01-16	20:17:52.76	140.842	10.934	25.0	6.52	6.59	NF	6.89	6.79	W.-CAROLINE-ISLANDS,-MIC
#488	2005-01-18	14:09:06.22	144.866	42.946	42.0	6.24	6.18	TF	6.11	6.54	HOKKAIDO,-JAPAN-REGION
#489	2005-01-19	06:11:36.40	141.491	34.064	28.0	6.39	6.54	TF	5.83	6.42	OFF-EAST-COAST-OF-HONSHU
#490	2005-01-22	20:30:17.35	159.475	-7.727	29.0	6.39	6.35	NF	5.90	6.45	SOLOMON-ISLANDS
#491	2005-01-23	20:10:12.15	119.933	-1.198	48.0	6.05	6.23	NF	6.00	6.13	SULAWESI,-INDONESIA
#492	2005-01-24	04:16:47.44	92.482	7.330	30.0	6.22	6.23	SS	6.48	6.42	NICOBAR-ISLANDS,-INDIA-R
#493	2005-02-07	20:02:17.69	153.187	-4.525	36.0	6.09	6.07	NCL	5.28	6.02	NEW-IRELAND-REGION,-P.N.
#494	2005-02-09	18:46:09.97	143.997	26.088	24.0	6.26	6.26	NF	5.97	6.46	BONIN-ISLANDS,-JAPAN-REG
#495	2005-02-14	23:38:08.66	79.440	41.728	22.0	5.96	6.08	NCL	5.69	6.12	KYRGYZSTAN-XINJIANG-BORD
#496	2005-02-15	14:42:25.85	126.421	4.756	40.0	6.40	6.50	TF	6.07	6.51	TALAUD-ISLANDS,-INDONESI
#497	2005-02-16	20:27:52.49	-16.558	-36.320	10.0	6.45	6.60	SS	6.63	6.41	SOUTHERN-MID-ATLANTIC-RI
#498	2005-02-19	00:04:43.59	122.129	-5.562	10.0	6.50	6.43	TF	6.30	6.91	SULAWESI,-INDONESIA
#499	2005-02-22	02:25:22.92	56.816	30.754	14.0	6.25	6.41	TF	6.15	6.69	NORTHERN-AND-CENTRAL-IRA
#500	2005-03-06	04:39:59.43	163.045	-11.045	10.0	6.15	6.02	SS	na	6.14	SOLOMON-ISLANDS
#501	2005-03-19	15:02:42.67	-174.337	-20.407	18.0	6.01	6.07	TF	5.79	6.22	TONGA-ISLANDS

#502	2005-03-20	01:53:41.83	130.131	33.807	10.0	6.44	6.58	SS	7.02	6.72	KYUSHU,-JAPAN
#503	2005-03-26	15:40:34.53	129.938	-4.894	10.0	6.12	6.15	SS	na	6.40	BANDA-SEA
#504	2005-03-28	16:09:36.53	97.108	2.085	30.0	8.05	8.61	NCL	8.28	8.30	NORTHERN-SUMATRA,-INDONE
#505	2005-04-02	12:52:36.59	6.098	78.607	10.0	6.07	6.15	SS	na	5.92	SVALBARD-REGION
#506	2005-04-07	20:04:41.06	83.662	30.491	11.0	6.19	6.28	NF	5.93	6.47	XIZANG
#507	2005-04-08	05:48:37.88	97.731	-0.215	21.0	6.09	6.10	SS	5.53	5.85	SOUTHWEST-OF-SUMATRA,-IN
#508	2005-04-10	10:29:11.28	99.607	-1.644	19.0	6.55	6.68	TF	6.78	6.90	SOUTHERN-SUMATRA,-INDONE
#509	2005-04-10	17:24:39.40	99.717	-1.591	30.0	6.37	6.12	NCL	5.93	6.29	SOUTHERN-SUMATRA,-INDONE
#510	2005-04-11	12:20:05.96	145.909	-3.484	11.0	6.44	6.63	SS	7.16	6.61	NEAR-N-COAST-OF-NEW-GUIN
#511	2005-04-11	17:08:53.94	170.612	-21.975	68.0	6.72	6.71	NCL	6.35	6.57	SOUTHEAST-OF-LOYALTY-ISL
#512	2005-05-05	19:12:21.41	-82.845	5.710	10.0	6.35	6.47	SS	6.45	6.35	SOUTH-OF-PANAMA
#513	2005-05-10	01:09:05.10	103.139	-6.226	17.0	6.19	6.27	TF	6.13	6.53	SOUTHWEST-OF-SUMATRA,-IN
#514	2005-05-16	03:54:14.62	-179.353	-32.589	34.0	6.57	6.50	TF	6.30	6.50	SOUTH-OF-KERMADEC-ISLAND
#515	2005-05-18	10:27:06.41	-173.240	-15.318	10.0	6.03	6.19	TF	5.44	5.98	TONGA-ISLANDS
#516	2005-05-19	01:54:52.85	97.041	1.989	30.0	6.65	6.85	NCL	6.19	6.84	NORTHERN-SUMATRA,-INDONE
#517	2005-05-21	05:11:35.39	-80.987	-3.286	40.0	6.28	6.35	SS	6.03	6.13	PERU-ECUADOR-BORDER-REGI
#518	2005-06-14	17:10:12.28	179.314	51.239	51.0	6.56	6.76	TF	6.45	6.52	RAT-ISLANDS,-ALEUTIAN-IS
#519	2005-06-15	02:50:54.19	-125.953	41.292	10.0	7.11	7.21	SS	7.54	7.02	OFF-COAST-OF-NORTHERN-CA
#520	2005-06-15	19:52:24.82	-80.562	-44.865	10.0	6.41	6.45	SS	na	6.04	OFF-COAST-OF-SOUTHERN-CH
#521	2005-06-17	06:21:42.59	-126.574	40.773	10.0	6.60	6.64	SS	7.16	6.71	OFF-COAST-OF-NORTHERN-CA
#522	2005-06-27	11:35:45.60	-107.298	18.781	16.0	6.20	6.15	SS	6.78	6.13	OFF-COAST-OF-JALISCO,-ME
#523	2005-07-04	11:36:05.65	42.370	-42.283	10.0	6.09	6.25	SS	na	6.05	PRINCE-EDWARD-ISLANDS-RE
#524	2005-07-10	04:46:31.24	-97.264	-36.310	10.0	6.10	6.01	SS	na	5.93	WEST-CHILE-RISE
#525	2005-07-24	15:42:06.21	92.190	7.920	16.0	7.14	7.23	SS	8.05	7.50	NICOBAR-ISLANDS,-INDIA-R
#526	2005-08-03	11:03:15.13	-85.541	11.247	14.0	6.24	6.25	SS	6.79	6.43	NICARAGUA
#527	2005-08-07	02:17:46.04	33.620	-47.090	10.0	5.96	6.16	SS	na	6.35	PRINCE-EDWARD-ISLANDS-RE
#528	2005-08-11	09:08:46.81	169.509	-22.677	10.0	6.21	6.13	SS	na	6.49	SOUTHEAST-OF-LOYALTY-ISL
#529	2005-08-16	02:46:28.40	142.039	38.276	36.0	7.05	7.19	TF	6.71	7.16	NEAR-EAST-COAST-OF-HONSH
#530	2005-08-26	18:16:33.62	52.365	14.417	10.0	6.17	6.14	SS	6.40	6.18	EASTERN-GULF-OF-ADEN
#531	2005-09-05	07:37:31.31	-142.392	-56.410	10.0	6.21	6.19	SS	6.57	6.13	PACIFIC-ANTARCTIC-RIDGE
#532	2005-09-25	12:55:46.60	167.801	-17.515	30.0	6.13	6.14	TF	5.71	6.06	VANUATU-ISLANDS
#533	2005-10-08	03:50:40.80	73.588	34.539	26.0	7.27	7.58	TF	7.35	7.65	PAKISTAN
#534	2005-10-15	10:06:17.01	154.113	46.816	43.0	6.01	6.10	TF	6.00	6.36	EAST-OF-KURIL-ISLANDS
#535	2005-10-29	04:05:56.04	96.898	-45.214	8.0	6.36	6.48	NF	6.04	6.55	SOUTHEAST-INDIAN-RIDGE
#536	2005-11-05	10:48:21.22	148.143	-3.149	25.0	6.30	6.40	SS	na	5.99	BISMARCK-SEA
#537	2005-11-14	21:38:51.42	144.896	38.107	11.0	6.83	6.98	NF	6.84	7.40	OFF-EAST-COAST-OF-HONSHU
#538	2005-11-19	14:10:13.03	96.786	2.164	21.0	6.46	6.32	TF	5.92	6.27	NORTHERN-SUMATRA,-INDONE
#539	2005-11-20	12:53:02.95	-164.093	53.843	30.0	6.01	6.15	TF	5.65	5.92	UNIMAK-ISLAND-REGION,-AL
#540	2005-11-22	15:11:31.58	145.284	-5.154	68.0	6.15	6.16	NCL	5.46	6.23	EASTERN-NEW-GUINEA-REG.,
#541	2005-11-30	16:53:42.47	124.029	6.270	13.0	6.19	6.39	TF	6.10	6.46	MINDANAO,-PHILIPPINES
#542	2005-12-02	13:13:09.52	142.122	38.089	29.0	6.42	6.46	TF	6.40	6.48	NEAR-EAST-COAST-OF-HONSH
#543	2005-12-05	12:19:56.62	29.830	-6.224	22.0	6.65	6.77	NF	6.32	6.70	LAKE-TANGANYIKA-REGION
#544	2005-12-07	23:32:51.55	-177.637	-30.012	21.0	6.28	6.40	TF	6.45	6.33	KERMADEC-ISLANDS,-NEW-ZE
#545	2005-12-11	14:20:45.00	152.223	-6.584	10.0	6.52	6.59	NF	6.35	6.95	NEW-BRITAIN-REGION,-P.N.
#546	2005-12-13	03:16:06.38	-178.571	-15.265	10.0	6.68	6.66	SS	7.06	6.72	FIJI-ISLANDS-REGION
#547	2005-12-16	18:32:16.42	141.900	38.506	43.0	5.93	6.02	TF	na	6.20	NEAR-EAST-COAST-OF-HONSH
#548	2005-12-20	05:51:12.56	140.995	12.232	23.0	6.07	6.11	NF	5.92	6.05	W.-CAROLINE-ISLANDS,-MIC
#549	2005-12-21	07:09:05.17	124.672	-0.066	25.0	6.22	6.34	TF	6.06	6.43	SOUTHERN-MOLUCCA-SEA
#550	2005-12-22	12:20:02.94	-135.868	-54.719	10.0	6.22	6.35	SS	na	6.01	PACIFIC-ANTARCTIC-RIDGE
#551	2005-12-30	18:26:43.90	-82.266	7.529	10.0	6.10	6.07	SS	na	5.98	SOUTH-OF-PANAMA
#552	2006-01-02	06:10:49.76	-21.606	-60.957	10.0	7.14	7.36	SS	7.59	7.33	EAST-OF-SOUTH-SANDWICH-I
#553	2006-01-04	08:32:32.40	-112.117	28.164	14.0	6.49	6.59	SS	7.07	6.59	GULF-OF-CALIFORNIA
#554	2006-01-06	03:39:58.55	-82.337	6.635	7.0	6.07	6.00	SS	6.57	6.35	SOUTH-OF-PANAMA
#555	2006-01-08	11:34:55.64	23.212	36.311	66.0	6.68	6.72	TF	6.71	7.11	SOUTHERN-GREECE
#556	2006-01-23	06:02:58.14	167.715	-17.391	32.0	6.30	6.39	TF	5.72	6.14	VANUATU-ISLANDS
#557	2006-01-23	20:50:44.98	-77.793	6.864	14.0	6.21	6.22	TF	6.23	6.55	NEAR-WEST-COAST-OF-COLOM

#558	2006-02-03	20:34:10.98	92.372	11.860	30.0	6.01	6.07	TF	5.96	6.09	ANDAMAN-ISLANDS,-INDIA-R
#559	2006-02-14	15:27:23.34	146.180	20.821	40.0	6.22	6.25	NCL	6.05	6.20	MARIANA-ISLANDS-REGION
#560	2006-02-18	15:59:22.09	152.053	-5.193	44.0	6.22	6.20	TF	5.83	6.16	NEW-BRITAIN-REGION,-P.N.
#561	2006-02-22	22:19:07.80	33.583	-21.324	11.0	7.04	7.01	NF	7.02	7.35	MOZAMBIQUE
#562	2006-02-28	07:31:02.65	56.865	28.120	18.0	5.96	6.02	TF	5.92	6.04	SOUTHERN-IRAN
#563	2006-03-06	18:13:08.43	78.486	-40.103	10.0	6.12	6.19	SS	na	5.95	MID-INDIAN-RIDGE
#564	2006-03-14	06:57:33.86	127.214	-3.595	30.0	6.72	6.71	SS	6.94	6.87	SERAM,-INDONESIA
#565	2006-03-24	12:27:05.38	143.144	-3.245	12.0	6.05	6.11	TF	6.09	6.12	NEAR-N-COAST-OF-NEW-GUIN
#566	2006-03-31	01:17:00.96	48.780	33.500	7.0	5.93	6.09	SS	5.90	6.37	WESTERN-IRAN
#567	2006-03-31	13:21:00.25	-176.768	-29.435	17.0	6.48	6.53	TF	6.50	6.51	KERMADEC-ISLANDS-REGION
#568	2006-03-31	21:14:45.20	126.344	3.798	55.0	6.20	6.11	NS	5.76	6.03	TALAUD-ISLANDS,-INDONESI
#569	2006-04-01	10:02:19.57	121.278	22.868	9.0	6.13	6.13	SS	6.57	6.48	TAIWAN-REGION
#570	2006-04-07	08:30:44.63	176.989	-16.527	22.0	6.42	6.46	SS	7.32	6.18	FIJI-ISLANDS-REGION
#571	2006-04-17	23:49:56.87	166.508	-12.475	31.0	5.96	6.09	TF	5.57	6.02	SANTA-CRUZ-ISLANDS
#572	2006-04-19	20:36:46.40	93.226	2.643	30.0	6.16	6.20	SS	6.65	6.12	OFF-W-COAST-OF-NORTHERN
#573	2006-04-20	23:25:02.15	167.089	60.949	22.0	7.25	7.58	TF	7.22	7.34	EASTERN-SIBERIA,-RUSSIA
#574	2006-04-21	04:32:43.82	165.816	60.527	9.0	na	6.12	TF	6.08	6.64	EASTERN-SIBERIA,-RUSSIA
#575	2006-04-21	11:14:15.33	167.525	61.354	12.0	6.07	6.03	TF	5.81	6.16	EASTERN-SIBERIA,-RUSSIA
#576	2006-04-25	18:26:17.15	96.995	1.994	21.0	6.13	6.32	NCL	6.02	6.19	OFF-W-COAST-OF-NORTHERN
#577	2006-04-26	01:46:03.86	147.568	-57.482	10.0	6.12	6.09	SS	na	5.92	WEST-OF-MACQUARIE-ISLAND
#578	2006-04-29	16:58:06.32	167.516	60.491	11.0	6.36	6.58	TF	6.43	6.75	EASTERN-SIBERIA,-RUSSIA
#579	2006-04-30	19:17:14.98	-71.022	-27.017	27.0	6.74	6.60	TF	6.48	6.48	NEAR-COAST-OF-NORTHERN-C
#580	2006-04-30	21:40:58.44	-71.056	-27.211	12.0	na	6.48	TF	6.15	6.58	NEAR-COAST-OF-NORTHERN-C
#581	2006-05-03	15:26:40.29	-174.123	-20.187	55.0	7.89	7.97	TF	8.03	8.27	TONGA-ISLANDS
#582	2006-05-07	14:17:35.17	78.545	-36.805	10.0	6.12	6.09	SS	na	5.82	MID-INDIAN-RIDGE
#583	2006-05-10	02:42:51.03	-169.256	52.515	18.0	6.27	6.41	TF	6.10	6.20	FOX-ISLANDS,-ALEUTIAN-IS
#584	2006-05-16	15:28:25.92	97.050	0.093	12.0	6.81	6.81	SS	7.54	7.41	NORTHERN-SUMATRA,-INDONE
#585	2006-05-19	14:44:24.90	124.713	-0.143	35.0	6.12	6.28	TS	5.89	6.22	SOUTHERN-MOLUCCA-SEA
#586	2006-05-22	11:12:00.80	165.743	60.772	16.0	6.51	6.61	SS	6.81	6.71	EASTERN-SIBERIA,-RUSSIA
#587	2006-05-22	20:53:57.41	126.811	-4.715	3.0	6.12	6.11	SS	na	6.24	BANDA-SEA
#588	2006-05-26	22:53:58.92	110.446	-7.961	12.0	6.35	6.35	SS	6.79	6.61	JAVA,-INDONESIA
#589	2006-05-28	03:12:08.76	151.133	-5.724	34.0	6.38	6.46	TF	5.73	6.08	NEW-BRITAIN-REGION,-P.N.
#590	2006-06-05	06:27:07.96	-28.065	1.175	10.0	5.91	6.02	SS	na	5.71	CENTRAL-MID-ATLANTIC-RID
#591	2006-06-14	04:18:42.51	177.082	51.752	14.0	6.43	6.47	SS	6.84	6.43	RAT-ISLANDS,-ALEUTIAN-IS
#592	2006-06-21	12:34:52.68	92.454	6.938	16.0	5.88	6.03	TF	5.87	6.34	NICOBAR-ISLANDS,-INDIA-R
#593	2006-06-24	21:15:00.92	123.195	-0.390	26.0	6.30	6.31	TS	6.31	6.27	MINAHASSA-PENINSULA,-SUL
#594	2006-06-27	02:39:32.90	176.158	52.230	17.0	6.17	6.23	SS	6.18	6.21	RAT-ISLANDS,-ALEUTIAN-IS
#595	2006-06-27	18:07:22.74	92.793	6.501	29.0	5.93	6.26	TF	5.73	6.07	NICOBAR-ISLANDS,-INDIA-R
#596	2006-07-07	07:26:12.53	-173.610	-15.244	35.0	5.96	6.02	NCL	5.53	5.88	TONGA-ISLANDS
#597	2006-07-08	20:40:00.98	-179.312	51.214	22.0	6.63	6.60	TF	6.00	6.39	ANDREANOF-ISLANDS,-ALEUT
#598	2006-07-16	11:42:41.41	-72.543	-28.715	10.0	6.23	6.19	NF	5.97	6.45	OFF-COAST-OF-CENTRAL-CHI
#599	2006-07-17	08:19:26.68	107.419	-9.284	34.0	7.21	7.71	NCL	7.09	7.20	SOUTH-OF-JAVA,-INDONESIA
#600	2006-07-17	15:45:59.82	108.319	-9.420	21.0	6.12	6.12	NF	5.85	6.24	SOUTH-OF-JAVA,-INDONESIA
#601	2006-07-19	10:57:36.88	105.389	-6.535	45.0	6.15	6.14	TF	5.67	5.97	SUNDA-STRAIT,-INDONESIA
#602	2006-07-19	11:48:58.29	150.684	-5.474	28.0	6.26	6.40	SS	na	6.15	NEW-BRITAIN-REGION,-P.N.
#603	2006-07-27	11:16:40.37	97.146	1.707	20.0	6.01	6.28	NCL	5.95	6.08	NORTHERN-SUMATRA,-INDONE
#604	2006-08-11	20:54:14.37	96.348	2.403	22.0	6.10	6.17	TF	5.87	6.16	NORTHERN-SUMATRA,-INDONE
#605	2006-08-20	03:41:48.04	-34.371	-61.029	10.0	6.96	6.98	SS	7.60	7.22	SCOTIA-SEA
#606	2006-08-24	21:50:36.65	157.522	51.148	43.0	6.46	6.46	TF	6.05	6.35	NEAR-EAST-COAST-OF-KAMCH
#607	2006-09-01	10:18:51.60	155.512	-6.759	38.0	6.75	6.74	TF	6.30	6.69	SOLOMON-ISLANDS
#608	2006-09-17	09:45:27.30	129.480	-2.870	17.0	na	6.33	TF	na	6.57	SERAM,-INDONESIA
#609	2006-09-28	06:22:09.73	-172.033	-16.592	28.0	6.68	6.89	NF	6.77	7.03	SAMOA-ISLANDS-REGION
#610	2006-09-29	13:08:26.16	-61.756	10.876	53.0	5.96	6.07	NCL	6.30	6.25	TRINIDAD
#611	2006-09-30	17:50:23.05	153.166	46.351	11.0	6.60	6.56	TF	6.72	6.70	KURIL-ISLANDS
#612	2006-10-01	09:06:02.32	153.240	46.470	19.0	6.45	6.55	TF	6.30	6.39	KURIL-ISLANDS
#613	2006-10-09	10:01:47.40	120.023	20.654	10.0	6.12	6.28	NF	6.12	6.51	PHILIPPINE-ISLANDS-REGIO

#614	2006-10-12	18:05:56.57	-71.368	-31.256	46.0	6.27	6.35	TF	5.90	6.31	NEAR-COAST-OF-CENTRAL-CH
#615	2006-10-15	17:07:49.25	-155.935	19.878	39.0	6.65	6.71	NS	6.73	6.70	HAWAII
#616	2006-10-17	01:25:12.23	150.982	-5.881	32.0	6.60	6.69	TF	6.54	6.67	NEW-BRITAIN-REGION,-P.N.
#617	2006-10-20	10:48:56.01	-76.677	-13.457	23.0	6.60	6.69	TF	6.43	6.43	NEAR-COAST-OF-PERU
#618	2006-10-22	08:55:16.76	95.987	-45.727	10.0	5.99	6.05	SS	na	6.14	SOUTHEAST-INDIAN-RIDGE
#619	2006-10-23	21:17:19.98	140.270	29.351	11.0	6.39	6.36	NF	6.31	6.63	SOUTHEAST-OF-HONSHU,-JAP
#620	2006-11-07	17:38:33.80	151.195	-6.482	10.0	6.36	6.55	NF	6.48	6.92	NEW-BRITAIN-REGION,-P.N.
#621	2006-11-12	18:21:26.14	151.050	-6.225	12.0	6.12	6.20	TF	5.90	6.42	NEW-BRITAIN-REGION,-P.N.
#622	2006-11-13	16:12:28.98	151.230	-6.380	11.0	6.07	6.21	NF	6.04	6.54	NEW-BRITAIN-REGION,-P.N.
#623	2006-11-15	11:14:13.57	153.266	46.592	39.0	7.89	8.30	TF	7.73	7.76	KURIL-ISLANDS
#624	2006-11-16	20:29:54.97	139.473	-51.996	10.0	6.13	6.06	SS	na	5.94	WESTERN-INDIAN-ANTARCTIC
#625	2006-11-17	18:03:12.26	129.895	28.591	22.0	6.09	6.16	TF	5.65	5.91	RYUKYU-ISLANDS,-JAPAN
#626	2006-11-29	01:32:17.92	128.283	2.520	39.0	6.17	6.22	SS	6.10	6.35	HALMAHERA,-INDONESIA
#627	2006-11-30	21:20:11.59	-134.359	-53.844	10.0	6.17	6.22	SS	na	5.94	PACIFIC-ANTARCTIC-RIDGE
#628	2006-12-01	14:01:44.26	118.753	-8.261	43.0	6.19	6.33	TF	5.83	6.27	SUMBAWA-REGION,-INDONESI
#629	2006-12-07	19:10:21.85	154.386	46.153	16.0	6.30	6.36	NF	6.48	6.82	EAST-OF-KURIL-ISLANDS
#630	2006-12-22	19:50:44.63	92.361	10.653	24.0	6.12	6.17	TF	5.97	6.21	ANDAMAN-ISLANDS,-INDIA-R
#631	2006-12-26	12:26:21.14	120.547	21.799	10.0	7.10	6.98	NF	6.93	7.38	TAIWAN-REGION
#632	2006-12-26	12:34:22.30	120.400	22.020	10.0	na	6.91	NCL	na	7.36	TAIWAN-REGION
#633	2006-12-30	08:30:49.79	51.365	13.313	15.0	6.51	6.62	SS	7.25	6.74	EASTERN-GULF-OF-ADEN
#634	2007-01-08	12:48:40.51	92.437	8.077	11.0	6.07	6.08	TF	6.00	6.16	NICOBAR-ISLANDS,-INDIA-R
#635	2007-01-08	17:21:49.91	70.312	39.803	16.0	6.01	6.04	SS	6.21	6.37	TAJIKISTAN
#636	2007-01-13	04:23:21.16	154.524	46.243	10.0	7.86	8.10	NF	8.15	8.57	EAST-OF-KURIL-ISLANDS
#637	2007-01-17	23:18:49.80	58.708	10.125	10.0	6.12	6.21	SS	na	6.17	CARLSBERG-RIDGE
#638	2007-01-20	06:21:04.56	-29.533	-55.419	10.0	6.10	6.21	SS	na	6.42	SOUTH-SANDWICH-ISLANDS-R
#639	2007-01-21	11:27:45.06	126.282	1.065	17.0	7.29	7.46	TF	7.48	7.74	NORTHERN-MOLUCCA-SEA
#640	2007-01-21	17:32:55.52	126.345	1.060	23.0	5.96	6.17	TF	6.01	6.04	NORTHERN-MOLUCCA-SEA
#641	2007-01-30	04:54:50.57	146.298	-54.740	11.0	6.80	6.85	SS	7.50	6.84	WEST-OF-MACQUARIE-ISLAND
#642	2007-01-30	21:37:44.37	144.705	20.980	30.0	6.52	6.58	NCL	6.82	6.77	MARIANA-ISLANDS
#643	2007-01-31	03:15:52.29	-178.002	-29.776	34.0	6.36	6.50	TF	6.13	6.55	KERMADEC-ISLANDS,-NEW-ZE
#644	2007-02-04	20:56:59.13	-78.518	19.372	10.0	6.19	6.19	SS	na	6.19	CUBA-REGION
#645	2007-02-12	12:45:31.70	126.073	5.561	29.0	5.96	6.09	TF	5.49	6.10	MINDANAO,-PHILIPPINES
#646	2007-02-20	08:04:25.28	126.976	-1.034	11.0	6.53	6.72	NS	6.57	7.01	SOUTHERN-MOLUCCA-SEA
#647	2007-02-24	02:36:23.65	-80.485	-7.006	23.0	6.30	6.34	TF	6.23	6.30	OFF-COAST-OF-NORTHERN-PE
#648	2007-02-28	23:13:15.61	-29.142	-55.245	10.0	6.22	6.11	NCL	6.13	6.59	SOUTH-SANDWICH-ISLANDS-R
#649	2007-03-06	03:49:38.90	100.498	-0.493	19.0	6.31	6.42	SS	6.98	5.98	SOUTHERN-SUMATRA,-INDONE
#650	2007-03-06	05:49:25.43	100.530	-0.488	20.0	6.10	6.28	SS	6.60	6.23	SOUTHERN-SUMATRA,-INDONE
#651	2007-03-09	07:27:31.22	66.255	-11.428	10.0	5.54	5.67	NF	na	5.89	MID-INDIAN-RIDGE
#652	2007-03-10	17:03:37.86	8.713	74.256	10.0	5.58	5.70	NF	na	6.17	GREENLAND-SEA
#653	2007-03-10	21:12:57.46	161.859	55.209	38.0	5.77	5.83	TF	5.63	6.25	NEAR-EAST-COAST-OF-KAMCH
#654	2007-03-11	07:09:26.71	147.891	43.988	49.0	5.75	5.69	TF	5.62	6.12	KURIL-ISLANDS
#655	2007-03-13	09:05:43.86	117.863	-8.128	10.0	5.52	5.62	NCL	na	5.76	SUMBAWA-REGION,-INDONESI
#656	2007-03-17	17:42:26.29	126.216	1.132	35.0	6.20	6.23	TF	6.14	6.21	NORTHERN-MOLUCCA-SEA
#657	2007-03-17	22:43:09.62	-78.536	4.551	10.0	5.91	6.00	NF	5.73	6.05	SOUTH-OF-PANAMA
#658	2007-03-18	02:11:05.30	-78.494	4.585	8.0	6.15	6.22	NF	6.28	6.59	SOUTH-OF-PANAMA
#659	2007-03-22	06:10:43.09	86.775	-3.388	21.0	5.88	5.90	SS	6.07	5.90	SOUTH-INDIAN-OCEAN
#660	2007-03-25	00:40:01.61	169.357	-20.617	34.0	7.09	7.13	TF	6.75	7.16	VANUATU-ISLANDS
#661	2007-03-25	00:41:57.82	136.588	37.336	8.0	6.57	6.67	TF	6.43	7.02	NEAR-WEST-COAST-OF-HONSH
#662	2007-03-26	07:27:55.83	142.975	22.036	10.0	5.45	5.50	NF	na	5.52	VOLCANO-ISLANDS,-JAPAN-R
#663	2007-03-28	21:17:10.65	29.673	-6.268	8.0	5.75	5.81	SS	5.96	6.13	LAKE-TANGANYIKA-REGION
#664	2007-03-31	12:49:03.71	-123.270	-56.083	10.0	6.16	6.23	SS	na	6.05	SOUTHERN-EAST-PACIFIC-RI
#665	2007-03-31	21:55:24.80	169.169	-20.514	10.0	5.61	5.66	TF	na	5.72	VANUATU-ISLANDS
#666	2007-04-01	20:39:58.71	157.043	-8.466	10.0	na	8.06	TF	7.54	8.15	SOLOMON-ISLANDS
#667	2007-04-02	23:20:23.27	157.386	-8.617	18.0	6.19	6.23	TF	5.92	6.19	SOLOMON-ISLANDS
#668	2007-04-04	21:40:18.77	141.673	30.926	9.0	5.60	5.71	TF	na	5.92	SOUTHEAST-OF-HONSHU,-JAP
#669	2007-04-05	03:56:50.48	-24.621	37.306	14.0	6.16	6.34	NF	6.00	6.33	AZORES-ISLANDS-REGION

#670	2007-04-06	05:54:20.42	-123.645	-55.373	10.0	5.81	5.92	NF	na	6.22	SOUTHERN-EAST-PACIFIC-RI
#671	2007-04-07	07:09:25.37	-24.494	37.306	8.0	5.96	6.05	NF	5.72	6.24	AZORES-ISLANDS-REGION
#672	2007-04-13	05:42:23.03	-100.198	17.302	34.0	6.01	5.95	TF	5.92	6.15	GUERRERO,-MEXICO
#673	2007-04-13	18:24:19.16	-108.836	-35.051	10.0	6.10	6.08	SS	na	6.16	SOUTHERN-EAST-PACIFIC-RI
#674	2007-04-16	13:20:38.23	147.964	-58.015	10.0	6.23	6.36	SS	na	6.21	WEST-OF-MACQUARIE-ISLAND
#675	2007-04-20	00:26:40.60	125.093	25.722	10.0	6.03	6.13	NF	na	6.29	SOUTHWESTERN-RYUKYU-ISL.
#676	2007-04-20	01:45:56.11	125.108	25.710	9.0	6.16	6.26	NS	6.37	6.60	SOUTHWESTERN-RYUKYU-ISL.
#677	2007-04-21	17:20:31.93	166.843	-13.838	41.0	5.92	6.04	TF	na	6.01	VANUATU-ISLANDS
#678	2007-04-25	13:34:14.23	166.863	-14.285	55.0	6.34	6.36	TF	5.90	6.35	VANUATU-ISLANDS
#679	2007-04-27	08:02:49.65	94.635	5.359	38.0	5.91	5.89	TF	5.72	6.24	NORTHERN-SUMATRA,-INDONE
#680	2007-04-28	14:02:37.91	-20.208	-60.789	10.0	5.91	6.05	SS	na	6.24	EAST-OF-SOUTH-SANDWICH-I
#681	2007-05-04	12:06:51.75	-14.921	-1.410	10.0	6.22	6.22	SS	6.09	6.08	NORTH-OF-ASCENSION-ISLAN
#682	2007-05-05	08:51:39.09	81.967	34.248	9.0	5.81	6.06	SS	5.57	6.11	XIZANG
#683	2007-05-16	08:56:14.12	100.732	20.503	24.0	6.16	6.28	SS	5.90	6.16	LAOS
#684	2007-05-29	09:36:05.60	127.343	-1.065	24.0	5.96	6.04	NF	na	6.18	HALMAHERA,-INDONESIA
#685	2007-06-02	21:34:57.78	101.052	23.028	5.0	6.05	6.09	SS	6.06	6.22	YUNNAN,-CHINA
#686	2007-06-07	00:40:38.13	146.761	-3.316	5.0	6.19	6.22	SS	na	6.25	BISMARCK-SEA
#687	2007-06-13	19:29:40.18	-90.618	13.554	23.0	6.54	6.67	TF	5.87	6.32	NEAR-COAST-OF-GUATEMALA
#688	2007-06-14	13:37:40.92	-100.152	-36.208	10.0	5.93	5.87	SS	na	6.05	SOUTHEAST-OF-EASTER-ISLA
#689	2007-06-18	06:18:45.68	150.962	-3.550	26.0	6.05	6.31	SS	6.72	6.07	NEW-IRELAND-REGION,-P.N.
#690	2007-06-24	00:25:18.40	-2.626	-55.645	10.0	6.33	6.48	SS	na	6.11	SOUTHERN-MID-ATLANTIC-RI
#691	2007-06-26	22:23:03.04	108.149	-10.492	10.0	5.93	6.00	NF	5.90	6.29	SOUTH-OF-JAVA,-INDONESIA
#692	2007-06-28	02:52:10.99	154.635	-7.979	10.0	6.74	6.68	NCL	7.09	6.87	SOLOMON-ISLANDS
#693	2007-07-03	08:26:00.81	-30.272	0.715	10.0	6.13	6.31	SS	na	6.33	CENTRAL-MID-ATLANTIC-RID
#694	2007-07-13	21:54:43.11	-176.280	51.838	50.0	5.85	5.96	TF	6.11	6.26	ANDREANOF-ISLANDS,-ALEUT
#695	2007-07-15	09:27:34.48	168.597	-15.383	46.0	6.01	6.14	TF	5.85	6.12	VANUATU-ISLANDS
#696	2007-07-15	13:08:01.68	-168.035	52.491	10.0	5.96	6.09	TF	5.85	6.31	FOX-ISLANDS,-ALEUTIAN-IS
#697	2007-07-16	01:13:22.37	138.446	37.535	55.0	6.47	6.62	TF	6.50	6.76	NEAR-WEST-COAST-OF-HONSH
#698	2007-07-17	14:10:42.46	36.362	-2.734	8.0	5.87	5.87	NF	5.35	5.96	TANZANIA
#699	2007-07-18	00:07:35.46	-177.738	-26.295	10.0	5.96	6.09	NF	na	6.31	SOUTH-OF-FIJI-ISLANDS
#700	2007-07-25	23:37:31.52	92.518	7.157	24.0	6.07	5.97	TF	5.70	5.85	NICOBAR-ISLANDS,-INDIA-R
#701	2007-07-26	05:40:16.10	127.464	2.872	45.0	6.89	6.93	TF	6.69	6.89	NORTHERN-MOLUCCA-SEA
#702	2007-07-27	14:46:26.88	170.939	-21.459	35.0	6.09	6.12	SS	na	6.11	SOUTHEAST-OF-LOYALTY-ISL
#703	2007-07-29	04:54:36.71	169.702	53.641	27.0	5.85	5.86	NCL	na	6.17	KOMANDORSKIYE-OSTROVA-RE
#704	2007-07-31	22:55:31.12	-17.795	-0.162	10.0	6.07	6.17	SS	6.13	6.06	NORTH-OF-ASCENSION-ISLAN
#705	2007-08-02	02:37:42.38	141.798	47.116	5.0	6.16	6.18	TF	na	5.87	SAKHALIN,-RUSSIA
#706	2007-08-02	03:21:42.82	-179.971	51.307	48.0	6.60	6.73	TF	6.26	6.60	ANDREANOF-ISLANDS,-ALEUT
#707	2007-08-03	00:41:14.30	145.306	-62.973	12.0	5.74	5.90	TF	5.81	6.34	SOUTH-OF-AUSTRALIA
#708	2007-08-05	09:28:39.83	168.718	-19.148	60.0	5.96	5.92	TF	5.31	5.93	VANUATU-ISLANDS
#709	2007-08-12	12:05:19.85	166.273	-11.378	42.0	5.99	6.03	TF	5.33	6.04	SANTA-CRUZ-ISLANDS
#710	2007-08-15	20:22:11.12	-177.548	50.322	21.0	na	6.46	NF	6.75	6.72	ANDREANOF-ISLANDS,-ALEUT
#711	2007-08-15	23:40:57.89	-76.603	-13.386	41.0	na	7.97	TF	7.71	7.95	NEAR-COAST-OF-PERU
#712	2007-08-16	08:39:28.44	159.465	-9.834	2.0	na	6.46	NCL	6.54	6.74	SOLOMON-ISLANDS
#713	2007-08-17	03:04:09.60	129.450	-5.240	10.0	na	6.43	SS	na	6.68	BANDA-SEA
#714	2007-08-18	02:52:35.40	-76.291	-13.805	35.0	na	6.02	TF	5.89	6.12	NEAR-COAST-OF-PERU
#715	2007-08-20	13:46:17.41	127.381	6.134	21.0	na	6.41	NF	6.63	6.77	PHILIPPINE-ISLANDS-REGIO
#716	2007-08-20	22:42:28.53	-39.251	8.037	10.0	na	6.54	SS	6.93	6.78	CENTRAL-MID-ATLANTIC-RID
#717	2007-09-01	19:14:22.64	-109.689	24.902	10.0	na	6.12	SS	6.16	5.84	GULF-OF-CALIFORNIA
#718	2007-09-02	01:05:18.15	165.762	-11.610	35.0	na	7.24	TF	6.57	6.85	SANTA-CRUZ-ISLANDS
#719	2007-09-06	17:51:26.19	122.219	24.340	63.0	na	6.25	TF	5.73	6.31	TAIWAN-REGION
#720	2007-09-10	01:49:11.78	-77.963	2.966	10.0	na	6.75	NF	6.45	6.82	NEAR-WEST-COAST-OF-COLOM
#721	2007-09-12	11:10:26.83	101.367	-4.438	30.0	na	8.48	NCL	8.13	8.20	SOUTHERN-SUMATRA,-INDONE
#722	2007-09-12	23:49:03.72	100.841	-2.625	10.0	na	7.87	TF	7.72	8.23	SOUTHERN-SUMATRA,-INDONE
#723	2007-09-13	03:35:28.72	99.627	-2.130	10.0	na	7.05	TF	6.96	7.38	SOUTHERN-SUMATRA,-INDONE
#724	2007-09-13	09:48:45.13	126.342	3.801	22.0	na	6.27	SS	6.48	6.40	TALAUD-ISLANDS,-INDONESI
#725	2007-09-13	16:09:16.87	101.524	-3.172	52.0	na	5.98	TF	6.04	6.42	SOUTHERN-SUMATRA,-INDONE

#726	2007-09-14	06:01:32.27	101.169	-4.075	35.0	na	6.36	NCL	6.12	6.53	SOUTHERN-SUMATRA,-INDONE
#727	2007-09-19	07:27:50.70	100.892	-2.746	35.0	5.86	5.98	TF	5.69	6.01	SOUTHERN-SUMATRA,-INDONE
#728	2007-09-20	08:31:14.49	100.141	-1.999	35.0	na	6.68	TF	6.89	6.74	SOUTHERN-SUMATRA,-INDONE
#729	2007-09-26	12:36:26.89	153.500	-4.990	33.0	6.72	6.75	TF	6.10	6.66	NEW-IRELAND-REGION,-P.N.
#730	2007-09-26	15:43:01.44	99.488	-1.787	28.0	6.01	6.11	TF	5.89	5.99	SOUTHERN-SUMATRA,-INDONE
#731	2007-09-27	19:57:44.00	169.283	-21.103	21.0	6.13	6.12	NCL	6.40	6.44	SOUTHEAST-OF-LOYALTY-ISL
#732	2007-09-28	01:01:49.18	169.362	-21.207	10.0	6.19	6.28	TF	6.04	6.55	SOUTHEAST-OF-LOYALTY-ISL
#733	2007-09-28	11:16:45.10	169.080	-21.450	10.0	na	5.86	TF	na	6.05	SOUTHEAST-OF-LOYALTY-ISL
#734	2007-09-30	02:08:30.17	145.718	10.454	10.0	6.87	6.95	SS	7.65	7.32	SOUTH-OF-MARIANA-ISLANDS
#735	2007-09-30	05:23:34.07	164.115	-49.271	11.0	6.93	7.40	TF	7.16	7.50	AUCKLAND-ISLANDS,-N.Z.-R
#736	2007-09-30	09:47:51.97	164.110	-49.138	10.0	6.52	6.60	TS	6.74	7.14	AUCKLAND-ISLANDS,-N.Z.-R
#737	2007-10-02	03:43:38.91	101.212	-4.240	35.0	5.85	5.90	TF	5.53	5.94	SOUTHERN-SUMATRA,-INDONE
#738	2007-10-02	18:00:06.87	-161.708	54.511	48.0	6.16	6.33	TF	6.19	6.44	ALASKA-PENINSULA
#739	2007-10-04	12:40:31.13	92.903	2.543	30.0	6.17	6.23	SS	6.34	6.00	OFF-W-COAST-OF-NORTHERN
#740	2007-10-06	12:38:49.17	147.148	18.730	64.0	6.01	6.06	NCL	6.34	6.61	MARIANA-ISLANDS-REGION
#741	2007-10-13	17:45:53.18	169.195	-21.230	40.0	6.13	6.05	NF	na	6.07	SOUTHEAST-OF-LOYALTY-ISL
#742	2007-10-15	12:29:34.86	167.553	-44.796	25.0	6.70	6.79	TF	6.54	6.66	SOUTH-ISLAND,-NEW-ZEALAN
#743	2007-10-24	21:02:50.61	101.020	-3.899	30.0	na	6.84	TF	6.20	6.64	SOUTHERN-SUMATRA,-INDONE
#744	2007-10-25	13:50:04.26	154.231	46.011	28.0	5.91	6.07	SS	6.39	6.11	EAST-OF-KURIL-ISLANDS
#745	2007-10-31	13:44:19.70	-178.400	51.420	35.0	na	6.02	TF	na	5.96	ANDREANOF-ISLANDS,-ALEUT
#746	2007-11-02	22:31:43.88	-128.966	-55.466	10.0	6.05	6.15	SS	na	5.85	PACIFIC-ANTARCTIC-RIDGE
#747	2007-11-10	01:13:43.90	161.230	-51.380	10.0	na	6.56	SS	na	6.09	NORTH-OF-MACQUARIE-ISLAN
#748	2007-11-14	15:40:50.53	-69.890	-22.247	60.0	na	7.72	TF	7.51	7.73	NORTHERN-CHILE
#749	2007-11-15	15:03:08.75	-70.407	-22.867	27.0	6.15	6.33	TF	5.90	6.03	NEAR-COAST-OF-NORTHERN-C
#750	2007-11-15	15:05:58.35	-70.237	-22.925	35.0	6.63	6.80	TF	6.65	6.61	NEAR-COAST-OF-NORTHERN-C
#751	2007-11-22	08:48:27.53	147.098	-5.757	53.0	6.72	6.75	TF	6.16	6.82	EASTERN-NEW-GUINEA-REG.,
#752	2007-11-25	16:02:15.75	118.370	-8.292	35.0	6.36	6.46	TF	6.00	6.58	SUMBAWA-REGION,-INDONESI
#753	2007-11-25	19:53:05.47	118.467	-8.224	35.0	6.38	6.46	TF	6.05	6.50	SUMBAWA-REGION,-INDONESI
#754	2007-11-27	11:49:58.01	162.149	-10.950	16.0	6.42	6.56	NCL	6.12	6.66	SOLOMON-ISLANDS
#755	2007-11-29	03:26:38.10	-98.350	-36.430	10.0	na	6.35	SS	na	5.94	WEST-CHILE-RISE
#756	2007-12-13	07:23:39.89	-70.549	-23.202	19.0	6.05	6.18	TF	5.76	6.03	NEAR-COAST-OF-NORTHERN-C
#757	2007-12-13	15:51:27.21	-172.367	-15.213	10.0	5.96	6.15	NF	5.76	6.33	SAMOA-ISLANDS-REGION
#758	2007-12-15	09:39:53.62	131.090	-6.622	50.7	6.32	6.40	SS	6.05	6.51	TANIMBAR-ISLANDS-REG.,-I
#759	2007-12-16	08:09:17.93	-70.182	-22.954	45.0	6.65	6.71	NCL	6.48	6.79	NEAR-COAST-OF-NORTHERN-C
#760	2007-12-19	09:30:27.93	-179.509	51.360	29.4	6.99	7.17	TF	6.52	6.93	ANDREANOF-ISLANDS,-ALEUT
#761	2007-12-20	07:55:15.84	178.291	-39.011	20.0	6.45	6.57	NF	6.31	6.64	OFF-E.-COAST-OF-N.-ISLAN
#762	2007-12-21	07:24:34.03	-178.979	51.366	30.0	na	6.26	TF	6.09	6.30	ANDREANOF-ISLANDS,-ALEUT
#763	2007-12-22	07:11:08.10	139.067	-2.407	27.0	6.07	6.21	TS	na	6.18	NEAR-NORTH-COAST-OF-IRIA
#764	2007-12-22	12:26:17.47	96.806	2.087	31.9	5.84	6.12	NCL	5.76	5.93	NORTHERN-SUMATRA,-INDONE
#765	2007-12-25	14:04:34.73	142.026	38.503	48.4	5.99	6.06	TF	na	5.92	NEAR-EAST-COAST-OF-HONSH
#766	2007-12-26	22:04:54.67	-168.221	52.558	35.4	6.21	6.36	TF	6.07	6.38	FOX-ISLANDS,-ALEUTIAN-IS
#767	2008-05-12	06:28:01.57	103.322	31.002	12.8	na	7.90	TF	7.66	8.26	SICHUAN,-CHINA
#768	2008-01-01	18:54:59.01	146.884	-5.878	34.0	6.13	6.29	TF	5.66	6.25	EASTERN-NEW-GUINEA-REG.,
#769	2008-01-04	07:29:18.30	101.032	-2.782	35.0	na	6.01	TF	5.99	6.01	SOUTHERN-SUMATRA,-INDONE
#770	2008-01-05	11:01:06.11	-130.746	51.254	10.0	6.52	6.59	SS	6.89	6.45	QUEEN-CHARLOTTE-ISLANDS
#771	2008-01-07	03:12:26.84	134.012	-0.795	12.0	5.78	5.87	TF	5.57	6.00	IRIAN-JAYA-REGION,-INDON
#772	2008-01-08	19:23:31.75	131.368	-3.913	2.0	5.69	5.79	TF	na	5.90	IRIAN-JAYA-REGION,-INDON
#773	2008-01-09	08:26:45.49	85.166	32.288	10.0	6.25	6.40	NF	6.45	6.60	XIZANG
#774	2008-01-09	14:40:00.96	-131.183	51.649	10.0	5.93	6.01	SS	na	5.72	QUEEN-CHARLOTTE-ISLANDS
#775	2008-01-10	01:37:19.00	-127.264	43.785	10.0	6.16	6.33	SS	6.15	5.90	OFF-COAST-OF-OREGON
#776	2008-01-13	12:15:35.60	120.989	17.048	10.0	5.55	5.74	SS	na	5.54	LUZON,-PHILIPPINES
#777	2008-01-14	13:38:35.99	92.869	10.413	43.0	5.64	5.83	TF	5.92	5.51	ANDAMAN-ISLANDS,-INDIA-R
#778	2008-01-16	11:54:44.12	85.158	32.331	9.0	5.68	5.89	NF	5.81	5.90	XIZANG
#779	2008-01-20	20:26:04.88	126.816	2.346	35.0	5.91	6.08	SS	na	6.18	NORTHERN-MOLUCCA-SEA
#780	2008-01-22	07:55:48.88	-175.348	-15.277	6.0	5.92	6.02	SS	na	5.85	TONGA-ISLANDS
#781	2008-01-22	17:14:57.95	97.442	1.011	20.0	6.19	6.20	TF	6.10	6.08	NORTHERN-SUMATRA,-INDONE

#782	2008-01-24	04:12:13.76	-82.383	6.943	10.0	5.71	5.86	SS	na	5.47	SOUTH-OF-PANAMA
#783	2008-01-24	22:29:53.06	146.619	-6.026	35.0	5.73	5.86	NCL	na	5.91	EASTERN-NEW-GUINEA-REG.,
#784	2008-01-30	07:32:42.80	127.688	-7.302	8.0	na	6.11	TF	6.09	6.44	BANDA-SEA
#785	2008-01-31	01:04:28.21	129.650	-6.132	10.0	5.66	5.82	SS	na	5.86	BANDA-SEA
#786	2008-02-03	07:34:12.18	28.900	-2.296	10.0	5.90	5.93	NF	5.76	5.91	LAKE-TANGANYIKA-REGION
#787	2008-02-04	17:01:29.98	-70.037	-20.166	44.0	6.26	6.33	TF	6.39	6.31	NEAR-COAST-OF-NORTHERN-C
#788	2008-02-05	05:56:46.96	118.070	-3.517	13.0	5.70	5.77	TF	na	6.02	SULAWESI,-INDONESIA
#789	2008-02-08	09:38:14.10	-41.899	10.671	9.0	6.80	6.94	SS	7.18	6.90	NORTHERN-MID-ATLANTIC-RI
#790	2008-02-09	18:34:01.60	125.084	-0.236	38.0	na	5.96	TF	5.44	5.73	SOUTHERN-MOLUCCA-SEA
#791	2008-02-10	12:22:02.65	-25.586	-60.797	8.0	6.49	6.54	NF	na	6.80	SOUTH-SANDWICH-ISLANDS-R
#792	2008-02-13	19:58:46.13	128.644	-8.158	19.0	5.96	6.17	TF	5.73	6.13	TIMOR-SEA
#793	2008-02-14	10:09:22.72	21.670	36.501	29.0	6.55	6.85	NCL	6.59	6.75	SOUTHERN-GREECE
#794	2008-02-14	12:08:55.79	21.863	36.345	28.0	na	6.54	NCL	6.11	6.53	SOUTHERN-GREECE
#795	2008-02-20	08:08:30.52	95.964	2.768	26.0	na	7.30	TF	7.06	7.02	OFF-W-COAST-OF-NORTHERN
#796	2008-02-20	18:27:06.00	21.775	36.288	10.0	5.91	6.16	SS	na	6.22	SOUTHERN-GREECE
#797	2008-02-21	02:46:18.19	18.571	77.079	10.0	5.99	6.07	NS	5.83	6.13	SVALBARD-REGION
#798	2008-02-21	14:16:02.71	-114.867	41.153	7.0	5.82	6.02	NF	5.70	6.02	NEVADA
#799	2008-02-21	23:55:36.46	99.880	-2.323	24.0	5.71	5.72	TF	na	5.88	SOUTHERN-SUMATRA,-INDONE
#800	2008-02-23	15:57:20.49	-23.433	-57.335	10.0	na	6.75	NS	6.90	6.97	SOUTH-SANDWICH-ISLANDS-R
#801	2008-02-24	14:46:21.47	99.931	-2.405	22.0	6.23	6.49	NCL	5.93	6.20	SOUTHERN-SUMATRA,-INDONE
#802	2008-02-25	08:36:33.03	99.972	-2.486	25.0	6.87	7.19	NCL	7.02	6.96	SOUTHERN-SUMATRA,-INDONE
#803	2008-02-25	18:06:03.90	99.891	-2.332	25.0	6.27	6.61	NCL	6.37	6.34	SOUTHERN-SUMATRA,-INDONE
#804	2008-02-25	21:02:18.42	99.808	-2.245	25.0	6.48	6.71	NCL	6.68	6.58	SOUTHERN-SUMATRA,-INDONE
#805	2008-02-26	18:18:27.53	101.067	-3.852	13.0	5.82	5.92	TF	5.40	5.75	SOUTHERN-SUMATRA,-INDONE
#806	2008-02-27	06:54:20.61	142.438	26.816	15.0	6.12	6.24	TF	6.24	6.25	BONIN-ISLANDS,-JAPAN-REG
#807	2008-03-03	02:37:27.12	99.823	-2.180	25.0	6.03	6.16	TF	5.73	5.85	SOUTHERN-SUMATRA,-INDONE
#808	2008-03-03	09:31:02.50	153.175	46.406	10.0	6.30	6.48	TF	6.40	6.58	KURIL-ISLANDS
#809	2008-03-03	13:49:40.42	121.334	19.913	10.0	5.77	5.98	TF	na	6.33	PHILIPPINE-ISLANDS-REGIO
#810	2008-03-03	14:11:14.62	125.630	13.351	24.0	6.77	6.87	NF	6.75	6.78	PHILIPPINE-ISLANDS-REGIO
#811	2008-03-12	11:23:34.06	167.335	-16.567	13.0	6.38	6.43	TF	5.65	6.19	VANUATU-ISLANDS
#812	2008-03-14	22:32:12.50	143.000	26.880	11.0	na	5.98	TF	na	6.12	BONIN-ISLANDS,-JAPAN-REG
#813	2008-03-15	14:43:26.50	94.596	2.708	20.0	5.90	6.03	TF	5.76	5.84	OFF-W-COAST-OF-NORTHERN
#814	2008-03-15	14:44:36.06	-126.835	42.412	10.0	5.63	5.71	NF	na	5.41	OFF-COAST-OF-OREGON
#815	2008-03-18	08:22:47.07	-177.440	-29.252	25.0	6.09	6.21	TF	5.83	5.96	KERMADEC-ISLANDS,-NEW-ZE
#816	2008-03-20	22:32:57.93	81.467	35.490	10.0	na	7.09	NF	6.68	6.91	SOUTHERN-XINJIANG,-CHINA
#817	2008-03-27	09:42:57.62	-84.835	17.199	10.0	5.60	5.63	SS	na	5.62	NORTH-OF-HONDURAS
#818	2008-03-28	00:16:19.90	25.345	34.758	45.0	5.58	5.54	TF	na	5.43	CRETE,-GREECE
#819	2008-03-28	22:41:32.22	121.949	20.251	10.0	5.66	5.80	SS	na	5.83	PHILIPPINE-ISLANDS-REGIO
#820	2008-03-29	03:01:30.32	125.684	13.283	18.0	5.70	5.66	NF	5.28	5.61	PHILIPPINE-ISLANDS-REGIO
#821	2008-03-29	17:30:50.15	95.296	2.855	20.0	6.27	6.34	NCL	5.99	6.01	OFF-W-COAST-OF-NORTHERN
#822	2008-04-02	08:48:49.73	102.717	-4.346	67.0	5.65	5.67	TF	na	5.85	SOUTHERN-SUMATRA,-INDONE
#823	2008-04-02	14:36:10.79	69.239	-4.879	10.0	5.63	5.71	NF	na	5.58	CHAGOS-ARCHIPELAGO-REGIO
#824	2008-04-09	11:13:17.69	168.861	-20.175	13.0	6.16	6.32	TF	5.76	6.16	LOYALTY-ISLANDS
#825	2008-04-09	12:46:12.72	168.892	-20.071	33.0	7.19	7.30	TF	6.88	6.84	LOYALTY-ISLANDS
#826	2008-04-10	01:10:07.00	168.710	-20.440	35.0	na	5.84	TF	na	5.62	LOYALTY-ISLANDS
#827	2008-04-11	16:36:01.20	168.810	-20.280	35.0	na	5.89	NF	na	5.45	LOYALTY-ISLANDS
#828	2008-04-11	17:45:01.94	168.839	-20.392	35.0	5.81	6.04	TF	5.67	5.77	LOYALTY-ISLANDS
#829	2008-04-12	00:30:12.60	158.453	-55.664	16.0	6.79	7.09	TF	6.83	7.30	MACQUARIE-ISLAND-REGION
#830	2008-04-15	03:03:04.66	-90.599	13.564	33.0	5.87	6.15	NCL	5.59	5.83	NEAR-COAST-OF-GUATEMALA
#831	2008-04-15	22:59:51.50	-179.361	51.856	10.0	6.36	6.45	SS	7.12	6.48	ANDREANOF-ISLANDS,-ALEUT
#832	2008-04-16	05:54:19.69	-179.165	51.878	13.0	6.50	6.59	SS	7.18	6.55	ANDREANOF-ISLANDS,-ALEUT
#833	2008-04-17	17:02:52.25	144.878	15.885	10.0	5.45	5.54	NF	na	5.73	MARIANA-ISLANDS-REGION
#834	2008-04-19	03:12:25.18	125.694	-7.815	13.0	5.99	6.07	SS	na	6.27	BANDA-SEA
#835	2008-04-19	05:58:42.25	168.796	-20.273	14.0	6.07	6.25	TS	na	6.54	LOYALTY-ISLANDS
#836	2008-04-19	10:21:12.50	125.722	-7.875	10.0	5.96	5.93	NCL	na	6.09	BANDA-SEA
#837	2008-04-20	13:01:20.49	125.685	-7.850	4.0	5.55	5.59	TF	na	5.70	BANDA-SEA

#838	2008-04-23	18:28:41.88	121.619	22.881	10.0	5.85	5.97	SS	na	5.85	TAIWAN-REGION
#839	2008-04-24	12:14:49.92	-23.471	-1.182	10.0	6.31	6.47	SS	na	5.82	CENTRAL-MID-ATLANTIC-RID
#840	2008-04-26	23:34:49.39	164.117	-49.091	10.0	6.13	5.93	TF	na	6.25	AUCKLAND-ISLANDS,-N.Z.-R
#841	2008-04-28	00:06:28.10	-100.171	17.846	57.0	5.70	5.83	NF	na	5.78	GUERRERO,-MEXICO
#842	2008-04-28	15:58:00.00	-24.150	-59.040	35.0	na	6.06	TF	na	5.60	SOUTH-SANDWICH-ISLANDS-R
#843	2008-04-28	18:33:34.20	168.953	-19.941	32.0	6.30	6.39	TF	6.18	6.40	VANUATU-ISLANDS
#844	2008-04-28	20:26:53.11	168.824	-20.238	35.0	5.90	6.03	NF	na	5.90	LOYALTY-ISLANDS
#845	2008-04-29	05:26:04.68	142.030	41.452	47.0	5.79	5.76	TF	na	5.83	HOKKAIDO,-JAPAN-REGION
#846	2008-05-01	04:57:50.19	168.878	-19.471	35.0	5.59	5.68	TF	na	5.67	VANUATU-ISLANDS
#847	2008-05-02	01:33:37.24	-177.528	51.864	14.0	6.52	6.59	SS	7.07	6.47	ANDREANOF-ISLANDS,-ALEUT
#848	2008-05-03	19:01:46.29	155.091	-6.640	35.0	5.58	5.70	TF	na	5.39	SOLOMON-ISLANDS
#849	2008-05-07	16:02:02.60	141.545	36.178	19.0	6.17	6.19	TF	6.06	5.95	NEAR-EAST-COAST-OF-HONSH
#850	2008-05-07	16:16:40.30	141.980	36.110	23.0	na	6.07	TF	na	6.22	NEAR-EAST-COAST-OF-HONSH
#851	2008-05-07	16:45:18.70	141.526	36.164	39.0	6.65	6.85	TF	6.55	6.44	NEAR-EAST-COAST-OF-HONSH
#852	2008-05-08	23:21:06.96	141.683	36.108	17.0	5.47	5.55	TF	na	5.85	NEAR-EAST-COAST-OF-HONSH
#853	2008-05-15	14:23:28.82	-25.483	-57.911	35.0	5.82	5.93	NCL	na	5.68	SOUTH-SANDWICH-ISLANDS-R
#854	2008-05-17	17:08:25.48	104.982	32.240	9.0	5.70	5.75	TF	5.96	6.07	SICHUAN,-CHINA
#855	2008-05-18	12:17:23.34	101.409	-3.202	35.0	5.55	5.70	TF	5.32	5.56	SOUTHERN-SUMATRA,-INDONE
#856	2008-05-19	14:26:45.02	99.147	1.640	10.0	5.90	6.01	SS	6.59	6.03	NORTHERN-SUMATRA,-INDONE
#857	2008-05-20	13:53:35.64	178.759	51.162	27.0	6.05	6.27	TF	5.87	6.02	RAT-ISLANDS,-ALEUTIAN-IS
#858	2008-05-23	19:35:34.78	-34.897	7.313	9.0	6.37	6.47	SS	6.95	6.41	CENTRAL-MID-ATLANTIC-RID
#859	2008-05-24	13:24:05.95	156.069	-7.181	29.0	5.79	5.89	TS	na	5.93	SOLOMON-ISLANDS
#860	2008-05-24	19:20:48.70	-73.790	4.320	9.0	na	5.87	SS	na	5.97	COLOMBIA
#861	2008-05-25	08:21:49.99	105.423	32.560	10.0	5.96	6.07	SS	na	6.43	SICHUAN,-CHINA
#862	2008-05-25	19:18:25.71	-153.780	56.087	20.0	5.96	5.88	TF	5.41	5.46	SOUTH-OF-ALASKA
#863	2008-05-26	15:01:33.64	-82.968	8.423	13.0	5.51	5.56	TF	na	5.49	PANAMA-COSTA-RICA-BORDER
#864	2008-05-27	05:51:15.70	147.370	-56.680	10.0	na	5.84	SS	na	5.61	WEST-OF-MACQUARIE-ISLAND
#865	2008-05-29	15:46:00.32	-21.013	64.005	10.0	6.17	6.29	SS	6.63	5.94	ICELAND
#866	2008-05-30	07:25:39.80	141.523	30.802	16.0	5.60	5.77	TF	na	5.72	SOUTHEAST-OF-HONSHU,-JAP
#867	2008-05-31	04:37:56.01	80.479	-41.198	10.0	na	6.40	SS	6.89	6.13	MID-INDIAN-RIDGE
#868	2008-06-01	01:57:23.69	121.350	20.124	35.0	na	6.33	TF	6.29	6.24	PHILIPPINE-ISLANDS-REGIO
#869	2008-06-01	14:31:03.01	149.660	-59.384	10.0	6.48	6.49	SS	na	6.21	WEST-OF-MACQUARIE-ISLAND
#870	2008-06-03	17:31:32.36	120.255	-8.166	14.0	5.71	5.88	TF	na	5.83	FLORES-REGION,-INDONESIA
#871	2008-06-03	21:03:46.70	120.265	-8.125	7.0	5.64	5.76	TF	na	5.71	FLORES-REGION,-INDONESIA
#872	2008-06-03	22:04:27.87	120.231	-8.100	14.0	5.84	6.00	TF	na	6.05	FLORES-REGION,-INDONESIA
#873	2008-06-05	02:16:46.93	-91.623	-38.844	10.0	5.87	5.99	SS	na	5.43	WEST-CHILE-RISE
#874	2008-06-08	12:25:29.71	21.525	37.963	16.0	6.20	6.37	SS	6.93	6.60	SOUTHERN-GREECE
#875	2008-06-13	23:43:45.36	140.881	39.030	8.0	6.79	6.87	TF	6.68	7.05	EASTERN-HONSHU,-JAPAN
#876	2008-06-17	17:42:09.67	-82.652	5.008	10.0	5.87	5.93	SS	na	5.65	SOUTH-OF-PANAMA
#877	2008-06-21	11:36:23.90	21.820	36.060	5.0	5.53	5.64	TF	na	5.66	SOUTHERN-GREECE
#878	2008-06-22	07:22:06.66	157.804	-8.865	10.0	5.84	5.76	TF	5.44	5.73	SOLOMON-ISLANDS
#879	2008-06-22	23:56:30.03	141.276	67.698	18.0	5.91	6.13	TS	6.50	6.10	EASTERN-SIBERIA,-RUSSIA
#880	2008-06-23	12:32:12.53	153.267	46.482	10.0	5.56	5.57	TF	na	5.72	KURIL-ISLANDS
#881	2008-06-25	02:53:25.44	97.191	1.344	16.0	5.54	5.69	TF	na	5.94	NORTHERN-SUMATRA,-INDONE
#882	2008-06-26	21:19:15.58	-173.342	-20.768	38.0	6.20	6.07	TF	5.57	6.03	TONGA-ISLANDS
#883	2008-06-27	11:40:13.99	91.824	11.005	17.0	6.42	6.56	NF	6.88	6.92	ANDAMAN-ISLANDS,-INDIA-R
#884	2008-06-28	12:54:46.36	91.712	10.847	15.0	6.13	6.07	NF	6.11	6.11	ANDAMAN-ISLANDS,-INDIA-R
#885	2008-06-30	06:17:43.02	-22.099	-58.227	19.0	6.85	6.96	SS	7.53	6.66	SOUTH-SANDWICH-ISLANDS-R
#886	2008-07-03	06:34:53.70	-60.442	10.281	34.0	5.48	5.69	NF	5.60	5.51	TRINIDAD
#887	2008-07-06	01:00:08.83	151.044	45.354	22.0	5.58	5.72	TF	na	5.68	KURIL-ISLANDS
#888	2008-07-06	09:08:21.29	150.965	45.387	10.0	na	5.73	TF	5.56	6.33	KURIL-ISLANDS
#889	2008-07-08	07:42:10.73	128.334	27.532	43.0	6.01	5.98	TF	5.85	6.08	RYUKYU-ISLANDS,-JAPAN
#890	2008-07-13	14:58:33.01	121.149	21.014	10.0	6.15	6.19	SS	6.78	5.97	TAIWAN-REGION
#891	2008-07-14	04:44:51.64	96.518	2.177	41.0	5.52	5.59	TF	5.24	5.47	NORTHERN-SUMATRA,-INDONE
#892	2008-07-15	03:26:34.70	27.860	35.800	52.0	6.27	6.39	SS	6.75	6.46	DODECANESE-ISLANDS,-GREE
#893	2008-07-16	08:11:04.00	-172.963	-16.599	10.0	5.59	5.66	TF	na	5.96	SAMOA-ISLANDS-REGION

#894	2008-07-19	02:39:28.70	142.214	37.552	22.0	6.83	6.91	TF	6.63	6.59	OFF-EAST-COAST-OF-HONSHU
#895	2008-07-19	09:27:01.46	164.493	-11.041	11.0	6.56	6.57	NF	6.36	6.57	SANTA-CRUZ-ISLANDS-REGIO
#896	2008-07-21	11:30:29.28	142.051	37.186	22.0	5.77	5.91	TF	5.87	5.96	OFF-EAST-COAST-OF-HONSHU
#897	2008-07-24	01:43:16.14	157.584	50.967	27.0	6.09	6.21	TF	5.83	6.00	KURIL-ISLANDS
#898	2008-07-24	07:09:31.80	105.550	32.820	10.0	na	5.57	SS	na	5.57	SICHUAN,-CHINA
#899	2008-07-25	00:29:22.97	178.982	51.279	21.0	5.73	5.86	TF	6.00	5.77	RAT-ISLANDS,-ALEUTIAN-IS
#900	2008-07-27	21:15:42.40	-18.287	-0.253	10.0	5.77	5.87	SS	6.43	6.07	CENTRAL-MID-ATLANTIC-RID
#901	2008-07-28	21:37:36.20	163.370	-10.500	10.0	na	5.90	SS	na	5.89	SOLOMON-ISLANDS
#902	2008-08-01	08:32:43.65	104.722	32.033	7.0	5.73	5.68	TF	6.03	6.13	SICHUAN,-CHINA
#903	2008-08-05	09:49:17.26	105.494	32.756	6.0	na	5.96	TF	6.08	6.19	SICHUAN,-CHINA
#904	2008-08-06	22:41:03.74	117.665	-8.131	31.0	5.74	5.93	SS	na	5.74	SUMBAWA-REGION,-INDONESI
#905	2008-08-07	18:30:03.07	-175.651	52.190	12.0	5.78	5.84	NS	5.83	5.71	ANDREANOF-ISLANDS,-ALEUT
#906	2008-08-08	06:37:41.91	101.076	-3.942	23.0	5.59	5.80	NCL	5.43	5.45	SOUTHERN-SUMATRA,-INDONE
#907	2008-08-09	06:02:03.80	153.380	-60.540	10.0	na	6.42	SS	na	6.01	WEST-OF-MACQUARIE-ISLAND
#908	2008-08-10	08:20:33.42	91.814	11.055	10.0	6.17	6.15	SS	6.85	6.16	ANDAMAN-ISLANDS,-INDIA-R
#909	2008-08-10	12:21:11.80	91.711	10.947	13.0	5.56	5.68	NF	na	5.51	ANDAMAN-ISLANDS,-INDIA-R
#910	2008-08-11	23:38:38.31	-21.843	-1.020	13.0	5.92	6.01	SS	na	5.77	CENTRAL-MID-ATLANTIC-RID
#911	2008-08-12	05:25:57.69	166.230	-11.432	38.0	5.88	5.80	TF	4.96	5.51	SANTA-CRUZ-ISLANDS
#912	2008-08-13	18:30:59.30	114.730	83.480	10.0	na	5.69	NF	na	5.34	NORTH-OF-SEVERNAYA-ZEMLY
#913	2008-08-16	04:01:08.60	98.207	52.272	12.0	5.57	5.71	SS	na	5.57	RUSSIA-MONGOLIA-BORDER-R
#914	2008-08-19	16:30:13.21	-173.476	-15.087	8.0	6.05	5.98	NCL	5.73	6.03	TONGA-ISLANDS
#915	2008-08-21	12:24:30.93	97.697	25.039	1.0	5.96	6.01	SS	6.55	5.84	MYANMAR-CHINA-BORDER-REG
#916	2008-08-22	07:47:39.58	65.394	-17.769	6.0	5.90	6.01	SS	na	5.79	MAURITIUS---REUNION-REGI
#917	2008-08-25	02:43:06.36	125.252	10.307	27.0	5.77	5.84	SS	na	5.58	LEYTE,-PHILIPPINES
#918	2008-08-26	03:07:29.50	104.469	-6.338	22.0	5.60	5.68	NS	na	5.98	SUNDA-STRAIT,-INDONESIA
#919	2008-08-27	06:46:19.48	41.469	-10.751	10.0	5.57	5.75	NF	na	6.02	NORTHWEST-OF-MADAGASCAR
#920	2008-08-27	21:52:38.11	47.350	32.308	10.0	5.67	5.78	SS	na	5.43	IRAN-IRAQ-BORDER-REGION
#921	2008-08-28	12:37:35.07	-129.628	50.165	10.0	5.76	5.89	SS	6.08	5.65	VANCOUVER-ISLAND,-CANADA
#922	2008-08-28	15:22:23.20	-17.358	-0.252	15.0	6.21	6.28	SS	6.63	6.14	NORTH-OF-ASCENSION-ISLAN
#923	2008-08-30	08:30:53.01	101.889	26.241	17.0	5.82	5.96	SS	6.10	5.99	YUNNAN,-CHINA
#924	2008-09-05	19:07:38.29	-13.955	-1.171	10.0	5.69	5.77	SS	na	5.74	NORTH-OF-ASCENSION-ISLAN
#925	2008-09-08	03:03:15.93	169.108	-19.964	36.0	6.12	6.18	TF	5.76	6.08	VANUATU-ISLANDS
#926	2008-09-09	12:22:49.07	158.261	-9.272	12.0	5.88	5.94	SS	6.26	6.18	SOLOMON-ISLANDS
#927	2008-09-10	11:00:34.09	55.828	26.743	12.0	5.83	6.09	TF	5.81	6.33	SOUTHERN-IRAN
#928	2008-09-10	13:08:14.69	-38.705	8.093	10.0	6.50	6.61	SS	6.87	6.64	CENTRAL-MID-ATLANTIC-RID
#929	2008-09-11	00:20:50.92	143.754	41.892	25.0	6.79	6.77	TF	6.64	6.74	HOKKAIDO,-JAPAN-REGION
#930	2008-09-14	00:00:09.07	126.855	-8.728	18.0	na	5.65	TF	5.14	5.76	TIMOR-REGION
#931	2008-09-16	11:15:42.20	127.050	-9.070	35.0	na	5.71	TF	na	5.74	TIMOR-REGION
#932	2008-09-18	01:41:03.01	-105.999	-4.554	10.0	5.88	6.01	SS	6.21	5.60	CENTRAL-EAST-PACIFIC-RIS
#933	2008-09-18	11:58:47.46	158.363	51.940	67.0	5.86	5.84	TF	5.28	5.73	NEAR-EAST-COAST-OF-KAMCH
#934	2008-09-24	02:33:05.56	-105.497	17.612	10.0	6.27	6.39	SS	6.61	6.10	OFF-COAST-OF-JALISCO,-ME
#935	2008-09-25	01:47:11.19	83.487	30.836	10.0	5.76	5.96	SS	5.93	5.77	XIZANG
#936	2008-09-26	18:46:18.57	65.316	3.074	10.0	5.57	5.65	NF	na	5.40	CARLSBERG-RIDGE
#937	2008-09-27	03:04:56.70	120.400	13.500	10.0	na	5.72	NF	na	5.70	MINDORO,-PHILIPPINES
#938	2008-09-27	03:09:04.82	120.548	13.477	10.0	na	5.90	NF	5.53	5.99	MINDORO,-PHILIPPINES
#939	2008-09-29	15:19:31.59	-177.683	-29.756	36.0	6.89	7.03	TF	6.59	6.85	KERMADEC-ISLANDS,-NEW-ZE
#940	2008-10-01	18:04:23.85	120.444	13.367	10.0	5.48	5.54	NF	na	5.32	MINDORO,-PHILIPPINES
#941	2008-10-02	23:28:09.12	169.861	-23.019	10.0	5.79	5.80	NF	na	5.92	SOUTHEAST-OF-LOYALTY-ISL
#942	2008-10-05	09:12:36.07	-177.176	-30.184	10.0	6.13	6.11	TF	6.05	6.26	KERMADEC-ISLANDS,-NEW-ZE
#943	2008-10-05	15:52:49.40	73.824	39.533	27.0	na	6.70	TF	6.45	6.54	TAJIKISTAN-XINJIANG-BORD
#944	2008-10-05	22:56:28.93	69.470	33.886	10.0	5.77	5.95	SS	na	5.75	SOUTHEASTERN-AFGHANISTAN
#945	2008-10-06	08:30:45.57	90.350	29.807	12.0	6.12	6.31	NF	6.02	6.29	XIZANG
#946	2008-10-07	10:00:48.12	-115.448	79.817	10.0	5.57	5.73	TF	5.73	5.75	ARCTIC-OCEAN
#947	2008-10-09	17:49:58.60	-174.420	-21.030	10.0	5.67	5.87	TF	na	6.10	TONGA-ISLANDS
#948	2008-10-11	09:06:10.77	46.254	43.372	16.0	5.65	5.81	TF	5.27	6.01	EASTERN-CAUCASUS
#949	2008-10-11	10:40:14.06	-64.833	19.161	23.0	5.96	6.06	SS	6.04	6.32	VIRGIN-ISLANDS

#950	2008-10-16	19:41:25.72	-92.364	14.423	24.0	6.44	6.65	TF	6.08	6.27	NEAR-COAST-OF-CHIAPAS,-M
#951	2008-10-19	05:10:33.91	-173.819	-21.863	29.0	6.83	6.90	TF	6.77	7.07	TONGA-ISLANDS
#952	2008-10-19	12:55:05.69	-173.700	-21.972	35.0	5.53	5.60	NF	na	5.66	TONGA-ISLANDS
#953	2008-10-28	16:00:03.24	145.867	-3.494	18.0	5.93	6.02	SS	na	5.51	NEAR-N-COAST-OF-NEW-GUIN
#954	2008-10-28	23:09:57.65	67.351	30.639	15.0	6.29	6.40	SS	6.68	6.68	PAKISTAN
#955	2008-10-29	11:32:43.13	67.455	30.598	14.0	6.21	6.42	SS	6.38	6.59	PAKISTAN
#956	2008-10-30	01:55:16.10	153.530	46.390	32.0	na	5.54	TF	na	5.32	KURIL-ISLANDS
#957	2008-10-30	15:15:46.40	-108.300	-9.080	10.0	na	6.05	SS	na	5.63	CENTRAL-EAST-PACIFIC-RIS
#958	2008-11-01	01:13:09.64	148.712	-3.399	10.0	5.90	5.97	SS	na	5.42	BISMARCK-SEA
#959	2008-11-02	13:48:42.82	-174.366	51.552	36.0	na	6.06	TF	5.52	5.91	ANDREANOF-ISLANDS,-ALEUT
#960	2008-11-03	19:21:58.45	97.253	1.145	10.0	5.71	5.75	TF	na	5.73	NORTHERN-SUMATRA,-INDONE
#961	2008-11-06	09:11:09.70	-176.950	-29.660	19.0	na	5.89	TF	na	5.72	KERMADEC-ISLANDS,-NEW-ZE
#962	2008-11-07	07:19:35.71	168.032	-14.829	13.0	6.23	6.37	TF	6.30	6.45	VANUATU-ISLANDS
#963	2008-11-07	16:04:28.60	129.240	-6.620	10.0	na	6.18	SS	na	6.25	BANDA-SEA
#964	2008-11-10	01:22:02.57	95.833	37.565	19.0	6.07	6.34	TF	6.38	6.39	QINGHAI,-CHINA
#965	2008-11-16	17:02:32.70	122.091	1.271	30.0	na	7.34	TF	7.05	7.05	MINAHASSA-PENINSULA,-SUL
#966	2008-11-17	12:55:22.79	-116.056	79.648	7.0	5.51	5.66	TF	na	5.83	ARCTIC-OCEAN
#967	2008-11-19	06:11:20.79	-82.967	8.267	32.0	6.12	6.25	SS	6.19	6.05	PANAMA-COSTA-RICA-BORDER
#968	2008-11-22	16:01:01.70	101.259	-4.348	24.0	6.34	6.33	TF	6.10	6.02	SOUTHERN-SUMATRA,-INDONE
#969	2008-11-22	16:01:39.38	171.199	-22.523	57.0	na	6.40	NF	na	6.16	SOUTHEAST-OF-LOYALTY-ISL
#970	2008-11-22	18:49:42.38	-13.933	-1.230	10.0	6.17	6.29	SS	na	6.17	NORTH-OF-ASCENSION-ISLAN
#971	2008-11-25	01:36:30.64	-177.876	-30.244	35.0	5.47	5.62	TF	na	5.46	KERMADEC-ISLANDS,-NEW-ZE
#972	2008-11-25	12:40:03.55	146.968	18.013	10.0	5.48	5.57	TF	na	5.53	MARIANA-ISLANDS
#973	2008-11-27	17:31:32.00	167.480	-17.990	10.0	na	5.52	NF	na	5.76	VANUATU-ISLANDS
#974	2008-11-28	08:50:47.91	101.764	-4.755	27.0	5.84	5.92	TF	5.89	5.72	SOUTHERN-SUMATRA,-INDONE
#975	2008-11-28	13:42:18.68	-126.978	40.348	10.0	5.83	5.94	SS	na	5.63	OFF-COAST-OF-NORTHERN-CA
#976	2008-12-03	23:16:54.87	142.878	38.589	14.0	5.78	5.77	TF	na	6.18	NEAR-EAST-COAST-OF-HONSH
#977	2008-12-08	18:39:09.48	106.823	-53.005	10.0	na	6.30	NF	5.93	6.44	SOUTHEAST-INDIAN-RIDGE
#978	2008-12-09	06:23:59.75	-176.924	-31.232	18.0	6.57	6.71	NF	6.61	6.53	KERMADEC-ISLANDS-REGION
#979	2008-12-09	22:52:37.62	67.404	30.442	10.0	5.47	5.67	SS	na	5.97	PAKISTAN
#980	2008-12-10	13:15:34.43	166.572	-12.337	51.0	6.01	5.99	TF	5.52	6.19	SANTA-CRUZ-ISLANDS
#981	2008-12-13	08:45:37.10	123.860	-49.120	10.0	na	5.93	NF	na	6.15	WESTERN-INDIAN-ANTARCTIC
#982	2008-12-18	21:19:28.38	-71.726	-32.458	18.0	6.03	6.13	TF	5.73	5.92	NEAR-COAST-OF-CENTRAL-CH
#983	2008-12-19	08:31:51.50	-27.290	47.006	2.0	5.86	5.85	NF	5.09	5.67	NORTHERN-MID-ATLANTIC-RI
#984	2008-12-20	10:29:23.10	142.425	36.541	19.0	6.24	6.33	TF	6.00	6.12	OFF-EAST-COAST-OF-HONSHU
#985	2008-12-21	09:16:44.74	142.317	36.541	13.0	5.82	5.87	NF	5.73	5.93	OFF-EAST-COAST-OF-HONSHU
#986	2008-12-23	11:15:18.47	154.943	-6.366	32.0	5.75	5.89	TF	5.29	6.12	SOLOMON-ISLANDS
#987	2008-12-24	09:11:34.29	-171.909	-17.290	9.0	na	5.97	NF	5.64	6.28	TONGA-ISLANDS-REGION
#988	2008-12-25	08:11:58.79	-128.621	49.128	10.0	5.79	5.82	SS	na	5.47	VANCOUVER-ISLAND,-CANADA
#989	2008-12-25	22:40:23.60	64.499	23.417	13.0	5.83	5.84	NS	5.68	5.97	OFF-COAST-OF-PAKISTAN
#990	2008-12-30	19:49:52.61	101.217	-4.297	20.0	5.87	5.92	TF	5.87	5.72	SOUTHERN-SUMATRA,-INDONE

Table A2: List of source, magnitude parameters, and tsunami data for the 89 tsumanigenic and tsunami earthquakes considered in section 3.4

#ID	MO/DA/YE	HH/MM/SS	Lat.	Lon.	h (km)	Mw(GCMT)	Ms	mb	Me(GS)	Me(GFZ)	Max. W.H. (m)	Runups	Mec. Type	Region
1	03/25/1990	13:22:54.9	9.89	-84.89	19	7.29	7.0	6.3	6.63	6.95	0.30	2	TF	Costa Rica
2	04/05/1990	21:12:38.7	15.23	147.53	32	7.41	7.5	6.5	7.50	7.71	0.60	34	NF	Mariana Islands Region
3	02/21/1991	02:35:32.4	58.42	-175.45	10	6.62	6.5	6.3	6.79	6.88	0.30	2	NF	Bering Sea
4	04/22/1991	21:56:51.9	9.68	-83.08	10	7.61	7.5	6.6	7.40	7.39	3.00	21	TF	Costa Rica
5	10/14/1991	15:58:14.4	-9.05	158.49	33	7.20	7.1	6.2	6.80	7.08	0.20	2	TF	Solomon Islands
6	04/25/1992	18:06:04.2	40.37	-124.32	15	7.15	7.1	6.4	7.01	7.17	1.80	14	NC	Near Coast of N. California
7	09/02/1992	00:15:57.5	11.76	-87.42	10	7.62	7.2	5.3	6.68	6.98	9.90	36	TF	Near Coast of Nicaragua
8	12/12/1992	05:29:27.4	-8.51	121.89	35	7.74	7.5	6.7	7.61	7.75	26.20	24	TF	Flores Region, Indonesia
9	07/12/1993	13:17:11.9	42.84	139.25	17	7.71	7.6	6.7	7.69	8.16	54.00	180	TF	Hokkaido, Japan Region
10	08/08/1993	08:34:25.0	12.96	144.78	61	7.74	8.1	7.2	7.62	7.93	2.13	50	TF	South of Mariana Islands
11	11/13/1993	01:18:04.2	51.92	158.70	34	7.00	7.1	6.5	6.39	6.83	0.05	1	TF	Near East Coast of Kamchatka
12	02/15/1994	17:07:42.8	-5.05	104.24	15	6.83	7.0	6.0	6.63	6.69	0.10	0	SS	Southern Sumatra, Indonesia
13	06/02/1994	18:17:36.8	-10.47	112.98	39	7.75	7.2	5.5	6.45	6.78	13.90	25	NC	South of Java, Indonesia
14	06/04/1994	00:57:53.5	-10.77	113.42	33	6.44	6.2	5.8	6.75	6.60	3.00	1	NF	South of Java, Indonesia
15	09/01/1994	15:15:53.2	40.41	-125.65	10	6.99	7.0	6.6	7.72	7.15	0.07	1	SS	Off Coast of N. California
16	10/04/1994	13:22:58.3	43.71	147.33	33	8.25	8.1	7.4	8.43	8.56	10.40	113	NC	Kuril Islands
17	10/09/1994	07:55:38.0	43.90	147.90	23	7.25	7.0	6.5	6.93	7.17	0.20	2	TF	Kuril Islands
18	11/14/1994	19:15:30.7	13.53	121.09	33	7.07	7.1	6.1	7.41	6.81	7.30	21	SS	Mindoro, Philippines
19	12/28/1994	12:19:23.6	40.45	143.49	33	7.73	7.5	6.4	7.50	7.68	0.53	13	TF	Off East Coast of Honshu, Japan
20	01/16/1995	20:46:51.1	34.55	135.00	16	6.86	6.8	6.4	7.02	7.04	0.20	2	SS	Near S. Coast of Western Honshu
21	04/07/1995	22:06:58.0	-15.19	-173.59	31	7.34	8.0	6.7	7.55	7.54	0.09	2	NC	Tonga Islands
22	04/21/1995	00:34:47.3	12.06	125.93	23	7.15	7.3	6.2	6.99	7.24	0.20	1	TF	Samar, Philippines
23	05/16/1995	20:12:45.6	-23.01	169.89	33	7.66	7.7	6.8	7.70	7.79	0.50	8	NF	Southeast of Loyalty Islands
24	05/27/1995	13:03:55.6	52.56	142.81	33	7.02	7.6	6.6	7.20	7.01	0.10	2	SS	Sakhalin, Russia
25	07/30/1995	05:11:23.5	-23.36	-70.31	47	7.99	7.3	6.6	7.56	7.80	3.00	90	TF	Near Coast of Northern Chile
26	08/16/1995	10:27:26.4	-5.81	154.21	16	7.71	7.8	6.4	7.24	7.83	0.60	0	TF	Solomon Islands
27	10/09/1995	15:35:55.7	19.15	-104.22	49	7.97	7.3	6.5	7.24	7.54	11.00	32	NC	Near Coast of Jalisco, Mexico
28	10/18/1995	10:37:26.3	27.92	130.34	27	7.10	6.8	6.5	6.91	7.20	2.59	42	NF	Ryukyu Islands, Japan
29	12/03/1995	18:01:07.7	44.62	149.32	22	7.88	na	5.6	7.32	7.50	1.10	35	TF	Kuril Islands
30	01/01/1996	08:05:11.9	0.72	119.98	33	7.86	7.7	6.2	7.36	7.50	3.43	15	NC	Minahassa Peninsula, Sulawesi

31	02/17/1996	05:59:29.7	-0.95	137.03	33	8.19	8.1	6.5	7.69	7.74	7.68	108	TF	Irian Jaya Region, Indonesia
32	02/21/1996	12:51:04.3	-9.62	-79.57	33	7.50	6.6	5.8	na	7.08	5.10	53	TF	Off Coast of Northern Peru
33	02/25/1996	03:08:18.8	16.20	-97.96	33	7.09	6.9	5.9	6.48	6.56	0.10	1	TF	Oaxaca, Mexico
34	06/10/1996	04:03:35.4	51.56	-177.63	33	7.87	7.6	6.6	7.40	7.61	0.51	64	TF	Andreanof Islands, Aleutian Islands
35	06/10/1996	15:24:56.0	51.48	-176.85	26	7.22	7.1	5.9	6.87	7.00	0.13	1	TF	Andreanof Islands, Aleutian Islands
36	09/05/1996	08:14:14.4	-22.12	-113.44	10	6.82	7.0	6.2	6.39	6.83	0.09	2	TF	Easter Island Region
37	11/12/1996	16:59:44.0	-14.99	-75.68	33	7.71	7.3	6.5	7.29	7.78	0.40	3	TF	Near Coast of Peru
38	04/21/1997	12:02:26.4	-12.58	166.68	33	7.69	7.9	6.4	7.68	7.91	3.00	39	TF	Santa Cruz Islands
39	12/05/1997	11:26:54.7	54.84	162.04	33	7.75	7.6	6.3	7.18	7.54	8.00	18	TF	Near East Coast of Kamchatka
40	05/03/1998	23:30:21.9	22.31	125.31	33	7.44	7.3	6.4	7.90	7.37	0.11	14	SS	Southeast of Taiwan
41	08/17/1999	00:01:39.1	40.75	29.86	17	7.57	7.8	6.3	7.67	7.37	2.52	18	SS	Turkey
42	11/26/1999	13:21:15.6	-16.42	168.21	33	7.42	7.3	6.4	7.22	7.38	6.00	43	TF	Vanuatu Islands
43	05/04/2000	04:21:16.2	-1.11	123.57	26	7.52	7.5	6.7	7.53	7.65	6.00	6	SS	Sulawesi, Indonesia
44	06/18/2000	14:44:13.3	-13.80	97.45	10	7.87	7.8	6.8	7.92	8.01	0.30	1	SS	South Indian Ocean
45	11/16/2000	04:54:56.7	-3.98	152.17	33	8.00	8.2	6.0	na	7.83	3.00	8	NC	New Ireland Region, P.N.G.
46	06/23/2001	20:33:14.1	-16.26	-73.64	33	8.38	8.2	6.7	8.04	8.16	7.00	92	TF	Near Coast of Peru
47	01/02/2002	17:22:48.8	-17.60	167.86	21	7.19	7.5	6.3	7.20	7.24	0.35	2	NC	Vanuatu Islands
48	03/05/2002	21:16:09.1	6.03	124.25	31	7.46	7.2	6.3	7.09	7.26	3.00	3	TF	Mindanao, Philippines
49	03/31/2002	06:52:50.5	24.28	122.18	33	7.09	7.4	6.4	6.87	7.07	0.20	11	TF	Taiwan Region
50	09/08/2002	18:44:23.7	-3.30	142.95	13	7.58	7.8	6.5	7.68	7.72	5.50	25	TF	Near N. Coast of New Guinea, PNG.
51	09/13/2002	22:28:29.5	13.04	93.07	21	6.47	6.7	6.2	6.37	6.65	na	3	TF	Andaman Islands, India Region
52	01/20/2003	08:43:06.1	-10.49	160.77	33	7.25	7.8	6.7	7.25	7.47	na	2	TS	Solomon Islands
53	01/22/2003	02:06:34.6	18.77	-104.10	24	7.47	7.6	6.5	7.35	7.34	0.61	3	TF	Near Coast of Jalisco, Mexico
54	05/21/2003	18:44:20.1	36.96	3.63	12	6.80	6.9	6.5	6.75	7.19	3.00	13	TF	Northern Algeria
55	09/25/2003	19:50:06.4	41.81	143.91	27	8.26	8.1	6.9	7.96	8.00	3.90	51	NC	Hokkaido, Japan Region
56	10/31/2003	01:06:28.3	37.81	142.62	10	6.97	6.8	6.1	6.65	7.01	0.32	4	NC	Off East Coast of Honshu, Japan
57	11/17/2003	06:43:06.8	51.15	178.65	33	7.75	7.2	6.2	7.31	7.45	0.33	20	TF	Rat Islands, Aleutian Islands
58	01/28/2004	22:15:30.7	-3.12	127.40	17	6.63	6.5	6.0	6.94	6.73	na	1	NC	Seram, Indonesia
59	09/05/2004	10:07:07.8	33.07	136.62	14	7.19	7.0	6.7	7.45	7.76	0.63	12	TF	Near S. Coast of Western Honshu
60	09/05/2004	14:57:18.6	33.18	137.07	10	7.37	7.1	6.2	7.41	7.84	0.93	24	TF	Near S. Coast of Honshu, Japan
61	11/02/2004	10:02:12.8	49.28	-128.77	10	6.56	6.4	5.8	6.91	6.46	0.11	2	SS	Vancouver Island, Canada Region
62	11/11/2004	21:26:41.2	-8.15	124.87	10	7.48	7.3	6.5	7.40	7.62	na	0	TF	Timor Region
63	11/21/2004	11:41:07.8	15.68	-61.71	14	6.29	6.1	6.3	6.32	6.63	0.70	7	NF	Leeward Islands

64	11/28/2004	18:32:14.1	43.01	145.12	39	6.97	6.7	6.4	6.96	7.27	0.11	2	TF	Hokkaido, Japan Region
65	12/23/2004	14:59:04.4	-49.31	161.35	10	8.07	7.7	6.5	8.43	8.02	0.30	5	SS	North of Macquarie Island
66	12/26/2004	00:58:50.0	3.30	95.78	10	9.00	8.8	7.0	8.50	8.79	50.90	716	NC	Off West Coast of Northern Sumatra
67	01/19/2005	06:11:36.4	34.06	141.49	28	6.54	6.4	5.8	5.83	6.42	0.39	1	TF	Off East Coast of Honshu, Japan
68	03/28/2005	16:09:36.5	2.09	97.11	30	8.61	8.4	7.2	8.28	8.30	3.00	15	NC	Northern Sumatra, Indonesia
69	04/10/2005	10:29:11.3	-1.64	99.61	19	6.68	6.7	6.4	6.78	6.90	0.40	1	TF	Southern Sumatra, Indonesia
70	06/15/2005	02:50:53.2	41.30	-125.97	10	7.21	7.1	6.2	7.54	7.02	0.10	5	SS	Off Coast of N. California
71	08/16/2005	02:46:28.4	38.28	142.04	36	7.19	6.8	6.5	6.71	7.16	0.05	1	TF	Near East Coast of Honshu, Japan
72	11/14/2005	21:38:51.4	38.11	144.90	11	6.98	6.8	6.7	6.84	7.40	0.42	1	NF	Off East Coast of Honshu, Japan
73	03/14/2006	06:57:33.9	-3.60	127.21	30	6.71	6.7	6.4	6.94	6.87	3.50	1	SS	Seram, Indonesia
74	05/03/2006	15:26:40.3	-20.19	-174.12	55	7.97	7.9	7.2	8.03	8.27	0.27	52	TF	Tonga Islands
75	07/17/2006	08:19:28.8	-9.25	107.41	34	7.71	7.2	6.1	7.09	7.20	10.00	20	NC	South of Java, Indonesia
76	09/28/2006	06:22:09.7	-16.59	-172.03	28	6.89	6.9	6.5	6.77	7.03	0.08	1	NF	Samoa Islands Region
77	11/15/2006	11:14:17.8	46.57	153.29	39	8.30	7.8	6.6	7.73	7.76	0.88	113	TF	Kuril Islands
78	01/13/2007	04:23:21.2	46.24	154.52	10	8.10	8.2	7.3	8.15	8.57	0.32	35	NF	East of Kuril Islands
79	03/25/2007	00:40:01.6	-20.62	169.36	34	7.13	7.1	6.5	6.75	7.16	0.08	2	TF	Vanuatu Islands
80	03/25/2007	00:41:57.8	37.34	136.59	8	6.67	6.8	6.1	6.43	7.02	0.10	2	TF	Near West Coast of Honshu, Japan
81	04/01/2007	20:39:56.4	-8.46	157.04	10	8.06	8.1	6.8	7.54	8.15	3.50	49	TF	Solomon Islands
82	07/16/2007	01:13:28.0	37.57	138.44	55	6.62	6.6	6.5	6.50	6.76	na	1	TF	Near West Coast of Honshu, Japan
83	08/02/2007	02:37:43.0	47.26	141.75	5	6.18	6.2	5.3	na	5.87	0.15	6	TF	Sakhalin, Russia
84	08/02/2007	03:21:46.0	51.36	-179.95	48	6.73	6.7	6.3	6.26	6.60	0.03	1	TF	Andreanof Islands, Aleutian Islands
85	08/15/2007	23:40:58.0	-13.32	-76.51	41	7.97	8.0	6.7	7.71	7.95	0.37	56	TF	Near Coast of Peru
86	09/12/2007	11:10:26.0	-4.52	101.38	30	8.48	8.5	6.9	8.13	8.20	0.98	20	NC	Southern Sumatra, Indonesia
87	09/30/2007	05:23:34.0	-49.42	163.84	11	7.40	7.4	6.4	7.16	7.50	0.11	3	TF	Auckland Islands, N.Z. Region
88	11/14/2007	15:40:53.0	-22.19	-69.84	60	7.72	7.7	6.7	7.51	7.73	0.13	6	TF	Antofagasta, Chile
89	09/29/2009	17:48:10.3	-15.49	-172.04	10	8.11	8.1	7.1	8.03	8.41	16.30	130	NF	Samoa Islands Region

CURRICULUM VITAE

Personal details:

Surname	Di Giacomo
First name	Domenico
Date of birth	16 December 1979
Place of birth	Potenza, Italy
Nationality	Italian
E-mail	domenico@gfz-potsdam.de
Telephone	+49 (0)331 288 28658

Education:

March 2004	Degree in Geological Science, University of Basilicata, Italy. Thesis: Analysis and modeling of seismic data in the presence of a velocity inversion. The case of Venosa (PZ).
July 2002 to December 2002	Erasmus stipend at GeoForschungsZentrum Potsdam (Germany) in cooperation with the University of Potsdam.
1998	Diploma at "G. Galilei" High School, Potenza, Italy.

Further Education:

2-7 September 2008	Young Scientist Training Course of the European Seismological Commission, held at the Laboratory of Geophysics and Seismology, Technological Institute of Crete, Chania, Crete, Greece.

Professional History:

Since March 2007	PhD student at Helmholtz Centre Potsdam GFZ German Research Centre For Geosciences in the section 2.1 "Earthquake Risk and Early Warning" in collaboration with the University of Potsdam. The focus of the PhD has been the development of a procedure to determine the energy magnitude Me for rapid response purposes.
April 2010	Convener at the annual meeting of the Seismological Society of America (SSA) in Portland (Oregon, USA) of the special session "*Recent advances in source parameters and earthquake magnitude estimations*".
September 2009	Lecture on "Introduction to source parameters derived from source spectra" during the "*International training course on*

	seismology, seismic data analysis, hazard assessment and risk mitigation", Potsdam, Germany.
April 2009	Lectures on "Introduction to observational seismology" and "Magnitude of seismic events" during the training course on "*Seismic network management and SeisComp3, Cross-border natural disaster prevention in Central Asia project*", Potsdam, Germany.
April 2009	Task Force Mission to L'Aquila (Italy) after the Mw 6.3 occurred the 6 April 2009. Installation of strong motion and velocimetric stations in the epicentral area.
May 2009	Single stations and array measurements of ambient seismic noise for the site characterization of the RAN stations. The work was performed in the context of the Italian DPC-project S4.
November 2008	Visit at the University of Alicante (Spain) in the context of the project "Acciones Integradas". The work aimed at implementing, in collaboration with J.J. Galiana-Merino, an alghorithm for automatic extraction and *P*-phase picking of earthquake data from continous streams recorded with the EarthDataLogger digitizers.
November 2005 to February 2007	Fellowship at the Istituto Nazionale di Geofisica e Vulcanologia, Sezione di Milano, Italy. The work concerned mainly the acquisition, the processing, the archiving of the seismic digital data of the seismic stations managed by the INGV-MI and their site effects evaluation.
October 2004 to May 2005	Fellowship at the Department of Physics of the University of Calabria, Cosenza, Italy. The work concerned the installation of seismometric stations in the region of Calabria (South Italy) and seismic monitoring. .

Publications:

Oth, A., D. Bindi, S. Parolai, and **D. Di Gi acomo** (2010). Spectral analysis of K- and KiK-net data in Japan II – On attenuation characteristics, source parameters and site response of borehole and surface stations, submitted to *Bull. Seism. Soc. Am.*

Di Giac omo, D. , D. Bindi, S. Parolai, and A. Oth (2010). Residual analysis of teleseismic P-wave energy magnitude estimates: inter- and intra-station variability, submitted to *Physics of the Earth and Planetary Interiors*.

Di Giacomo, D., and S. Parolai (2010). Is the detection of earthquakes depleted in their high frequency content sufficient for tsunami warning systems?, submitted to *Natural Hazards*.

Bormann, P., and **D. Di Giacomo** (2010). The moment magnitude M_w and the energy magnitude M_e: common roots and differences, submitted to *Journal of Seismology*.

Parolai, S., S. Orunbaev, D. Bindi, A. Strollo, S. Usupaev, M. Picozzi, **D. Di Giacomo**, P. Augliera, E. D'Alema, C. Milkereit, B. Moldobekov and J. Zschau (2010). Site effect assessment in Bishkek (Kyrgyzstan) using earthquake and noise recording data, *Bull. Seism. Soc. Am.*, in press.

Picozzi, M., R. Ditommaso, S. Parolai, M. Mucciarelli, C. Milkereit, M. Sobesiak, **D. Di Giacomo**, M.R. Gallipoli, M. Pilz, M. Vona, and J. Zschau (2010). Real time monitoring of structures in task force missions: the example of the Mw = 6.3 Central Italy earthquake, April 6, 2009, *Natural Hazards*, **52**(2), 253-256, DOI 10.1007/s11069-009-9481-1.

Di Giacomo, D., S. Parolai, P. Bormann, H. Grosser, J. Saul, R. Wang, and J. Zschau (2010). Suitability of rapid energy magnitude estimations for emergency response purposes, *Geophys. J. Int.*, **180***,* 361-374, doi: 10.1111/j.1365-246X.2009.04416.x.

Di Giacomo, D., S. Parolai, P. Bormann, H. Grosser, J. Saul, R. Wang, and J. Zschau (2010). Erratum to "Suitability of rapid energy magnitude estimations for emergency response purposes", *Geophys. J. Int.*, **181***,* 1725-1726, doi: 10.1111/j.1365-246X.2010.04610.x.

Massa, M., S. Lovati, **D. Di Giacomo**, S. Marzorati, E. D'Alema, and P. Augliera (2009). A microtremor survey in the area shocked by the Ml 5.2 Salò earthquake (North Italy): an empirical approach to determine the effects of ground motions, *Journal of Earthquake Engineering,* **13**(7), 1029-1046.

Luzi, L., S. Lovati, E. D'Alema, S. Marzorati, **D. Di Giacomo** , S. Hailemikael, E. Cardarelli, M. Cercato, G. Di Filippo, G. Milana, G. Di Giulio, M. Rainone, P. Torrese, P. Signanini, G. Scarascia Mugnonzza, S. Rivellino, and A. Gorini (2009). Italian accelerometric archive: geological, geophysical and geotechnical investigations at strong-motions stations, *Bulletin of Earthquake Engineering,* DOI:10.1007/s10518-009-9153-2.

Di Giacomo, D., H. Grosser, S. Parolai, P. Bormann, and R. Wang (2008). Rapid determination of Me for strong to great shallow earthquakes, *Geophys. Res. Lett.*, **35**, L10308, doi:10.1029/2008GL033505.

Massa, M., S. Marzorati, E. D'Alema, **D. Di Giacomo** , and P. Augliera (2007). Site classification assessment for estimating empirical attenuation relationship for Central-Northern Italy earthquakes, *Journal of Earthquake Engineering,* **11**(6), 943-967.

Di Gi acomo, D. , M. R. Gallipoli, M. Mucciarelli, S. Parolai, and S. Richwalski (2005). Analysis and modelling of HVSR in the presence of a velocity inversion. The case of Venosa (Italy), *Bull. Seism. Soc. Am.*, **95**(6), 2364-2372.

Mucciarelli, M., M. R. Gallipoli, **D. Di Giacomo**, F. Di Nota, and E. Nino (2005). The influence of wind on measurements of seismic noise, *Geophys. J. Int.*, **161**, 303-308.

Selected Meeting Presentations:

- Comparisons of different teleseismic magnitude estimates from global earthquake datasets and assessment of influence of site and propagation effects.
  Di Giacomo D., S. Parolai, P. Bormann, J. Saul, D. Bindi, R. Wang, H. Grosser.
  2010 SSA Annual Meeting, Portland, OR, USA.
- Rapid determination of the energy magnitude Me.
  Di Giacomo D. , S. Parolai, J. Saul, H. Grosser, P. Bormann, R. Wang, J. Zschau.
  XXXI General Assembly of the European Seismological Commission 2008, Hersonissos, Crete, Greece.
- Rapid determination of energy magnitude from P-waves of teleseismic seismograms.
  Di Giacomo D., H. Grosser, S. Parolai, P. Bormann, R. Wang.
  General Assembly of the European Geosciences Union 2008, Vienna, Austria.
- Fast determination of energy magnitude from P-waves of teleseismic seismograms.
  Di Giacomo D., H. Grosser, S. Parolai, R. Wang, P. Bormann.
  68th Annual Meeting of the German Geophysical Society 2008, Freiberg, Germany.
- Strong motion stations: installations in North Italy.
  Augliera P., E. D'Alema, **D. Di Giacomo**, S. Marzorati, M. Massa.
  25th National Conference of the G.N.G.T.S. 2006, Rome, Italy.
- Analysis and modelling of HVSR in the presence of a velocity inversion. The case of Venosa (Italy).
  Di Giacomo D., M. R. Gallipoli, M. Mucciarelli, S. Parolai, S. Richwalski.
  General Assembly of the European Geosciences Union 2005, Vienna, Austria
- Velocity inversion and its effects on HVSR characteristics.
  Di Giacomo D., M. R. Gallipoli, M. Mucciarelli, S. Parolai, S. Richwalski.
  Poster presentation at XXIX General Assembly of the European Seismological Commission 2004, Potsdam, Germany.
- Influence of wind on microtremor measurements.
  Mucciarelli M., M. R. Gallipoli, **D. Di Giacomo**, E. Nino.
  XXIX General Assembly of the European Seismological Commission 2004, Potsdam, Germany.

Computer skills

- Excellent knowledge of the Linux operating system, of many seismological software (SAC, TauP, PITSA, Hypoellipse, FPFIT), of the Generic Mapping Tools (GMT), and of the PASSCAL suite software.
- Good shell-scripts programming and knowledge of the Fortran and AWK programming languages. Basic knowledge of Matlab programming language.
- Good knowledge of MS-Windows and MS-DOS operating systems.

Language skills

Mother language: Italian.
Other languages: good knowledge of English, basic German and French.

Awards:

- Winner of the national prize "G. Pialli" 2004 for the best diploma thesis in the field of seismic risk reduction.
- Winner of the 2nd prize at GFZ PhD-Day, 1st December 2008; with the poster *"Rapid determination of the energy magnitude Me*".

Domenico Di Giacomo